INTERNATIONAL ASSOCIATION FOR GONDWANA RESEARCH 2024 CONVENTION AND 21ST INTERNATIONAL CONFERENCE ON GONDWANA TO ASIA

Global Synergy for Geoscience Innovation: Uniting Continents, Advancing Knowledge

18-22 NOVEMBER 2024
WATERFRONT HOTEL, KUCHING
SARAWAK, MALAYSIA

IAGR 2024 ABSTRACT VOLUME

The IAGR annual conventions and Gondwana to Asia international conference series provide an excellent platform for the dissemination of new research results and exchange of scientific knowledge on Geodynamics and Tectonics, Metallogeny, Life evolution and paleo environment, Geo energy and future sustainability , Sustainable resources & geoengineering, Natural Hazards and Geoheritage research. The annual conventions of IAGR have a high reputation as venues for the advancement of science and one of the best platforms for interaction with renowned geoscientists.

Table of Contents

Welcoming Message from Professor Simon Leunig

Pro Vice-Chancellor, President and Chief Executive, Curtin University Malaysia

On behalf of Curtin University Malaysia, it is my great pleasure to welcome you to the 2024 Annual Convention of the International Association for Gondwana Research (IAGR) and the 21st International Conference on Gondwana to Asia. We are deeply honoured to host this prestigious event here in Kuching, Malaysia, in collaboration with the IAGR.

This conference is a significant gathering of the world's foremost geoscientists, and it provides an exceptional platform for sharing pioneering research and exchanging scientific knowledge across a broad spectrum of geoscience disciplines.

The focal themes for this year - ranging from Geodynamics and Tectonics to Geoenergy and Future Sustainability - are both timely and critical as we collectively address some of the most pressing challenges facing our planet today. With a focus on advancing understanding in areas such as natural resource management, renewable energy, sustainable geoengineering, and disaster mitigation, this conference plays a crucial role in shaping the future of geoscience and its impact on society.

Curtin University Malaysia is proud to be at the forefront of research and education in these areas. Our commitment to sustainable practices, innovative geoengineering solutions, and cutting-edge energy research aligns closely with the themes of this conference. We are excited by the opportunities for collaboration and knowledge exchange that this event presents, and we look forward to fostering meaningful partnerships with researchers, academics, and industry leaders from around the globe.

I would like to extend my sincere gratitude to the IAGR for entrusting Curtin Malaysia with the honour of co-organising this event, and to our supporters and partners - Business Events Sarawak, Inno Lab Engineering Sdn Bhd, and Press Metal - for their invaluable contributions.

As you engage in the sessions, discussions, and presentations over the course of this conference, I encourage you to explore new ideas, forge new connections, and work together towards advancing geoscience research for the benefit of our global community.

Once again, welcome to the IAGR 2024 Annual Convention and the 21st International Conference on Gondwana to Asia. I wish you all a productive and inspiring conference.

Warmest regards

Prof. Simon Leunig

Welcome message from IAGR Secretary General

We extend a hearty welcome to the delegates of the International Association for Gondwana Research (IAGR) 2024 Convention and 21st International Conference on Gondwana to Asia held in Kuching, Malaysia during November 18-22, 2024, organized by the Curtin University Malaysia, jointly with the IAGR. We also welcome the Officials of IAGR, Patrons, Editors of "Gondwana Research" and "Geoscience Frontiers", our Awardees, students, friends and well-wishers to this elite gathering.

In the mid-1980s Prof. Masaru Yoshida from Osaka City University of Japan visited Trivandrum, the capital city of Kerala in southern India where he met with M. Santosh at the Center for Earth Science Studies and their collaboration and friendship paved the way to the building of the "Gondwana Research Group" (GRG). Subsequently, they were awarded a UNESCO-IGCP project on Proterozoic Events in East Gondwana under which they gathered a few hundred participants from over 40 countries around the world. The GRG started publishing the "Gondwana Newsletter" (GNL), with Prof. Joseph Meert from USA joining hands, and taking the lead to start its first online version. GNL, which was later incorporated for some time in the Journal of African Earth Sciences. The GRG grew into the International Association for Gondwana Research (IAGR) and GNL changed into a full-fledged and independent international multidisciplinary journal, "Gondwana Research" (GR), the first issue of which was published in October 1997. GR rapidly gained visibility and reach as a reputed journal and eventually Elsevier came forward to publish the journal on a partnership basis with IAGR from 2005. GR, the official publication of IAGR, is now one of the highest-ranking journals in its field.

IAGR holds the reputation as one of the largest fraternity of geoscientists on the globe with no membership fee. During the past three decades, the Society has organized its annual meetings in different countries including India, China, Japan, Korea, Australia, Thailand, and also previous workshops in South Africa and South America, among other countries. The Society has also joined many other conferences as co-sponsors. It is the first time that we are organizing our Annual Convention in Malaysia. The IAGR annual conventions and Gondwana to Asia international conference series provide an excellent platform for dissemination of new research results and exchange of scientific knowledge on Geodynamics and Tectonics, Metallogeny, Life evolution and paleo environment, Geo energy and future sustainability, Sustainable resources & geoengineering, Natural Hazards and Geoheritage research, among other themes. The annual conventions of IAGR have high reputation as venues for the advancement of science. The 2024 conference in Kuching, Malaysia commences with ice breaker on November 18, and oral and poster sessions for 2 days during 19 and 20 November 2024. This is followed by a one-day field excursion to the Kuching area on 21st Nov 2024, and a local trip on 22nd Nov 2024.

We thank the organizers of this conference, particularly Prof. R. Nagarajan and his team members at the Curtin University of Malaysia for hosting this conference in Malaysia. We wish you a productive time at the conference attending the keynote talks, and oral and poster presentations. We hope you will also enjoy the local geology, culture and cuisine. We also wish you fruitful interactions and exchange of ideas, renewing associations, and building new friendship and collaborations. On behalf of IAGR, I thank you once again for your valuable patronage and goodwill through your participation.

M. Santosh,
Secretary General, International Association for Gondwana Research

Welcome message from the Chairman of the IAGR 2024 Conference

On behalf of the Organising Committee, I am delighted to welcome all the VIP guests, keynote speakers and delegates from various parts of the globe to Kuching, Sarawak, Malaysia for the International Association for Gondwana Research (IAGR) 2024 convention and 21st International Conference on Gondwana to Asia, Sarawak Malaysia. The IAGR annual conventions and Gondwana to Asia international conference series provide an excellent platform for the dissemination of new research results and exchange of scientific knowledge on Geodynamics and Tectonics, Metallogeny, Life evolution and paleoenvironment, Geo energy and future sustainability, Sustainable resources & geoengineering, Natural Hazards and Geoheritage research. The annual conventions of IAGR have a high reputation as venues for the advancement of science and one of the best platforms for interaction with renowned geoscientists.

The theme of IAGR is "Global Synergy for Geoscience Innovation: Uniting Continents, advancing knowledge". Exponential population growth and industrial development are increasing pressures on the available resources and the earth; thus, challenges arise for food, water and energy supplies, environmental issues and climate change. In addition, inadequate management and unsustainable approach lead to various hazards. Over-exploitation of resources led to an exhaust of materials and challenges. These grand challenges for humanity require immediate solutions in sustainable ways without harming the environment and thus create opportunity for the geoscientist to explore more for new resources, sustainable mining, extraction and protect the earth from natural hazards in interdisciplinary and multidisciplinary approaches. In addition, in the challenging world interaction between industry and academia and the collaboration between various disciplinary researchers is key essential to the sustainable future. Therefore, IAGR 2024 brings together a community of Geoscientists, Geo engineers, social scientists and other related researchers from Malaysia and Asia region and beyond to discuss the latest innovations, advances and best practices of geological solutions in industry and academic for sustainable future of the earth.

We are very pleased to announce that the number of delegates to IAGR to be more than 150, including international participants from China, India, Japan, Malaysia, Italy, Republic of Korea, Australia, Russia, Mexico, UK, Taiwan, Thailand, Indonesia, Saudi Arabia, Brunei, France, USA, Vietnam and Sri Lanka.

IAGR 2024 will not be successful without the support from various parties. Therefore, I would like to thank IAGR as an organising partner, all the participants and sponsors such as Inno lab, Press metal, Curtin Malaysia for making this symposium possible.

Finally, all members of the Organising Committee wish you a fruitful internal conference experience and a memorable stay in Kuching, Sarawak, Malaysia.

Best Regards
Nagarajan Ramasamy
The Chair of IAGR 2024

IAGR 2024 Organising Committee

Chair: Prof. R.Nagarajan (Curtin University, Malaysia)
Co-Chairs: Prof. M. Santosh (China University of Geosciences, Beijing, China)
Dr. Vijay Sundarrajan (Curtin University, Malaysia)
Dr. Bridgid Chin Lai Fui (Curtin University, Malaysia)

Members:
Prof. Mu.Ramkumar (Periyar University, India)
Dr. Yun Peng Dong (China)
Prof. J.G. Meert (Australia)
Dr. S. Kwon (South Korea)
Prof. T. Tsunogae (Japan)
Prof. I. Safonova (Russia)
Prof. A. Festa (Italy)
Dr. D. Lingley (Japan)
Prof. E. Shaji (India)
Dr. Cheng-Xue Yang (China)

ADVISORY BOARD
Prof. Simon Leunig, Pro Vice Chancellor, Curtin University, Malaysia
Prof.Vincent Lee, Deputy Pro Vice Chancellor, Curtin University, Malaysia

Members
Prof. Tuong Thuy Vu, Curtin University, Malaysia
Dr. Pauline Ho, Curtin University, Malaysia
Mr. John Jong, Malaysia
Prof. M.V Prasanna (Curtin University, Malaysia)
Dr. Dominique Dodge-Wan (Curtin University, Malaysia)
Mr. Franz Kessler, Germany
Dr. Armstrong Altrin-Sam, UNAM, Mexico
Dr. Datu.Lulie Melling, TROPI, Malaysia
Dr. M.P.Jonathan, Instituto Politecnico Nacional (IPN) Mexico
Prof. T.Subramani, Anna University, India
Prof. Pon Selvan, Curtin University, Dubai
Dr. Ryan McKenzie, Hong Kong
Dr. Isnu Hajar Silistyawan, Geological Museum, Indonesia

SECRETARIAT
Dr. Perumal Kumar (Chair)
Prof Sujan Debnath (Co-Chair)

TREASURER
Ms. Daisy Christy Saban (Chair)
Ms. Eradania Winston Anak Juti

PROCEEDINGS AND PUBLICATION COMMITTEE
Dr. Tan Inn Shi (Chair)
Dr. Christine Yeo Wan Sieng
Dr. Henry Foo Chee Yew
Dr. Lee Yeong Huei
Dr. Adrian Tiong

PROGRAM & LOGISTIC COMMITTEE
Dr. Bridgid Chin Lai Fui (Chair)
Dr. Jibrail Kansedo

Dr. Evelyn Chiong Tung
Dr.Angnes Tiong Ngieng Tze
Dr. Lee Yih Nin
Dr. Yong Leong Kong
Ms. Siti Nurbaya Binti Mohamad Basir
Ms. Florence Singa

FIELD LOGISTICS (Volunteers)
Dr. Vijay Sundarrajan (**Chair**)
Mr. Sharveen Ravichandran
Mr. Ranjen Chandrasekaran
Mr. Abdulmajid Ali Muhammad
Mr. Mano Balaji
Ms. Patricia Henry
Ms. Natasha Cindy Richard

SPONSORSHIP COMMITTEE
Mr. Basil Jason John (Chair)
Prof. R.Nagarajan

EXTERNAL LINKAGES AND PUBLICITY
Prof. R.Nagarajan **(Chair)**
Dr. Vijay Sundarrajan
Dr. Bridgid Chin Lai Fui

WEBSITE/Media
Dr. Henry Foo Chee Yew

CONFERENCE MC
Mr.Ricky Donald Anak Berji (Curtin Malaysia)

Key Note Abstracts

The nexus of sustainability and climate change conundrum: Planet Earth in Transitional Era

M. Santosh[1,2,3*]

[1]*China University of Geoscience Beijing, China*
[2]*University of Adelaide, Australia*
[3]*Kochi University, Japan*

*Corresponding Author:
E-mail address: santosh@cugb.edu.cn (M.Santosh)

It took nearly four billion years for the Earth to become a habitable planet. Plate tectonics drives the tectonic plates on the globe, builds continents and a wealth of mineral resources, opens and closes oceans, and assembles continental fragments into large supercontinents. Plumes act as giant energy pipes transferring heat and material from the deep mantle. The birth of primitive life on our planet is considered to be linked to energy from either chemotrophy or photography. Following the protracted evolution of life and the appearance of humans and the growth of civilization, carbon-based fuels came into use. Approximately 85% of the world's energy currently comes from fossil fuels, including coal, petroleum products, and natural gas. The spiraling growth in population and fast depletion of metallic resources pose a major challenge to the sustainability of our civilization. Energy resources of the planet are limited, and the world is faced with severe challenges of resource depletion, pollution, and environmental degradation. In addition, some of the biased concepts on global warming and sea level changes also need to be evaluated in a more logical and integrated scientific perspective if we have to effectively address the challenges of the planet's sustainability.

The Paradox that is the Vindhyan Basin: Why is it so Important and Vexing?

Joseph G Meert[1*], Samuel Kwafo[1], Manoj K. Pandit[2], Anup K. Sinha[3]

[1]*Neil Opdyke Paleomagnetic Laboratory, Department of Earth and Planetary Sciences, University of Florida, Gainesville, FL 32611 USA.*
[2]*Department of Geology, University of Rajasthan, Jaipur 302004, Rajasthan, India*
[3]*Geomagnetic Research Laboratory, Regional Center of Indian Institute of Geomagnetism, Allahabad, 221 505, India*

*Corresponding Author:
*E-mail address:*jmeert@ufl.edu (J.G.Meert)

The Vindhyan Basin is in north-central India and is the largest of several "Purana" (=ancient) sedimentary basins in Peninsular India. The basin covers more than 1.6 million square kilometers with a total estimated sedimentary thickness of ~5000 meters and is divided into two (sometimes three) geographic regions in Rajasthan and Son Valley (**Fig. 1**). The Lower Vindhyan (Semri Group) is separated from the Upper Vindhyan sequence by an angular unconformity (**Fig. 1**). Numerous U-Pb

and Pb-Pb ages on interbedded ash units along with less well-constrained Pb-Pb ages on carbonates bracket the depositional history of the Semri Group to between ~1800-1600 Ma. These geochronologic results from the Lower Vindhyan have largely settled debates about its absolute age and therefore continued claims of Ediacaran fossils in the Lower part of the Vindhyan are perplexing. The ages of the Upper Vindhyan Kaimur, Rewa and Bhander Groups are unresolved after more than one hundred years of scientific debate. Taken at face value, the ages from the Semri Group indicate that the Upper Vindhyan sequence is younger than ~1600 Ma. The lowermost Kaimur sandstone is intruded by the 1073 Ma Majhgawan kimberlite indicating that subsidence was well underway during the Stenian. A less well-defined Re-Os age of 1210 ± 52 Ma was obtained from the Biyagarh shale within the upper part of the Kaimur. The Rewa shale rests conformably over the Kaimur sandstone and traces of diamond are known from the Rewa sandstone. Assuming that the diamonds are sourced from nearby Mesoproterozoic kimberlites, the Rewa must be younger than ~1073 Ma. Other isotopic age determinations in the Upper Vindhyan yield conflicting ages. For example, a K-Ar glauconite age in the Upper Kaimur Group is 300 Myr younger than the immediately underlying shales and only 2 myr older than a Pb-Pb carbonate age in the overlying Bhander limestone (**Fig. 2**). There are fission track and Sr-isotope estimates for the ages of units within the Upper Vindhyan that vary between 650-750 Ma (**Fig. 2**). Pb-Pb carbonate ages from the Bhander/Rewa carbonates yielded disparate results ranging from 1073 Ma to 866 Ma (**Fig. 2**). Attempts to 'date' the Upper Vindhyan sequence using fossil evidence are also contentious. De (2003) presented 'fossils' which he identified as *Hiemalora* and *Ediacaria* but admitted that these were tentative conclusions due to the poor preservation. Several have argued that the Bhander limestone is Ediacaran in age based on fossil findings of *Arumberia* and *Beltanelliformis*. The latter fossil was recently categorized as cyanobacteria. The nature of the enigmatic fossil/structure of *Arumberia* is controversial with various authors suggesting that it is a sedimentary structure or organic-sedimentary structure whilst others point to a biological origin most likely microbial or algal. McMahon et al. (2022) argue that *Arumberia* is restricted to the 560-520 Ma interval; however, older *Arumberia* occurrences are known from Baltica (573 Ma) and Scotland (~1.0 Ga). Recently, Retallack et al. (2021) reported *Dickinsonia tenuis* in the Maihar sandstone at Bhimbetka. Because *Dickinsonia* is temporally restricted to the Ediacaran this would seemingly solidify arguments regarding the age of the Upper Bhander at ~550 Ma. Meert et al. (2023) re-visited 'Dickinsonia' at Bhimbetka and demonstrated that the 'fossil' was a remanent of a modern beehive. Xiao et al. (2016) identified the microfossil *Trachyhystrichosphaera aimika* in the Sirbu shale (Upper Vindhyan) and correlative strata in the Ganga Valley (Himalayan Foreland Basin). *T. aimika* has been identified in strata ranging in age from 1150-720 Ma. Controversies about the fossil evidence in both the Lower and UpperVindhyan sedimentary sequences continue unabated.

Contradictory evidence for the age of the Upper Vindhyan is also found in detrital zircon studies. Several detrital zircon studies of the Upper Vindhyan sequence yielded similar spectra and, notably, no detrital zircon ages younger than ~1000 Ma. Lan et al. (2020) catalogued a single youngest detrital zircon from the Maihar sandstone with an age of 548 Ma in the Son Valley region. No other zircons younger than 1000 Ma were documented in that study, but the authors concluded that the fossil evidence cited above along with the isolated 548 Ma age confirmed an Ediacaran age for the Maihar (Bhander) sandstone. Lan et al. (2021) also reported detrital zircon ages from the same sandstone ~300 meters away and found no zircons younger than 1000 Ma. McKenzie et al. (2011) were able to correlate sedimentary successions beneath the Gangetic plains in northern India with the Upper Vindhyan strata. Those successions also lacked detrital zircon populations younger than 1000 Ma (**Figure 2** shows all DZ data from the Upper Vindhyan Sequence). Meert et al. (2021) summarized paleomagnetic data available from the Upper Vindhyan, Majhgawan kimberlite (1073 Ma; Gregory et al., 2008) and a ~1100 Ma dyke from Mahoba intruding the Bundelkhand granite (Pradhan et al., 2012). These three studies all show similar paleomagnetic directions, which led to the conclusion that Upper Vindhyan sedimentation was largely confined to the Stenian-Kleisian interval. Unfortunately, none of those paleomagnetic studies had field tests to demonstrate the primary nature of magnetization. Both the Majhgawan kimberlite and Mahoba dyke directions are based on limited sampling and therefore do not average paleosecular variation (PSV). Malone et al. (2008) argued that the stratabound reversals in the Upper Vindhyan provided strong evidence for a primary remanence, but Meert et al. (2020) noted that

field tests such as a fold or intraformational conglomerate tests are more important in defining the age of remanence. Therefore, it is possible that the directional similarities resulted from a remagnetization of the igneous rocks during Upper Vindhyan deposition or less likely that all rocks were remagnetized at a younger time. There are no presently known younger poles from India that correspond to directions isolated in the Upper Vindhyan. Some Ediacaran-Cambrian poles from western Gondwana, when rotated into Indian coordinates, do resemble the Bhander-Rewa poles so the possibility exists that the Bhander-Rewa poles are Ediacaran in age and the igneous rocks are remagnetized or that the similarity is fortuitous (Pivarunas et al., 2018).

Carbon isotopic studies yielded negative $\delta^{13}C$ (~-5.5‰) values in the Lakheri limestone (Rajasthan sector) whereas the assumed cross-basinal equivalent Bhander Limestone (Son Valley) showed more positive values. Kumar et al. (2005) associated the negative excursion in the Lakheri limestone with the Sturtian glaciation. In their interpretation, the Lhakeri limestone is *Cryogenian* in age and the younger Bhander limestone is *Ediacaran*. To date, there is no unequivocal evidence for glacially derived sediments in the Vindhyan basin. Gilleaudeau et al. (2018) re-examined the same Upper Vindhyan rocks and obtained conflicting results compared to the earlier studies. They found relatively constant positive $\delta^{13}C$ values between +2 and 3‰ in the Lakheri limestone and posited a *Mesoproterozoic-early Kleisian* age and argued that the more positive $\delta^{13}C$ values between +4 and 6‰ in the Bhander limestone (Son Valley region) indicate a later *Kleisian* (>811 Ma) age. In their study, neither limestone showed extreme negative values such as might be expected if deposition occurred during the Bitter Springs (811 Ma), Islay (735 Ma), Trezona (~650 Ma) or Shuram (574-567 Ma) anomalies. Nevertheless, they concluded that previous intrabasinal correlations between the two limestones should be reviewed and perhaps basinal closure in the west took place earlier than in the east. Basu et al. (2021) agreed that there may be differences in source material between the Rajasthan and Son Valley sectors but reasoned that the $\delta^{13}C$ values may reflect variations in the local carbon cycle rather than a global signal indicating different ages for the two limestones. Age interpretations using stable isotopes range from ~58 0Ma - 1.1 Ga for the Lahkeri limestones. Paleomagnetic data from both Lakheri and Bhander limestones are limited (3 sites from each; Malone et al., 2008). Due to the low number of samples, both poles have large errors, but they are statistically indistinguishable.

Indirect evidence for an *Stenian-Kleisian* age of basin closure in the Upper Vindhyan is suggested by the presence of orogenic belts to the west (Aravalli-Delhi) and south (Central Indian Tectonic Zone) that experienced significant tectonism between ~1.1-0.85 Ga (McKenzie et al., 2013; Bhowmik, 2019; Biswal et al., 2022). It is argued that the development of these mountainous regions resulted in the closure of the Upper Vindhyan basins around the same time. Lastly, the Marwar Basin that lies to the west of the Aravalli-Delhi fold belt is undoubtedly of the Ediacaran age. Davis et al. (2014) obtained limited paleomagnetic data from the Marwar sequence that are statistically distinct from the Upper Vindhyan, Majhgawan and Mahoba paleomagnetic data cited above. In this talk, we examine some new data that support a Tonian age for the Upper Vindhyan sequence.

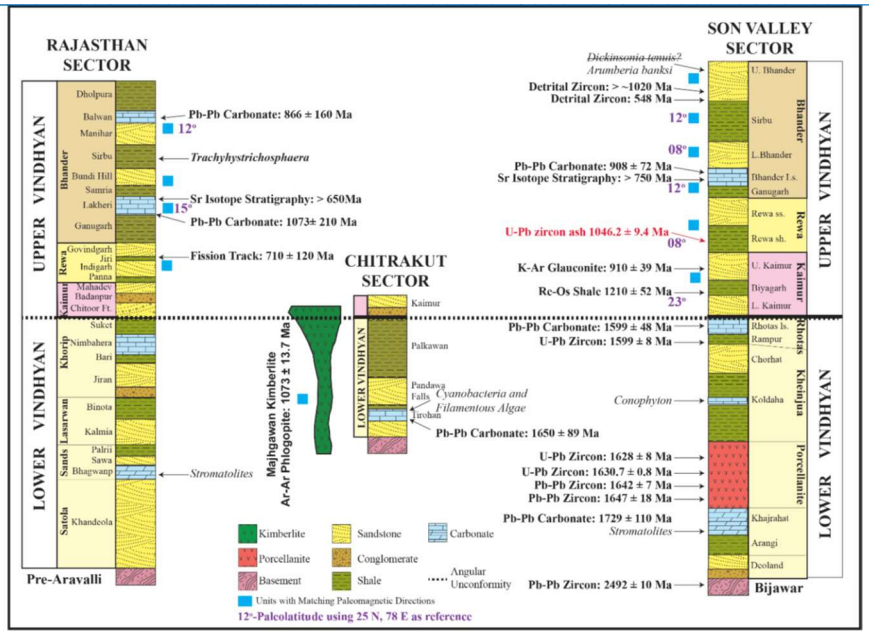

Figure 1. Generalized stratigraphy of the Vindhyan Basin showing geochronological, paleontological, and stable isotope age constraints on various units within the Upper and Lower sedimentary units. The figure is modified from Gilleaudeau et al. (2018). Note the new 1046 Ma concordia age from an ash bed in the Rewa shale at Teonthar. Purple numbers represent paleolatitude estimates from paleomagnetism using 25° N, 78° E as reference site.

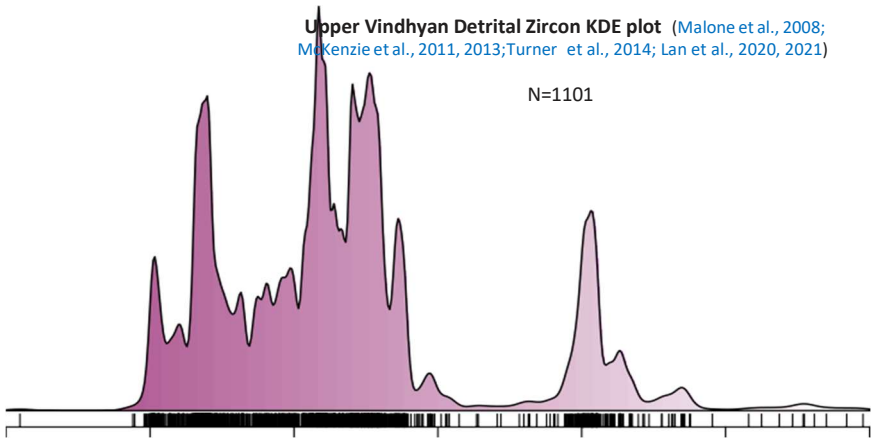

Figure 2: Kernel Density Estimator (KDE) plot of compiled Upper Vindhyan (Kaimur, Rewa, Bhander) detrital zircon data. The rug plot indicates the distribution/density of the individual data points.

References

Basu, P., Banerjee, A., Chakrabarti, R., 2021. A combined geochemical, Nd, and stable Ca isotopic investigation of provenance, paleo-depositional setting and sub-basin connectivity of the Proterozoic Vindhyan Basin, India. Lithos 388–389, 106059. https://doi.org/10.1016/j.lithos.2021.106059.

Bhowmik, S.K., 2019. The current state of orogenesis in the Central Indian Tectonic Zone: A view from the southern margin. Geological Journal 54, 2912–2934.

Biswal, T. K., Pradhan, R. M., Sharma, N. K., Tiwari, S. K., Beniest, A., Behera, B. M., Singh, S., Saraswati, R., Bhardwaj, A., Umasankar, B. H., Singh, Y. K., Sarkar, S., Mahadani, T., Saha, G., 2022. A review on deformation structures of different terranes in the Precambrian Aravalli-Delhi Mobile Belt (ADMB), NW India: Tectonic implications and global correlation. Earth-Science Reviews 230, 1-22. 104037. https://doi.org/10.1016/j.earscirev.2022.104037

Davis, J.K., Meert, J.G., Pandit, M.K., 2014. Paleomagnetic analysis of the Marwar Supergroup, Rajasthan, India and proposed interbasinal correlations. Journal of Asian Earth Sciences 91, 339–351.

De, C., 2003. Possible organisms similar to Ediacaran forms from the Bhander Group, Vindhyan Supergroup, Late Neoproterozoic of India. Journal of Asian Earth Sciences 21(4), 387-395. https://doi.org/10.1016/S1367-9120(02)00036-6.

Gilleaudeau, G.J. Sahoo, S.K. Kah, L.C. Henderson, M.A. Kaufman, A.J., 2018. Proterozoic carbonates of the Vindhyan Basin, India: Chemostratigraphy and diagenesis. Gondwana Research 57, 10-25. https://doi.org/10.1016/j.gr.2018.01.003.

Gregory, L. C., Meert, J. G., Pradhan, V., Pandit, M. K., Tamrat, E., Malone, S. J., 2008. A paleomagnetic and geochronologic study of the Majhgawan kimberlite, India: Implications for the age of the Upper Vindhyan Supergroup. Precambrian Research 149(1–2), 65-75. https://doi.org/10.1016/j.precamres.2006.05.005

Kumar, S., Schidlowski, M., Joachimski, M.M., 2005. Carbon isotope stratigraphy of the Paleoneotrprozoic Vindhyan Supergroup, central India: implications for basin evolution and intrabasinal correlation. The Paleontological Society India 50, 65–81.

Lan, Z., Zhang, S., Li, X.-H., Pandey, S.K., Sharma, M., Shukla, Y., Ahmad, S., Sarkar, S., Zhai, M., 2020. Towards resolving the 'jigsaw puzzl' and age-fossil inconsistency within East Gondwana. Precambrian Research 345, 105775. https://doi.org/10.1016/j.precamres.2020.105779.

Lan, Z, Pandey, S.K., Zhang, S., Sharma, M., Gao, Y., Wu, S., 2021. Precambrian crustal evolution in Northern India block: evidence from detrital zircon U-Pb ages and Hf-isotopes, Precambrian Research 361, 106238. https://doi.org/10.1016/j.precamres.2021.106238.
Malone, S.J., Meert, J.G., Banerjee, D.M., Pandit, M.K., Tamrat, E., Kamenov, G.D., Pradhan, V.R., Sohl, L.E., 2008. Paleomagnetism and detrital zircon geochronology of the Upper Vindhyan sequence, Son Valley and Rajasthan, India: A ca. 1000 Ma closure age for the Purana basins? Precambrian Research 164, 137–159.
McKenzie, N.R., Hughes, N.C., Myrow, P.M., Xiao, S., Sharma, M., 2011. Correlation of Precambrian-Cambrian sedimentary successions across northern India and the utility of isotopic signatures of Himalayan lithotectonic zones. Earth Planetary Science Letters 312, 471–483.
McKenzie, N. R. Hughes, N. C. Myrow, P. M. Banerjee, D.M. Deb, M. Planavsky, N. J. 2013. New age constraints for the Proterozoic Aravalli–Delhi successions of India and their implications, Precambrian Research 238, 120-128.
McMahon, W.J., Davies, N.S., Liu, A.G., Went, D.J., 2022. Engima Variations: Characteristics and Likely Origin of the Problematic Structure Arumberia, as recognized from an exceptional bedding plane exposure and the global record. Geological Magazine 159, 1–20.
Meert, J.G., Pivarunas, A.F., Evans, D.A.D., Pisarevsky, S.A., Pesonen, L.J., Li, Z.X., Elming, S.A., Miller, S.R., Zhang, S., Salminen, J., 2020. The magnificent seven: A proposal for the modest revision of the Van der Voo (1990) quality index. Tectonophysics 790, 228549. https://doi.org/10.1016/j.tecto.2020.228549.
Meert, J.G., Pivarunas, A.F., Miller, S.R., Pandit, M.K., Sinha, A.K., 2021. Chapter 10. The Precambrian drift history and paleogeography of India. In: Pesonen, L.J, Salminen, J., Veikkolainen, T., (eds) Ancient Supercontinents and the Palaeogeography of the Earth. 305-332, Elsevier. https://doi.org/10.1016/B978-0-12-818533-9.00004-7
Meert, J.G., Pandit, M.K., Kwafo, S., Singha A., (2023) Stinging News: 'Dickinsonia' discovered in the Upper Vindhyan of India not worth the buzz. Gondwana Research 117, 1–7. https://doi.org/10.1016/j.gr.2023.01.003
Pivarunas, A.F., Meert, J.G., Miller, S.R., 2018. Assessing the intersection/ remagnetization puzzle with synthetic apparent polar wander paths. Geophysical Journal International 214 (2), 1164-1172. https://doi.org/10.1093/gji/ggy216.
Pradhan, V.R., Meert, J.G., Pandit, M.K., Kamenov, G.D., Mondal, E.A., 2012. Tectonic evolution of the Precambrian Bundelkhand craton, central India: Insights from paleomagnetic and geochronological studies on the mafic dyke swarms. Precambrian Research 198–199, 51–76.
Retallack, G.J., Matthews, N.A., Master, S., Khangar, R.G., Khan, M., 2021. Dickinsonia discovered in India and late Ediacaran biogeography. Gondwana Research 90, 165–170.
Turner, C.C., Meert, J.G., Pandit, M.K., Kamenov, G.D., 2014. A detrital zircon U-Pb and Hf isotopic transect across the Son Valley sector of the Vindhyan basin, India: Implications for basin evolution and paleogeography. Gondwana Research 26, 348–364.
Xiao, S., Tang, Q., Hughes, N. C., McKenzie, N. R. and Myrow, P. M. 2016. Biostratigraphic and detrital zircon age constraints on the basement of the Himalayan Foreland Basin: implications for a Proterozoic link to the Lesser Himalaya and cratonic India. Terra Nova 28, 419–426

Mélanges and their significance in the evolution of subduction-accretionary complexes and future perspectives

Andrea Festa[1, 2*]

[1]*Department of Earth Sciences, University of Torino, Via Valperga Caluso 35, 10125 Torino, Italy.*
[2]*National Research Council of Italy, Institute of Geosciences and Earth Resources Via Valperga Caluso 35, 10125 Torino, Italy.*

*Corresponding Author:
E-mail address: andrea.festa@unito.it (A.Festa)

Mélanges and, chaotic units represent significant components of most subduction complexes (i.e., accretionary, and not-accretionary margins) and orogenic belts around the world, regardless of their age (from Precambrian to present day), tectonic evolution, and location (e.g., from the circum-Pacific region to the circum- Mediterranean area, up to the Alpine-Himalayan and Asian orogenic belts and suture zones). However, nearly 100 years after the introduction of the term "mélange" (Greenley, 2019), the mode and nature of processes responsible for mélanges formation, and the geological environments in which different mélange types form are still a topic of controversy. The main challenge is the recognition of their original, diagnostic block-in-matrix fabric, which provides critical clues for where and how these chaotic rock assemblages formed and what they tell us about the nature of and interplay between crustal and submarine processes during their development.

Tectonic, sedimentary, and diapiric processes and their interaction have been documented to form different types of mélanges and/or chaotic units (i.e., tectonic, sedimentary, diapiric and polygenetic; e.g., Raymond, 1984; Festa et al., 2010). Nevertheless, most of the chaotic units preserved in exhumed subduction complexes, particularly metamorphic ones, are commonly interpreted as the product of

tectonic processes acting from intermediate (250 °C < *T* < 400 °C, corresponding to about 10–15 km depth) to great depths (*T* > 400 °C, corresponding to > 15 km depth) during convergent stages. The transfer of isolated slices and blocks, detached from the downgoing slab to the upper plate and/or within the plate boundary interface due to tectonic underplating, and the return flow (i.e., flow mélanges), undoubtedly represents an effective mixing mechanism for mélanges formation at those depths. However, our observations on both modern and ancient subduction complexes clearly show that the different types of mélanges and chaotic units already form at shallow structural levels (*T* < 250 °C, corresponding to < 10–15 km depth), indicating that (i) mixing mechanisms are not exclusive of deep processes, (ii) the internal architecture of exhumed subduction complexes may be highly heterogeneous already at shallow structural levels, and (iii) tectonics is not the exclusive process of mélange formation (see Raymond, 1984; Pini, 1999; Festa et al. 2019 and references therein). These observations suggest that part of mélanges occurring in exhumed metamorphic and polydeformed subduction complexes and orogenic belts do not necessarily represent the exclusive product of intermediate to deep processes, but they may document the subduction-related tectonic reworking of chaotic rock units formed at shallower structural levels (Festa et al., 2022).

Using field-based stratigraphic and structural criteria, we show that mélanges are characterized and distinguished from each other by different internal fabrics and diagnostic block-in-matrix arrangements. Hence, the study of mélanges through well-constrained field observations and diagnostic criteria, may provide important constraints in the reconstruction of the tectonic evolution of subduction accretionary complexes, and of various paleoenvironments within different tectonic settings with significant implications for a better understanding of the tectonic evolution of Precambrian to Phanerozoic subduction complexes and metamorphic orogenic belts around the world.

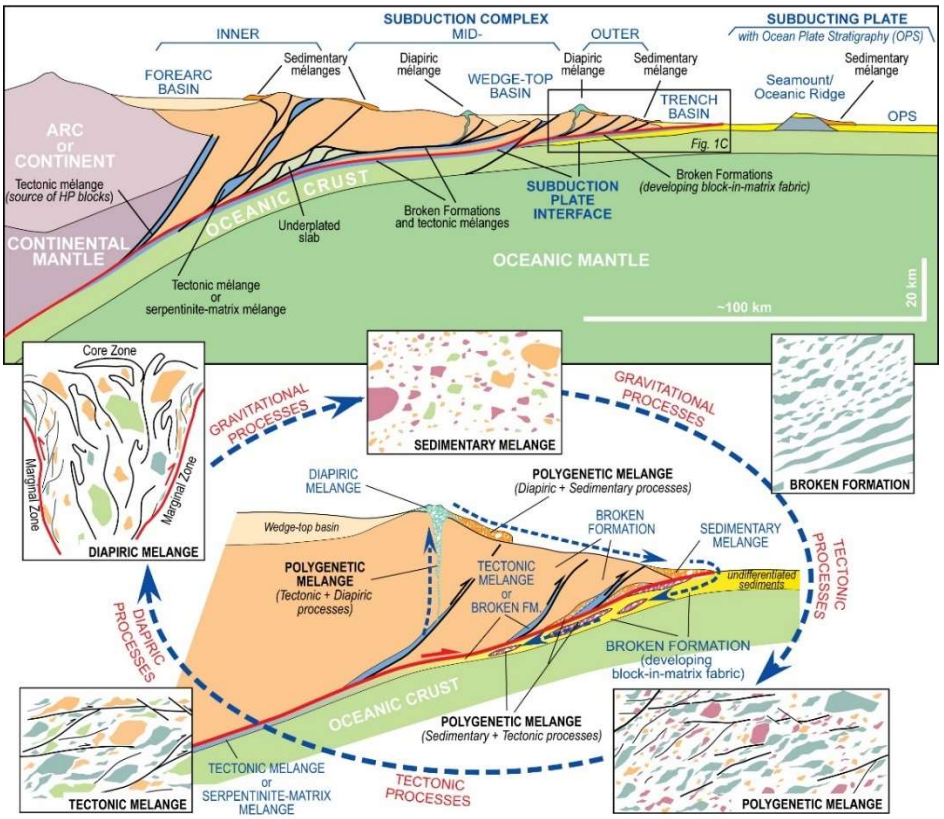

Figure 1. Different mechanisms and nature of blocks concur to form different types of mélanges and broken formations during the tectonic evolution of a subduction complex, according to different forming processes (tectonic, sedimentary, and diapiric). Polygenetic mélanges represent the product of the interplay and superposition of different processes (modified from Festa et al., 2022).

References

Festa, A., Barbero, E., Remitti, F., Ogata, K, and Pini, G.A., 2022. Mélanges and chaotic rock units: Implications for exhumed subduction complexes and orogenic belts. Geosystems and Geoenvironment 1, 100030. https://doi.org/10.1016/j.geogeo.2022.10 0 030

Festa, A., Pini, G.A., Dilek, Y., Codegone, G., 2010. Mélanges and mélange-forming processes: a historical overview and new concepts. International Geology Review 52 (10–12), 1040–1105. https://doi.org/10.1080/00206810903557704.

Festa, A., Pini, G.A., Ogata, K., Dilek, Y., 2019. Diagnostic features and field-criteria in recognition of tectonic, sedimentary and diapiric mélanges in orogenic belts and exhumed subduction-accretion complexes. Gondwana Research 74, 11–34.

Greenly, E., 2009. The geology of Anglesey. Vol. I & II. Memoirs of the Geological Survey HM Stationary Office, London 390–980, 1–388.

Pini, G.A., 1999. Tectonosomes and olistostromes in the Argille Scagliose of the Northern Apennines, Italy. Geological Society of America Special Papers 335, 73 pp.

Raymond, L.A., 1984. Classification of mélanges. Raymond, L.A. (Ed.), Mélanges: Their Nature, Origin and Significance. Geological Society of America Special Papers 198, 7–20.

Neoproterozoic tectonics, paleoenvironment and early life in the Yangtze Block, South China

Yunpeng Dong[1*]

[1]*State Key Laboratory of Continental Dynamics, Department of Geology, Northwest University, Northern Taibai Str. 229, Xi'an 710069, China*

*Corresponding Author:
E-mail address: dongyp@nwu.edu.cn (Yunpeng Dong)

The correlation between Neoproterozoic tectonics, paleoenvironment and early life are crucial for understanding the evolution of the Earth's habitability. The Yangtze Block preserves plenty of essential records to investigate these topics. The early Tonian tectonics of the Yangtze Block was characterized by exterior spreading to its west and north, and coeval interior subduction along its eastern margin, resulting in the passive continental marginal basins on the western and northern margins, and arc-related basins along the eastern margin. In the middle Tonian, the long-term exterior subduction-accretion on the west and north resulted in numerous arc-type igneous rocks and associated clastic deposits. In the east, the continuous interior subduction generated an active conti- nental margin, with back-arc and retro-arc basins filled with volcanic and clastic rocks, and finally led to the collision between the Yangtze and Cathaysia blocks at ca. 820 Ma. Some typical Neoproterozoic microfloras were flourishing. During the late Tonian, the exterior subduction generated the arc-related volcanic basins in the western and outer northern margins, while the interior post-collisional rifting resulted in a rift basin in the eastern margin, filled by shallow-marine to bathyal facies sediments. Influenced by the marginal volcanism, the paleoclimate was warm and humid in the early period, and transition to rather cold and dry in the late period. The microfloras remained the dominant paleontological taxonomy, but some macroalgal fossil fragments appeared. In the Cryogenian, along with termination of the exterior subduction, most parts of the Yangtze Block entered an extensional tectonics. Together with global paleoclimate cooling, the various tectonic backgrounds and paleogeographical frameworks of individual margins accumulated different glacial-interglacial sequences on the eastern, northern and western margins. These multi-stage deposits record paleoclimate cycles of cold-dry glacial periods and warm-humid interglacial periods. Subject to more extreme paleoclimate and paleoenviron- ment, early life was still dominated by microfloras (Monosphaeritae and Prismatomorphitae of Sphaer- omorphida) with minor macroalgal fossil fragments. During the Ediacaran, the entire Yangtze Block evolved into an extensional-subsidence tectonics, with carbonate platform (inner shelf and outer shelf) to abyssal-bathyal (slope-basin) facies gradually developing from northwest to southeast. Episodic atmospheric and oceanic oxygenation events resulted in positive shifts in paleoclimate and paleoenvironment. The advantageous condi- tions induced several global Ediacaran biotas on the Yangtze Block, which are known as the prologue and first phase of the Cambrian explosion, including the Lantian, Weng'an, Miaohe, Shibantan and Gaojiashan biotas. The transition from the Ediacaran to Cambrian constitutes a

critical inflection point in geological history, marking a co-evolution of organisms and paleoclimates that flourished by mutations. Appropriate external conditions made the early life further radiate, and the second and third phases of the Cambrian explosion were unveiled. They are represented by the Meishucun small shelly fossils (SSFs) on the western margin, and the Chengjiang biota and the contemporaneous Qingjiang biota on the western and northern margins of the Yangtze Block, respectively. Such manifestations indicate that the Cambrian explosion in the Yangtze Block was most likely related to the Neo- proterozoic subduction and continental arcs, which could provide sufficient nutrients for the later early life radiation.

Subduction erosion at Pacific-type convergent margins

Inna Safonova[1*], M. Santosh[2]

[1]*South-West Jiaotong University, FGEE, Chengdu 610031, Sichuan, China*
[2]*School of Earth Sciences and Resources, China University of Geosciences, Beijing 100083, China*

*Corresponding Author:
E-mail address: inna03-64@mail.ru (I.Safonova)

Pacific-type convergent margins (PCM) or orogenic belts form over subduction zones, where the oceanic lithosphere is submerged under intra-oceanic arcs or active continental margins. PCMs are very important geological entities because they are major sites of juvenile crust formation on the Earth, but also places of strong crust destruction via subduction erosion (Clift and Vanucchi, 2004). The most challengeable issue of the reconstruction of fossil magmatic arcs is the probable disappearance of arc igneous formations from geological records due to subduction erosion. The main agents of subduction erosion are horst-graben topography of subducting oceanic plate, orthogonal subduction of intra-oceanic arcs and ridges and accretion of oceanic rises (seamounts) (von Huene and Ranero, 2003). There are two contrast types of Pacific-type convergent margins – accreting and eroding (Scholl and von Huene, 2007). The accreting margins form accretionary complexes and grow oceanward. The eroding margins are characterized by the shortening distance between the arc and trench and subsequent subduction erosion of accretionary wedge, fore-arc prism and volcanic arc.

The first evidence for the tectonic erosion at Pacific-type convergent margins came from seismic reflection profiles made across the Tonga and Nankai trenches. The modern Pacific is surrounded by 75% of eroding convergent margins and 25% of accreting margins (Scholl and von Huene, 2007). The fast-subducting Pacific plate provides high-rate subduction erosion of the hanging walls of the western Pacific margins. Evidence for the subduction erosion comes from the proximity of coeval accretionary and supra-subduction complexes, the presence of supra-subduction igneous rocks as blocks in exhumed serpentinite mélange, trench jumping landward and related, magmatic lulls and the disappearance of U–Pb zircon age peaks in younger clastic rocks. For example, the Costa Rica consuming boundary in South America witnesses high rates of sediment destruction (Vanucchi et al., 2016), and the Cretaceous Shimanto accretionary prism in Japan is spatially adjacent to the coeval granitoids of the Ryoke belt suggesting that older accreted units were eroded (Safonova et al., 2015).

The present Western Pacific is the most probable actualistic analogue of the Paleo-Asian Ocean (PAO), which suturing formed the Phanerozoic Central Asian Orogenic Belt (CAOB) (Safonova et al., 2011). Accordingly, we suggest that the processes of subduction erosion were probably active at the PAO active margins. Evidence for this comes from the Chatkal-Atbashi arc in the middle Kyrgyz Tianshan, the Itmurundy and Tekturmas zones of central Kazakhstan, Ulaanbaatar accretionary complex (AC) in Mongolia and Char zone in eastern Kazakhstan, all in the western CAOB. The Chatkal-Atbashi complex includes coeval and spatially adjacent Early Devonian arc granitoids, ophiolites and accretionary units. In the Itmurundy and Tekturmas zones, the middle-late Cambrian

igneous rocks of supra-subduction origin have been diagnosed only as blocks in serpentinite mélange. In addition, in the Itmurundy and Tekturmas zones, the accreted oceanic units are located very close to the coeval supra-subduction complexes. The Itmurundy, Tekturmas and Char zones host thick greywacke units of mafic to andesitic composition, which detrital zircons those greywackes show unimodal U-Pb age curves, disappeared older peaks in younger sediments and positive epsilon Hf values. There are nil arc magmatic formations in the Ulaanbaatar AC, but the graywacke sandstones therein show unimodal distributions of U-Pb detrital zircon ages and positive values of epsilon Nd (whole-rock) and Hf (in zircon) (Savinskiy et al., 2022). All these facts suggest that that that the Cambrian magmatic arc that once existed in the PAO was eroded (Safonova and Perfilova, 2023). Therefore, the processes of subduction erosion in the western PAO were similar to those in the modern Circum-Pacific, for example, over the Guatemala-Costa Rica-Chile (eastern Pacific), Tonga (SW Pacific) and Nankai-Japan (western Pacific) subduction zones (von Huene and Ranero, 2003).

References

Clift, P.D., Vannucchi, P., 2004. Controls on tectonic accretion versus erosion in subduction zones: Implications for the origin and recycling of the continental crust. Reviews of Geophysics 42, RG2001.

Safonova, I., Seltmann, R., Kröner, A., Gladkochub, D., Schulmann, K., Xiao, W., Komiya, T., Sun, M., 2011. A new concept of continental construction in the Central Asian Orogenic Belt (compared to actualistic examples from the Western Pacific). Episodes 34, 186–194.

Safonova, I., Maruyama, S., Litasov, K., 2015. Generation of hydrous-carbonate plumes in the mantle transition zone linked to tectonic erosion and subduction. Tectonophysics 662, 454-471.

Savinskiy, I., Safonova, I., Perfilova, A., Kotler, P., Sato, T., Maruyama, S., 2021. A story of Devonian ocean plate stratigraphy hosted by the Ulaanbaatar accretionary complex, northern Mongolia: implications from geological, structural and U–Pb detrital zircon data. International Journal of Earth Sciences 111, 2469-2492.

Safonova, I., Perfilova, A., 2023. Survived and disappeared intra-oceanic arcs of the Paleo-Asian Ocean: evidence from Kazakhstan. National Science Review 10 (2), nwac215.

Scholl, D., von Huene, R., 2007. Crustal recycling at modern subduction zones applied to the past. Issues of growth and preservation of continental basement crust, mantle geochemistry, and supercontinent reconstruction. In: Hatcher, R.D., Jr., Carlson, M.P., McBride, J.H., Martínez Catalán, J.R. (Eds.), 4-D framework of continental crust. Geological Soceity of America Memoir 200, 9–32.

Vanucchi, P., Morgan, J.P., Balestrieri, M.L., 2016. Subduction erosion, and the de-construction of continental crust: The Central America case and its global implications. Gondwana Research 40, 184-198.

von Huene, R., Ranero, C.R., 2003. Subduction erosion and basal friction along the sediment-starved convergent margin off Antofagasta, Chile. Journal of Geophysical Research 108 (B2), 2079

Concatenation of biogeochemical processes and mineralization in the Archean Oceans

C. Manikyamba[1*]

[1]*CSIR-National Geophysical Research Institute, Uppal Road, Hyderabad 500 013*

*Corresponding Author:
E-mail address: cmaningri@gmail.com (C.Manikyamba)

The Archean greenstone belts comprising the most diverse rock types on the Earth's surface are unparalleled archives of the planet's evolution including the origin of the proto-oceans and their physico-chemical properties, evidence of plate tectonic processes, formation of oceanic crust and its role in the development of continental crust with vast mineral deposits. Although it is established that the tectono-magmatic processes operative on the primordial Earth played a pivotal role in shaping the planet's hydrosphere, atmosphere and biosphere, thus moulding the planet habitable for complex life forms, the processes governing the interactions between these spheres for mineralization remain unclear. The Dharwar Craton of southern peninsular India is a natural geological museum with well-preserved volcano-sedimentary assemblages present in the greenstone belts along with TTG-granitoid sequences and intruded dyke activity, documenting a billion-year crust formation history that is contemporaneous with the evolving mantle heterogeneity, ocean oxygenation, origin and evolution of

life and corresponding biogeochemical processes, mineralization and the gradual transformation of an inhabitable Earth. ~35 greenstone belts accounting to ~75,000 km^2 area are situated within the vast gneissic, granitoid terrane in the Dharwar Craton (~4,50,000 km^2), which ranges in age from 3.5-2.5 Ga. Based on the age, lithological associations, and metamorphism, the Dharwar Craton has been classified into the Sargur Group, and Bababudan-Chitradurga Groups collectively termed as the Dharwar Supergroup, which are preserved in the southern and western parts of the craton. The greenstone belts confined to the eastern part of the craton are orogenic gold bearing belts classified as the 'Kolar type'. The tectonic framework of the older to younger greenstone belts present in the southern, western and eastern regions of Dharwar Craton indicates predominant mantle plume, plume-arc and prevalence of arc volcanism that collectively contributed to the development of enriched and depleted mantle reservoirs, which gave rise to chromite, baryte, Platinum group elements (PGE), iron, manganese and gold mineralization etc.

The banded iron (BIFs) and Manganese formations, stromatolitic carbonates and carbonaceous shales of Sandur, Shimoga and Chitradurga greenstone belts provide significant information on the Archean ocean water chemistry, temperature, and the development of various depositional environments at the Meso-Neoarchean shelves. The higher thermal state of the Archean Earth led to enormous volcano-exhalative processes creating alkaline to acidic, reducing to oxygenic and chemically enriched ocean waters. The evolution of cyanobacteria driven through the material circulation between ocean, atmosphere and landmass forming the habitable trinity environment is largely attributed to the availability of nutrients released from abundant volcanism. The oxygen released due to the cyanobacterial activity is responsible for the deposition of BIFs, and Mn formations at the Archean shallow shelves with effective preservation of the decayed organic matter. The carbonaceous shales deposited in the deep ocean environment provide evidence for the Neoarchean biogeochemical processes in the Dharwar Craton. Graphitic carbon is preserved in the mineral lattice of BIFs as crystalline and poorly crystalline graphite with $\delta^{13}C_{gra}$ values of -28.5‰ from the sulphidic BIFs of Sandur belt coinciding with the $\delta^{13}C_{org}$ of associated Mn formations (-23.5 to -27‰ VPDB) and carbonaceous phyllites ($\delta^{13}C_{org}$= -24.8‰ to -29.2‰ VPDB). Though the mode of formation of these rocks and their mineral assemblages at different parts of Archean oceans vary from shelf to deeper basin, ranging from purely detrital to chemical precipitation, their carbon isotopic signatures unite them in terms of biological influence. The carbonaceous phyllites from the Chitradurga ($\delta^{13}C_{org}$= -38.3‰ to 14.2‰ VPDB), Gadag ($\delta^{13}C_{org}$= -24.3‰ to -8.06‰ VPDB) and Shimoga belts ($\delta^{13}C_{org}$= -24.6‰ to -11.8‰ VPDB) also corroborate the organic carbon signatures and the role of biogenic activity in these basins. The Rare Earth Element (REE) anomalies combined with the $^{13}C_{org}$ values from the stromatolitic carbonates (-1.61‰ to -0.01‰VPDB) from the Sandur, Chitradurga (-2.35‰ to 1.35‰VPDB) and Shimoga (-0.39‰ to 1.39‰ VPDB) belts together indicate fluctuating oxic-anoxic, acidic-alkaline conditions in the Archean oceans during their deposition. Negative values of $\delta^{18}O$ in these stromatolites (-20.95‰ to -12.24‰ in Sandur; -9.96‰ to -18.7‰ in Chitradurga and -7.72‰ to -9.85‰ in Shimoga belts) indicate local fluctuation in the seawater temperatures due to the influence of hydrothermal solutions (**Fig. 1**). The relationship between the oxygen and carbon isotopic ratios indicates a temperature range of 25-75ºC during the deposition of these stromatolites in the Dharwar proto-ocean. The combined geological, geochemical, geochronological, and stable isotope evidence from the clastic and chemical sediments of the Dharwar Craton together suggest that the Neoarchean peak of crustal growth attained through abundant magmatic activity influenced the stromatolitic growth and proliferation, which collectively favoured the precipitation of iron and manganese formations in the Archean oceans through the gradual oxygen build-up by the end of Neoarchean era. The successive detoxification of the Archean oceans and atmosphere from toxic gases and metals has thus rendered the planet habitable, fostering the growth and diversification of advanced/complex life forms.

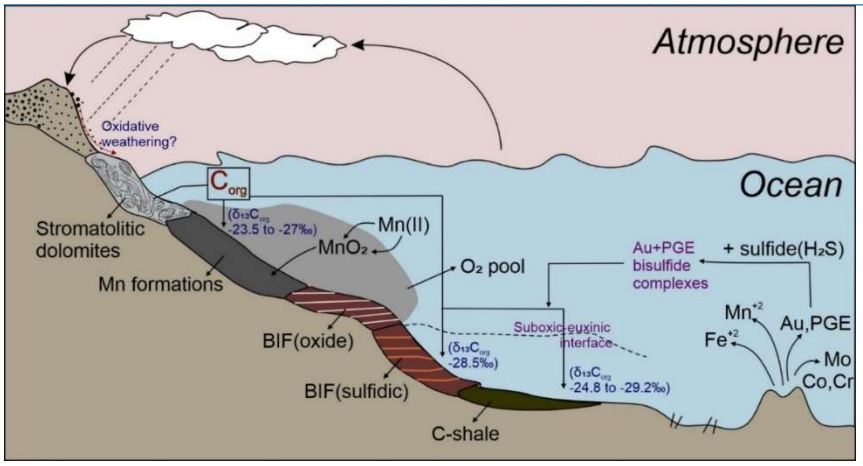

Figure 1. Different depositional environments in the Archean Ocean and their biological connection

Phanerozoic tectonic evolution of the proto-Korean Peninsula from polyphase orogenies recorded in the northeastern Okcheon Belt, Korea

Yirang Jang[1*], Sanghoon Kwon[2], Vinod O. Samuel[2]

[1] *Department of Earth and Environmental Sciences, Chonnam National University, Gwangju 61186, Republic of Korea*
[2] *Department of Earth System Sciences, Yonsei University, Seoul 03722, Republic of Korea*

*Corresponding Author:
E-mail address: yirang@jnu.ac.kr (J.Yirang)

The Korean Peninsula, a key fragment of the East Asian continental margin, lies between the North and South China cratons and the Japanese islands. The vast Paleozoic metasedimentary successions within a major orogenic belt of the Korean Peninsula reveal multiple tectonic systems, highlighting interactions such as subduction, collision and extension, documenting the geodynamic evolution of the Paleozoic basins in East Asia (e.g., Liu, 1998; Lee and Lee, 2003; Wu and Zheng, 2013; An et al., 2017; Han et al., 2017; Kim et al., 2017; Liu et al., 2017; Kim and Lee, 2018; Cho et al., 2021).

The Taebaeksan Zone of the northeastern Okcheon Belt, which consists of the most extensive Paleozoic strata in South Korea, has been a focal point for studying the Phanerozoic amalgamation of the North and South China cratons and the intervening microcontinents (e.g., Ernst and Liou, 1995; Metcalfe, 2006; Zhang et al., 2009). The Paleozoic sequences of the Taebaeksan Zone comprise the Lower Paleozoic Joseon and Upper Paleozoic Pyeongan supergroups, with a Middle Paleozoic hiatus, deposited on the intracontinental rift strata between the Gyeonggi and Yeongnam massifs in the southern Korean Peninsula.

The detrital zircon U-Pb ages and Lu-Hf isotope results from the Paleozoic sequences of the Taebaeksan Zone indicate that they predominantly contain Paleoproterozoic and Paleozoic zircons, with rare Meso- to Neoproterozoic ones. The zircon populations exhibit the following characteristics, informing their sedimentary provenances: (1) Paleoproterozoic zircons (ca. 1.85 Ga and 2.50 Ga) with similar ranges of εHf(t) values are common in the basement rocks of the Korean Peninsula, sourced from both the Gyeonggi and Yeongnam massifs. (2) Meso- to Neoproterozoic zircons, found only in Middle to Late Cambrian clastic sedimentary rocks within the carbonate sequences, likely indicate proximal provenance. (3) The youngest Paleozoic zircons in each formation, aligning closely with their deposition ages, suggest syndepositional magmatism and proximal magmatic sources during deposition. (4) Cambrian–Ordovician zircons in the Lower Paleozoic sequences, but rare in the Upper

Paleozoic sequences, indicate a provenance change following the hiatus between the two sedimentary successions. (5) Permian zircons with varying εHf(t) values suggest diverse detrital sources at that time.

Our integrated results suggest that the provenance variability is linked to diverse tectonic environments, reflecting the prolonged subduction-related crustal evolution of the proto-Korean Peninsula during the Paleozoic.

References

An, F., Zhu, Y., Wei, S., Lai, S., 2017. The zircon U-Pb and Hf isotope constraints on the basement nature and Paleozoic evolution in northern margin of Yili Block, NW China. Gondwana Research 43, 41–54.

Cho, M., Cheong, W., Ernst, W.G., Kim, Y., Yi, K., 2021. U-Pb detrital zircon ages of Cambrian-Ordovician sandstones from the Taebaeksan Basin, Korea: Provenance variability in platform shelf sequences and paleogeographic implications. GSA Bulletin 133 (3–4), 488–504.

Ernst, W.G., Liou, J.G., 1995. Contrasting plate-tectonic styles of the Qinling–Dabie–Sulu and Franciscan metamorphic belts. Geology 23, 353–356.

Han, S., de Jong, K., Yi, K., 2017. Detrital zircon ages in Korean mid-Paleozoic metasandstones (Imjingang Belt and Taean Formation): Constraints on tectonic and depositional setting, source regions and possible affinity with Chinese terranes. Journal of Asian Earth Sciences 143, 191–217.

Kim, M.G., Lee, Y.I., 2018. The Pyeongan Supergroup (upper Paleozoic-Lower Triassic) in the Okcheon Belt, Korea: A review of stratigraphy and detrital zircon provenance, and its implications for the tectonic setting of the eastern Sino-Korean Block. Earth-Science Reviews 185, 1170–1186.

Kim, S.W., Park, S.-I., Jang, Y., Kwon, S., Kim, S.J., Santosh, M., 2017. Tracking Paleozoic evolution of the South Korean Peninsula from detrital zircon records: implications for the tectonic history of East Asia. Gondwana Research 50, 195–215.

Lee, Y.I., Lee, J.I., 2003. Paleozoic sedimentation and tectonics in Korea: a review. Island Arc 12, 162–179.

Liu, S.F., 1998. The coupling mechanism of basin and orogen in the western Ordos Basin and adjacent regions of China. Journal of Asian Earth Sciences 16, 369–383.

Liu, Y., Li, W., Feng, Z., Wen, Q., Neubauer, F., Liang, C., 2017. A review of the Paleozoic tectonics in the eastern part of Central Asian Orogenic Belt. Gondwana Research 43, 123–148.

Metcalfe, I., 2006. Paleozoic and Mesozoic tectonic evolution and paleogeography of East Asian crustal fragments: the Korean Peninsula in context. Gondwana Research 9, 24–46.

Wu, Y.-B., Zheng, Y.-F., 2013. Tectonic evolution of a composite collision orogen: an overview on the Qinling–Tongbai–Hong'an–Dabie–Sulu orogenic belt in central China. Gondwana Research 23, 1402–1428.

Zhang, R.Y., Liou, J.G., Ernst, W.G., 2009. The Dabie-Sulu continental collision zone: a comprehensive review. Gondwana Research 16, 1–26.

Unlocking the Future: Can Explainable AI Revolutionize Climate Hazard Assessment via Spatial Intelligence Modeling?

Biswajeet Pradhan[1*]

[1]*Centre for Advanced Modelling and Geospatial Information Systems (CAMGIS), Faculty of Engineering and IT, University of Technology Sydney, CB11.06.106, Building 11 81 Broadway, Ultimo NSW 2007 (PO Box 123), Australia*

*Corresponding Author:
E-mail address: Biswajeet.Pradhan@uts.edu.au (B.Pradhan)

In this keynote talk, we delve into the transformative potential of Explainable Artificial Intelligence (AI) in revolutionizing climate hazard assessments through spatial intelligence modeling. As AI continues to evolve, it is reshaping the way we understand and manage natural hazards. By leveraging machine learning algorithms and big data analytics, AI allows for the efficient processing and interpretation of extensive spatial datasets, resulting in highly accurate and timely hazard assessments.

The real-time integration of geospatial information enhances our ability to anticipate and prepare for disasters, enabling swift and precise responses to emerging threats. Furthermore, AI introduces a paradigm shift in the analysis of natural hazards by uncovering intricate spatial patterns and relationships that were previously undetectable. These advanced algorithms reveal subtle correlations and hidden trends, deepening our understanding of complex environmental processes and informing more effective risk reduction strategies and resilient infrastructure development.

Through a series of case studies and cutting-edge applications, this keynote will demonstrate how AI-driven models and interpretations are fundamentally changing our approach to climate hazard assessment. By embracing this innovative convergence of technology and geoscience, we can unlock a safer and more resilient future, where Explainable AI plays a pivotal role in mitigating the impacts of natural disasters and safeguarding vulnerable communities.

Laser Ablation Lu-Hf Geochronology: A Novel and Robust Method to Rapidly Date Metamorphic, Mafic and Hydrothermal Minerals

Stijn Glorie[1*]

[1]*Department of Earth Sciences, The University of Adelaide, Adelaide SA 5005 Australia*

*Corresponding Author:
E-mail address: stijn.glorie@adelaide.edu.au (S.Glorie)

Lu-Hf geochronology traditionally involves laborious chemical separation processes in specialized laboratories. The novel laser ablation approach, recently developed at the University of Adelaide (Simpson et al., 2021, 2023), enables rapid Lu-Hf isotopic data acquisition at high spatial resolution, directly from rock blocks or thin sections. Applied to garnet, the method can be conducted in a campaign-style approach to rapidly reveal the metamorphic history of a terrane and has the capability to unravel polymetamorphic histories. Apatite Lu-Hf is more robust to isotopic disturbances compared to the U-Pb system (higher closure temperature) and can be used to directly date the timing of magmatic crystallization in rocks where zircons are absent (such as mafic rocks). Apatite, as well as calcite/dolomite, fluorite and allanite, are commonly associated with mineralization and can be dated by the Lu-Hf method to gain insights into hydrothermal processes. The presentation will go through a series of examples to illustrate the power of the Lu-Hf method to date a variety of geological processes that are difficult to time-constrain by other, more traditional methods.

References

Simpson, A., Gilbert, S., Tamblyn, R., Hand, M., Spandler, C., Gillespie, J., Nixon, A., Glorie, S., 2021. In-situ Lu-Hf geochronology of garnet, apatite and xenotime by LA ICP MS/MS. Chemical Geology 577, 120299.

Simpson, A., Glorie, S., Hand, M., Spandler, C., Gilbert, S., Cave, B., 2022. In situ Lu–Hf geochronology of calcite. Geochronology 4, 353–372.

Syn-emplacement ophiolites and relationship to supercontinent cycle

Peter A. Cawood[a*], Andrew S. Merdith[b,c] and J. Brendan Murphy[d]

[a] *School of Earth, Atmosphere and Environment Science, Monash University, Clayton, Victoria, 3800, Australia*
[b] *School of Earth and Environment, University of Leeds, Leeds, LS2 9JT, UK*
[c] *School of Physics, Chemistry and Earth Sciences, University of Adelaide, Adelaide, 5005, Australia*
[d] *Department of Earth Sciences, St Francis Xavier University, Antigonish, Nova Scotia, B2G 2W5, Canada*

*Corresponding Author:
E-mail address: Peter.cawood@monash.edu (P.A.Cawood)

Ophiolites are fragments of oceanic lithosphere now entrained within continents. Some ophiolites, such as the Bay of Islands ophiolite in the Appalachian-Caledonian Orogen and the Semail ophiolite in the Alpine-Himalayan Orogen, are characterized by a metamorphic sole along their structural base. The sole records metamorphism along a subduction zone interface between upper and lower plates with structural imbrication resulting in an inverted metamorphic assemblage of higher grade over lower grade. The sole is juxtaposed with the ophiolite, which forms through extension in the upper plate of the subduction zone, during attempted subduction of, and subsequent emplacement onto, a continental margin. We argue that such ophiolites form in small interior ocean basins during supercontinent breakup with the generation and expansion of these oceans compensated by lithospheric compression and initiation of multiple subduction zones. Subduction initiation is induced adjacent to a continental margin, likely along lithospheric discontinuities such as transform systems that formed during continental lithospheric extension and interior ocean basin formation. In such newly formed subduction zones, the subducting plate has limited lateral extent enabling its rapid evolution through trench rollback leading to ophiolite generation in the upper plate. This infant subduction system consumes the narrow tract of oceanic lithosphere adjacent to the continental margin leading to ophiolite obduction through attempted margin underthrusting. The establishment of these secondary subduction systems within small interior ocean basins corresponds temporally with the termination of convergent plate interaction and plate reorganization elsewhere in the global plate network, which we argue is the likely primary driver, triggering a cascading sequence of events, that induces the initiation of these transient secondary systems.

The Bio-geochemical Record of Late Devonian Mass Extinctions in the Woodford Shale of Southeast Laurentia: Midcontinent USA

Andrew Cullen[1*]

[1]*Big Hill Adventures, 810 Hoover, Norman OK 73072, USA*

*Corresponding Author:
E-mail address: abcullen@hotmail.com (A.Cullen)

Phanerozoic increases in the Earth's biosphere diversity have been disrupted by episodic extinction events, five of which were sufficiently severe and rapid to be considered mass extinctions. Since the possible causes of these extinctions, massive volcanism, supercontinent assembly, increases in seafloor spreading rates, and extraterrestrial events, are not mutually exclusive; relative weightings of primary-secondary drivers need to be resolved. The Late Devonian-Carboniferous extinction occurred in two separate pulses at the Frasnian-Famennian (Kellwasser events) and Famennian-Tournaisian (Hangenburg event) stage boundaries against the backdrop of rapid expansion of deep-rooted vascular land plants, rising atmospheric oxygen levels, and widespread anoxia-dysoxia in epeiric seas of the Rheic Ocean. This talk compares bio-geochemical aspects of the Late Devonian-Early Carboniferous Woodford Shale, (USA Midcontinent) to age equivalent black shales globally. The Woodford is an algal-dominated world-class siliceous marine source rock (3-16% TOC) reaching 200m in thickness. The Woodford was deposited during a 2nd order eustatic cycle. The transgressive lower member, spanning the Frasnian-Famennian extinction, is mostly siliceous mudstone. The middle member is dominated by pyritic argillaceous mudstone deposited in euxenic bottom waters during the maximum highstand. Siliceous mudstones and cherts of the regressive upper Woodford span the end of Devonian extinction. The upper Woodford has a 3-10m interval with abundant large (0.5-10cm) phosphate nodules that cover >30,000 km^2. REE and biomarker data indicate phosphogenesis was driven by an influx of terrestrial nutrients related to the extinction of extensive *Archaeopteris* forests and massive wildfires. Woodford Shale deposition post-dates known major Devonian impact events. Preliminary Hg

data, lacking isotopic analyses, are ambiguous with respect to volcanic activity as a driver of either of the Late Devonian mass extinctions. Paradoxically, increasing Devonian atmospheric oxygen levels may have not only enhanced algal and radiolarian blooms leading to eutrophication/anoxia of the shallow marine seas but also intensified massive forest fires at low latitudes.

Towards a Sustainable Transportation Fuel: Biofuel Technology vs EV

Lee Keat Teong[1*]

School of Chemical Engineering, Engineering Campus, Universiti Sains Malaysia, 14300 Nibong Tebal, Pulau Pinang

*Corresponding Author:
E-mail address: ktlee@usm.my (K.T.Lee)

Decarbonization of the transport sector has become an urgent priority and will be instrumental in winning the global race against climate change. The transport sector is responsible for approximately one-quarter of greenhouse gas emissions. 95% of the world's transport energy still comes from fossil fuels such as gasoline, diesel, jet fuel and natural gas. For 45% of countries transport is the largest source of energy-related emissions. For the rest of the countries, it is the second largest source. In addition to that, one important truth, humanity has only about 30 years to bring greenhouse gas emissions (GHG) to net zero if there is any chance of limiting global warming to 1.5 °C and GHG emissions need to fall by about half by 2030. In order to immediately overcome this, many perceive that EVs are the single most important technology for decarbonizing the transport sector. However, for the remaining some, biofuels, which include ethanol, methanol, biodiesel, biocrude, and methane derived from biomass seem to be a more promising potential, especially for the immediate future. In this presentation, some facts on the potential of EVs to decarbonize the transportation sector and options for using biofuel will be presented.

Keywords: Biofuel, Decarbonization, EVs, Transportation

Developing an Earthquake Resilient Society

Harsh K. Gupta[1*]

[1]CSIR-National Geophysical Research Institute, Hyderabad 500007, India

*Corresponding Author:
E-mail address: harshg123@gamil.com (H.K.Gupta)

We are presently in the 24th year of the 21st Century. In the past 23 years, the human lives lost due to earthquakes and the resultant tsunamis have far exceeded the total lives lost globally in the 20th Century. This is despite all the scientific, technical, and administrative developments.

Himalaya is seismically one of the most active continental regions globally, having hosted the strongest continental earthquake of Mw 8.7 on 15 August 1950 in northeast India. After 1950, no Mw ≥ 8 earthquake has occurred in the Himalayan belt. It is generally believed and accepted that a great earthquake could occur any time anywhere in the Himalayan seismic belt. Where and when it would

occur cannot be foretold with any certainty. Even if it is forecasted that an earthquake of Mw 7.5 would occur in the vicinity of Delhi next Sunday at noon time, can everyone leave Delhi? That is not possible. So, we need to learn to live with earthquakes. A very successful exercise in this regard was conducted by creating scenarios as to what would happen if the 1905 Kangra M ~ 8 earthquake repeats today (Gupta, 2023), by the National Disaster Management Authority (NDMA) Govt. of India in collaboration with other agencies. A hypothetical earthquake of Mw 8.0 was postulated at Mandi (near the epicenter of the 1905 Kangra earthquake). Isoseismals were generated using the 2011 Census data for demography and building typology, it was estimated that if the earthquake occurred at mid-night, the number of human lives lost would be ~ 0.9 million combining the states of Himachal Pradesh, Punjab, Haryana, and the Union Territory of Chandigarh. NDMA took up detailed preparatory exercises involving the state and center bodies for Rapid Visual Screening (RVS) of life-line buildings; school sensitizing events; Incident Response System (IRS); and awareness generation programs involving local celebrities and local media. National Disaster Response Force (NDRF), and State Disaster Response Forces played a very important role. After year-long preparations, Mega-mock drills were conducted for the hypothetical Mw 8 earthquake occurring at 11 am on 13 February 2013 for the 3 states (Himachal Pradesh, Punjab, and Haryana), and the UT of Chandigarh. The Public participated wholeheartedly. The performance of all the sectors was evaluated by independent observers. Quite a few shortcomings were found. Overall, it was a very successful exercise. With this success, a similar exercise was conducted for the 8 northeast Indian states for the repeat of the 1897 Mw 8.7 earthquake with equal success.

It is also of utmost importance to observe an annual Earthquake Day. There are ample examples that the countries that observe annually an earthquake day have done better when an earthquake occurs. 'Elementary Seismology', written by Charles Richter (1958) is one of the most popular textbooks read globally. Chapter 5 of this book, entitled 'Some Great Indian Earthquakes' mentions the 1819 Cutch earthquake (Oldham, 1928), the 1897 Shillong earthquake, the 1905 Kangra earthquake, the 1934 Bihar-Nepal earthquake, the 1935 Quetta earthquake and the 1950 Assam earthquake (**Fig. 1**). It has been found that in the 21st Century, earthquakes of magnitude like the 1819 Kutch, 1905 Kangra and 1934 Bihar-Nepal occurred, and the number of human lives lost was several folds reflecting the increase in population and infrastructure. The only exception was the Gurkha earthquake of 15 April 2015, where the lives lost were less compared to the 1934 earthquake, despite a several-fold increase in the population. One of the reasons is that Nepal observes 16 January every year as the earthquake safety day.

There are examples, worthy of following up, on how a determined approach to developing an earthquake-resilient society has provided excellent results (e.g. Gupta et al. 2020). For example, on 12 January 2010, a Mw 7.0 earthquake claimed ~ 316000 human lives in the Haiti in the Caribbean. A determined approach to improve the situation showed improvement when an Mw 7.2 earthquake occurred in Haiti on 14 August 2021, near the epicenter of the 2010 earthquake and claimed only ~ 3000 human lives. A more recent example is from Taiwan. The Chichi earthquake of Mw 7.6 on 21 September 1999 claimed ~ 2400 human lives, while the Mw 7.2 earthquake on 3 April 2024 claimed only 9 human lives.

Another important issue is the installation of the Earthquake Early Warning System along the entire length of the Himalayan seismic belt. The state of Uttarakhand has successfully deployed such a system, which is operating very effectively (Kumar et al. 2023). In a nutshell, earthquakes cannot be forecasted accurately as of now nor can be done away with. It is of utmost importance to learn to live with earthquakes and develop an earthquake-resilient society.

The six earthquakes (top; **Table 1**) are the ones included in Richter (1958). The bottom 3 (**Table 2**) are the earthquakes that occurred in India and its immediate vicinity during the 21st Century. It is noteworthy that a larger number of human lives lost in the Bhuj and Muzaffarabad earthquakes are a manifestation of the increase in population and infrastructure (Gupta et al. 2009). However, that is not the case with the Gorkha earthquake.

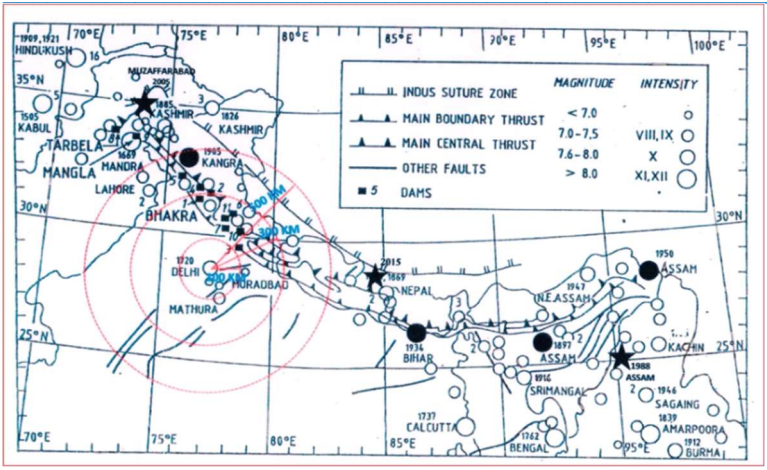

Figure 1. Earthquakes of M≥7.0, epicentral intensity ≥ VIII, and/or recent damaging earthquakes that caused fatalities in the Himalayas and the vicinity (25°- 37° N, 69°- 83° E; 20°- 30° N, 83°- 100° E). Four great earthquakes of M ≥8 are shown with filled circles. Stars: East is the 6 August 1988 M 7.3; west 8 October 2005 M 7.6 Muzaffarabad and Center: 25 April M 7.8 Nepal earthquake. Circles around Delhi indicate epicentral distances of 100, 300 and 500 km from Delhi. Updated from Chandra (1978).

Table 1: Indian Earthquakes included by Richter (1958), and M ≥ 7.5 in India and its vicinity:

S. No.	Date	Region	Magnitude (M)	Human lives lost	India's population in Earthquake Year
1	16 June 1819	Cutch	~8.0	~1,500	200
2	12 June 1897	Shillong	~8.7	~1,550	220
3	04 April 1905	Kangra	~8.0	~20,000	250
4	15 Jan 1934	Bihar-Nepal	~8.0	~15,000	360 (Nepal 5)
5	30 May 1935	Quetta	~8.0	~30,000	365
6	15 Aug 1950	Assam	~8.7	~4,800	400

Table 2. Destructive earthquakes of M ≥ 7.5 in India and in the vicinity in the 21st Century

S. No.	Date	Region	Magnitude (M)	Human lives lost	India's population in Earthquake Year
1	26 Jan 2001	Bhuj	~7.7	~20,000	1000
2	08 Oct 2005	Muzaffarabad	~7.6	~87,000	1150 (Pakistan 170)
3	15 April 2015	Gorkha(Nepal)	~7.9	~10,000	1320 (Nepal 27)

References:

Chandra, U., 1978. Seismicity, earthquake mechanisms and tectonics along the Himalayan Mountain range and vicinity. Physics of the Earth Planetary Interiors 16, 109-131

Gupta, H.K., Purnachandra, R., Yeats, R., 2009. Guest Editorial: The Devastating Muzaffarabad Earthquake of 8 October 2005. Journal of Seismology 13(3), 313-314.

Gupta, H.K., Kanchan A. Sabnis, Duarah, R., Saxena, R.S., Saurabh Baruah, 2020). Himalayan Earthquakes and Developing an Earthquake Resilient Society. Journal of the Geological Society of India 96, 433-446.

Gupta, H.K., 2023. If a Magnitude ~8 Earthquake Occurs in India Today….. . Journal of Geological Society of India 99, 299-302.

Kumar P., Kamal, Sharma, M.L., Pratibha, Jakka, R.S., Ashok Kumar, Joshi, G.C., Piyoosh Rautela 2023. Successful alert issuance with sufficient lead time by Uttarakhand state earthquake early warning system: Case study of Nepal earthquakes. Journal of Geological Society of India 99, 303-310.

Metych, Michele. "natural disaster". *Encyclopedia Britannica*, 7 Mar. 2024, https://www.britannica.com/science/natural-disaster. Accessed 16 April 2024

Oldham, R.D., 1928. The Cutch (Kachh) earthquake of 16th June 1819, with a revision of the great earthquake of 12th June 1897, ibid., 46, 71- 147.

Richter, C.F., 1958 Elementary Seismology, W. H. Freeman and Company, Inc., 768p.

Deep-Sea Mineral Deposits as a Source of Critical Metals

V. Balaram[1*]

[1]*CSIR-National Geophysical Research Institute (NGRI), Hyderabad -500 007, India*

*Corresponding Author:
E-mail address: balaram1951@yahoo.com (V. Balaram)

Marine sedimentary deposits such as ferromanganese nodules, ferromanganese crusts, massive sulphides, marine muds, and phosphorites on seamounts represent a major reservoir of various critical metal elements such as rare earth elements (REE), Co, Cu, Ni, and Li, and hold substantial economic value (**Fig.1**). Manganese nodules contain mainly manganese and iron, but also valuable metals like nickel, cobalt, and copper as well as REE and platinum. Total REE concentrations up to 2,511 µg/g were found in the ferromanganese crusts from the Indian Ocean, and deep-sea mud enriched in REE (> 2000 µg/g) was found in the western North Pacific Ocean. However, these deposits usually have lower REE grades than land-based REE deposits such as carbonatite-hosted deposits but form greater potential volumes. Though the mining companies and their sponsoring countries are in the process of developing the required technologies to mine the three deep-sea environments: abyssal plains, seamounts, and hydrothermal vents, due to severe concerns about the possible environmental damages, the International Seabed Authority (ISA) has not granted any mining permissions so far.

Introduction

For the whole world to deliver net zero by 2050 to limit global warming to 1.5ºC compared with pre-industrial times, large-scale mining is more critical for metals such as lithium, cobalt, platinum, palladium, REE, gallium, tungsten, tellurium, and indium as these metals are essential for green technology applications such as making wind turbines, solar panels, fuel-cells, electric vehicles, energy storage systems, and data storage systems required to transition to a low-carbon economy (Balaram, 2023a). Since land-based mineral deposits are depleting fast, sea-bed resources are seen as a new resource frontier for mineral exploration, mining, and extraction (Hein et al. 2023; Balaram, 2023).

Several studies worldwide indicated the potential of deep-sea for critical metals. For example, sediment cores collected near topographic highs in the Central Pacific Ocean showed a maximum REY content of 4,489 µg/g (Ohta et al., 2021). Widespread distributions of ferromanganese nodules, ferromanganese crusts, and REY-rich mud prompted many studies during the last several decades (Zhang et al., 2023). Among the variety of possible seabed resources, massive sulphide deposits in the midocean ridge areas indicated the potential for supply of Cu, Co, and Ni (Juliani and Ellefmo, 2018). The Figure indicates the occurrence of manganese nodules, ferromanganese crusts, massive sulphide deposits, REE-rich mud, and phosphorites at the ocean basins, mid-oceanic ridges, seamounts, and continental margins in the oceans.

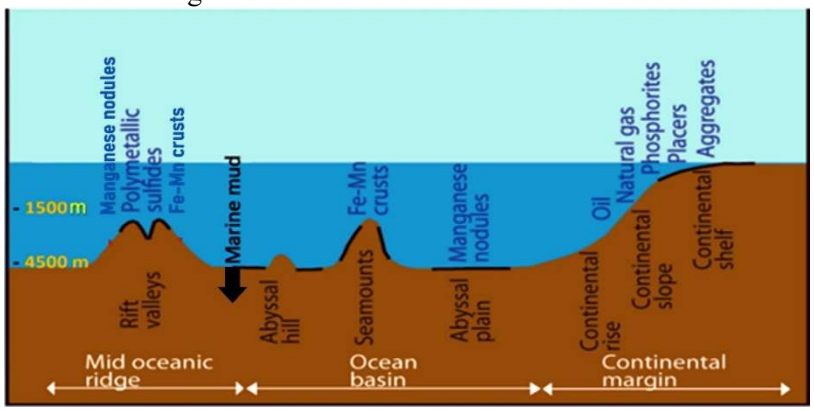

Figure 1: Occurrence of manganese nodules, ferromanganese crusts, massive sulphide deposits, REE-rich mud, and phosphorites at the ocean basins, mid-oceanic ridges, seamounts, and continental margins in the oceans (Modified after Balaram, 2023b).

Exploration of the seamount crust at the Afanasy Niktin Seamount (ANS) in the Indian Ocean

Recent studies on the exploration of the Afanasy Niktin Seamount (ANS) in the Eastern Equatorial Indian Ocean, have indicated that different types of seafloor sediments harbour high concentrations of REE and some other critical elements (**Table 1**). High concentrations of REE ranging from 1,727 to 2,511 µg/g and Co up to 6580 µg/g were found in crust samples collected from the Afanasy Nikitin Seamount (ANS) in the Indian Ocean.

Marine vs. Land-based resources

Though the marine deposits have lower REE contents than the well-known land deposits, their sizes are very extensive, much higher than the land-based deposits (Papavasileiou, 2021). Hein et al. (2013) took the critical metal content of the Clarion Clipperton Zone (CCZ) in the Pacific Ocean for comparison. A comparison between two of the largest on-land REE deposits, i.e., Bayan Obo in China and Mountain

Pass in the U.S. and the contents of REE in the Mn–Fe oxides nodules from the Clarion Clipperton Zone (CCZ) deposits and Co-rich ferromanganese crusts from the Pacific Ocean reveal that although the two land-based deposits are higher in grade, their tonnages are considerably lower than those of the CCZ (Papavasileiou, 2021).

Some countries have already started deep-sea mining in their respective EEZs

Some countries including China, India, Japan, and South Korea determined to start commercial exploitation of deep-sea minerals (Editorial, 2024). Norway and Japan are currently actively exploring pathways to mine the deep sea of its exclusive economic zone (EEZ) to lessen reliance on imported mineral resources needed for advanced and green technologies.

Table 1. Concentrations of ∑REE and some other trace elements (µg/g) in the ferromanganese crust samples collected from the ANS

Element	CC-1-DR-12	CC-2-ADR-20	ABP 37/10Q(D)	AA-8	ABP37/10D	CC2-ADR-24	CCE-ADR-25
∑REE	2462	2029	1737	2520	2244	2070	2110
V	1217	949	865	918	1706	739	600
Co	6420	4997	3363	6580	5942	4622	6460
Ni	3981	4502	3903	4384	4735	2977	3437
Cu	1260	1030	1248	624	1569	497	882
Zn	731	628	605	546	687	494	492
Sr	1870	1623	1333	1693	1728	1265	1352
Zr	669	568	401	345	475	457	514
Nb	213	36	88	28	33	28	92

Conclusions

As an alternative to traditional mining on land to meet the current demand for critical metals, seabed mineral resources deserve attention when we have technologies ready to conserve marine ecosystems. With the current technological developments in deep-sea mining, some of them can be scaled to create underwater robots that can mine the seafloor with minimum disturbance to the marine ecosystem. On the other hand, some are cautioning the world that deep-sea mining plans should not be rushed, and we should exercise care as deep seas are the least explored parts of our planet.

References

Balaram, V., 2023a. Combating Climate Change and Global Warming for a Sustainable Living in Harmony with Nature. Journal of Geographical Research 6(3): 1-17. https://doi.org/10.30564/jgr.v6i3.5706.

Balaram, V., 2023b. Deep-sea mineral deposits as a future source of critical metals, and environmental issues. Minerals and Mineral Materials, 2. 5. 1-17. https://doi.org/10.20517/mmm.2022.12.2023.100210

Balaram, V., Banakar, V.K., Subramanyam, K.S.V., Roy, P., Satyanarayanan, M., Mohan, M.R., and Sawant, S. S., 2012. Yttrium and rare earth element contents in seamount cobalt crusts in the Indian Ocean, Current Science 110 (11), 1334-1338.

Editorial. 2024. Deep-sea mining plans should not be rushed. Nature. 627, 8005, 704. https://doi.org/10.1038/d41586-024-00890-3.

Hein, J.R., Mizell, K., Koschinsky, A., Conrad, T.A., 2013. Deep-ocean mineral deposits as a source of critical metals for high- and green-technology applications: Comparison with land-based resources. Ore Geology Reviews 51, 1–14. https://doi.org/10.1016/j.oregeorev.2012.12.001

Juliani, C., Ellefmo, S.L., 2018. Resource assessment of undiscovered seafloor massive sulfide deposits on an Arctic mid-ocean ridge: Application of grade and tonnage models. Ore Geology Reviews 102, 818-828. https://doi.org/10.1016/j.oregeorev.2018.10.002.

Ohta, J., Yasukawa, K., Nakamura, K., Fujinaga, K., Iijima, K., Kato, Y., 2021. Geological features and resource potential of deep-sea mud highly enriched in rare-earth elements in the Central Pacific Basin and the Penrhyn Basin, Ore Geology Reviews 139, 104440, http://creativecommons.org/licenses/by/4.0/

Papavasileiou, K.A., 2021. Critical Review on Evaluation of the Marine Resources Mining versus the Land-Based Ones for REE. Materials Proceedings 5, 112. https://doi.org/10.3390/materproc2021005112

Zhang, W., Liu, Y., Zhao, W., 2023. Occurrence and enrichment of cobalt in ferromanganese nodules from the Western Pacific, Ore Geology Reviews 163, 105758. https://doi.org/10.1016/j.oregeorev.2023.105758.

Conference Theme 1: Geodynamics and Tectonics

GDT 01: Geodynamic setting, petrological and geochemical criteria for the formation of the foidolite-foidosyenite Darya complex in Ket-Kap–Yuna igneous province of the Aldan shield, Russia

Polin Vladimir Fyodorovich[1*]

[1]*Far East Geological Institute of Far East Branch of Russian Academy of Sciences, Russian Federation Vladivostok, 690022, 100 letia Vladivostoku.*

*Corresponding Author:
E-mail address: vfpolin@mail.ru (V.F. Polin)

The interest in alkali rocks associated with granitoids, widely distributed within the zones of the late Mesozoic tectono-magmatic activation of the Aldan shield, is caused by the coexistence of contrasting Na-K and K-Na subalkaline and potassic alkaline rocks, scarce occurrence of potassic alkaline rocks and their insufficient study. In addition, the problem of geodynamic settings of occurrence of polyformational late Mesozoic magmatism in the zones of tectono-magmatic activation has long attracted the attention of researchers and remains relevant. In connection therewith, the formation of the early Aptian (Polin et al., 2014) foidolite-foidosyenite hypabissal Darya complex in the Ket-Kap–Yuna igneous province, located in the east of the Aldan shield, is of great interest. In light of the above-mentioned facts, this paper aimed to determine the geodynamic setting of the formation of the Darya complex based on the new petrological and geochemical data on the composition of rocks that build up the complex.

Mineralogical and petrographic typification of the Darya complex: The Darya complex is composed of foidolites of ultrabasic (melteigite, ijolite) and basic (malignite and melanocratic malignite), alkaline foid-bearing gabbroids (theralite, shonkinite, essexite and ferruginous essexite), feldspathoids and alkaline foid-bearing syenites (foyaite, lujavrite, ledmorite, miaskite, pulaskite, foid-laurvikite, pseudoleucitolite, and vary rarely laurvikite and corundum pulaskite). Dykes and veins are represented by essexite, shonkinite, vishnevite-bearing syenite-porphyry, tinguaite, sölvsbergite and aponepheline alkaline pegmatite. The occurrences of fenite and autometasomatite are related to certain intrusive bodies of the complex.

Petrochemical systematics: The results of the petrological and geochemical studies show that the complex is composed of rocks of two series with many ***contrasting*** parameters: *kamafugite* and *tephrite-leucitite* series. The latter itself is divided into two groups: low-Ca group, which is dominant in terms of volume, and high-Ca group, which is scarcely represented. Compared to the early Cretaceous Bokur and late Cretaceous Kurung complexes of the foid and alkaline rocks in the Ket-Kap–Yuna igneous province (KKYIP) (Polin and Sakhno, 2004; Polin and Ostapenko, 2024), the Darya complex is characterized by a wider range of concentrations of silica (36-63 % SiO_2), alumina (5-24 %), calcium oxides (1-22 %) and alkali metals (1-12 % Na_2O and 1-9 % K_2O). The vast majority of rocks of both series correspond to high-alkali rocks rich in either Na, K, K-Na or Na-K, the last two variants being dominant.

Geodynamic setting of formation of the Darya complex: Initially, the late Mesozoic alkaline igneous rocks of the Aldan shield (AS) were considered to be connected with the rifting caused by the Mesozoic tectono-magmatic activation (TMA) of this global structure. The later models of the Mesozoic magmatism of the AS suggested that its manifestation was related either to the collision of the East-

Siberian and Chinese plates or to the setting of a Californian-type transform continental margin. There are also reasons to believe that it has a supra-plume or supra-subduction origin.

Results of discriminant geodynamic analysis: Taking into account that existing views on the geodynamic setting of formation of early Cretaceous igneous rocks of the AS are controversial, and aiming at identifying additional criteria of the geodynamic setting, in which the Darya complex formed, the author analyzed several discriminant diagrams, which allow discerning igneous rocks formed in different geodynamic settings. For this purpose, the diagrams of Fershtater (1981; in Russian), Simonov (1998; in Russian) and Grebennikov and Khanchuk (2021) were used.

The analysis of positions of the Darya plutonic rocks in the "Rb-Sr" diagram of Fershtater (1981) (**Figure 1A**) led to a conclusion that the distribution of figurative points of most rocks in the composition field of compositions (above the FL line) typical for "igneous rocks in stable zones, subplatform stages of mobile zones developed on the continental crust" is rather consistent with the geological position of the complex. In the diagrams of Simonov (1988) (**Figure 1 B**) enabling discrimination of volcanic and plutonic rocks from the areas of intercontinental collision, seafloor spreading, subduction and continental rifting, the figurative points of igneous rocks of the Darya complex fall in the fields of continental-rifting igneous rocks similar to the rocks found in African rifts. The discriminant diagrams of Grebennikov and Khanchuk (2021) provide similar results and allow distinguishing supra-subduction igneous rocks from igneous rocks formed at divergent plate boundaries, especially at those where plates slide horizontally past each other. One of the diagrams of this author is given in this paper (**Figure 1C**), and it shows that igneous rocks of the Darya complex definitely fall into the field of rocks from the areas of lithospheric plate sliding, which *in general* is consistent with the results yielded from the discriminant diagrams of Simonov (1988).

Conclusions: Summarizing the results of geodynamic discrimination of igneous rocks from the Darya complex, it should be noted that the distribution of their compositions in all used diagrams indicates the continental rifting-related origin of the studied rocks. These findings are consistent with the earlier interpretation of the geodynamic position of zones of the late Mesozoic TMA of the AS. Considering the geophysical and petrogenetic data and results of the geodynamic typification of rocks, the most *plausible* hypothesis is the one inferring that the complex formed during continental rifting related to the sliding of lithospheric plates: Siberian continent and Amur superterrane, in the Late Jurassic–Early Cretaceous (Khanchuk, 2006). The research was conducted as part of the state assignment for the Far East Geological Institute FEB RAS.

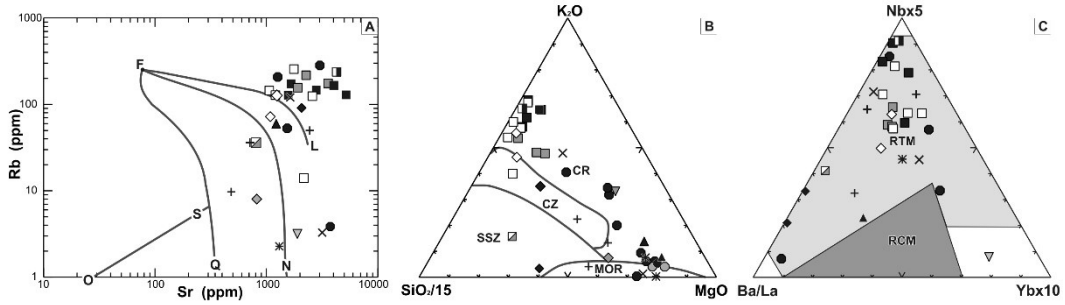

Fig. 1, A-C. Geodynamic discriminant diagrams of the Darya complex rocks. A. – after (Fershtater, 1981). Fields of rock compositions inherent in different geodynamic settings: OSQ – derivatives of oceanic tholeiites; QFN – derivatives of continental tholeiites; NFL – derivatives of continental andesites. Above the FL line is the area of alkaline–magma derivatives: igneous rocks in stable zones, subplatform stages of mobile zones developed on the continental crust; B. - after (Simonov, 1998). Composition fields of igneous rocks in type geodynamic settings: MOR – mid-ocean ridges; SSZ – suprasubduction zone setting; CZ – continental collision zones; CR – continental rifts; **C.** − after (Grebennikov and Khanchuk, 2021); discriminant diagram used to interpret the geodynamic settings associated with magmatism at convergent plate boundaries and transform margins. Fields of igneous rocks in different settings: RTM – transform margins; RCM – convergent plate margins; triangles with light gray filling indicate overlapping areas of fields of different settings.

References:

Fershtater, G.B., 1981. Rb–Sr diagrams for analysis of the geodynamic regime of formation of igneous rock series, in: Yearbook-1980: Information materials [in Russian]. Sverdlovsk, pp. 86–88.
Grebennikov, A.V., Khanchuk, A.I., 2021. Geodynamics and magmatism of the Pacific-type transform margins: aspects and discriminant diagrams. Russian Journal of Pacific Geology 40 (1), 3–24.
Khanchuk, A.I. (Ed.), 2006. Geodynamics, Magmatism and Metallogeny of the Russian East. In 2 books [in Russian]. Dal'nauka, Vladivostok, Book 2.
Polin, V.F., Sakhno, V.G., 2004. Petrogenesis of alkaline volcanic rocks of the Ketkap-Yuna magmatic province of Aldan. Doklady Earth Sciences 394 (1), 28–31.
Polin, V.F., Glebovitskii, V.A., Mitsuk, V.V., Kiselev, V.I., Budnitskiy, S.Yu., Travin A.V., Rizvanova, N.G., Barinov, N.N., Ekimova, N.I., Ponomarchuk, A.V., 2014. Two stage formation of the alcaline volcano-plutonic complexes in the Ketkap–Yuna igneous province of the Aldan Shield: New isotopic data. Doklady Earth Sciences 459, 1322–1327.
Polin, V.F. Ostapenko D.S. 2024. Alkaline–Salicic Kurung Complex of the Ket-Kap–Yuna Igneous Province (Aldan Shield, Russia): Petrogenesis and Geodynamic Conditions of Formation. Russian Geology and Geophysics 65:1–24.
Simonov, D.A., 1998. Late Cenozoic Geodynamics and Volcanism of Alpine folded belt in Aegean-Caucasian Segment. PhD Thesis [in Russian]. MGU, Moscow

GDT 02: The petrogenesis of the syn-collisional and post-collisional granitoid rocks in the eastern Gangdese belt: Evidence from whole-rock geochemistry and Sr-Nd-Hf-O isotopes

Haoqi Yuan[1*], Yuanku Meng[1]

[1]*Shandong University of Science and Technology, P. R. China.*

*Corresponding Author:
E-mail address: yyyuanhaoqi@163.com (H.Yuan)

The formation of granites is associated with large-scale partial melting and growth/transformation of the crustal materials, but the balancing act and detailed petrogenetic processes of granite forming mechanism are unclear on the Earth. A comprehensive study of whole-rock and mineral geochemical, Sr-Nd-Hf-O isotopic, and geochronological analyses were carried out on a granodiorite pluton (dated at 53 Ma) and two granitic plutons (dated at 28 Ma) from the eastern Gangdese belt, Southern Tibet, to constrain evolutionary processes and tectonic implications of the magma sources. The Eocene granodiorite pluton displays positive whole-rock $\varepsilon_{Nd}(t)$ (+1.34 to +2.08) and zircon $\varepsilon_{Hf}(t)$ (+0.69 to +7.43) values, indicating juvenile recycling of the mafic lower crustal compositions in the eastern Gangdese belt. The Sr-Nd-Hf-O isotopic compositions of the Eocene granodiorite pluton are slightly enriched and higher than those of the juvenile lower crust, suggesting the addition of the Nyingchi ancient basement. The middle rare earth elements deficit and thermodynamic modeling of the Eocene granodiorite pluton indicate the unbalanced partial melting of the basic rocks with the residual pyroxene. The Eocene granodiorite pluton shows arc-type geochemical features, corresponding to a low-pressure environment (2.27 to 2.86 kbar). The formation mechanism of the Eocene granodiorite pluton is the partial melting of the juvenile lower crust related to the asthenosphere upwelling caused by subducted Neo-Tethys slab rollback or break-off. The two Oligocene granitic plutons have slightly enriched whole-rock Sr compositions ($^{87}Sr/^{86}Sr)_i$ (0.706063 to 0.706095 and 0.705948 to 0.705898), and negative $\varepsilon_{Nd}(t)$ values (−0.58 to −2.96 and +0.80 to −2.22), but show positive zircon $\varepsilon_{Hf}(t)$ values (+1.24 to +6.77 and +0.12 to +8.04) and wide ranges of oxygen compositions ($\delta^{18}O$ = 5.64‰ to 8.33‰ and 4.46‰ to 8.23‰), respectively. The magma of two Oligocene granitic plutons consists of juvenile lower crust with minor Indian continent materials, precluding the magma mixing/crust contamination. The trace and major elemental thermodynamic modeling further provides a new perspective on the petrogenesis of the Oligocene granitic plutons that the magma underwent insignificant differentiation with the removal of hornblende, rutile, and garnet during the magmatic evolution, reflecting a medium pressure setting (6.46 to 7.39 kbar). The geodynamic mechanism of two Oligocene granitic plutons is depicted as follows: the tearing of the low-angle subducted Indian slab released slab melt

metasomatized the overlying mantle wedge and continental lithospheric mantle and formed ultrapotassic magma. The ultrapotassic magma provided massive heat and water for the fluid-fluxed melting of the crustal rocks, to generate the Oligocene adakitic magma.

Keywords: Granitoid rocks; Petrogenesis; Rhyolite-MELTS simulation; Sr-Nd-Hf-O isotopes; Gangdese belt

GDT 03: Provenance characteristics of Late Mesozoic sedimentary rocks of the back-arc basin, southern Tibet and their response to tectonic evolution

Qingling Wang[1*], Yuanku Meng[1], Youqing Wei[1]

[1]*College of Earth Science and Engineering, Shandong University of Science and Technology, Qingdao, China*

*Corresponding Author:
E-mail address: 2511527240@qq.com (Q.Wang)

The Gangdese magmatic belt (southern Lhasa terrane) is located in the southernmost margin of the Eurasian continent. The Gangdese belt records a great deal of key information, including the Neo-Tethyan subduction, the uplift of the Tibetan Plateau and the India-Asia collision, thus it is an ideal site for unraveling the aforementioned dynamic processes. In the Gangdese belt, most of the previous studies have focused on igneous petrogenesis and tectonic implications by geochronology and geochemical methods, but little attention has been paid to the Late Mesozoic volcanic-sedimentary sequences in the back-arc basin of the southern Lhasa terrane. Here we undertook petrography, systematic detrital zircon U-Pb geochronology, zircon Lu-Hf isotopic and Carbon and Oxygen (C-O) isotopic studies on the sedimentary rocks in the back-arc basin of the Gangdese belt, southern Tibet. On this basis, the sedimentary strata of the back-arc basin, including depositional timing, formational environment, tectonic evolution and provenance, are discussed in detail. Our study plays a key role in the provenance-drainage system of the back-arc basin and highlights evolution of the southern Tibet during the Late Mesozoic.

By integrating detrital zircon U-Pb age populations and Hf isotopic characteristics with previous studies, we concluded that the dominant detrital provenance of the Shexing Formation was from the Gangdese magmatic arc. The Shexing Formation is well-constrained at ~83.1 Ma evidenced by the youngest detrital zircon age cluster. The Chumulong and the Takena Formation samples yielded a depositional timing of 109 Ma and 105 Ma, with primary sedimentary provenances being sourced from the central Lhasa terrane, whereas the Gangdese magmatic arc played an insignificant role in the detrital provenance. Furthermore, the youngest detrital zircon age clusters indicate that the stratigraphic depositional timing of the Bima, Linbuzong, Duodigou and Quesangwenquan Formations are well-defined at circa 123 Ma, 137 Ma, 149 Ma, and 156 Ma respectively. The results demonstrate that these sedimentary strata are sourced from the central Lhasa terrane, and the northern and southern Lhasa terranes also provide detrital materials to some extent. The main source area of the sedimentary strata in the back-arc basin of the Gangdese belt experienced significant changes during the Late Jurassic to the Late Cretaceous. In addition, C-O isotope results of carbonate rocks indicate that the Duodigou Formation was deposited in a marine environment, but the Shexing Formation was in a terrestrial environment. During the interval between the Duodigou and the Shexing Formations, the sedimentary environment of the southern Lhasa terrane changed from marine to terrestrial facies. We interpret these changes to be resulted from a complicated tectonic mechanism, concerning the northward subduction of Neo-Tethys oceanic lithosphere beneath the Lhasa terrane, the southward subduction of the Bangong Co-Nujiang Ocean and the Lhasa-Qiangtang collision. The complicated dynamic mechanism is described below.

With the northward subduction of Neo-Tethys oceanic lithosphere beneath the Lhasa terrane and the subduction of the Bangong Co-Nujiang Ocean, the Lhasa terrane has experienced multiple periods of tectonic evolutions. Accompanied by the subduction of the Neo-Tethyan oceanic slab, the Lhasa terrane has undergone crustal compression and thickening, and there was continuous magmatism during the Middle Jurassic. During the Late Jurassic-Early Cretaceous, the Lhasa terrane experienced a back-arc extension due to the roll-back of the Neo-Tethyan subduction slab, resulting in crustal thinning in southern Tibet. During the Early Cretaceous, the continuous northward subduction of the Neo-Tethys oceanic lithosphere and Lhasa-Qiangtang collision led to the thickening and uplift of the central and northern Lhasa terranes, in which the central Lhasa terrane served as the primary source area for the back-arc basin. The central Lhasa terrane suffered from rapid uplift and denudation, then the exhumated and eroded materials were transported into the back-arc basin. Subsequently, during the Early-Late Cretaceous, the Gangdese magmatic arc was formed and began to carry materials into the back-arc basin as the secondary source area. During the Late Cretaceous, the Neo-Tethyan oceanic slab subducted at a low angle, resulting in the crustal thickening in the southern Lhasa terrane. The Gangdese magmatic arc had a relatively high relief and became the main depositional source for the back-arc basin. During the lately Late-Cretaceous, the Gangdese magmatic arc was eroded significantly with a low relief, the drainage systems were well-developed leading to massive detrital materials being transported into the Neo-Tethys Ocean forearc basin from the central Lhasa terrane.

Keywords: Back-arc basin; Detrital zircon U-Pb age; Zircon Lu-Hf isotope; Provenance analysis; Tectonic evolution

---

GDT 04: Unveiling the Hidden Back-Arc Suture Zone in Penyu Basin Using High-Resolution FTG, Aeromagnetic and 3D Seismic Data

Nor Syazwani Zainal Abidin[a,b*], Muhammad Firdaus Abd Halim[a], Muhammad Noor Amin Zakariah[a], Nur Huda Mohd Jamin[a], Zuraida Mat Isa[a], Sulaiman Chee At-Saat[c], Mohd Firdaus Ali[c], Azirul Liana Abdullah[c], Wei Boon Hock[c], Herry Maulana[c], Azwa Jannah Abu Bakar[c], Ong Swee Keong[c], Zulhaimi A Rahman[c]

[a]*Geoscience Department, Faculty of Science and Information Technology (FSIT), Universiti Teknologi PETRONAS, 32610, Seri Iskandar, Perak, Malaysia.*
[b]*Southeast Asia Clastic & Carbonate Research Laboratory (SEACARL), Institute of Hydrocarbon Recovery for Enhanced Oil Recovery, Universiti Teknologi PETRONAS, 32610 Bandar Seri Iskandar, Perak, Malaysia.*
[c]*Basin Strategy and Management (BSM), Resource Exploration (REX), Malaysian Petroleum Management, Level 20, Tower 1, PETRONAS Twin Towers, Kuala Lumpur City Centre, 50088 Kuala Lumpur, Malaysia.*

*Corresponding Author:
E-mail address: norsyazwani.z@utp.edu.my (N.S.Zainal Abidin)

The recent paradigm shift of a 40-year dispute in regional Thai geology identifies the Nan-Uttaradit-Sra Kaeo Suture Zones as an onshore back-arc suture zone, distinct from the Palaeo-Tethys Suture Zone, yet its offshore continuation is obscured by thick younger sequences in the Tertiary Basins of Pattani, Malay, and Penyu Basins. In this study, the optimisation of newly acquired aeromagnetic and Full-Tensor Gradiometry (FTG) data supported by 3-Dimensional seismic data has unveiled this hidden back-arc suture zone in the Penyu Basin areas. Regional aeromagnetic anomalies primarily reflect deep crustal features, while airborne gravity anomalies' depth (Z) tensors indicate shallow subsurface structures, with dominant NW-SE orientations suggestive of complex tectonic processes and minor E-

W trends indicating half-graben extensional features. These E-W structural trends align with observed 3D seismic reflection data, particularly in the eastern region (**Table 1**). Analysis of satellite-derived gravity and magnetic data highlights a significant relationship between the Indochina block and the Sukhothai Terrain, extending seamlessly offshore and characterizing the back-arc suture zone, now termed the "Penyu Suture Zone," which delineates the boundary between the Permian Sukhothai island-arc system and the Indochina Block (**Fig. 1**). This discovery consequently extends the hydrocarbon exploration within the so-called "basement" interval following the proven play pursued in the existing Malay Basin. The delineation of the southern back-arc suture zone extension holds significant promise for future predictions of potential leads, enhancing the overall understanding of the geological landscape and its implications for hydrocarbon exploration.

Table 1. Summary of structural analyses of FTG Contact Lineament Processed (CLP) and magnetic maps.

Data Type	**Major Trend**	**Minor trend**	**Depth Range**
3D Seismic	E-W		Shallow - Deep
CLP for Txx	NNW-SSE, NNE-SSW	NW-SE	Shallow - Intermediate
CLP for Txy	NW-SE, NE-SW		Shallow - Intermediate
CLP for Txz	NNW-SSE, NNE-SSW		Shallow - Intermediate
CLP for Tyy	E-W, NW-SE		Shallow - Intermediate
CLP for Tyz	NW-SE, E-W	NE-SW	Shallow - Intermediate
CLP for Tzz	NW-SE	NE-SW	Shallow (High frequency)
Total Magnetic Intensity (TMI)	NW-SE	NE-SW	Magnetic Basement
Total Magnetic Intensity Reduced to the Equator (TMI_RTE)	NW-SE, E-W	NE-SW	Magnetic Basement (corrected)
Analytical Signal of the First Derivatives for 20 Residual (RTE_AS_20res)	NW-SE	NE-SW	Shallow Magnetic Basement
Analytical Signal of the First Derivatives for 50 Residual (RTE_AS_50res)	NW-SE, NE-SW		Shallower Magnetic Basement
Analytical Signal of the First Derivatives for 20 Regional (RTE_AS_50reg)	NW-SE	NE-SW	Deep Magnetic Basement
Analytical Signal of the First Derivatives for 50 Regional (RTE_AS_50reg)	NW-SE	NE-SW	Deeper Magnetic Basements

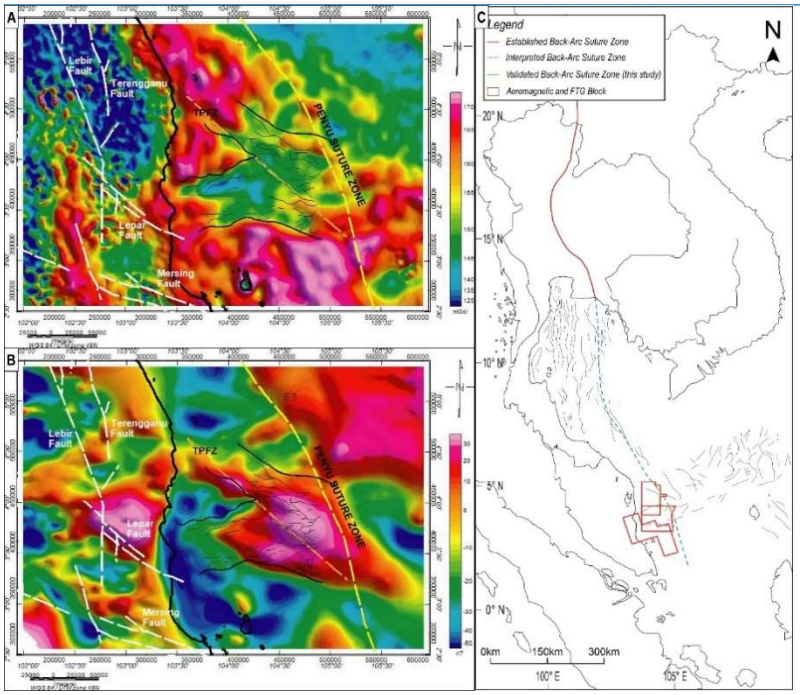

Figure 1. A) Bouguer gravity anomaly in the onshore to offshore Peninsular Malaysia, specifically at Pahang and Penyu Basin regions. Interpreted Penyu Suture Zone is shown in the offshore Penyu Basin. B) Magnetic gravity anomaly in the onshore to offshore Peninsular Malaysia, specifically at Pahang and Penyu Basin regions. Interpreted Penyu Suture Zone is shown in the offshore Penyu Basin. C) Proposed "Penyu Suture Zone" for the identified back-arc suture zone in the Penyu Basin region.

GDT 05: Tectonothermal evolution of the NE Tibetan Plateau since the Paleo-Tethys subduction: Insights from thermochronological records in the Longshou Shan

Ni Tao[1,2*], Ruohong Jiao[3], Martin Danišík[4], Yiduo Liu[5], Meinert Rahn[6], Yunpeng Dong[2], Jun Duan[1], Jiangang Jiao[1], Noreen J. Evans[4], Hanjie Wen[1]

[1]*School of Earth Science and Resources, Chang'an University, Xi'an, China*
[2]*State Key Laboratory of Continental Dynamics, Department of Geology, Northwest University, Xi'an, China*
[3]*School of Earth and Ocean Sciences, University of Victoria, Victoria, Canada*
[4]*John de Laeter Centre, Curtin University, Perth, Australia*
[5]*Institute of Mountain Hazards and Environment, Chinese Academy of Sciences, Chengdu, China*
[6]*Institute of Geo- and Environmental Sciences, University of Freiburg, Freiburg, Germany*

*Corresponding Author:
E-mail address: ni.tao@chd.edu.cn (Ni Tao)

Constraining exhumation and tectonic processes along the boundary of a plateau provide important insights for understanding the mechanism leading to the plateau expansion and crustal evolution. The Longshou Shan Thrust Belt (LSSTB) bounds the Tibetan Plateau along its northeast margin from the North China Craton. In this study, the spatiotemporal characteristics of the exhumation and fault deformation along the LSSTB are investigated by detailed analysis and numerical modeling of published and new thermochronological data. We dated five Proterozoic basement and intrusion samples which yielded the Cretaceous apatite fission-track central ages (126 ± 7–74 ± 5 Ma with mean track lengths of 12.6 ± 1.7–13.3 ± 1.9) and Late Cretaceous to Eocene apatite (U-Th)/He mean ages (84 ± 3–51 ± 5 Ma). Inverse modelling of thermal history reveals multi-stage exhumation of LSSTB in the Permian-Triassic, Late Mesozoic, Eocene, and post-middle Miocene. Permotriassic exhumation hints for a >250 Ma-old peneplain surface related to the closure of the Paleo-Tethys and Paleo-Asian Oceans.

Late Mesozoic episodic exhumations are the result of intracontinental deformations responding to tectonic processes at the Eurasian continental margins. Eocene exhumation is simultaneous with and best interpreted by the initial India-Asia collision. Post-middle Miocene uplift along the reactivated Longshou Shan thrusts is driven by the northeastward expansion of the Tibetan Plateau. Our results support the LSSTB as a long-lived block boundary since the Permotriassic, which now represents the active boundary of the northeastern Tibetan Plateau.

Key words: NE Tibetan Plateau; Longshou Shan; tectonics; thermochronology; thermo-kinematic modelling

GDT 06: Detection of knickpoints using LSDTopoTools and evaluation of their causative factors in the Cauvery Basin, South India

T. Abhijith[a], K.Balasubramani[b*], AL Fathima[c], Mu. Ramkumar[c], M.J. Mathew[d]

[a]*Department of Earth and Space Sciences, Indian Institute of Space Science and Technology, Thiruvananthapuram, India*

[b]*Department of Geography, Central University of Tamil Nadu, Thiruvarur, India*

[c]*Department of Geology, Periyar University, Salem, India*

[a]*Department of Geography, Geology and the Environment, Kingston University, Kingston Upon Thames KT1 2EE, United Kingdom.*

*Corresponding Author:
E-mail address: geobalas@cutn.ac.in (K.Balasubramani)

Analysis and interpretation of the relationships between the earth's surface processes and their influence on the landscape are attempted through various tools and techniques, including remote sensing and Geographic Information Systems (GIS). Recent developments in greater access and spatial coverage of satellite-based digital elevation models (DEM) have invigorated the application and testing of topography-based algorithms to understand and model landscape dynamics. In this study, we bring a semi-automated approach by implementing LSDTopoTools (Gailleton et al., 2019; Mudd et al., 2014, 2021), a Linux-based open-source software that offers a suite of algorithms, for extracting knickpoints to analyze the geodynamics in the Cauvery River Basin, Southern India. This basin is chosen for this study as it encompasses diverse landscapes developed under the influences of interplay between tectonic, climatic, and other processes and factors. The river's long low-gradient profile sections are generally separated by short reaches of steep gradient, i.e. knickpoints. The recognition of knickpoints or knickzones along the river profile helps interpret the dynamic topographic processes in the basin.

This study attempted a comprehensive and rigorous process of knickpoint identification. Initially, we derived the Shuttle Radar Topography Mission's Digital Elevation Model (SRTM DEM) with a 30m resolution to delineate the basin and sub-basins. From this, channel networks for chi-mapping analysis and knickpoints identification were extracted. The concavity index was then calculated for 14 sub-basins using the slope-area and chi disorder methods. By integrating the drainage area, we transformed the longitudinal river profiles into a chi-elevation profile using the integral method. The transformed profiles were statistically segmented, each with a gradient and intercept (Perron and Royden, 2013; Royden and Taylor Perron, 2013). Finally, we used the knickpoint detection algorithm to identify the locations of abrupt changes in the channel profiles. The obtained knickpoint locations were plotted using Python-based plots and mapped using ArcGIS software. Ground truth validation of extracted knickpoints was conducted in all major catchment sub-basins wherever the accessibility permits us to perform the field study. As we found the best fit for knickpoints with the field

observations, locating knickpoints through this automated method is the best alternative for large basins like Cauvery.

This study has identified 1,446 knickpoints, a significant number of which (807) have a magnitude greater than or equal to 1. These knickpoints, determined using the extensive topographic data from 617,474 locations in 14 subbasins of the Cauvery River Basin, provide crucial insights into the landscape dynamics of the basin. The knickzones generated by the algorithm were plotted over the spatial extent of geological supergroups, and it was found that a large number of knickpoints were identified in the Southern Granulite Complex supergroup (**Fig. 1**). High drainage density and a concentration of knickpoints and knickzones in the middle reaches of the Cauvery River suggest upliftment due to regional neotectonics. The most knickpoints (334) are identified in the Bhavani sub-basin, which drains through this supergroup. The sub-basin is also observed to have the highest magnitude of change in segment elevation (192.2 m) among all the basins. The Shimsha sub-basin is characterized by a low concavity index. However, there is a sudden change in elevation near the trunk stream, marked by a series of negative changes in channel steepness value. The Shimsha Fall, a major knickpoint located near the basin's outlet, and an abrupt fall in channel elevation at Chunchi waterfall (Arkavathi) near the trunk stream suggest the presence of a fluvial hanging valley.

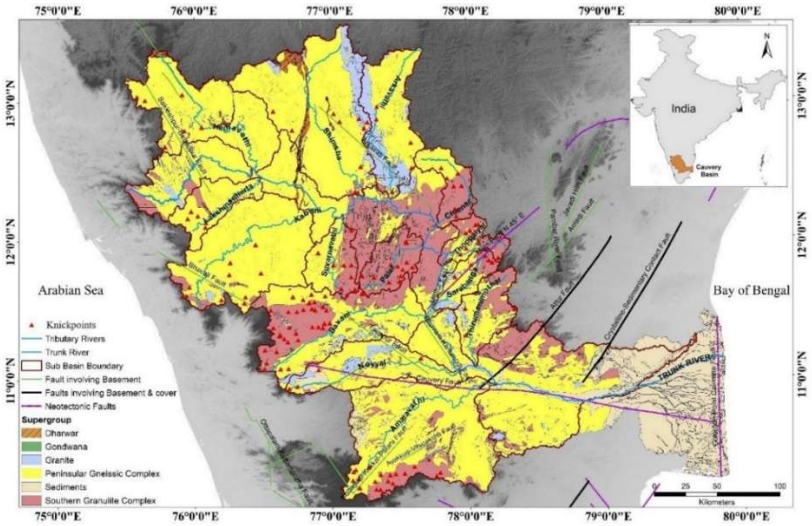

Figure 1: Major knick points on Supergroups in the Cauvery Basin, South India

One of the limitations of our approach is relying on the integral method of profile transformation, in which the value of the concavity index should be known as a *priori*. Kale et al. (2014) employed a 90-meter SRTM DEM to extract longitudinal river profiles of the Cauvery River Basin, identified evidence of fluvial hanging valleys in the Shimsha, Arkavathi, and Chinnar tributaries of the Cauvery and interpreted tectonic control over their formation. These authors applied a reference concavity index of 0.45 to sub-basin analysis, revealing a statistically significant increase in channel steepness within the middle reach of the Cauvery River compared to the upper and lower reaches. As sub-basins of large rivers like Cauvery may have different concavity indices, it is inappropriate to utilise a single concavity index value for all sub-basins, as it may result in erratic channel steepness (K_{sn}) and Chi. Therefore, it is recommended that sub-basins with varying concavity index should be examined individually (Gailleton et al., 2019). Accordingly, our method used the concavity index calculated for respective sub-basins to generate a chi-elevation profile and to derive K_{sn}.

The transformed chi-elevation profile helps observe the response of different channels to a common driving force, such as a regional uplift or a change in base level. Knickpoints are the surface realisations of river adjustments to such transient perturbations. Understanding the celerity of such perturbations is vital to understanding the landscape dynamics. Thus, our extraction of the knickpoints and knickzones holds significant implications for understanding the transient signals of the Cauvery River Basin. The identified knickpoints and knickzones can also be used to correlate sediment yield, erosion rate, bedrock incision rate, hill slope dynamics, and other numerical datasets for comprehending the basin's landscape

dynamics. Furthermore, the study presents a scalable and reproducible methodology for identifying and quantifying knickpoints, which can be applied elsewhere for modelling and monitoring the geodynamics of large river basins.

References

Gailleton, B., Mudd, S.M., Clubb, F.J., Peifer, D., Hurst, M.D., 2019. A segmentation approach for the reproducible extraction and quantification of knickpoints from river long profiles. Earth Surface Dynamics 7(1), 211–230. https://doi.org/10.5194/ESURF-7-211-2019.

Kale, V. S., Sengupta, S., Achyuthan, H., Jaiswal, M. K., 2014. Tectonic controls upon Kaveri River drainage, cratonic Peninsular India: Inferences from longitudinal profiles, morphotectonic indices, hanging valleys and fluvial records. Geomorphology 227, 153–165. https://doi.org/10.1016/J.GEOMORPH.2013.07.027

Mudd, S.M., Attal, M., Milodowski, D.T., Grieve, S.W.D., Valters, D.A. 2014. A statistical framework to quantify spatial variation in channel gradients using the integral method of channel profile analysis. Journal of Geophysical Research: Earth Surface, 119(2), 138–152. https://doi.org/10.1002/2013JF002981

Mudd, S.M., Clubb, F.J., Grieve, S.W.D., Milodowski, D.T., Gailleton, B., Hurst, M.D., Valters, D.V., Wickert, A.D., Hutton, E.W., 2021. LSDTopoTools2 v0.5. https://doi.org/10.5281/ZENODO.5788576

Perron, J. T., Royden, L., 2013. An integral approach to bedrock river profile analysis. Earth Surface Processes and Landforms 38(6), 570–576. https://doi.org/https://doi.org/10.1002/esp.3302

Royden, L., Taylor Perron, J., 2013. Solutions of the stream power equation and application to the evolution of river longitudinal profiles. Journal of Geophysical Research: Earth Surface 118(2), 497–518. https://doi.org/10.1002/JGRF.20031

GDT 07: Timing and Style of Final Closure of the Paleo-Asian Ocean: Perspectives from the Big Geodata Analysis and Machine Learning Model

Jixiang Xue[1], Keda Cai[1*], Zhenjie Zhang[1], Kai Wang[1]

[1]*School of Earth Science and Resources, and Frontiers Science Center for Deep-time Digital Earth, China University of Geosciences, Beijing 100083, China.*

*Corresponding Author:
E-mail address: caikd@cugb.edu.cn (K.Cai)

The Paleo-Asian Ocean (PAO) once existed between the Siberian Craton and Tarim-North China Craton, and its subduction-closure history has been important for studying the evolution of the Central Asian Orogenic Belt that may have unidentified impact on paleoclimate. However, when and how the PAO closed remains controversial. In addition, the potential link between the Permian aridification in the North China Craton and the subduction-closure processes of the PAO remains uncertain. The closure locations of the western, middle, eastern, and easternmost segments of the PAO are located at the South Tianshan Belt, Beishan Belt, Solonker Belt, and Changchun-Yanji Belt, respectively. Here, we propose a LightGBM algorithm-based machine learning model to reveal the evolution of the crustal thickness of the four segments, which is integrated with big geodata analysis methods (Zircon Hf time series and Zircon age Spatial analysis) and available geological evidence to address these scientific issues. The ~300Ma, ~280M, ~260Ma, and ~240Ma crustal thickening and corresponding zircon $\varepsilon_{Hf}(t)$ isotopic pull-downs of the four belts, coupled with flora distribution, sedimentary records and paleomagnetic data, suggest that the PAO closed diachronously in a scissor style from west to east during the Late Carboniferous to the Middle Triassic. The new crustal thickness of northern North China estimated by the LightGBM algorithm is 47 km during the Early Triassic, which is less than the average crustal thickness (~58 km) predicted by whole-rock La/Yb ratios, indicating that there is no Andean-type orogenic plateau that led to the Permian aridification in the northern North China.

Keywords: Paleo-Asian Ocean; TNCC; Machine Learning Model

GDT 09: Kinematics of Different Types of Shear Zones around Salem Region, Tamil Nadu, India: Its Implications Over Geodynamics and Tectonics of The SGT

Thirukumaran Venugopal[1*]

[1]*Department of Geology, Government Arts College (Autonomous), Salem-636007, Tamil Nadu, India*

*Corresponding Author:
E-mail address: mailkumaran75@gmail.com (**V. Thirukumaran**)

The geodynamic processes and tectonic events s are recorded in shear zones. Shear zones are often localized in narrow, sub-parallel-sided zones reflecting the natural deformations of the earth's crust. Consequent upon the type, nature and intensities of these geodynamic processes and tectonic events, the resultant shear zones respond in terms of Brittle-, Brittle-ductile, and Ductile in character. Accordingly, each character indicates a prevalent unique kinematic and geodynamic process. Occurrences of individual, multiple and or all the types of shear zones in a region may indicate a prolonged and varied geodynamic history.

The Salem region (**Fig. 1**) is occupying the central part of the Southern Granulite Terrain (SGT). It is one such place where a host of minerals formed in a long-drawn tectono-magmatic-deformation-mineralization history. It is one of the best geo-ecosystems around the world bridging the low-grade greenstone–granite domain and high-grade granulite facies rocks.

A wide variety of lithologies including charnockite, pyroxenite, amphibolites, banded magnetite-quartzite, garnetiferous metagabbro, anorthosite, ultramafite, and vast areas of, hornblende-biotite gneiss, granite gneiss, quartzite, metapelites, sillimanite schist represent different stratigraphic units of diverse ages ranging from late Archean to Tertiary in various tectonic blocks surrounding the study area. Most of the hills viz., Biligirirangan- Shevaroy-Kalrayan Hills, Kollimalai-Pachaimalai Hills, Bodamalai Hills, and other minor hills expose high-grade rocks comprising massive, structureless or poorly banded charnockite, mafic granulite, and amphibolites. The gneiss and supracrustal rocks are bounded by the eastern extension of Moyar Bhavani shear zone (MBSZ) called **Salem -Attur Shear Zone** (SASZ) in the middle of Attur valley, which is marked by intense development of mylonite, (**Fig.2 A&B**) mylonitised pyroxene granulite, quartzo-feldspathic gneiss, and garnet amphibolite (Biswal et al., 2009; 2010). A similar Mylonitized zone occurs near Mettur (**Fig.2 C&D**), which is part of the NE-SW trending **Mettur Shear Zone (MSZ).** The mylonites of MSZ are crisscrossed by Pseudotachylyte veins. The NE- SW trending, a km wide **Gangavalli Shear Zone (GSZ)** runs for about 50km. This shear zone is characterized by pseudotachylytes (**Fig.2 E&F**) and cataclasites within a linear charnockite ridge, forming a classic example of a brittle shear zone, (Behera et al., 2017). The North-South trending **Sitampundi–Kanjamalai Shear Zone (SKSZ)** is characterized by showing internal discontinuities, extension fractures, sigmoidal veins and mega porphyroclasts (**Fig.2 G&H**) and amphibolites (retrograded Meta gabbro), Mylonitized Quartzo-feldspathic gneiss. Apart from quartz ribbons, the mylonites consist of feldspar clasts of σ, δ, and Φ types (Thirukumaran et al., 2019). The feldspar clasts are of different sizes and shapes; some are marked by intragranular faults.

This paper discusses the complex tectonic history of the Salem region, covering various periods from the Early Archean to the Paleozoic. The region showcases several significant geological features, including the Salem Attur Shear Zone, Mettur Shear Zone, Gangavalli Shear Zone (GSZ), and Sitampundi-Kanjamalai Shear Zone (SKSZ), each exhibiting distinct deformation characteristics and associated geological phenomena.

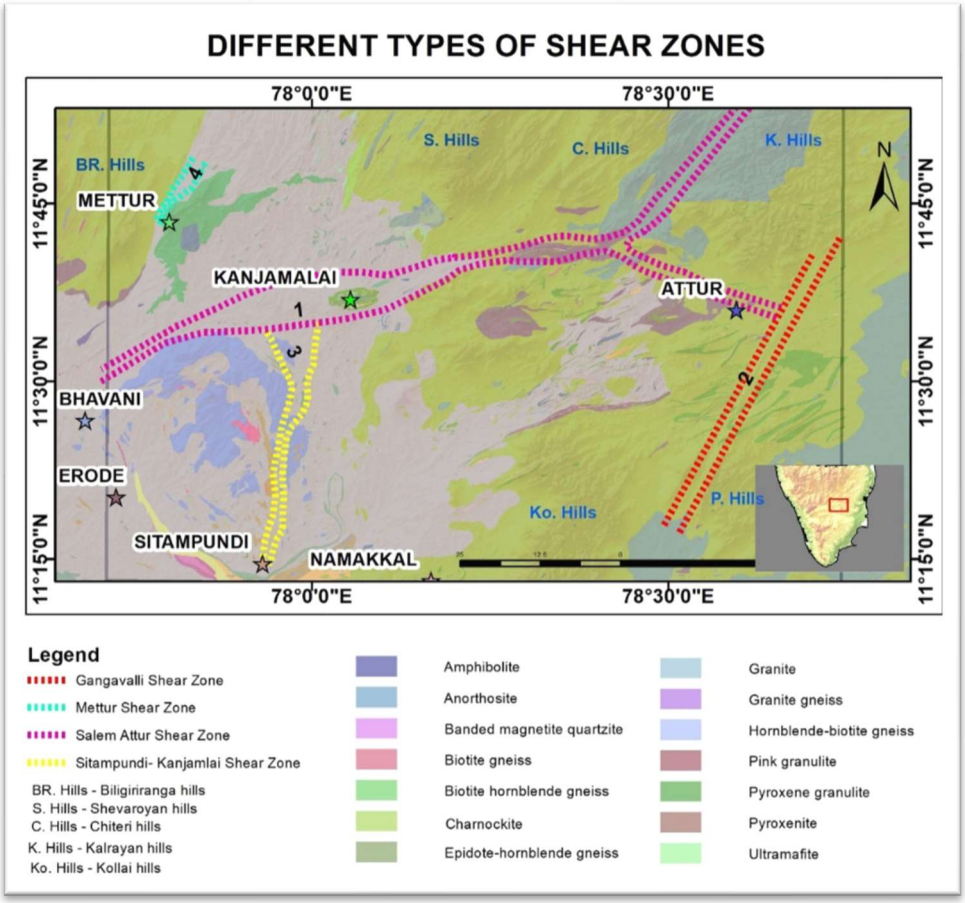

Figure 1. Salem region in southern India showing multiple types of shear zones (Insert location of Study area in South India)

1. **Salem Attur Shear Zone**: This zone has experienced multiple deformation stages from D1 to D4. The superimposition of F2 and F3 folds over F1 has resulted in the creation of type 1, type 2, and type 3 interference folds. This zone has undergone significant deformation, indicating a prolonged tectonic history (Behera et al., 2019).
2. **Mettur Shear Zone**: Primarily associated with D2 deformation, this zone displays NE-SW trending open to tight and upright to NW inclined F2 folds, suggesting a buckling origin. Various deformation characteristics such as parasitic folds, cleavage refraction, compositional band boudins, and folded boudins are observed, indicating a complex deformation history.
3. **Gangavalli Shear Zone (GSZ)**: This brittle shear zone represents the last recorded phase of deformation (D4). Despite primarily exhibiting strike-slip characteristics, stereoplots and Mohr's 3D stress plot suggest a vertical stress tensor corresponding to normal faults. This stress behavior indicates a flip-flop of stress vectors from horizontal to vertical along the GSZ.
4. **Sitampundi-Kanjamalai Shear Zone (SKSZ)**: Characterized by larger internally porphyroclasts, boudinaged veins, and folds associated with D4 deformation, this zone indicates significant rheological influences brought about by magma. The emplacement of the Sankari Granite, corresponding to the Pan-African Orogeny, has pervaded the foliations of amphibolites, further highlighting the region's complex geological history.

Overall, these shear zones provide valuable insights into the tectonic evolution of the Salem region, reflecting a series of deformations and associated geological processes spanning multiple geological periods.

Figure 2 A. S-C Mylonite from Salem-Attur Shear Zone (SASZ), B. Porphyroclasts in thin section from Sarkar Natarmangalam, SASZ, C. Mylonites of Mettur Shear Zone (MSZ), D. Thin section of mylonite from MSZ- Fractured Porphyroclast displaying dextral sense. E. Pseudo-tachylyte in Charnockite from Gangavalli, GSZ, F. Microlites of albite in thin section of pseudo-tachylyte, Udayaturgate, GSZ, G. Sigmoidal por- phyroclasts in mylonites from Tiruchengode, SKSZ, H. quartz ribbon in mylonites from SKSZ.

Keywords: Ductile shear Zone, Brittle shear Zone, Salem-Attur Shear Zone, Gangavalli Shear Zone, Mettur Shear Zone, Sitampundi-Kanjamalai Shear zone, SGT

References:

Behera, B.M. Waele, B.D. Thirukumaran, V. Sundaralingam, K. Narayanan, S.Sivalingam, B. Biswal, T.K., 2019. Kinematics, strain pattern and geochronology of the Salem-Attur shear zone: Tectonic implications for the multiple sheared Salem-Namakkal blocks of the Southern Granulite terrane, India, Precambrian Research 324, 32-61. https://doi.org/10.1016/j.precamres.2019.01.022.

Thirukumaran V., Biswal T.K., Sundaralingam K., Sowmya K., Boopathi S., Mythili R., 2019. Strain Pattern Analysis of Mylonites from Sitampundi-Kanjamalai Shear Zone, Thiruchengode, South India. International Journal of Civil, Environmental and Agricultural Engineering 1(1), 25-34. https://doi.org/10.34256/ijceae1914.

Behera, B.M., Thirukumaran, V., Soni, A., Mishra, P.K., Biswal, T.K., 2017. Size distribution and roundness of clasts within pseudotachylites of the Gangavalli Shear Zone, Salem, Tamil Nadu: An insight into its origin and tectonic significance. Journal of Earth System Science 126 (4), 46

Biswal, T.K., Thirukumaran, V., Ratre, K., Sundaralingam, K., 2009. Study of the Salem-Attur shear zone, east of Salem, Tamil Nadu: a new kinematic interpretation. Current Science 96 (10), 1–4.

Biswal, T.K., Thirukumaran, V., Ratre, K., Bandyapadhaya, K., Sundaralingam, K., Mondal, A.K., 2010. A Study of mylonites from parts of the Salem-Attur shear zone (Tamil Nadu) and its Tectonic Implications. Journal of the Geological Society of India 75, 128–136.

GDT 10: Multi-stage Phanerozoic mafic magmatism in the NE Pamir: implications for the evolution from Proto- to Paleo-Tethys Ocean

Zhihao Song[a], Chuanlin Zhang[a*], Masumeh Sargazi[a], Xiaoqiang Liu[b], Xiantao Ye[a], Yan Jing[a], Hongran Wang[a], Zahid Hussain[a]

[a]*College of Oceanography, Hohai University, Nanjing, People's Republic of China, 210016*
[b]*College of Geology and Mining Engineering, Xinjiang University, Urumqi, People's Republic of China, 830046*

*Corresponding Author:
E-mail address: zhangchuanlin@hhu.edu.cn (C.L. Zhang)

The Pamir Plateau/Syntax, located in the northwest of the Tibet-Plateau, lies at the western end of the Tethys domain in China, recording essential information about the evolution from the opening of the Proto-Tethys to the final closure of the Neo-Tethys (Li et al., 2018; Robinson et al., 2012; Yin and Harrison, 2000). During this long-term evolution, the details of subduction polarity and timing of the Proto- and Paleo-Tethys Oceans remain controversial (Liu et al., 2023; Rembe et al., 2021; Song et al., 2024; Zhang et al., 2018). Our field observation and systematic geochronological studies reveal four stages of Phanerozoic mafic magmatic flare-ups with tholeiitic series, occurring at 512-539 Ma, 320 Ma, 277 Ma, and 203-211 Ma in the northeastern (NE) Pamir (**Fig. 1**).

The Qushiman hornblende gabbro (539 Ma) and amphibole plagiogneiss (512 Ma) exhibit high concentrations of large-ion lithophile elements (LILEs, Rb, Ba, and Sr), low high-field-strength elements (HFSEs, Nb, Ta, Zr, and Hf), and slightly to steep right-leaning REE patterns. The variation in zircon $\varepsilon_{Hf}(t)$ values (-2.7 to -0.9) for hornblende gabbro, and amphibole plagiogneiss (-1.6 to +2.3), along with elevated zircon $\delta^{18}O$ values (5.97 ~ 7.66‰) and negative $\varepsilon_{Nd}(t)$ values (-6.94 and -2.36) of amphibole plagiogneiss, suggest that they were derived from a metasomatized sub-continental lithospheric mantle source.

The Oytagh basalts (320 Ma) of biomodal volcanic sequence show mid-oceanic-ridge basalt-like geochemical features with flat to depleted light rare earth element trends [$(La/Yb)_N$ = 0.68 ~ 1.82], depleted whole-rock $\varepsilon_{Nd}(t)$ (6.44 ~ 7.85), and zircon $\varepsilon_{Hf}(t)$ (6.3 ~ 10.1) values, suggesting they are primitive magmas derived from a depleted mantle source metasomatized by earlier subduction, in line with their low Nb/La ratios (0.30 ~ 0.64). Consequently, a back-arc basin setting is more consistent with the interpretation of the sedimentary sequence in this area.

The Permian Dabudaer gabbro (277 Ma) display nearly flat to slightly right-leaning REE patterns (La/Yb=0.97 ~ 5.16), $\varepsilon_{Nd}(t)$ values (-2.66 ~ +4.74), and zircon $\varepsilon_{Hf}(t)$ values (-7.3 ~ +1.6). Conversely, the Triassic Dabudaer gabbros (206 Ma) exhibit positive anomalies in Nd, Ta. Rb, and Ba, resembling Oceanic island basalt (OIB)-like patterns in chondritic-normalized and primitive mantle-normalized diagrams, with $\varepsilon_{Nd}(t)$ values of (+1.87 ~ +1.96). These evidences suggest the Permian Dabudaer gabbros were derived from a fertile lherzolite source in a fore-arc environment. Additionally, the late Triassic OIB-like gabbro may have originated in an E-MORB source under a subduction setting. The Tashkorgan olivine gabbro (211 Ma) is enriched in Nb-Ta, Zr, and Hf, with a slightly right-leaning distribution of REE patterns, variable negative Ba, Sr, and Ti. Mantle-like zircon $\delta^{18}O$ contents (5.05 ~ 6.69‰), and positive $\varepsilon_{Nd}(t)$ value (+4.21) suggest they were derived partial melting of an asthenosphere mantle source. The Tashkorgan hornblende gabbro exhibits positive Rb, Ba, and Sr, and displays right-leaning in the PM-normalized trace element diagram, with $\varepsilon_{Nd}(t)$ value (+0.37), suggesting the same magma source as olivine gabbro but crystallized at different depth.

Figure 1 Representive field photographs and hand specimens of mafic rocks in the NE Pamir. (A) Oytagh-Gaizi bimodal volcanic sequence, the intermediate - acid volcanic rocks conformably overlie the basalts. (B) Oytagh basalts (322 Ma). (C) Oytagh andesite (288 Ma). (D) Gabbro dyke intrudes in the Cambrian Bulunkuole Group. (E) The massive mafic intrusions intrude in the Wenquangou Group. (F) Tashkorgan cumulate olivine gabbro (211 Ma). (G-H) Dabudaer gabbros (277 Ma). (I) Dabudaer olivine gabbro (206 Ma).

Our findings, combined with the previous data on mafic magmatism in the NE Pamir, the following conclusions can be summarized: (1) They provide new evidence for the southward subduction of the Proto-Tethys Ocean, and we speculate on the possible occurred at the early Paleozoic (539 Ma) in the NE Pamir. (2) They construct a detailed evolution process of the initial subduction of the Paleo-Tethys Ocean, i.e., the extension of the filled residual Proto-Tethys Ocean between the Tarim and Northern Pamir induced by the northward subduction in the early Carboniferous. (3) We speculate that the bi-direction subduction of the Paleo-Tethys Ocean started at ca. 277 Ma and did not close before ca. 206 Ma.

Keywords: Phanerozoic; Mafic magmatism; Geochemistry; Tethys Ocean; NE Pamir

Acknowledgement: This study was funded by the National Key Research and Development Program (2021YFC2901904), National Nature Sciences Foundation (42172062), and National 305 Project of China (2019B00011-1).

References:

Li, S.Z., Zhao, S.J., Liu, X., Cao, H.H., Yu, S., Li, X.Y., Somerville, L., Yu, S.Y., Suo, Y.H., 2018. Closure of the Proto-Tethys Ocean and Early Paleozoic amalgamation of microcontinental blocks in East Asia. Earth Science Reviews 186, 37-75.

Liu, X.Q., Zhang, C.L., Zou, H.B., Ye, X.T., 2023. Diverse metavolcanic sequences in the Cambrian accretionary complex at the Pamir Syntax: Implications for tectonic evolution from Proto-Tethys to Paleo-Tethys. Journal of Asian Earth Sciences 241, 105481.
Rembe, J., Sobel, E.R., Kley, J., Zhou, R.J., Thiede, R., Chen, J., Valla, P., 2021. The Carboniferous Arc of the North Pamir. Lithosphere 2021(1), 6697858.
Robinson, A.C., Ducea, M., Lapen, T.J., 2012. Detrital zircon and isotopic constraints on the crustal architecture and tectonic evolution of the northeastern Pamir. Tectonics 31(2), TC2016.
Song, Z.H., Zhang, C.L., Sargazi, M., Hussain, Z., Liu, X.Q., Ye, X.T., Wang, H.R., 2024. Carboniferous bimodal volcanic sequences along the Northeastern Pamir: Evidence for back-arc extension due to northward subduction of the Paleo-Tethys. GSA Bulletin. 136 (9-10): 3769–3785. doi: https://doi.org/10.1130/B37153.1
Yin, A., Harrison, T.M., 2000. Geologic evolution of the Himalayan-Tibetan orogen. Annual review of Earth and Planetary Sciences 28, 211-280.
Zhang, C.L., Zou, H.B., Ye, X.T., Chen, X.Y., 2018. Tectonic evolution of the NE section of the Pamir Plateau: New evidence from field observations and zircon U-Pb geochronology. Tectonophysics 723, 27-40.

GDT 11: Laser ablation Lu-Hf detrital apatite of the Pilbara craton: insights into early Earth crust

Melissa Kharkongor[1*], Stijn Glorie[1], Jack Mulder[1], Christopher L. Kirkland[2], Sarah Gilbert[1,5], Peter Cawood[3], Chris Hawkesworth[4]

[1]*Department of Earth Sciences, University of Adelaide, SA 5005, Australia*
[2]*Timescales of Mineral Systems Group, School of Earth and Planetary Sciences, Curtin University, WA 6102, Australia*
[3]*Monash University, VIC 3800, Australia*
[4]*School of Earth Sciences, University of Bristol, Bristol BS8 1RJ, UK*
[5]*Adelaide Microscopy, University of Adelaide, SA 5005, Australia*

*Corresponding Author:
E-mail address: melissa.kharkongor@adelaide.edu.au (M.Kharkongor)

Studying the evolution of continental crust is key to understand the processes that shaped our habitable planet. Continental growth models propose that a significant portion of today's continental crust formed by the end of the Archean, but the geodynamic setting of this early crust formation remains debated (Cawood et al., 2022). While granite- greenstone terranes, often considered to have formed from thickened mafic crust above mantle upwellings, are prominent in discussions, there's growing evidence suggesting they developed on pre-existing continental substrates (Kamber, 2015; Petersson et al., 2019). The East Pilbara Terrane (EPT) in Western Australia is the archetypal granite-greenstone terrane, presenting a unique opportunity to study Archean crustal foundations. The EPT exhibits volcano-sedimentary cycles and tonalite- trondhjemite-granodiorite (TTG) plutonism dating back to 3.52 Ga. Evidence of older crustal substrates include Eoarchaean xenocrystic, detrital and enclave-hosted zircon grains found in younger rocks across the Pilbara Craton (Kemp et al., 2015). However, the zircon record (Hickman, 2021) is strongly biased towards felsic sources with mafic rocks being poorly represented. Here we present geochronology results and trace element compositions for detrital apatites from the EPT. Compared to zircon, apatite has a broader lithological range and is labile in the sedimentary cycle, providing insights into proximal sources. The detrital apatite U-Pb dates range from 2.5 Ga to 3.4 Ga, while Lu-Hf analyses from the same crystals yield generally older dates of 2.8 – 3.7 Ga. The population of Eoarchean detrital apatite grains from the EPT are the oldest terrestrial apatites ever dated. The trace element compositions suggest the Eoarchaean apatites were derived from TTG and mafic sources, supporting the notion of a protocrust forming in the earliest Eoarchean, potentially representing the primary sites of early continental growth.

References

Cawood, P. A., Chowdhury, P., Mulder, J.A., Hawkesworth, C. J., Capitanio, F. A., Gunawardana, P. M., Nebel, O., 2022. Secular evolution of continents and the Earth system. Reviews of Geophysics 60, e2022RG000789. https://doi.org/10.1029/2022RG000789

Hickman, A.H., 2021. East Pilbara Craton: a record of one billion years in the growth of Archean continental crust. Geological Survey of Western Australia, Report 187, 143 p. https://dmpbookshop.eruditetechnologies.com.au/product/east-pilbara-craton-a-record-of-one-billion-years-in-the-growth-of-archean-continental-crust.do
Kemp, Anthony I.S., Hickman, Arthur H., Kirkland, Christopher L., and Vervoort, Jeffery D., 2015. Hf isotopes in detrital and inherited zircons of the Pilbara Craton provide no evidence for Hadean continents. Precambrian Research 261, 112-126.
Petersson, A., Kemp, A.I., Whitehouse, M.J., 2019. A Yilgarn seed to the Pilbara Craton (Australia)? Evidence from inherited zircons. Geology 47(11), 1098–1102. https://doi.org/10.1130/G46696.1

GDT 12: Numerical modeling on geodynamical processes of intra-oceanic arcs and oceanic plateaus along convergent margin: insights into continental crust growth of the largest Phanerozoic accretionary orogen

Shengxuan Tang[1*], Kai Wang[2], Keda Cai[1], and Hao Zhou[2]

[1] *School of Earth Sciences and Resources, and Frontiers Science Center for Deep-time Digital Earth, China University of Geosciences, Beijing 100083, China.*
[2] *Department of Earth and Space Sciences, Southern University of Science and Technology, Shenzhen 518055, China.*

*Corresponding Author:
E-mail address: 3001220005@email.cugb.edu.cn (T. Shengxuan)

Modern subduction-accretion of intra-oceanic arcs and seamounts/oceanic plateaus in the western Pacific regions show that the amount of accretion depends on the rheological structure of the subducted oceanic lithosphere. Whether seamounts/ oceanic plateaus are accreted or not relies on the bulk thermal state at the time when these tectonic units approach the active margin. Researches on the vertical structure of global intra-oceanic arcs suggest that a weak rheological layer exists in the middle arc crust (e.g., the Izu-Bonin arc) or the bottom (e.g., the Lesser Antilles arc) with observations of the layered intermediate to felsic intrusions or ultramafic magma reservoirs and partial molten regions, respectively. Such a rheological stratification is generally determined by the maturity of the intra-oceanic arc (Tatsumi et al., 2008; Takahashi et al., 2009; Tetreault and Buiter, 2014). The contrasting fates of oceanic plateaus and seamounts that formed in the same period mainly depend on the time when they reached the active margin, such as the subducted Caribbean oceanic plateau and the accreted Gorgona oceanic plateau (Kerr and Tarney, 2005).

Here, we use two-dimensional numerical simulations to investigate the subduction-accretion processes and the accretion efficiency of intra-oceanic arcs and oceanic plateaus (**Fig. 1**). The initial model includes a continental plate fixed on the left wall and an investigated terrane located on the subducting oceanic plate. Based on the seismic P-wave detection (including active arcs, rear arcs, and accreted arcs; Tetreault and Buiter, 2014), the intra-oceanic arc has an average thickness of 28 km and a lateral width of 200 km, which is divided into 3 to 4 layers. Four test models are developed to investigate the subduction and accretion of the intra-oceanic arcs constituted by different crustal compositions and internal low-rheological-strength layers (Model A-1 to Model A-4). In contrast to the normal oceanic crust, the oceanic plateau generally has a 20-km-thick crust and can extend to a width of 200 km, thus is divided into 2 to 3 layers. In our numerical models, three experiments are conducted based on different thermal states of the oceanic plateau (Model S-1 to Model S-3). Details of the crustal structures and lithological compositions are shown in **Table 1**.

Our findings suggest that the deeper the weak layer positioned in the intra-oceanic arc crust, the larger the volume of the arc crust that is accreted, corresponding to a high accretion efficiency, up to ~70%. However, because the more number of weak layers makes the arc crust difficult to form stable lateral accretion but more conductive for the arc crust to be subducted into the mantle through subduction erosion, increasing the number of weak layers in the intra-oceanic arc crust cannot enhance the accretion efficiency (**Fig. 2**), comparing the Model A-2 (one weak layer positioned only in the crust-

mantle transition layer) with the Model A-4 (two weak layers positioned in both the crust-mantle transition layer and the middle crust). In addition, the hotter the oceanic plateau reaches the active margin, the easier and more it is to be accreted (>22%) when the bottom lower crust remains in a partially molten state (Model S-2 and S-3) (**Fig. 3**). Relatively low topography of oceanic plateaus causes the main accretion style of underplating, with crustal fragments entering the accretionary wedge.

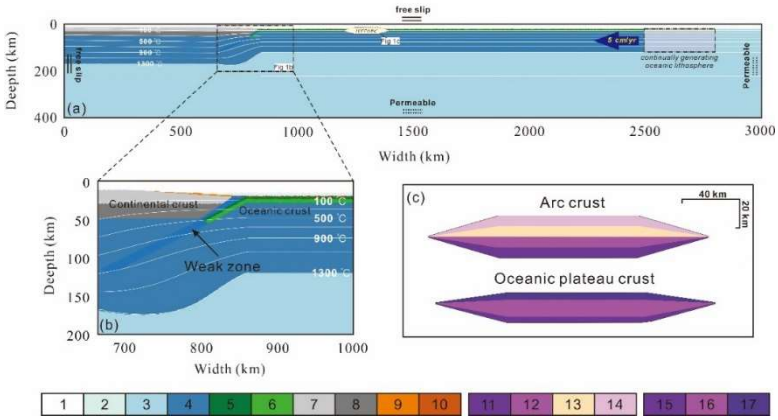

Figure 1. The initial model setting includes an active continental margin, subducting terrane, and oceanic plate. Figure 1b is a diagram containing crustal layering patterns, thickness, and length of terrane crusts classified by intra-oceanic arc crust and oceanic plateau crust, which vary in viscosity structure and thermal states. 1, 2, 9 (and 10), denote stick air, sticky water, and sediments, respectively. 3 and 4 refer to the lithosphere mantle and asthenospheric mantle. 5 and 6, and 7 and 8, represent oceanic upper and lower crust, and continental upper and lower crust, respectively. 11, 12, 13, and 14 represent the intra-oceanic arc crustal-mantle transition zone, lower crust, middle crust, and upper crust, respectively. 15, 16, and 17 are respectively the base of the oceanic plateau lower crust, oceanic plateau lower, and upper crust. Figure 1c is the enlarged diagram of the terrane crust including intra-oceanic arc and oceanic plateaus. The intra-oceanic arc crust is divided into four layers and the oceanic plateau crust is divided into 3 layers with an extremely thick lower crust.

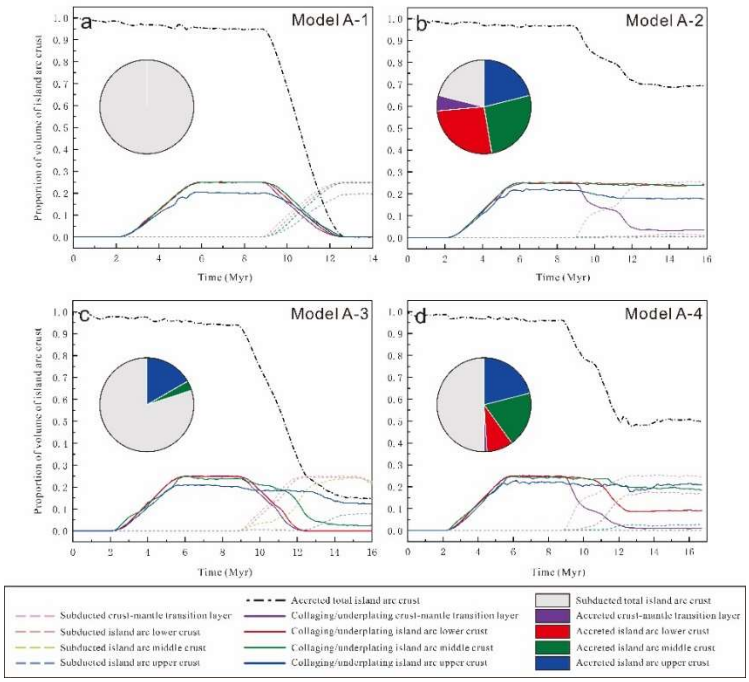

Figure 2. Accretion efficiencies of intra-oceanic arcs of Model A-1 to Model A-4. The vertical and horizontal coordinates are proportions of the volume of intra-oceanic arc crust (0-1) and Time in million years, respectively. In the four diagrams, dashed lines refer to the proportions of subducted intra-oceanic arc crust layers and solid lines refer to the proportions of accreted intra-oceanic arc crust layers. Different colored dashed or solid lines correspond to different layers in the subducted or accreted crust, see legend for details. Where the black dots with long dashed lines refer to the total accretionary efficiencies of the intra-oceanic arc crust. The colored areas in pie charts for each model correspond to the accreted proportion of each crustal layer and the grey areas refer to total subducted proportions of intra-oceanic arc crust when the subduction-accretion processes reach final steady state.

These preliminary studies provide insights, for the first order, into the geodynamics of the Central Asian Orogenic Belt which is one of the largest accretionary orogens formed by amalgamations of numerous intra-oceanic arcs and oceanic plateaus/seamounts (**Fig. 4a**) (Safonova et al., 2016, 2017; Yang et al., 2019). Exposed rocks along regional geotransects are dominated by fragments of the shallow crust of intra-oceanic arcs and seamounts (**Fig. 4b-d**), which may be associated with ubiquitously shallow positions of the weak layer within intra-oceanic arcs and the hot thermal state of oceanic plateaus.

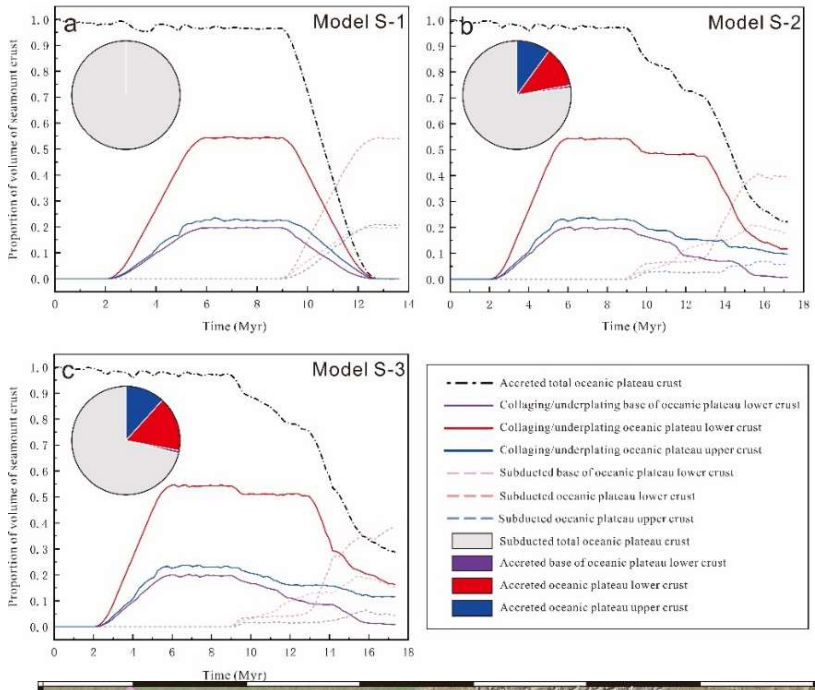

Figure 3. Accretion efficiencies of oceanic plateaus of Model S-1 to Model S-3. The vertical and horizontal coordinates are proportions of the volume of oceanic plateau crust (0-1) and Time in million years, respectively. The comments on the legend are the same as the note in Figure 2.

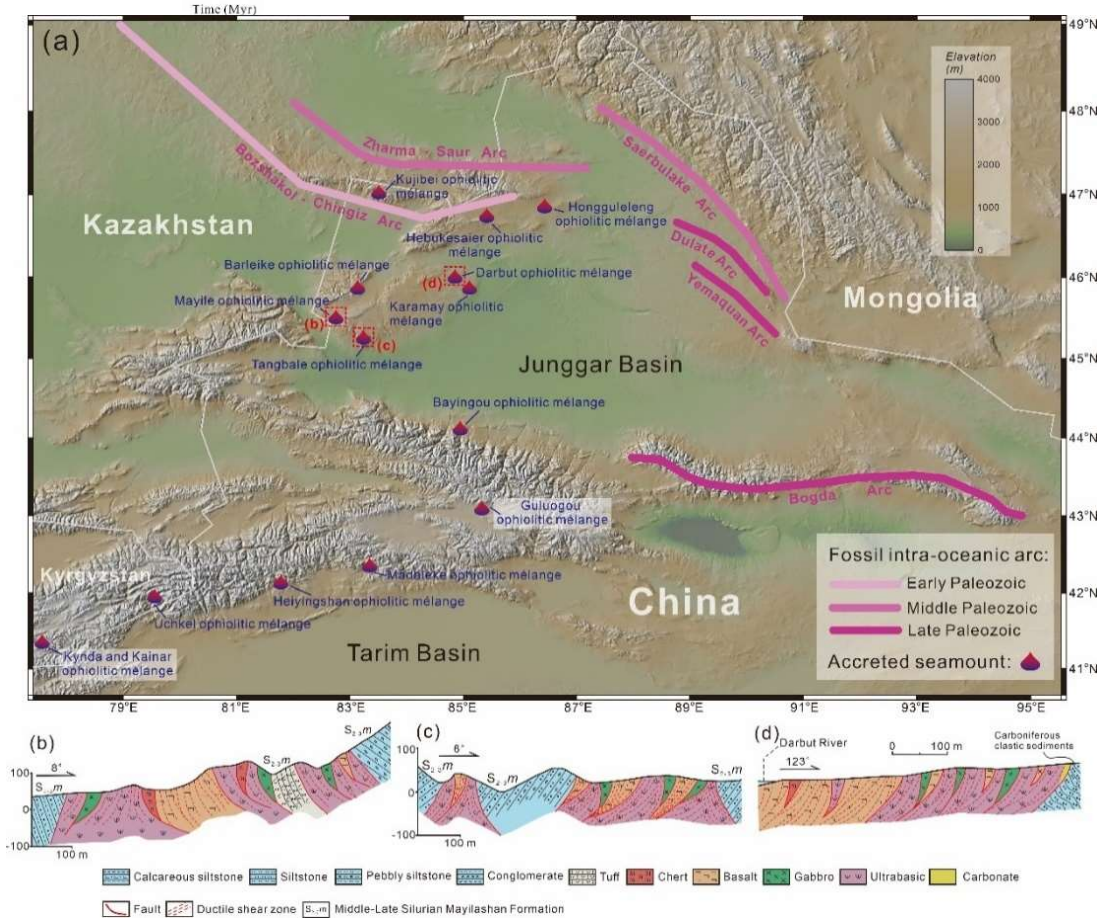

Figure 4. (a) Distribution of fossil intra-oceanic arcs and accreted seamounts in Tianshan, Junggar and Chinese Altai. (b) The tectonic section of Mayile ophiolitic mélange (modified from Yang et al., 2012b). (c) The tectonic section of Tangbale ophiolitic mélange (modified from Yang et al., 2012b). (d) The tectonic section of Darbut ophiolitic mélange (modified from Yang et al., 2012a).

Table 1. Crustal structure and flow law of intra-oceanic arc and oceanic plateau crust in each model

Terrane type	Crustal layer	Lithology	Flow law	Reference density [kg/m^3]	[a]References	Applied model
Intra-oceanic arc	Crust-Mantle Transition Layer	Ultramafic cumulates	Clinopyroxene	3200	3	Model A-1/3
		Molten mantle peridotite	Molten dry olivine	2900	1, 2	Model A-2/4
	Lower crust	Gabbro	Plagioclase (An^{75})	3000	1, 2	Model A-1/2/3/4
	Middle crust	Felsic intrusive rock	Wet quartzite	2700	4	Model A-1/2
		Molten felsic rock	Molten wet quartzite	2400	4	Model A-3/4
	Upper crust	Basalt/Volcaniclastics	Wet quartzite	3000	1, 2	Model A-1/2/3/4
Oceanic plateau	The base of lower crust	Mantle peridotite	Dry olivine	3300	1, 2	Model S-1
		Molten mantle peridotite	Molten dry olivine	2900	1, 2	Model S-2/3
	Lower crust	Gabbro	Plagioclase (An^{75})	3000	1, 2	Model S-1/2/3
	Upper crust	Basalt/Volcaniclastics	Wet quartzite	3000	1, 2	Model S-1/2/3

[a] References 1-4: 1. Bittner and Schmeling (1995); 2. Turcotte and Schubert (2002); 3. Chen et al. (2006); 4. Dingwell (1999) respectively.

References:

Bittner, D., Schmeling, H., 1995. Numerical modeling of melting processes and induced diapirism in the lower crust. Geophysical Journal International 123, 59–70.

Chen, S., Hiraga, T., Kohlstedt, D.L., 2006. Water weakening of clinopyroxene in the dislocation creep regime. Journal of Geophysical Research 111, B08203, doi:10.1029/2005JB003885.

Dingwell, D. B., 1999. Rheology of granitic melts. Understanding Granites: Modern and Classical Approaches. Geological Society of London Special Publication 168 27-38.

Kerr, A. C., and Tarney, J., 2005. Tectonic evolution of the Caribbean and northwestern South America: The case for accretion of two Late Cretaceous oceanic plateaus. Geology, 33(4), 269-272.

Safonova, I., Biske, G., Romer, R. L., Seltmann, R., Simonov, V., Maruyama, S., 2016. Middle Paleozoic mafic magmatism and ocean plate stratigraphy of the South Tianshan, Kyrgyzstan. Gondwana Research 30, 236-256.

Safonova, I., Kotlyarov, A., Krivonogov, S., Xiao, W., 2017. Intra-oceanic arcs of the Paleo-Asian Ocean. Gondwana Research 50, 167-194.

Takahashi, N., Kodaira, S., Tatsumi, Y., Yamashita, M., Sato, T., Kaiho, Y., Miura, S., No, T., Takizawa, K., Kaneda, Y., 2009. Structural variations of arc crusts and rifted margins in the southern Izu-Ogasawara arc–back arc system. Geochemistry Geophysics Geosystems 10(9) Q09X08.

Tatsumi, Y., Shukuno, H., Tani, K., Takahashi, N., Kodaira, S., Kogiso, T., 2008. Structure and growth of the Izu-Bonin-Mariana arc crust: 2. Role of crust-mantle transformation and the transparent Moho in arc crust evolution. Journal of Geophysical Research: Solid Earth 113(B2).

Tetreault, J. L., Buiter, S.J.H., 2014. Future accreted terranes: a compilation of island arcs, oceanic plateaus, submarine ridges, seamounts, and continental fragments. Solid Earth 5(2), 1243-1275.

Turcotte, D.L., Schubert, G., 2002. Geodynamics. Cambridge University Press, Cambridge, UK.

Yang, G., Li, Y., Tong, L., Wang, Z., Duan, F., Xu, Q., Li, H., 2019. An overview of oceanic island basalts in accretionary complexes and seamounts accretion in the western Central Asian Orogenic Belt. Journal of Asian Earth Sciences 179, 385-398.

Yang, G.X., Li, Y.J., Santosh, M., Yang, B.K., Yan, J., Zhang, B., Tong, L.L., 2012a. Geochronology and geochemistry of basaltic rocks from the Sartuohai ophiolitic melange, NW China: implications for a Devonian mantle plume within the Junggar Ocean. Journal of Asian Earth Sciences 59, 141–155.

Yang, G.X., Li, Y.J., Gu, P.Y., Yang, B.K., Tong, L.L., Zhang, H.W., 2012b. Geochronological and geochemical study of the Darbut ophiolitic complex in the west Junggar (NW China): implications for petrogenesis and tectonic evolution. Gondwana Research 21, 1037–1049.

GDT 13: Geological and Tectonic Features of Manipur: Implications on Deformation and Evolution of the Indo-Myanmar Ranges of Northeast India

Soibam Ibotombi[1*], Khundrakpam Kumarjit Singh[1] and Thokchom Nilamani Singh[1]

[1]*Department of Earth Sciences, Manipur University, Imphal-795003, India*

*Corresponding Author:
E-mail address: soibamibotombi@gmail.com (S. Ibotombi)

Geological and tectonic features of Indo-Myanmar Ranges (IMR) in general and Manipur Hills, in particular, have distinct entities in the geotectonic framework of Southeast Asia, for they represent both collisions as well as subduction mechanisms between the Indian and Myanmar plates. In the process, the IMR evolved as an accretionary prism where an older group of lithounits lie and lean over the younger ones in the form of an imbricate thrust system. Consequently, older lithounits are exposed on the eastern side while the younger ones are on the western side (**Fig. 1a**). As a result, the tectonostratigraphic sequence of the range is practically an inversion of the stratigraphic sequence.

Analysis of structural and tectonic features indicates nearly E-W (WNW-ESE) compression and N-S (NNE-SSW) extension of the range. Plate kinematic studies in and around Manipur reveal that such regional compression and extension can result from a dextral shear coupling deformation between the Indian and Myanmar plates. Drainage analysis and topographic inversion studies further indicate the successive evolution stages of the Manipur Hills that the eastern part of the state was uplifted first followed by the western part **(Fig. 1b**).

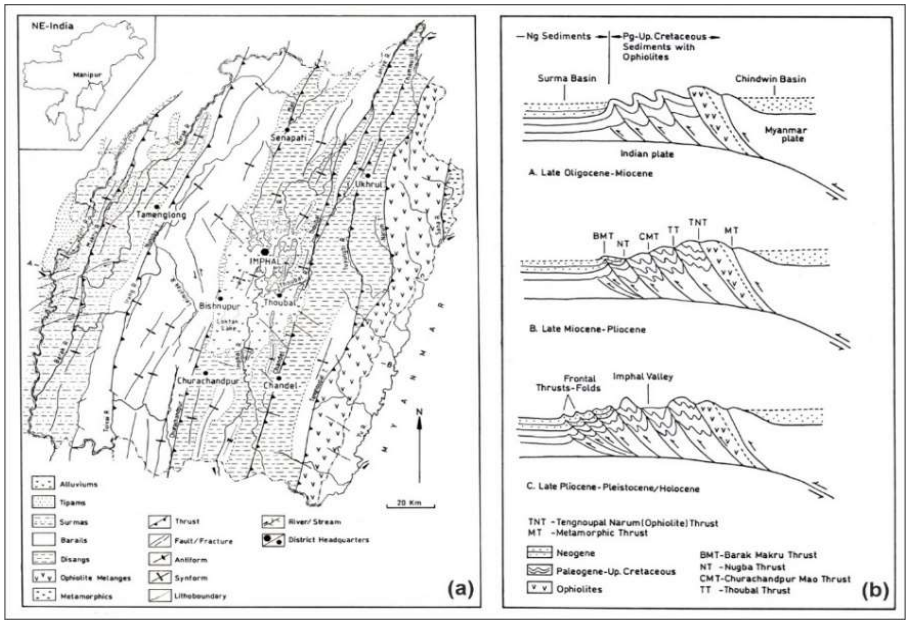

Fig. 1:a) Geological map of Manipur showing various lithounits and major structural features

b) Evolutionary stages of Manipur Hills of the IMR constructed based on topographic inversion.

Keywords: Accretionary prism, Manipur, Thrust system, Myanmar plate, Topographic inversion

GDT 15: Banded iron formation drives subduction initiation and onset of global plate tectonics at ca. 2.45 Ga

Shuan-Hong Zhang[1,2,3]*, Yue Zhao[1,2], Jun-Ling Pei[2,4]

[1]*Institute of Geomechanics, Chinese Academy of Geological Sciences, Beijing 100081, China*
[2]*MLR Key Laboratory of Paleomagnetism and Tectonic Reconstruction, Beijing 100081, China*
[3]*SinoProbe Laboratory, Chinese Academy of Geological Sciences, Beijing 100037, China*
[4]*School of Earth Sciences, East China University of Technology, Jiangxi 330013, China*

*Corresponding Author:
E-mail address: tozhangshuanhong@163.com; shzhang@cags.ac.cn (S.H. Zhang)

The Earth is the only known planet where plate tectonics is active. However, when and how plate tectonics began to operate on Earth has been highly debated, with estimated ages ranging from >4.0 Ga to ca. 0.85 Ga (e.g., Palin et al., 2020 and references therein). Earth's evolution involves transforming the formerly ductile asthenosphere into a thick, rigid lithosphere, and rigid lithosphere is considered to be a necessary pre-condition for the onset of plate tectonics (Cawood et al., 2018). Subduction initiation is a key process for plate tectonics, and it requires density differences between two rigid blocks along their boundary (Stern and Gerya, 2018). Therefore, the development of lithosphere-scale weak zones after the formation of rigid lithosphere and density differences are two important necessary pre-conditions for the onset of plate tectonics.

Banded iron formation (BIF) is one of the densest sedimentary rocks (>3.4 g cm^{-3}, up to 3.9 g cm^{-3}) on Earth (Dobson and Brodholt, 2005). Development of giant dyke swarms (defined as those >300 km long, Ernst and Buchan, 1997; Ernst, 2014) are important indicators for lithosphere-scale extension after the stabilization of cratons. Our analyses on temporal and spatial distributions of the Precambrian BIFs (Huston and Logan, 2004; Bekker et al., 2014; Konhauser et al., 2017) and giant dyke swarms (Ernst, 2014) show that ca. 2.45 Ga is the main peak age for deposition of vast volumes of BIFs (especially the voluminous Superior-type), which is accompanied by global development of rectilinear giant dyke swarms. The global appearance of rectilinear giant dyke swarms from ca. 2.45 Ga indicates the existence of rigid lithosphere and lithosphere-scale weak zones during this period. Deposition of thick and vast volumes of BIFs in large marine sedimentary basins, especially the Superior-type BIFs, resulted in significant density differences near basin margins and induced subduction initiation along lithosphere-scale weak zones and the global onset of plate tectonics.

Our results show that deposition of thick and vast volumes of BIFs and the global appearance of rectilinear giant dyke swarms at ca. 2.45 Ga provide two important necessary prerequisites for plate tectonics at a global scale, indicating the onset of global plate tectonics at ca. 2.45 Ga, essentially coincident with the Archean-Proterozoic boundary. We proposed that BIFs, especially the Superior-type BIFs drive subduction initiation and onset of plate tectonics at a global scale from the Archean-Proterozoic transition at ca. 2.45 Ga. We suggest that the onset of global plate tectonics results in a rapid increase in Earth's subaerial surface and enhancing of silicate and carbonate weathering, which may thus have promoted the subsequent Siderian low-latitude glaciation and Great Oxidation Event started from ca. 2.43 Ga and Lomagundi-Jatuli Event started from ca. 2.22 Ga (Duncan and Dasgupta, 2017; Eguchi et al., 2020).

Acknowledgment: This research was financially supported by the National Natural Science Foundation of China (41920104004, U2244213, 41725011) and the Fundamental Research Fund of Chinese Academy of Geological Sciences (JKYZD202320).

References

Bekker, A., Planavsky, N., Krapež, B., Rasmussen, B., Hofmann, A., Slack, J.F., Rouxel, O.J., Konhauser, K.O., 2014. Iron formations: their origins and implications for ancient seawater chemistry. In: Holland, H.D., Turekian, K.K. (Eds.), Treatise of Geochemistry (2nd ed.), 9. pp. 561–628, Elsevier.

Cawood, P.A., Hawkesworth, C.J., Pisarevsky, S.A., Dhuime, B., Capitanio, F.A., Nebel, O., 2018. Geological archive of the onset of plate tectonics. Philosophical Transactions of the Royal Society A, 376, 20170405.
Dobson, D., Brodholt, J., 2005. Subducted banded iron formations as a source of ultralow-velocity zones at the core–mantle boundary. Nature 434, 371–374.
Duncan, M.S., Dasgupta, R., 2017. Rise of Earth's atmospheric oxygen controlled by efficient subduction of organic carbon. Nature Geoscience 10(5), 387–392.
Eguchi, J., Seales, J., Dasgupta, R., 2020. Great Oxidation and Lomagundi events linked by deep cycling and enhanced degassing of carbon. Nature Geoscience 13, 71–76.
Ernst, R.E., Buchan, K.L., 1997. Giant radiating dyke swarms: their use in identifying pre-Mesozoic large igneous provinces and mantle plumes. AGU Geophysical Monograph 100, pp. 297–333.
Ernst, R.E., 2014. Large Igneous Provinces. Cambridge University Press, Cambridge. 653 p.
Huston, D.L., Logan, B.W., 2004. Barite, BIFs and bugs: Evidence for the evolution of the Earth's early hydrosphere. Earth and Planetary Science Letters 220, 41–55.
Konhauser, K.O., Planavsky, N.J., Hardisty, D.S., Robbins, L.J., Warchola, T.J., Haugaard, R., Lalonde, S.V., Partin, C.A., Oonk, P.B.H., Tsikos, H., Lyons, T.W., Bekker, A., Johnson, C.M., 2017. Iron formations: A global record of Neoarchaean to Palaeoproterozoic environmental history. Earth-Science Reviews 172, 140–177.
Palin, R.M., Santosh, M., Cao, W., Li, S.-S., Hernández-Uribe, D., Parsons, A., 2020. Secular change and the onset of plate tectonics on Earth. Earth-Science Reviews 207, 103172.
Stern, R.J., Gerya, T., 2018. Subduction initiation in nature and models: A review. Tectonophysics 746, 173–198.

GDT 16: P-T conundrum: A comprehensive debate on Conventional vs. High-Resolution Thermobarometric modelling from NW Kumaun Himalaya, India

Biraja Prasad Das[1*], Shubham Patel[2], Mallickarjun Joshi[2]

[1]*Department of Geology, Dharanidhar University, India*
[2]*Department of Geology, Banaras Hindu University, India*

*Corresponding Author:
E-mail address: birajageology@gmail.com (D.Biraja Prasad)

Pressure-temperature reconstructions are common to constrain the tectono-thermal history of Himalaya (Walker et al., 2001; Joshi and Tiwari, 2009; Celerier et al., 2009b; Kohn, 2014). Conventional thermobarometry has been used for several decades to calculate the P-T conditions for the Himalayan metamorphic rocks. In this study, we report multiple pressure-temperature (P-T) path modellings for the first time to deduce the tectono-thermal evolution of one of the representative klippen, viz. Askot Klippe, NW Kumaun Himalaya. High-resolution garnet P-T path modelling using Theriak-Domino, conventional geothermobarometric approach, and Isochemical phase section modelling are used for the metapelitic rocks to unravel their P-T history. With the advent of modern computer programmes, High-Resolution (spatial resolution) P-T path modelling in garnet from core to rim is in progress for the last few years (Moynihan and Pattison, 2013; Kelly et al., 2015; Catlos et al., 2018; Etzel et al., 2019; Catlos et al., 2020) to obtain more precise thermobarometric modelling in the metamorphic rocks.

This paper stresses more on the conventional as well as high-resolution P-T path and timing of peak metamorphic conditions of the metapelites of the Askot Klippe to unwarp their recorded Paleoproterozoic metamorphic histories. In the present work, we use both conventional and High-Resolution thermobarometric approaches along with the Isochemical Phase Section modelling of the metapelitic rocks of the Askot Klippe and compare the results with textural and mineralogical assemblages for the metamorphic assemblages exposed in the central part of Askot Klippe to demonstrate their P-T evolution. We compare the results of the three samples using both modelling approaches to verify the data consistency. It is likely that the constraints used in the Theriak PT path modelling for the metapelitic gneisses do not correspond with the physical conditions that prevailed during the metamorphism of the rocks under investigation, unlike schists where both conventional as well as High-Resolution P-T path modelling show nearly identical results. The present P-T path results for both the metapelitic schists and gneisses using two modelling approaches are compared with the

results of the Almora Nappe, Askot Klippe and the MCT of Higher Himalaya to strengthen their tectono-thermal correlation. With the compelling evidences found from both petrochemical results and Isochemical phase section modelling in comparison with the two P-T modelling approaches, it can be postulated that the conventional P-T path modelling approach for the metapelitic schists lies close to the Theriak-Domino P-T path modelling approach, but in case of metapelitic gneisses, it is quite distinct, which suggests that the calculations below 600°C are valid only for metapelitic schists in view of the limitations of the Theriak PT path modelling approach and the temperature exceeding 600°C clearly violates the assumption made for the P-T modelling by Theriak PT path, particularly for the metapelitic gneisses.

References

Catlos, E.J., Lovera, O.M., Kelly, E.D., Ashley, K.T., Harrison, T.M., Etzel, T., 2018. Modeling high-resolution pressure-temperature paths across the Himalayan Main Central Thrust (Central Nepal): Implications for the dynamics of collision. Tectonics 37, 2363-2388.

Catlos, E.J., Perez, T.J., Lovera, O.M., Dubey, C.S., Schmitt, A.K., Etzel, T.M., 2020. High-resolution P-T-Time paths across himalayan faults exposed along the bhagirathi transect NW India: Implications for the construction of the Himalayan orogen and ongoing deformation. Geochemistry Geophysics Geosystems 21, 1-29.

Celerier, J., Harrison, T.M., Beyssac, O., Herman, F., Dunlap, W.J., Webb, A.A.G., 2009b. The Kumaun and Garwhal Lesser Himalaya, India: Part 2. Thermal and deformation histories. Geological Society of America Bulletin 121, 1281-1297.

Etzel, T.M., Catlosm E.J., Ataktürk, K., Lovera, O.M., Kelly, E.D., Çemen, I., Diniz, E., 2019. Implications for thrust-related shortening punctuated by extension from P-T paths and geochronology of garnet-bearing schists, Southern (Çine), Menderes Massif, SW Turkey. Tectonics 38, 1974-1998.

Joshi, M., Tiwari, A.N., 2009. Structure events and metamorphic consequences in Almora Nappe during Himalayan collision tectonics. Journal of Asian Earth Sciences 34, 326-335.

Kelly, E.D., Hoisch, T.D., Wells, M.L., Vervoort, J.D., Beyene, M.A., 2015. An Early Cretaceous garnet pressure-temperature path recording synconvergent burial and exhumation from the hinterland of the Sevier orogenic belt, Albion Mountains, Idaho. Contributions to Mineralogy and Petrology 170, 1-22.

Kohn, M.J., 2014. Himalayan metamorphism and its tectonic implications, Annual Review of Earth and Planetary Sciences. 42, 381-419.

Moynihan, D., Pattison, D.R.M., 2013. An automated method for the calculation of P-T paths from garnet zoning, with application to metapelitic schist from the Kootenay Arc, British Columbia, Canada. Journal of Metamorphic Geology 31, 525-548.

Walker, C.B., Searle, M.P., Waters, D.J., 2001. An integrated tectonothermal model for the evolution of the High Himalaya in western Zanskar with constraints from thermobarometry and metamorphic modelling. Tectonics 20, 810-833.

GDT 18: Eocene SSZ-type ophiolite from Banggi Island, Sabah (Northern Borneo), Malaysia: Age, geochemical characteristics and tectonic implications

Rezal Rahmat[1,2,3,4*], Sun-Lin Chung[2,3,5], Chih-Tung Chen[3], Azman Abd Ghani[6], Hao-Yang Lee[2], Yoshiyuki Iizuka[2] and Long Xiang Quek[7]

[1]*Taiwan International Graduate Program (TIGP) - Earth System Science, Academia Sinica and National Central University, Taiwan*
[2]*Institute of Earth Sciences, Academia Sinica, Taipei, Taiwan*
[3]*College of Earth Sciences, National Central University, Taiwan*
[4]*Geology Program, Faculty of Science and Natural Resources, Universiti Malaysia Sabah, Malaysia*
[5]*Department of Geosciences, National Taiwan University, Taipei, Taiwan*
[6]*Department of Geology, University of Malaya, Kuala Lumpur, Malaysia*
[7]*College of Earth and Planetary Sciences, University of Chinese Academy of Sciences, Beijing, China*

*Corresponding Author:
E-mail address: rezal.rahmat@g.ncu.edu.tw (R.Rezal)

Ophiolites in Sabah are dispersed in a band-shaped region stretching from Darvel Bay in the southeast to Banggi Island in the northmost part of Sabah. This study reports the first set of zircon U-Pb ages and whole-rock geochemical data of the Banggi Ophiolite, conventionally regarded as part of the regional Triassic-Eocene "Chert-Spilite Formations", named as the Sabah Ophiolite, and interpreted as remnants of exposed oceanic crust from the proto-South China Sea. LA-ICPMS analyses of zircon separated from

five gabbro and two diorite samples gave a short range of $^{206}Pb/^{238}U$ ages of ~55–51 Ma (Early Eocene), with high and positive zircon $\varepsilon_{Hf}(t)$ values from +16.6 to +10.2 indicating their magma source from a relatively depleted or juvenile mantle. The crustal sequence of Banggi Ophiolite, including basalt, gabbro, and diorite, is divided into two types in terms of geochemical characteristics, a depleted type (i.e., depleted in light rare earth elements) and an enriched type, respectively. The majority of both types display various degrees of enrichment in LILE (large ion lithophile elements) and depletion in Nb and Ta, geochemical signatures typical of arc magmas from intra-oceanic subduction zones and comparable to the SSZ (supra-subduction zone) type ophiolites reported from two nearby islands in Palawan and Mindoro, western Philippines. The formation age of Banggi Ophiolite (Eocene) is slightly older than the Palawan (~40-34 Ma) and Mindoro (~33-23 Ma) ophiolites. Integrating our new data with regional geology information, we argue that the Banggi Ophiolite is an SSZ-type ophiolite that formed in the forearc regime at the initial stage of the southward subduction of the proto-South China Sea plate. The subduction initiation started in Sabah, giving rise to a stratigraphic unconformity in its surrounding areas, and propagated north-eastward to Palawan and then Mindoro, eventually resulting in a volcanic arc exposed as the Cagayan Ridge.

Keywords: Borneo, Sabah, zircon U-Pb geochronology, geochemistry, SSZ-type ophiolite, subduction initiation.

GDT 19: Hierarchical Focal Depth Study of Earthquakes in the Indo-Myanmar Ranges of Northeast India and Its Tectonic Implications

Khundrakpam Kumarjit Singh[1*], Soibam Ibotombi[1] and Sanoujam Manichandra[1]

[1]*Department of Earth Sciences, Manipur University, Imphal-795003, India*

*Corresponding Author:
E-mail address: khkumarjitsingh1@gmail.com (K. Kumarjit Singh)

The Indo-Myanmar Ranges (IMR) of Northeast India are recognized as active subduction mountain ranges within the broader scope of global tectonics, illustrating characteristics akin to an island arc with an oblique subduction process. The IMR exhibits a notable frequency of seismic activity, indicative of ongoing tectonic stresses due to the convergent activity between the Indian and Myanmar plates, particularly within the NNE-SSW (N-S) trending arcuate belt of the IMR. The tectonic significance of the sedimentary column is evident through geological, superficial structural and tectonic lineament analyses. The resultant strain ellipse and associated stress regime, as inferred from field studies and supported by analyses of superficial structural features and tectonic lineaments, suggest a WNW-ESE compression and NNE-SSW extension, consistent with the geological and tectonic strike of the range.

Analysis of Fault Plane Solutions (FPS) reveals a nuanced stress pattern within the IMR, exhibiting variability across different depths. When the entire focal depth range is considered, the orientation of Principal Stresses (σ_1 or P = maximum, σ_2 or N = intermediate, and σ_3 or T = minimum) indicates NNE-SSW contraction and WNW-ESE extension, contrary to the stress pattern inferred from superficial structural features and tectonic lineament studies, suggesting a different deformation mechanism for the IMR. However, hierarchical focal depth analysis of FPS of earthquakes reveals a distinct stress pattern (**Fig. 1**). Deeper earthquakes, occurring at focal depths of 50 km and more, exhibit consistent NNE-SSW contraction and WNW-ESE extension showing principal stress orientation patterns of σ_1 = 029°/03°, σ_2 = 273°/58°, σ_3 = 115°/25° for 50-90 km focal depth (Zone-III), and σ_1 = 016°/05°, σ_2 = 283°/26°, and σ_3 = 108°/56° for > 90 km focal depth (Zone-IV). Conversely, shallower earthquakes with focal depths ranging between 20-50 km (Zone-II) demonstrate a polarised stress orientation pattern (σ_1 = 226°/07°, σ_2 = 336°/65°, and σ_3 = 120°/20°), while ultra-shallow earthquakes or Zone-I (focal

depth < 20 km) demonstrate nearly E-W compression and N-S extension ($\sigma_1 = 080°/01°$, $\sigma_2 = 037°/81°$, and $\sigma_3 = 353°/03°$).

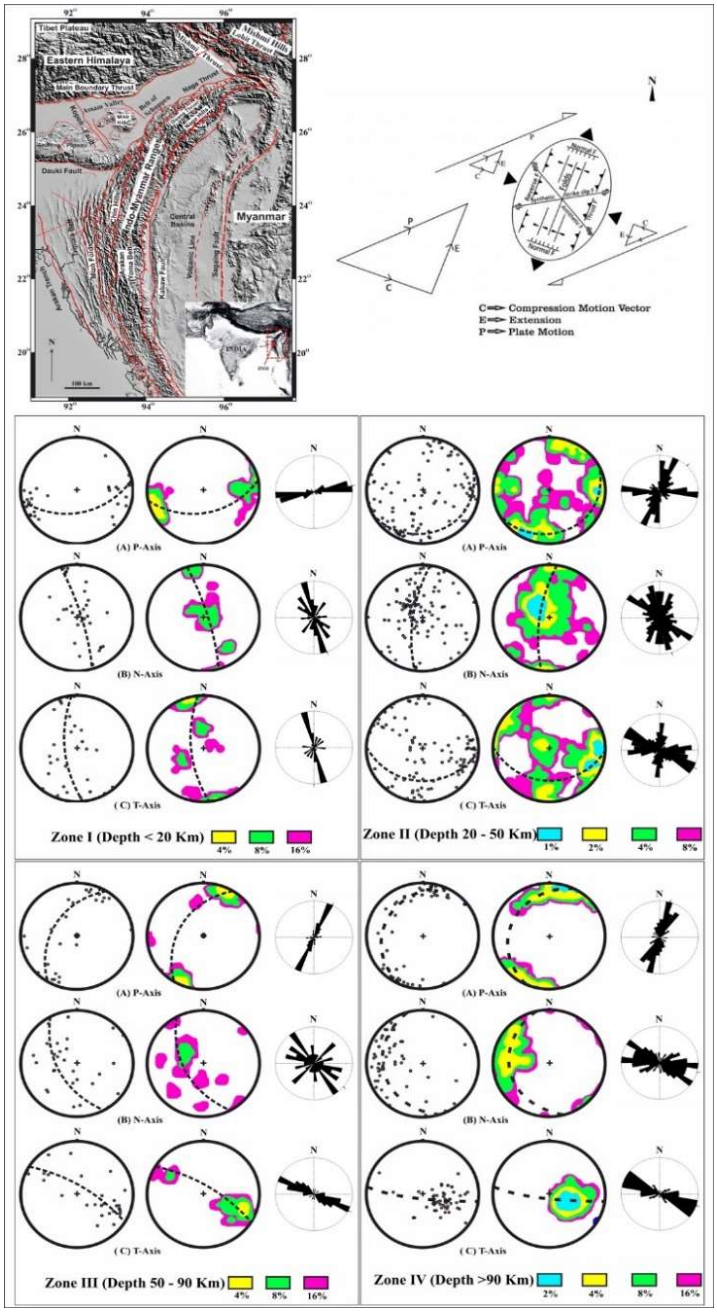

Figure 1: Top Left: Morphotectonic map of the IMR displaying the arcuate nature of the mountain range (adapted from Nandy 2001; Murthy et al. 1969; and Kayal 1998). **Top Right**: Dextral simple-shear deformation mechanism of the IMR (modified from Soibam 2006, Soibam et al. 2015). **Bottom**: Pole, contour and rosette diagrams of the three principal stresses of FPS for focal depths: Zone-I, II, III & IV.

The results of hierarchical focal depth analysis highlight the complexity of tectonic processes within the IMR, indicating that stress patterns vary not only horizontally but also vertically. Deeper earthquakes situated within the Indian Plate have been probably influenced by the NNE movement of the Indian Plate relative to the Eurasia Plate, consistent with the observed stress orientations. While the ultra-shallow earthquakes, displaying nearly E-W compression, consistent with superficial structural, topographic, and tectonic features, might have been controlled by the dextral shear coupling between the India plate and Myanmar microplate, especially the sedimentary pile of the IMR.

Keywords: Deformation mechanism, Fault plane solutions, Focal depths, Indo-Myanmar Ranges, Principal stresses

References:
Kayal, J.R., 1998. Seismicity of North East and surrounding— development over the past 100 years. Journal of Geophysics 29(1), 31–67
Murthy, M.V.N., Talukdar, S.C., Batthacharya, A.C., 1969. The Dauki Fault of Assam. Bulletin of Oil and Natural. Gas Commission 6, 57–64.
Nandy, D.R., 2001. Geodynamics of Northeastern India and the adjoining region. ACB publication, Calcutta, 209p
Soibam, I., 2006. Relative plate motions in and around Manipur and its implications on the tectonics of the Indo-Myanmar Ranges. Himalayan Geology 27, 111–122
Soibam, I., Khuman, M. CH., and Subhamenon, S.S., 2015. Ophiolitic rocks of the Indo-Myanmar Ranges, NE India: relicts of an inverted and tectonically imbricated hyper-extended continental margin basin? 413:301-331. https://doi.org/10.1144/sp413.12

GDT 21: Geomorpho-Tectono-Climatic Influence on Landscape Evolution and Natural Hazards in The Western Ghat of Indian Peninsula

S. Abdul Rahaman[1*] and Subhash Anand[2]

[1]*Delhi School of Climate Change and Sustainability, University of Delhi*
[2]*Department of Geography, Delhi School of Economics, University of Delhi*

*Corresponding Authors:
E-mail address: abdulatgeo@gmail.com (S. Abdul Rahaman)

Landscapes are gradually changing, and numerous natural hazards are increasing daily due to the tectonic upliftment, changing climatic patterns and seismicity influences in the Western Ghats region. More specifically, relatively active tectonic/neotectonic at a slow pace, whereas landslides and floods are the major events happening frequently every year. It causes the loss of several human life, properties, and the environment. This hazardous situation leads to disasters, which impact the forming of new landscapes. In order to understand the nuances and their nature of characteristics, the present study focused on geomorphic-tectonic and climatic influences on landscape evolution and natural hazards in the western ghat regions.

The Western Ghat is internationally recognized as a region of immense global importance for conserving biological diversity, besides containing areas of high geological, cultural and aesthetic values. The Western Ghat is a mountain range that in a stretch of 1,600 km (990 mi) parallel to the western coast of the Indian peninsula, traversing the states of Gujarat, Maharashtra, Goa, Karnataka, Kerala and Tamil Nadu (**Fig.1a**). The mountain chain of the Western Ghat represents geomorphic features of immense importance with unique biophysical and ecological processes, which is older than the Himalayan mountains (UNESCO). The most peculiar feature of the western ghat is the elevated passive margin with a well-defined escarpment (**Fig.1a**), which is the western continental margin of India (Kale, 2007, 2008; Radhakrishna et al., 2018). Geological evidence indicates that it was formed during the breakup of the Gondwana supercontinent ~150 million years ago (late Jurassic and early Cretaceous). Apart from their stunning beauty, the Western Ghats act to regulate weather and ecological patterns over the entire Indian peninsula. Running parallel to the western coast from Gujarat to Kerala, the Western Ghats "influence the Indian monsoon weather patterns that mediate the warm tropical climate of the region, presenting one of the best examples of the tropical monsoon system on the planet".

The landscape evolution and its upliftment in the western ghat margin is one of the complex assessments. During the last five decades, various researchers assumed a sustained uplift in the western continental margin of India (Athavale and Anjaneyulu, 1972; Powar, 1993; Radhakrishna, 1993; Widdowson and Cox, 1996; Gunnell, 2001; Valdiya, 2001; Campanile et al., 2008; Mukhopadhyay et al. 2008; Kale, 2008). Valdiya (2001) argued that the mega-feature cannot be just ascribed to isostatic uplift but to neotectonic resurgence. From this perspective, the present study focuses on understanding the neotectonic activities for landscape evolution. The researchers followed several assessment methods in this study to evaluate tectonic activity based on geomorphic proxies; it is a more efficient method (Kale, 2007, 2008; Ramkumar et al., 2019. 2024).

Similarly, climate has played a crucial role in landscape development and the formation of past climatic conditions. The unpredicted rainfall pattern and temperature variations lead to the development of new fluvial landscapes due to erosional and depositional features. However, this climatic change further leads to natural hazards such as landslides and floods in the high-altitude mountain terrain and the coastal plain regions of the Western Ghats. To evaluate this historical climate data, morphometric assessments are handy tools (Ramkumar et al., 2019; Yunus et al., 2021; Abdul Rahaman, 2021).

The Western Ghat has various natural and spectacular landscapes such as escarpments, plateaus, valleys, gorges, hill ranges, and cliffs – natural wonders that reflect the geological, structural and weathering process. These are one-way other ways that make important, influential factors for natural disasters like landslides, earthquakes, and floods. Yet, recurring floods and landslides in the mountains, hills, and areas downstream (between the Ghat and the sea) show that India must rethink its environmental law to balance the needs of nature and humans. There is much evidence for the multi-hazards in the Western Ghat, which has been studied individually or collectively. Landslides: Intense and excess rainfall in the Western Ghats region of Kerala, Karnataka and Tamil Nadu resulted in thousands of landslides. NRSC team mapped 6,970 landslides covering 22.6sqkms in the Western Ghats in August 2018, of which 83.2% were triggered by very high rainfall. This is the fourth consecutive year that Kerala has faced devastating landslides and loss of life. “Post the 2018 Kerala floods and major landslides in 2019 and 2020 in Puthumala (Biju and Shaji, 2013) and Pettimudi. In Karnataka state Chikkamagaluru, Kodagu landslide and floods in 2020, 2022. Every year, the Nilgiris have been facing landslides since 1900 in Tamil Nadu (Abdul Rahaman et al., 2014).

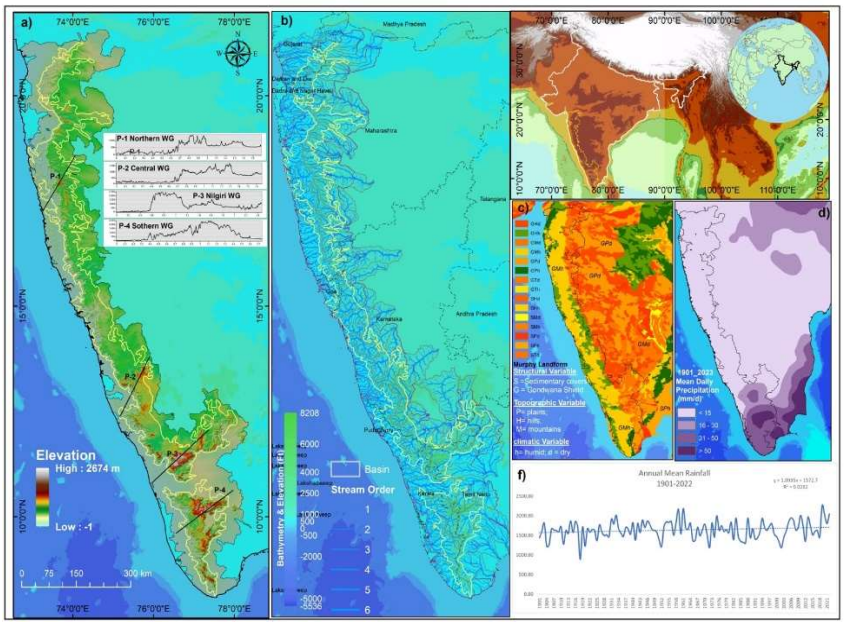

Figure 1: a) Western Ghat region elevation and its cross profile (P-1, 2, and 3) shows the escarpment. b) stream network and basins c) Landforms Based on the structural, topographic, and climatic variables; d-e) Historic mean daily precipitation data shows the spatial distribution and graph shows the mean annual rainfall variation in the western ghat region.

Overall, the goal is to assess the neotectonic activity-based landscape development and climatic interaction for the natural hazards in the western Ghat region. The entire study region was evaluated at watershed level, for that, it was demarcated into around a hundred basins (**Fig.1b**). Further, Geomorphotectonic proxies such as Asymmetry factor (Af), basin shape (Bs), valley width-height ratio (Vf), stream gradient-length ratio (SL), Mountain front (MF), Sinosity index (Si), basin elongation ratio (Re), Longitudinal profile, Hypsometric curve and integral (HI& HC) were calculated. Although selected morphometric attributes, i.e. Bifurcation ratio (Rb), Drainage Density (Dd), Circularity ratio(Cr), Length of overland flow (Lof), Relief ratio, and Melton Ruggednes (Mr), were computed to understand the linkage between natural hazards (landslides and floods). For that, the Shuttle Radar Topography Mission (SRTM) digital elevation model (DEM) has a spatial resolution of 30m. To investigate the climatic implication in the study region towards landscape development and natural hazards, 100-plus-year climatic variables were assessed. Historic gridded rainfall data (1901-2023), having the spatial resolution of 0.25 * 0.25 from the Indian Meteorological Department (**Fig. 1 d&f**).

The experimental study mainly elucidates the interlinking between tectonic activity and climate interaction on landscape development and natural hazards. Further, identify the emergence of new landscapes due to landslides and floods. This study will help geoscientists, academicians, and hazard and disaster mitigation agencies.

Keywords: Morpho-tectonic, Western ghat, Landslides and Floods, Geomorphic proxies

References:

Abdul Rahaman, S., Aruchamy, S., Jegankumar R., 2014. Geospatial approach on landslide hazard zonation mapping using multi criteria decision analysis: a study on Coonoor and Ooty, part of Kallar watershed, The Nilgiris, Tamil Nadu. The International Archives of the Photogrammetry, Remote Sensing and Spatial Information Sciences XL-8, 1417-1422. https://doi.org/10.5194/isprsarchives-XL-8-1417-2014

Abdul Rahaman, S., 2021. Morphometric assessment of hydrogeomorphic processes and landscape evolution in the Kallar watershed (Western Ghats, India): regionalisation and prioritization, Arabian Journal of Geosciences 14, 1861. https://doi.org/10.1007/s12517-021-08105-z

Athavale, R.N., Anjaneyulu, G.R., 1972. Palaeomagnetic results on the Deccan Trap lavas of the Aurangabad region and their tectonic significance; Tectonophysics 14, 87–103.

Biju A.P., Shaji, E., 2013. Landslide hazard zonation in and around Thodupuzha-Idukki-Munnar road, Idukki district, Kerala: A geospatial approach. Journal of the Geological Society of India 82, 649–656. https://doi.org/10.1007/s12594-013-0203-7

Campanile, D., Nambiar, C.G., Bishop, P., Widdowson, M., Brown, R., 2008. Sedimentation record in the Konkan–Kerala Basin: Implications for the evolution of the Western Ghats and the Western Indian passive margin. Basin Research 20 3–22.

Gunnell, Y., 2001. Dynamics and kinematics of rifting and uplift at the western continental margin of India: Insights from geophysical and numerical models; Geological Society of India Memoir 47, 475–496.

Kale, V.S., Rajaguru, S.N., 1988. Morphology and denudation chronology of the coastal and Upland river basins of western Deccan Trappean landscape India: A collation; Zeitschrift f¨ ur Geomorphologie 32, 311–327.

Kale V.S., Shejwalkar, N., 2007. Western Ghat escarpment Evolution in the Deccan Basalt Province: Geomorphic observations based on DEM analysis. Journal of the Geological Society of India 70, 459–473.

Kale V.S. Shejwalkar, N., 2008. Uplift along the western margin of the Deccan Basalt Province: Is there any geomorphometric evidence?. Journal of Earth System Science 117(6), 959–971.

Mukhopadhyay, R., Rajesh, M., De, S., Chakraborty, B., Jauhari, P., 2008. Structural highs on the western continental slope of India: Implications for regional tectonics; Geomorphology 96, 48–61.

Powar, K.B., 1993. Geomorphological evolution of Konkan coastal belt and adjoining Sahyadri uplands with reference to Quaternary uplift; Current Science 64, 793–796.

Radhakrishna, B.P., 1993. Neogene uplift and geomorphic rejuvenation of the Indian peninsula. Current Science 64 787–793

Radhakrishna, T., Mohamed, A.R., Soumya G.S., Prachiti P. K., 2019. Mechanism of rift flank uplift and escarpment formation evidenced by Western Ghats, India, Scientific Reports 9, 10511. https://doi.org/10.1038/s41598-019-46564-3

Ramkumar, M., Santosh, M., Abdul Rahaman, S., Balasundareshwaran, A., Balasubramani, K., Mathew, M.J., Sautter, B., Siddiqui, S.N., Usha, K., Sreerhishiya, K., Prithiviraj, G., Nagarajan, R., Thirukumaran, V., Menier, D., Kumaraswamy, K., 2019. Tectono-morphological evolution of the Cauvery, Vaigai and Thamirabarani River basins: Implications on timing, stratigraphic markers, relative roles of intrinsic and extrinsic factors and transience of southern Indian landscape. Geological Journal 54, 2870–2911.

Ramkumar, M., Nagarajan, R., Juni, K.J., Manobalaji, A., Balasubramani, K., Roy, P.D., Kumaraswamy, K., Fathima, A.L., Pramod, A., Sharveen, R., Rahman, S.A., Siddiqui, N.A., Menier, D., Sharma, R., 2024. Tectono-climatic and depositional environmental controls on the Neolithic habitation sites, Vaigai River Basin, Southern India. Geological Journal, 1199-1218. https://doi.org/10.1002/gj.4919

Yunus, A.P. Fan, X., Siva Subramanian, S., Jie, D., Xu Q., 2021. Unraveling the drivers of intensified landslide regimes in Western Ghats, India. Science of the Total Environment 770, 145357. https://doi.org/10.1016/j.scitotenv.2021.145357

Widdowson, M., Cox, K.G., 1996. Uplift and erosional history of the Deccan Traps India: Evidence from laterites and drainage patterns of the Western Ghats and Konkan coast; Earth and Planetary Science Letters 137, 57–69.

Valdiya, K.S., 2001. Tectonic resurgence of the Mysore plateau and surrounding regions in cratonic southern India. Current Science 81, 1068–1089.

GDT 22: Lithospheric Architecture of the Singhbhum Craton: New insights from Gravity Investigations

A. Vasanthi[1*]

[1]*CSIR-National Geophysical Research Institute, Hyderabad-500007, India.*

*Corresponding Author:
E-mail address: vasanthi@ngri.res.in (A.Vasanthi)

The construction and destruction of cratons, continents and supercontinents on the globe involved multiple events of the plume, rifting, subduction-accretion, and collision through the long history of evolution of our planet. Archean cratons preserve the records of continent building in the early Earth,

and understanding their lithospheric architecture is fundamental in building geodynamic models. The Singhbhum craton is one among the five Archean cratons of Peninsular India that preserves some of the oldest continental nuclei. High-resolution ground gravity data of the Singhbhum Craton has been analyzed to understand the regional lithospheric architecture and the geodynamic evolution of the craton. The residual gravity anomaly (**Fig. 1**), deduced by using the Finite Element Method, clearly demarcated the boundaries of major geotectonic units of the Craton. The conspicuous presence of high-order residual gravity low anomalies, together with low estimated densities, suggests voluminous presence of Singhbhum granitic batholiths that built the dominant crustal architecture. The isolated residual gravity highs correspond to the mafic and ultramafic volcanic suites like Dhanjori, Simlipal and Dalma, while the relatively low gravity anomalies observed over the western volcanic suites like Malangtoli, Jagannathpur and Ongarbira, indicate their relatively felsic nature. The estimated lithospheric thickness of about ~ 130 km below the granitic batholithic region, and about 110 km beneath the Precambrian volcanic terranes, together with low effective elastic thickness (T_e) of only about 30 km, suggest a thin and weak lithosphere. The craton witnessed extensive lithospheric destruction with the removal of nearly 100–150 km of the cratonic root. The decratonization may be linked to persistent thermo-dynamic activities, mantle upwelling induced rise of mantle isotherms, together with mantle plumes at different times, suggesting a combined mechanical, thermal and chemical erosion of the cratonic keel.

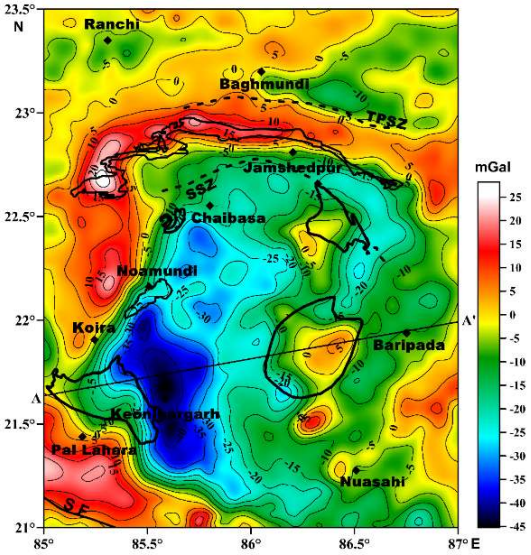

Fig.1: Residual gravity anomaly map of Singhbhum Craton. Black polygons represent the boundaries of different volcanic suites. AA' is an E-W Profile along which 2.5D gravity modelling has been carried out in order to delineate the crustal and lithospheric architecture beneath this Craton.

GDT 23: Strain analysis using different markers and their tectonic implications on Indo-Myanmar Ranges of North-East India

Thokchom Nilamani[1*] and Soibam Ibotombi[1]

[1]*Department of Earth Sciences, Manipur University, Canchipur*

*Corresponding Author:
E-mail address: thokchomnila@gmail.com (T.Nilamani)

The Indo-Myanmar Ranges (IMR), a tectonic belt resulting from the oblique subduction of the Indian Plate beneath the Myanmar (Burmese) microplate, exhibits a stress regime characterized by east-west (WNW-ESE) compression and north-south (NNE-SSW) extension. Geologically, the eastern part of the IMR comprises metamorphic rocks atop an ophiolite mélange zone, while the central part is dominantly

flysch sediments, and to the west, relatively younger molassic sequence is common (**Fig. 1a**). This study aims to elucidate the deformation mechanism and tectonic history of the IMR by analyzing the strain parameters of conglomerate pebbles and concretionary mud balls found in the Nagaland and Manipur sections (Field photographs as shown in **Fig.1b,c,d and e**). Using Flinn Plots and the Rf/φ method for strain measurement, we examine conglomerate pebbles from the Ukhrul (Manipur) and Thewati (Nagaland) regions. These pebbles fall within the constriction and flattening fields on the Flinn Plots, exhibiting LS-tectonite structures (**Fig. 1g, h**). Notably, the Nagaland section displays higher strain intensity compared to that of Manipur. In contrast, concretionary mud balls from the flysch sediments of the Imphal Valley (Manipur) predominantly exhibit S-tectonite, showing layer parallel compression (**Fig. 1i**). The long strain axis has an orientation of 11°/017° (**Fig. 1d, f**), aligning with the regional extension direction, NNE of IMR. Mud balls from the Pfutsero region (Nagaland) also lie within the flattening and constriction fields (**Fig. 1i**), indicating a transpression and transtension regime. Rf/φ plot analysis reveals tectonic strain (Rs) values of 1.4 and 2.4, in the Ukhrul region whereas in the Akhen region of Nagaland, the Rs value is 1.89, indicating low tectonic strain and moderate to high fluctuations in both the regions. These findings provide critical insights into the states of strain across the IMR of Northeast India.

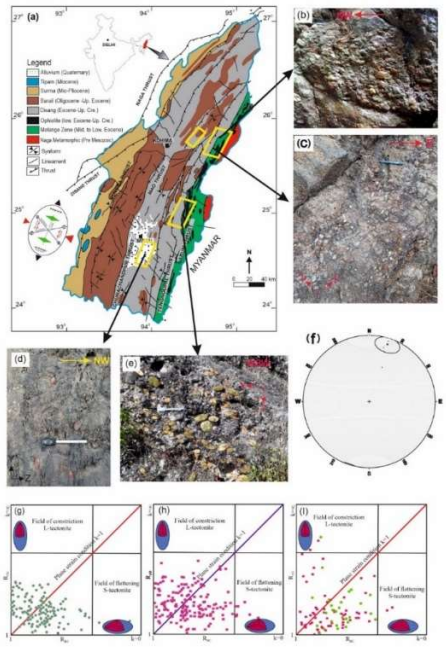

Figure 1: (a) Geological map of the Manipur and Nagaland regions of the Indo-Myanmar Ranges, study area highlighted in yellow boxes; (b),(c),(e) Field photographs showing different conglomerate exposures in Thewati, Reguri and Ukhrul region respectively. (d) Field photograph showing YZ-plane of mudballs associated with flysch sediments of the Disang Shale of Imphal valley; (f) Stereo plot illustrating the orientation of the maximum strain axes direction; (g) and (h) Flinn plots showing distribution of conglomerate pebbles of Thewati and Ukhrul regions, respectively; and (i) Flinn plots displaying the distribution of mud balls of Pfutsero (red dots) and the Imphal Valley (green dots).

GDT 24: Geochemical Study of Serpentinised Peridotite from Indian Ocean: Insights into Mantle Evolution and Tectonic Settings

Mrunali Pilgaonkar[1*]

[1]*Applied Geology Programme, School of Earth, Ocean and Atmospheric Science, Goa University, Goa, India*

*Corresponding Author:
E-mail address: mrunalipilgaonkar29@gmail.com (M.Pilgaonkar)

The present study delves into the petrography, mineral chemistry, and whole-rock chemistry of serpentinite peridotite, obtained from a depth of 2700 meters at latitude 06° 38.506' S and longitude 68° 19.340' E, situated between the Vityaz and Vema Fracture Zones on the Central Indian Ridge. These samples were collected in 2003 during the Sagar Kanya SK-195 cruise (DR#9) organized by the

National Institute of Oceanography in Dona Paula, Goa. Our study aims to elucidate the geochemical systematics of abyssal peridotites, focusing on the impact of hydrothermal alteration on their composition. Through this research, we seek to enhance the understanding of the geochemical budget of the lithosphere at slow and ultraslow spreading ridges. Detailed petrographic analysis revealed high-relief olivine and clinopyroxene, with orthopyroxene showing high-temperature deformation along with the presence of opaque Cr spinel and magnetite minerals. Mesh and Brucite textures are prominent. The degree of Serpentinization was confirmed by the presence of antigorite, lizardite, and chrysotile, examined through EPMA and BSE imaging. With the help of the data obtained from the mentioned analytical techniques various observations were made, and along with EPMA, Major and Whole Rock Geochemistry with special emphasis on the certain Trace element is made in order to understand the origin, the genesis and the setting in which the rock must have originally formed. Geochemical data indicated a harzburgitic protolith with iron-rich lizardite and significant Fe enrichment in chromiferous spinel. Spinel, a quantitative melting indicator of mantle residues, exhibits compositional diversity and relative proportions of Cr, Fe, and Al in spinel-group minerals. This variation in melting extent highlights the influence of spreading rates on the degree of mantle melting and underscores the utility of $Cr^{\#}$ values in assessing magma extraction processes in mantle-derived rocks. REE (**Fig. 1**) patterns showed a distinct U-shape with a positive Eu anomaly, suggesting the absence of plagioclase feldspar. Major element analyses, supported by MgO/SiO_2 vs. Al_2O_3/SiO_2 trends, indicated 25-30% of partial melting, and also negative magnesium loss trend was observed, Contrary to the conventional seafloor weathering patterns, differentiation processes manifested through mineral transformations from olivine to serpentine may present distinctive characteristics. This study explores the implications of such mineralogical changes, where serpentinization, driven by hydrothermal alteration and mantle dynamics, results in unique weathering profiles. The stability, chemical composition, and physical properties of serpentine contrast sharply with those of olivine, leading to variances in seafloor topography and erosion. Understanding these transformative processes offers critical insights into the complex interactions within oceanic geological and hydrological systems. The peridotites of the Central Indian Ridge (CIR) present a strikingly diverse array of compositions, driven by both melt-rock interactions and the pervasive influence of hydrothermal alteration. The intricate behavior of highly incompatible elements (HFSE) and rare earth elements (REE) plays a pivotal role in shaping these variations across different sites. Abyssal peridotite samples have elucidated the profound impact of regional geological processes and environmental conditions. The $Cr^{\#}$ and $Mg^{\#}$ ratios in spinel, alongside variations in Th, Zr, and Nb concentrations, reflect intricate melt-rock interactions. The characteristics of serpentinized peridotites suggest a heterogeneous origin influenced by multiple tectonic episodes and common source material. These insights advance our understanding of serpentinization, mantle melting processes, and the geochemical evolution of oceanic peridotites.

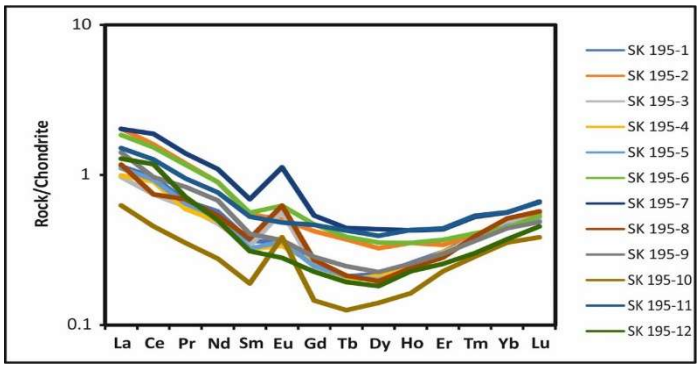

Figure 1. Chondrite normalised REE patterns showed a distinct U-shape with a positive Eu anomaly for the Serpentinised Peridotite

GDT 26: Mantle potential temperature and felsic continental crust control the initiation and cessation of plate tectonics

Liangliang Wang[1,2], Liming Dai[1,2], Sanzhong Li[1,2*], Peter A. Cawood[3], Robert Stern[4], Taras Gerya[5], Zhong-Hai Li[6], Xiaohui Li[1,2], Wenyong Duan[1,2], Shihua Zhong[1,2], Guozheng Sun[1,2], Shengyao Yu [1,2]

[1]*Frontiers Science Center for Deep Ocean Multispheres and Earth System, Key Lab of Submarine Geosciences and Prospecting Techniques, MOE and College of Marine Geosciences, Ocean University of China, Qingdao 266100, China*
[2]*Laboratory for Marine Mineral Resources, Laoshan Laboratory, Qingdao 266100, China*
[3]*School of Earth, Atmosphere and Environment, Monash University, Melbourne, VIC, 3800, Australia*
[4]*Department of Sustainable Earth Systems Sciences, U Texas at Dallas, Richardson, TX 75080, USA*
[5]*Swiss Federal Institute of Technology (ETH-Zurich), Zurich, Switzerland*
[6]*Key Laboratory of Computational Geodynamics, College of Earth and Planetary Sciences, University of Chinese Academy of Sciences, Beijing, China*

*Corresponding Author:
E-mail address: sanzhong@ouc.edu.cn (Sanzhong Li)

Understanding the initiation of plate tectonics on Earth is crucial for unraveling our planet's geological history and understanding its unique tectonic regime. The roles of mantle cooling and continental crust growth in triggering plate tectonics remain controversial, in part due to the paucity of quantifiable evidence. We employ two-dimensional numerical models to investigate the process, timing, and underlying mechanism of tectonic regime transitions throughout the Earth's history. Our simulations reveal two pivotal transition points, i.e., initiation and cessation timings, that divide the evolution of global plate tectonics into three stages. These transitions reflect the thickening and strengthening of the lithosphere with long-term cooling of Earth's mantle. Initially, subduction initiation (SI) was difficult, and Earth's tectonic regime was characterized by vertical dripping and delamination. This transitioned into a second stage where SI is easier, requiring forces only slightly greater than the ridge push force, and is when plate tectonics became possible. Finally, in the third stage, SI is again difficult, with excessively large initiation forces required, signifying the cessation of global plate tectonics. We demonstrate that the lithospheric density and strength, as well as the contrasts between oceanic and continental lithospheres, governed by mantle cooling and influenced by continental growth, orchestrated the interplay between plate rigidity and localized weakening under horizontal motion, driving these tectonic transitions. Integrating our models with the geological record suggests that a transition to plate tectonics became possible by 2.4 Ga-1.8 Ga, whereas the eventual cessation of plate tectonics is likely to occur in 2.1 Ga into the future. Progressive strengthening of the lithosphere with mantle cooling is generally applicable to planetary evolution and may provide valuable insights for the tectonic evolution of other active silicate planets, including Mars and Venus.

GDT 27: Locating South China and Tarim In the Assembly of Greater Malani Supercontinent

Naresh Kochhar[1*]

[1]*Department of Geology, Panjab University, Chandigarh, 160014, India*

*Corresponding Author:
E-mail address: Nareshkochhar2003@yahoo.com (Naresh Kochhar)

Abstract: The palaogeographic position of South China and Tarim in the Rodinia Supercontinent-peripheral or central is debatable. We present here evidence, which indicates that this duo was attached to the Trans-Aravalli Block of the North-Western Indian shield and formed a part of the Late Proterozoic Greater Malani Super Continent.

Keywords: Malani Magmatism, Rajasthan, Supercontinent, South Chine, Tarim, Oxygen Isotope, Palaeomagnetism

Introduction

The Trans Aravalli - Block (TAB) is unique in the geological evolution of the Indian shield as it marks a major period of anorogenic (A-type), 'Within Plate', high heat producing (HHP) magmatism represented by the Malani igneous suite of rocks (MIS). The Neoproterozoic Malani igneous suite (55,000 km²; 732 Ma) comprising peralkaline (Siwana), metaluminous to mildly peralkaline (Jalor), and peraluminous (Tusham and Jhunjhunu) granites with cogenetic carapace of acid volcanics (welded tuff, trachyte, explosion breccia and perlite etc.) are characterized by volcano-plutonic ring structures and radial dykes (**Fig. 1**). The suite is bimodal in nature with minor amounts of basalt, gabbro, and dolerite dykes. The Siwana ring structure (30 km in EW 25 km in NS direction) is the most spectacular feature of the Thar Desert (**Fig. 2**). The representatives of Malani suite also occur at Kirana Hills, and at Nagar Parkar, Sindh, Pakistan. The Malani magmatism is controlled by NE SW trending lineaments (zones of extension and high heat flow) of fundamental nature (mantle) and owes its origin to mantle plume (for review, Kochhar 2015, 2019, Eby and Kochhar 1990, Om Prakash et al. 2020).

The Greater Malani Supercontinent: The period ca. 732 Ma B.P. marks a major Pan African tectono magmatic event of widespread magmatism of alkali granites and comagmatic acid volcanic (anorogenic, A-type) in the Trans- Aravali block of the Indian shield, central Iran, Somalia, Nubian-Arabian shield and Madagascar and south China, Somalia. In view of the widespread ca. 750 Ma alkaline magmatism, which is so widespread, and well documented in TAB, central Iran, Arabian- Nubian shield, Madagascar and S. China, Somalia, Seychelles, Siberia, Tarim, Mongolia, Kazakhstan (Kochhar, 2007, 2008, 2013 and 2019) proposed that all these microcontinents were characterized by common crustal stress pattern, rifting, thermal regime, Strutian glaciation and subsequent desiccation and similar paleo- latitudinal positions which could be attributed to the existence of a supercontinent-the Greater Malani Supercontinent (**Table 1**). This assembly and subsequent breakup marked rift to drift tectonic environment.

South China and Tarim: The paleogeographic position of major continental blocks in Rodinia and Gondwana has been accepted but for South China, Tarim and India during the transition from Rodinia to Gondwana remains debatable (Wen et al., 2017). We suggest that South China, Tarim were connected to the Trans Aravalli Block (TAB) of the Northwestern Indian shield during the late Proterozoic.

Kochhar (2007) was probably the first to suggest that South China was attached to the TAB (Trans Aravalli Block) of the North Western Indian shield during the late Proterozoic. In the Yangtze craton of South China, peralkaline to alkaline 'within plate magmatic rocks (pre-rift 830-795 Ma) with the coeval swarms of mafic dykes have been attributed superplume. This syn-rift Chengian magmatism has been correlated with the Malani magmatism (Li et al., 2003). It has also been suggested that the South China –India duo was connected to India during the Neo-proterozoic- Early Cambrian time. This separation took place due to the opening of Proto-Tethys. Liu et al. (2020) have also suggested the location of the Tarim craton between South China and North India in the periphery of Rodinia. The Yangtze block of South China and NorthWest India share similar Late Tonian rift-related siliciclastic volcanics succession, cryogenic glaciogenic diamictites succession, Edicara carbonate succession and early Cambrian phosphorite and clastic succession (Wang and Li 2003; Qi et al., 2020). This set of data suggests that South China remains closely linked with India and formed a South China- India duo (c.f. Cawood et al., 2013; Liu et al., 2023).

Recent paleomagnetic data also shows $\delta^{13}C$ excursion hosted by Doushantio member corresponding with Krol B $\delta^{13}C$ (Himalaya) and poles from Marwar Supergroup, Jodhpur Indicate South China was close to Rajasthan during Ediacara (Zhang et al., 2015).

The Ca 820-710 Ma sedimentation and bimodal magmatism due to Nanhua rifting across South

China also match well with rifting-related episodes of Tarim (Yao et al., 2019). These thermo tectonic events comparison indicates Tarim and S. China were more related to India before 0.9 Ga (Chang et al., 2023; Wang et al., 2022). As in the TAB Tarim basin also, rhyolites and granites of A-type (735±10 Ma) existed during the Nanhua period in response to the break up of the Rodinia Supercontinent (Wu et al., 2018; Cawood et al., 2016). Based on provenance studies, (Han et al., 2024) have suggested that the Northern part of the Yangtze craton was an extensional tectonic setting before 526 Ma and the collision between the Yangtze block and Gondwana was completed at 526 Ma which was related to the closure of Yangtze associated Proto-Tethys ocean.

Paleomagnetic data: The AAPW paleomagnetic poles at ca. 800 Ma B.P. place South China at 55-70° N (Li et al., 2004) at par with the paleolatitudes of India during Malani Rhyolite period 'ca. 750 Ma. Around 700 Ma B/P India started drifting towards the tropical latitudes and around 600 Ma, India was near the equator (Poornachandra Rao et al., 1997). India and South China were located at high latitude at 800 Ma, and paleomagnetic data suggest that they underwent a 35^0 counterclockwise rotation 720 Ma (Merdith et al., 2017).

Archean xenocryst zircon from Mauritius: Recent discovery by Ashwal et al. (2017), of 3.2 Ga Archean crust (BGC protolith) beneath Mauritius supports Seychelles, Madagascar and Arabian shield were connected with the Northwestern shield in the configuration of the Greater Malani Supercontinent.

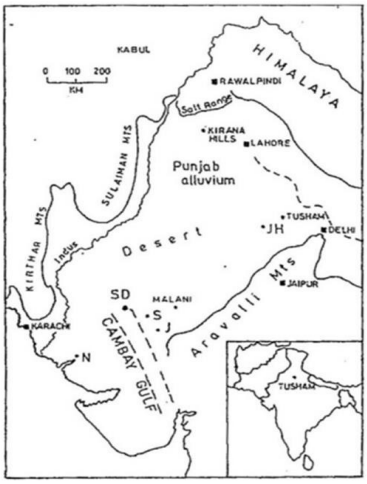

Figure 1. Location map of Malani Igenous Suite, India. J: Jalor, JH: Jhunjhunu, S: Siwana , N: Nagarparkar, SD: Sarnu-Dhandali

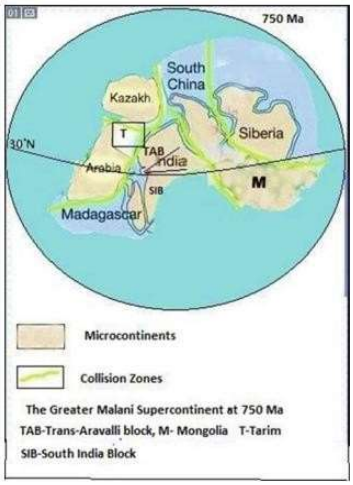

Figure 2. Assembly of the Greater Malani supercontinent at 750 Ma

Conclusions: From the aforesaid, it is obvious that comparison of plume-related bimodal, anorogenic magmatism, paleogeogrpahic position, sedimentation, carbon and oxygen isotope data support that South China and Tarim were part of the Greater Malani Supercontinnt during late Proterozoic.

Table 1 Summary of similarities between TAB, Seychelles, Nubian-Arabian Shield, South China, Kazakhistan, Siberia,and Mongolia (Kochhar, 2013, Levashova et al., 2011, Jahn, 2004, Tucker et al., 2001).

	TAB NW Indian shield	**Seychelles**	**Nubian-Arabian shield**	**S. China Yangtze block**	**Kazakhistan**	**Siberia**	**Mongolia**
Alkali magmatism granites	Siwana Jalor Tusham CA 745 Ma	Mahe, Ste Anna Praslin 700 – 755 Ma	Jabal-Al Hasasin Jabal- As Sawal Dahul 700-760 Ma	Chengjian 780-745 Ma	Kopa formation 775 Ma Red gneissgranite	SW Margin Tataraka -Ishimila suture zone Srednetalar-ska pluton 671-774 Ma Mafic Dykes (Nersal) 740 Ma	Barguzinsky block 850-700 Ma
Protolith	Archean BGC	Archean BGC	Paleo Proterozoic or older crustal precursor	-	Anrakhai Terrane 1789±0.6 Ma 2187±0.5 Ma εNd (t)-6.4	-	Ust. Angara complexes εNd (t) +8 to -6 Juvenilecrust
Paleople	55-70°N	30°N	-	70°N	-	-	-

Strutian glaciations	Pokhran, Salt range boulder bed	-	Haqf super group	Linatua and Nantua deposits	Upper part of sequence underling Karatan	Norlhein Siberna	Olokit graben
Evaporite/ carbonate sequence	Hanseran, Nagaur-BikanerBasin	-	Hormuz series	Late Sinian Late Pre cambrian carbonates and phosphates	South Tyan Shan	Kuonanm Black Shale	Darkhat and Khubsugul Series

Acknowledgement: This research is supported by Panjab University, Chandigarh and University Grant Commission, New Delhi, UGC Emeritus fellowship. This is IGCP 648 contribution.

References

Ashwal, L. D., Wiedenbeck, M., Torsvik, T. H. 2017. Archaean zircons in Miocene oceanic hotspot rocks establish ancient continental crust beneath Mauritius. Nature Communications 8(1), 14086.

Cawood, P. A., Wang, Y., Xu, Y., Zhao, G., 2013. Locating South China in Rodinia and Gondwana: A fragment of greater India lithosphere?. Geology 41(8), 903-906.

Cawood, P. A., Strachan, R. A., Pisarevsky, S. A., Gladkochub, D. P., and Murphy, J. B., 2016, Linking collisional and accretionary orogens during Rodinia assembly and breakup: Implications for models of supercontinent cycles: Earth and Planetary Science Letters 449, 118–126. https://dx.doi.org/10.1016/j.epsl.2016.05.049

Chang, H., Hou, G., Huang, S., Luo, C., Xia, J., Zhong, Z., ... Wei, L., 2023. Analysis of proto-type Tarim Basin in the late Precambrian and the dynamic mechanism of its evolution. Plos one 18(6), e0286849.

Eby, G. N., Kochhar, N., 1990. Geochemistry and petrogenesis of the Malani igneous suite, North Peninsular India. Journal of the Geological Society of India 36(2), 109-130.

Han, Y., Ran, B., Santosh, M. Liu, S., Li, Z., Ye, Y., Lv, F., Wang, H., Li, C., 2024. The Cambrian collision of the Yangtze Block with Gondwana: Evidence from provenance analyses. GSA Bulletin https://doi.org/10.1130/B37470.1

Jahn, B. M., 2004. The Central Asian Orogenic Belt and growth of the continental crust in the Phanerozoic. Geological Society, London, Special Publications, 226(1), 73-100.

Kochhar, N., 2015. The Malani Supercontinent. The Frontiers of Earth Science 122-136.

Kochhar, N., 2007. Was Yangtze craton. S. China attached to the Trans-Aravali Block of the NW Indian shield during Late Proterozoic? Current Science 92, 295-297.

Kochhar, N., 2008. Geochemical signatures of the A-type Malani magmatism, NW peninsular India, and the assembly of Late Proterozoic Malani supercontinent. Geological Society of India Memoir 73, 21-36.

Kochhar, N., 2019. Archean Continental Crust Beneath Mauritius, and Low Oxygen Isotopic Compositions from the Malani Rhyolites, Rajasthan, (India): Implication for the Greater Malani Supercontinent with Special Reference to South China, Seychelles and Arabian-Nubian Shield. In The Structural Geology Contribution to the Africa-Eurasia Geology: Basement and Reservoir Structure, Ore Mineralisation and Tectonic Modelling: Proceedings of the 1st Springer Conference of the Arabian Journal of Geosciences (CAJG-1), Tunisia 2018 (pp. 41-45). Springer International Publishing.

Kochhar, N., 2013. The Greater Malani Supercontinent: Siberia, Mongolia, Kazakhstan and Tarim connection during late Proterozoic. Rodinia 2013: Supercontinent cycle and Geodynamics Symposium, Moscow University, Russia, Abstract-volume, 44.

Li, Z.X., Id, X.H., Kinney, P.D., Wang, J. Zhang, S., Zhou, H., 2003, Geochronology of Neoproterozoic syn-rift magmatism in the Yangtze craton, S. China and associated rocks and correlation with other continents: evidence for a mantle superplume that broke up Rodinia. Precambrian Research 22, 85-109.

Li, Z. X., Evans, D. A. D., Zhang, S., 2004. A 90 spin on Rodinia: possible causal links between the Neoproterozoic supercontinent, superplume, true polar wander and low-latitude glaciation. Earth and Planetary Science Letters 220(3-4), 409-421.

Levashova, N. M., Gibsher, A. S., Meert, J.G., 2011. Precambrian microcontinents of the Ural-Mongolian Belt: New paleomagnetic and geochronological data. Geotectonics 45(1), 51-70.

Liu, B., Peng, T., Fan, W., Zhao, G., Gao, J., Dong, X., ... Peng, B., 2023. Correlation between South China and India and development of double rift systems in the South China–India Duo during late Neoproterozoic time. GSA Bulletin 135(1-2), 351-366.

Liu, Q., Zhao, G., Li, J., Yao, J., Han, Y., Wang, P., Tsunogae, T., 2020. Detrital zircon U-Pb-Hf isotopes of middle Neoproterozoic sedimentary rocks in the Altyn Tagh Orogen, southeastern Tarim: insights for a Tarim-South China-North India connection in the periphery of Rodinia. Lithosphere 2020(1), 8895888.

Merdith, A. S., Collins, A. S., Williams, S. E., Pisarevsky, S., Foden, J. D. Archibald, D. B., Blades, M. L., Alessio, B.L., Armistead, S., Plavsa, D., Chris Clark, Müller, R. D., 2017. A full-plate global reconstruction of the Neoproterozoic. Gondwana Research 50, 84-134.

Poornachandra Rao, G. V. S., Mallikarjuna Rao, J., Chako, S. T., Subrahmanyam, K.. 1997. Palaeomagnetism of Baghain Sandstone Formation, Kaimur Group. Journal of Geophysical Union 1, 41-48.

Om Prakash, Singh A.P., Prasad, K.N.D., Nageswara Rao, B., Pandey, A.K., 2020. Remnant plume head under Neoproterozoic Malani igneous suite, western India. Tectonophysics 792, 228576.

Qi, L., Cawood, P. A., Xu, Y., Du, Y., Zhang, H., Zhang, Z., 2020. Linking south China to North India from the late Tonian to Ediacaran: Constraints from the Cathaysia block. Precambrian Research 350, 105898.

Tucker, R. D., Ashwal, L. D., Torsvik, T. H., 2001. U–Pb geochronology of Seychelles granitoids: a Neoproterozoic continental arc fragment. Earth and Planetary Science Letters 187(1-2), 27-38.

Wang, J., Li, Z. X. 2003. History of Neoproterozoic rift basins in South China: implications for Rodinia breakup. Precambrian Research 122(1-4), 141-158.

Wang, P., Zhao, G., Cawood, P. A., Han, Y., Yu, S., Liu, Q., ... Zhang, D., 2022. South Tarim tied to north India on the periphery of Rodinia and Gondwana and implications for the evolution of two supercontinents. Geology 50(2), 131-136.

Wen, B., Evans, D.A.D., Li, Y-X., 2017. Neoproterozoic paleogeography of the Tarim Block: An extended or alternative "missing-link" model for Rodinia? Earth and Planetary Science Letters 458, 92-106 https://doi.org/10.1016/j.epsl.2016.10.030

Wu, G., Xiao, Y., Bonin, B., Ma, D., Li, X., Zhu, G., 2018. Ca. 850 Ma magmatic events in the Tarim Craton: Age, geochemistry and implications for assembly of Rodinia supercontinent: Precambrian Research 305, 489–503, https://dx.doi.org/10.1016/j.precamres.2017.10.020

Yao, J., Cawood, P. A., Shu, L., Zhao, G., 2019. Jiangnan orogen, South China: a~ 970–820 Ma Rodinia margin accretionary belt. Earth-

Science Reviews 196, 102872.
Zhang, S., Li, H., Jiang, G., Evans, D. A., Dong, J., Wu, H., ... Xiao, Q., 2015. New paleomagnetic results from the Ediacaran Doushantuo Formation in South China and their paleogeographic implications. Precambrian Research 259, 130-142.

GDT 28: Neoarchean orogenic belt evolution in the northeast North China Craton: Implications for the reconstruction of early Earth's microplates

Guozheng Sun[1,2*], Sanzhong Li[1,2*], Shuwen Liu[3*], Timothy M. Kusky[4], Fangyang Hu[5], Han Bao[3], Lei Gao[6], Yalu Hu[7], Shengyao Yu[1,2], Liming Dai[1,2], Lintao Wang[1,2], Xi Wang[1,2]

[1]*Frontiers Science Center for Deep Ocean Multispheres and Earth System, Key Lab of Submarine Geosciences and Prospecting Techniques, MOE and College of Marine Geosciences, Ocean University of China, Qingdao 266100, PR China*
[2]*Laboratory for Marine Mineral Resources, Qingdao National Laboratory for Marine Science and Technology, Qingdao 266237, PR China*
[3]*Key Laboratory of Orogenic Belts and Crustal Evolution, Ministry of Education, Peking University, Beijing 100871, PR China*
[4]*State Key Lab for Geological Processes and Mineral Resources, Center for Global Tectonics, School of Earth Sciences, China University of Geosciences, Wuhan, 430074, China*
[5]*Key Laboratory of Mineral Resources, Institute of Geology and Geophysics, Chinese Academy of Sciences, Beijing 100029, China*
[6]*School of Earth Sciences and Resources, China University of Geosciences Beijing, Beijing 100083, PR China*
[7]*Development Research Center, China Geological Survey, Beijing 100037, PR China*

*Corresponding Authors:
E-mail address: sunguozheng@ouc.edu.cn (Guozheng Sun); sanzhong@ouc.edu.cn (Sanzhong Li); swliu@pku.edu.cn (Shuwen Liu)

Identification and detailed studies of ancient orogens are one of the most important scientific problems for understanding the formation and evolution of early continental crust. However, it is very difficult to identify the original architecture of ancient orogenic belts due to the strong disturbances of late tectonothermal events, which makes it hard to reconstruct the formation mechanism and evolution process of early microplates. Here we used spatial-temporal evolution of Neoarchean tectono-magmatism to trace orogenic processes of the Neoarchean continental crust of the North China Craton (NCC). Regional investigations in lithological assemblages, structural geology, chronology, geochemistry and isotopic characteristics suggest that the Archean crystalline basement of the Eastern Liaoning Range in the northeastern NCC may be divided into three tectonic zones, each with its own independent tectono-thermal evolution. We suggest therefore that these are independent terranes, namely microplates. Anshan-Benxi microplate (ABM) in the southwest is a ~3.8 to ~2.9 Ga ancient continental nucleus with abundant Neoarchean (2.54–2.49 Ga) crust-derived K_2O-rich granitoids. Waitoushan-Weiziyu-Jiubing microplate (WWJM) in the center is mainly composed of ~2.7 Ga tonalite-trondhjemite-granodiorite suite and 2.6–2.5 Ga diversified granitoids with some remnants of ancient oceanic lithosphere. Liaobei microplate (LBM) in the northeast contains mainly late Neoarchean (2.57–2.52 Ga) magmatic rocks with minor Mesoarchean (~3.1 Ga) crustal materials. We summarize the formation mechanism, essential features, and identification marks of the Archean orogenic belt, and conclude that the Eastern Liaoning Range experienced the following four stages of Neoarchean geodynamic evolution. (1) In the early Neoarchean (2.71–2.68 Ga), intra-oceanic subduction generated the ~2.7 Ga island arc belt (proto-WWJM); (2) The 2.60–2.56 Ga warm subduction of oceanic slabs reformed proto-LBM, and re-deformed the residual ~2.7 Ga island arc belt; (3) During 2.56–2.54 Ga, the WWJM and LBM were amalgamated by an 'arc-arc' collision; (4) At the

end of Archean (2.54–2.50 Ga), the WWJM+LBM and proto-ABM were finally aggregated through the 'arc-proto-continental' collision, forming a unified crystalline basement of the Eastern Liaoning Range. Our work suggests that the short-term, small-scale subduction-collision orogenic cycles within pristine plate tectonic regimes played a crucial role in the Neoarchean crustal growth and evolution of the NCC.

Keywords: Archean microplates; Spatial-temporal evolution of tectono-magmatism; Ancient orogenic belt; Subduction-collision orogenic cycles; Northeastern North China Craton.

GDT 30: The late Triassic Red Beds and their Significance for Unravelling Convergent Tectonics along the Chiang Mai-Chiang Rai Suture Zone

Thikapong Thata[a], Rattanaporn Fongngern[a,*], Weerapan Srichan[a], Niti Mankhemthong[a], and Kwan-Nung Pang[b]

[a]*Department of Geological Science, Faculty of Science, Chiang Mai University, Chiang Mai, 50200, Thailand*
[b]*Institute of Earth Sciences, Academia Sinica, Taipei, 11529, Taiwan*

*Corresponding Authors:
E-mail address: rattanaporn.f@cmu.ac.th (Rattanaporn Fongngern); thikapong_th@cmu.ac.th (Thikapong Thata)

This study investigated a succession of coarse-grained red beds, and their adjacent rocks exposed in Chae Hom District of Lampang Province, northern Thailand, which is tectonically situated in the easternmost side of Chiang Mai-Chiang Rai suture zone (**Fig. 1**).

The red beds, named here Chae Hom Red Beds (CHRBs), overly metamorphic and deformed sedimentary rocks and in turn, are overlain by turbidite sequences. The CHRBs are dominated by conglomerates at the lower part of the succession and grade upward to sandstone and siltstone towards the top. Most conglomerate beds have stratification and occasionally show fining upward trend. The most abundant clasts in conglomerates are quartz, red siltstone, limestone, silicified shale, and reddish sandstone, respectively. The sandstones, classified as sublithic arenite and lithic wacke, contain dominantly igneous rocks (volcanic rocks) and metamorphic rock fragments. The CHRBs were interpreted to deposit in a braided stream-alluvial fan system during 216-205 Ma or the late Triassic period, and the zircon grains in turbidite sequences indicate the age 234-213 Ma, based on U-Pd age dating. This age range is much younger than previously documented. According to the geochronological data the outcrop exposed on the westside of the Chae Hom Basin could have been a preserved piece of the suture that records the very last events before the collision between the Sibumasu and Indochina Terranes was completed. The turbidite sequences might have been deposited in the deep forearc basin with substantial subsidence during crustal relaxation, which coincided with the felsic volcanic activity in the late Triassic. Upon the final phase of collision, compression caused reduced subsidence and uplift of the accretionary prism, the metamorphic and deformed sedimentary rocks, which then became the source of the CHRBs.

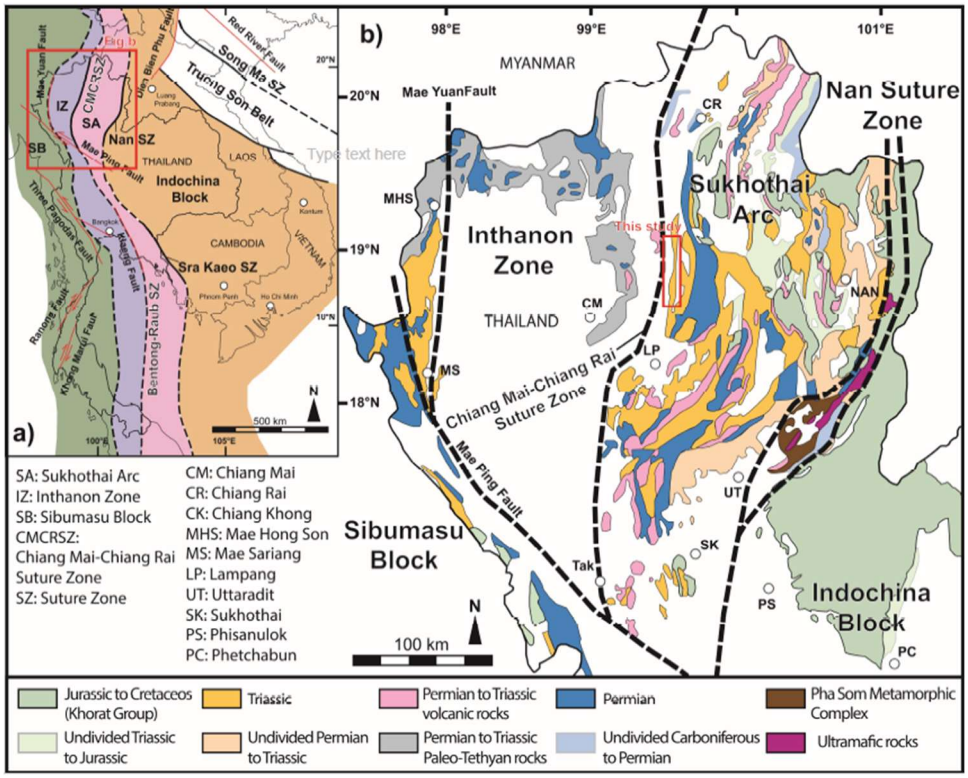

Fig. 1 a) Tectonic map of Southeast Asia showing major geological units and fault zones, modified from Sone and Metcalfe (2008), Metcalfe (2011a, 2011b, 2013, 2017, 2021), Ueno et al. (2018), and Hara et al. (2020). b) Geological map of northern Thailand highlighting the study area location, based on the 1:1,000,000 scale geological map of Thailand (Department of Mineral Resources, 1999).

Keywords: Detrital zircon U–Pb dating, Paleo-Tethys, Chiang Mai-Chiang Rai Suture Zone

References

Hara, H., Ito, T., Tokiwa, T., Kong, S., Lim, P., 2020. The origin of the Pailin Crystalline Complex in western Cambodia, and back-arc basin development in the Paleo-Tethys Ocean. Gondwana Research 82, 299–316.

Metcalfe, I., 2011a. Palaeozoic-Mesozoic history of SE Asia. In: Hall, R., Cottam, M., Wilson, M.)Eds.(, The SE Asian Gateway: History and Tectonics of Australia– Asia Collision. Geological Society of London Special Publications 355, 7–35.

Metcalfe, I., 2011b. Tectonic framework and Phanerozoic evolution of Sundaland. Gondwana Research 19, 3–21.

Metcalfe, I., 2013. Gondwana dispersion and Asian accretion: tectonic and palaeogeographic evolution of eastern Tethys. Journal of Asian Earth Sciences 66, 1–33.

Metcalfe, I., 2021. Multiple Tethyan ocean basins and orogenic belts in Asia. Gondwana Research 100, 87-130.

Metcalfe, I., Henderson, C.M. and Wakita, K., 2017. Lower Permian conodonts from Palaeo-Tethys Ocean plate stratigraphy in the Chiang Mai-Chiang Rai suture zone, northern Thailand. Gondwana Research 44, 54-66.

Sone, M., Metcalfe, I., 2008. Parallel Tethyan Sutures inmainland SE Asia: new insights for Palaeo-Tethys closure. Comptes Rendus Geoscience 340, 166–179.

Ueno, K., Kamata, Y., Uno, K., Charoentitirat, T., Charusiri, P., Vilaykham, K., Martini, R., 2018. The Sukhothai Zone)Permian–Triassic island-arc domain of Southeast Asia(in Northern Laos: insights from Triassic carbonates and foraminifers. Gondwana Research 61, 88–99.

GDT 31: Structural, petrochronological and geochemical analysis of migmatites in the Assam-Meghalaya Gneissic Complex: Insights on Proterozoic crustal evolution in NE India

Rahul Nag[1*], Nathan Cogné[2], Hrushikesh, H[3], Prabhakar, N[1], Dhananjay Mishra[1]

[1]*Department of Earth Sciences, Indian Institute of Technology Bombay, Powai, Mumbai, Maharastra-400076, India*
[2]*Géosciences Rennes, UMR6118, CNRS Université de Rennes, France*
[3]*Geological Survey of India, Northeastern Region, Guwahati, Assam-781005*

*Corresponding Author:
E-mail address: rahulnag10feb@gmail.com (Rahul Nag)

Migmatites record crucial information regarding partial melting processes and the rheological behavior of the lower to middle continental crust. The present study focuses on extensively migmatised basement rocks in Guwahati and adjoining areas in the Assam-Meghalaya Gneissic Complex (AMGC). Field observations show mesoscopic evidence of partial melting, such as lensoidal patches and veins of leucosomes in migmatitic quartzo-feldspathic gneisses and migmatites occurring as metatexites and diatexites exhibiting schollen and schlieren structures. Microtextures like cuspate-shaped grain boundaries and silicic films indicate the former presence of melt along the grain boundaries. Three distinct deformation episodes (D_1, D_2 and D_3) were identified in the gneisses and amphibolites. Both these lithologies witnessed migmatisation during the D_2 deformation. Phase equilibrium modelling constrained peak *P–T* conditions for the quartzo-feldspathic gneisses and amphibolites at 6.0–8.0 kbar/700–740 °C and 5.8–7.0 kbar/690–700 °C, respectively. Based on the melt-reintegration approach, the prograde metamorphism in quartzo-feldspathic gneisses is characterized by the subsolidus breakdown of muscovite, which was followed by biotite breakdown during the peak metamorphism. U–Pb zircon dating of gneisses and amphibolites show upper intercept ages of 1624–1612 Ma, representing the inherited igneous protolith ages. Discordant lower intercept ages (512–426 Ma) and U–Th–total Pb monazite ages (499–470 Ma) determine the timing of high-grade metamorphism and partial melting in the central AMGC. The geochemical characteristics show that the leucosomes hosted in gneisses and amphibolites are enriched in K and Ca contents, respectively. According to trace element and REE patterns, the K-rich and Ca-rich leucosomes originated from the partial melting of granitic or metasedimentary protoliths and mafic protoliths, respectively. The integration of thermobarometry data and geochronological results presented in this study with the existing data indicate that the central AMGC evolved in a hinterland region during a Late Neoproterozoic (499–470 Ma) collision event. The correlation of Late Neoproterozoic partial melting, high-grade metamorphism and magmatism in the Guwahati region with similar events in western Australia and Antarctica indicate that the central and eastern AMGC was a part of the convergent zone that evolved during the assembly of the Gondwana supercontinent.

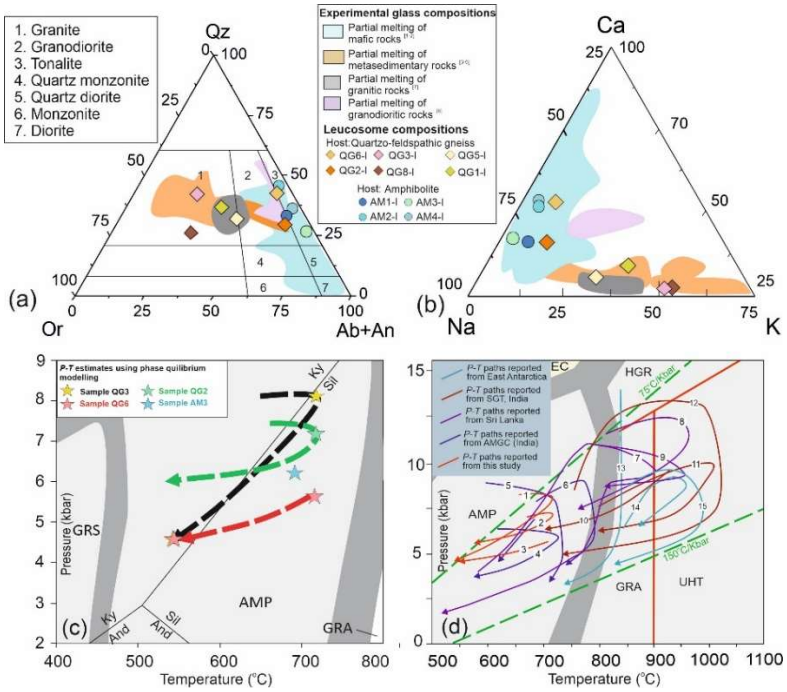

Figure 1: (a-b) Comparison of leucosome samples (hosted in migmatitic quartzo-feldspathic gneisses and amphibolites) with glasses derived from experimental partial melting of mafic rocks, metasedimentary rocks and granitic-granodioritic rocks. References for experimental glass compositions: [1] Rapp and Watson (1995), [2] Prouteau et al., 2001, [3] Patiño Douce and Johnston (1991), [4] Pickering and Johnston (1998), [5] Castro et al. (1999), [6] Castro et al., (2000), [7] Acosta-Vigil et al. (2006) and [8] Johnston and Wyllie (1988). (c) Pressure-Temperature diagram showing a compilation of P-T paths derived from migmatitic quartzo-feldspathic gneisses (Samples QG3, QG2, QG6) and amphibolite (Sample AM3) in this study. (d) Summary of P-T paths compiled from Late Neoproterozoic to Early Cambrian high-grade metamorphic rocks from this study (red) and previous studies from AMGC, Southern Granulite Terrain and East Antarctica. References: 1, 2 and 3–present study; 4–Chatterjee et al. (2007); 5 and 6–Nag et al. (2024); Sri Lanka: 7–Dharmapriya et al. (2017); 8–Takamura et al. (2015); 9–Dharmapriya et al. (2015). Southern Granulite Terrain: 10–Dev et al. (2021); 11–Tiwari and Sarkar (2020); 12–Brandt et al. (2011). East Antarctica: 13–Chen et al. (2018); 14–Kelsey et al. (2007); 15–Wang et al. (2022).

References:

Acosta-Vigil, A., London, D., Morgan VI, G.B., 2006. Experiments on the kinetics of partial melting of a leucogranite at 200 MPa H_2O and 690–800°C: compositional variability of melts during the onset of H_2O-saturated crustal anatexis. Contributions to Mineralogy and Petrology 151, 539–557. https://doi.org/10.1007/s00410-006-0081-8

Brandt, S., Schenk, V., Raith, M.M., Appel, P., Gerdes, A., Srikantappa, C., 2011. Late Neoproterozoic PT evolution of HP-UHT granulites from the Palni Hills (South India): new constraints from phase diagram modelling, LA-ICP-MS zircon dating and in-situ EMP monazite dating. Journal of Petrology 52, 1813–56.

Castro, A., Patiño, E., Corretgé, L.G., de la Rosa, J., El-Biad, M., ElHmidi, H., 1999. Origin of peraluminous granites and granodiorites, Iberian Massif, Spain: an experimental test of granite petrogenesis. Contributions to Mineralogy and Petrology 135, 255–276.

Castro, A., Guillermo Corretgé, L., El-Biad, M., El-Hmidi, H., Fernández, C., Patiño Douce, A.E., 2000. Experimental constraints on Hercynian anatexis in the Iberian Massif, Spain. Journal of Petrology 41, 1471–1488.

Chatterjee, N., Mazumdar, A.C., Bhattacharya, A., Saikia, R.R., 2007. Mesoproterozoic granulites of the Shillong-Meghalaya Plateau: evidence of westward continuation of the Prydz Bay Pan-African suture into Northeastern India. Precambrian Research 152, 1–26.

Chen, L., Wang, W., Liu, X., Zhao, Y., 2018. Metamorphism and zircon U-Pb dating of high-pressure pelitic granulites from glacial moraines in the Grove Mountains, East Antarctica. Advances in Polar Science 29, 118–134.

Dev, J.A., Tomson, J.K., Sorcar, N., Nandakumar, V., 2021. Combined U-Pb/Hf isotopic studies and phase equilibrium modelling of HT-UHT metapelites from Kambam ultrahigh-temperature belt, south India: constraints on tectonothermal history of the terrane. Lithos 406, 106531.

Dharmapriya, P.L., Malaviarachchi, S.P., Santosh, M., Tang, L., Sajeev, K., 2015. Late-Neoproterozoic ultrahigh-temperature metamorphism in the Highland Complex, Sri Lanka. Precambrian Research 271, 311–333.

Dharmapriya, P.L., Malaviarachchi, S.P., Kriegsman, L.M. Andrea Galli, Sajeev, K., Chengli Zhang, 2017. New constraints on the P–T path of HT/UHT metapelites from the Highland Complex of Sri Lanka. Geoscience Frontiers 8(6), 1405-1430. https://doi.org/10.1016/j.gsf.2016.12.005.

Johnston, A.D., Wyllie, P.J., 1988. Interaction of granitic and basic magmas: experimental observations on contamination processes at 10 kbar with H_2O. Contributions to Mineralogy and Petrology 98, 352–362 https://doi.org/10.1007/BF00375185

Kelsey, D.E., Hand, M., Clark, C., Wilson, C.J.L., 2007. On the application of in situ monazite chemical geochronology to constraining P-T–t histories in high temperature (> 850°C) polymetamorphic granulites from Prydz Bay, East Antarctica. Journal of the Geological Society 164, 667–683.

Nag, R., Hrushikesh, H. Cogné, N., Prabhakar, N., 2024. Late Neoproterozoic to early Cambrian high-grade metamorphism from Mikir Hills (Assam-Meghalaya gneissic Complex, northeast India): Implications for eastern Gondwana assembly. Geoscience Frontiers, 15, (5) 101850. https://doi.org/10.1016/j.gsf.2024.101850.

Patiño Douce, A.E. Johnston, A.D., 1991. Phase equilibria and melt productivity in the pelitic system: implications for the origin of peraluminus granitoids and aluminous granulites. Contributions to Mineralogy and Petrology 107, 202–218.

Pickering, J.M., Johnston, D.A., 1998. Fluid-Absent Melting Behavior of a Two-Mica Metapelite: Experimental Constraints on the Origin of Black Hills Granite. Journal of Petrology 39, 1787–1804.

Prouteau, G., Scaillet, B., Pichavant, M. Maury, R.C, 2001. Evidence of mantle metasomatism by hydrous silicic melts derived from subducted oceanic crust. Nature 410, 197–200.
Rapp, R.P., Watson, E.B., 1995. Dehydration melting of metabasalt at 8-13 kbar: implications for continental growth and crust mantle recycling. Journal of Petrology 36, 891–931.
Takamura, Y. Tsunogae, T. Santosh, M. Malaviarachchi, S.P.K., Tsutsumi, Y., 2015. Petrology and zircon U-Pb geochronology of metagabbro from the Highland complex, Sri Lanka: implications for the correlation of Gondwana suture zones. Journal of Asian Earth Sciences 113, 826-841.
Tiwari, A.K., Sarkar, T., 2020. P-T-t evolution of sapphirine-bearing semipelitic granulites from Vadkampatti in Eastern Madurai Domain, southern India: Insights from petrography, pseudosection modelling and in-situ monazite geochronology, Precambrian Research 348, 105866, https://doi.org/10.1016/j.precamres.2020.105866.
Wang, W., Zhao, Y., Wei, C., Daczko, N.R., Liu, X., Xiao, W., Zhang, Z., 2022. High-ultrahigh temperature metamorphism in the Larsemann Hills: insights into the tectono-thermal evolution of the Prydz Bay Region, East Antarctica. Journal of Petrology 63(2), egac002. https://doi.org/10.1093/petrology/egac002

GDT 32: Tracing the eastern Gondwana amalgamation in Eastern Himalaya: Implications for early Paleozoic tectonic evolution along the northern Indian passive margin

Athokpam Krishnakanta Singh[a,b]

[a]*Department of Applied Geology, Dr. Harisingh Gour University, Sagar - 470003, India*
[b]*Wadia Institute of Himalayan Geology, 33 GMS Road, Dehradun - 248001, India*

*Corresponding Author:
E-mail address: aksingh_wihg@rediffmail.com (A. Krishnakanta Singh)

The Tibet-Himalayan region witnessed multiple magmatic episodes during the Gondwana assembly and subsequent activity of break-up events. The Early Paleozoic magmatism is due to either formation of an Andean-type active continental margin at the northern Gondwana when the proto-Tethyan oceanic crust is subducted southward or magmatism occurs in a post-collisional extensional environment after the amalgamation of Gondwana. To comprehensively investigate the possible mechanism of the tectonic evolution during the amalgamation of Gondwana in the eastern Himalaya, magmatic rocks exposed in the core of the Siang window of the eastern Himalaya were studied. It involves analyses of whole-rock geochemistry and zircon U-Pb dating of mafic-felsic rocks. The mafic intrusive rocks are enriched in TiO_2 (1.59-3.72 wt.%) and large ion lithophile elements (K, Pb, Sr) and depleted in Nb/Y < 0.54 with slightly enriched light rare earth elements and flat heavy rare earth elements pattern [(La/Yb)cn = 2.64 to 5.77]. The samples have strong characteristics of enriched mid-ocean ridge basalts to oceanic island basalts, which forbids the possibility of a subduction origin. The timing of emplacement of the mafic intrusive rocks is constrained by zircon U-Pb ages between 502 and 476 Ma, suggesting the Early Paleozoic magmatism in eastern Himalaya is part of the Gondwana supercontinent. The mantle source modeling further suggests partial melting of the primitive-type mantle with garnet in the source, which supports a deeper mantle melting related to a plume source. It further suggests that the mafic rocks of the Siang window were generated in an intraplate tectonic setting at the passive continental margin of Gondwana after the termination of the southward subduction of the proto-Tethyan oceanic crust. The associated A-type felsic rocks display low MgO (0.35-1.12 wt.%), CaO (< 4.33 wt.%), light rare earth elements and large ion lithophile element enrichment, and depletion in heavy rare earth elements, with strong negative Eu-anomaly. They yield zircon U–Pb ages of 139-133 Ma, indicating they were likely to have been generated by the interaction of the upwelling Kerguelen mantle plume and the pre-existing crust during the initiation of the eastern Gondwana break-up during the early Cretaceous. All these observations indicate that the early Paleozoic magmatic rocks in the eastern Himalaya formed in a post-collisional extensional environment affected by a plume upwelling at the passive margin along the northern margin of Gondwana. Later, the subsequent eastern Gondwana breakup is responsible for the magmatism in the

Siang window of eastern Himalayan syntaxis due to the outbreak of the Kerguelen plume during the early Cretaceous. This plume initiated large-scale extension and development of deep normal faults leading to thinning of the overlying lithosphere, which further caused the separation of the Greater Indian plate from the Australian plate along with seafloor spreading and formation of oceanic island basalt-type mafic rocks. It was probably the timing for the initial impact of the plume on the plate margin, thereby producing a Large Igneous Province, for which heat from the Kerguelen mantle plume aided the melting along the circum-eastern Gondwana.

GDT 33: Late Neoproterozoic–Early Cambrian magmatic and metamorphic events from the Mikir Hills, Assam-Meghalaya gneissic complex (NE India): metamorphic history, geochronology and implications for Gondwana supercontinent assembly

Prabhakar N[1*], Rahul Nag[1], N Cogné[2], Hrushikesh H[3]

[1]*Indian Institute of Technology Bombay, Mumbai, Maharashtra-400076, India*
[2]*Univ Rennes, CNRS, Geosciences Rennes, UMR 6118, 35000 Rennes, France*
[3]*Geological Survey of India, Northeastern Region, Assam-781005, India*

*Corresponding Author:
E-mail address: prabhakarnaraga@iitb.ac.in (N.Prabhakar)

Granitoids, migmatised pelitic gneisses and quartzo-feldspathic gneisses are extensively distributed in the Mikir Hills region, representing the eastern portion of the Assam-Meghalaya Gneissic Complex (AMGC; NE India). This study presents the U–Pb zircon geochronology and whole-rock compositions of granitoids and the *P–T–t* evolution of migmatitic gneisses. Zircons from two granitoids from Panbari and Dolamara yielded crystallization ages of 534 ± 5 Ma (n = 5; MSWD = 0.65) and 518 Ma ± 6 Ma (n = 3; MSWD = 0.79). Geochemically, these granitoids show weakly peraluminous, alkali-calcic to calc-alkalic and ferroan characteristics. Pronounced negative Eu anomaly, enrichment in U, Th and LILEs (Rb, Pb and K), and relative depletion of HFSEs (Hf, Zr, Ti and Nb) classify these rocks as A-type granites that were derived from crustal protoliths. The migmatised gneisses witnessed three deformation events (D_1, D_2 and D_3) and are dominated by a prominent ENE–WSW striking and shallow-moderately dipping (<40°) S_2 gneissic foliation. Phase equilibria modelling (MnNCKFMASHTO system) of migmatised gneisses constrained clockwise *P–T* paths, involving partial melting during peak metamorphism (8.0–8.6 kbar/768–780 °C) followed by near isothermal decompression at 4.0–5.0 kbar/720–765 °C. In addition, the melt-reintegrated pseudosections revealed that the pelitic gneisses may have produced 12-18 vol% of melt at the peak metamorphic conditions. The zircons from migmatised pelitic and quartzo-feldspathic gneisses show concordant ages of 1647 ± 11 Ma and 1590 ± 7 Ma, respectively. These Late Paleoproterozoic dates represent the inherited ages of gneissic basement in the AGMC. In contrast, the monazites from pelitic and quartzo-feldspathic gneisses show ages between 496 ± 7 Ma and 467 ± 16 Ma. Based on high Th/U ratios, these dates are interpreted as the timing of migmatisation in the Mikir Hills region. The dominance of Late Neoproterozoic to Early Cambrian migmatisation and magmatism in the Mikir Hills indicate that the eastern AMGC represent an active convergent margin during the assembly of the eastern Gondwana supercontinent (**Fig. 1**). The tectono-magmatic events recorded in the AMGC are broadly consistent with those observed in Western Australia and East Antarctica of the Gondwana assembly.

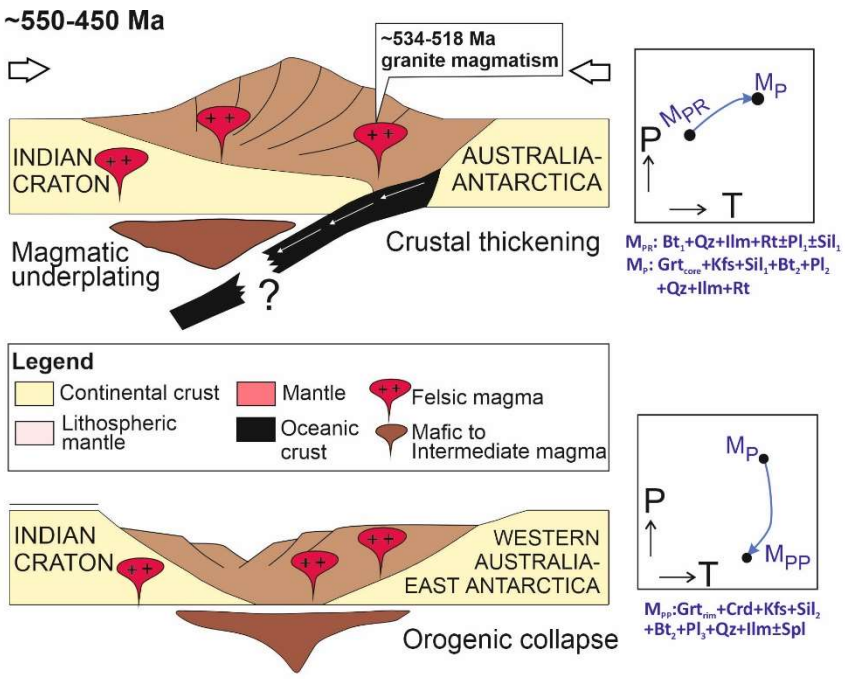

Figure 1: A schematic diagram (not to scale) showing tectono-thermal processes operated during the Eastern Gondwana supercontinent assembly at 550–450 Ma. Collision between India-Australia-Antarctica cratons led to contractional deformation and crustal thickening in the AMGC, leading to the emplacement of granitoids (534–518 Ma; this study) and high-grade metamorphism in the gneisses of the AMGC (after Nag et al., 2024).

Reference:

Nag, R., Hrushikesh, H. Cogné, N., Prabhakar, N., 2024. Late Neoproterozoic to early Cambrian high-grade metamorphism from Mikir Hills (Assam-Meghalaya gneissic Complex, northeast India): Implications for eastern Gondwana assembly. Geoscience Frontiers, 15, (5) 101850. https://doi.org/10.1016/j.gsf.2024.101850.

Theme 2: Metallogeny

MET 02: Genesis of Au mineralization in the Kattamadavu area of Southern Granulite Terrain (SGT), Tamil Nadu, Southern India.

Ramprasad, R[a,b*], Roy, S[a], Mariappan, S[a], Madhavan, K[b], Vijay Anand, S[c]

[a] *Geological Survey of India, Chennai – 600 032, India.*
[b]*Department of Civil Engineering, National Institute of Technology, Calicut – 673 601, India*
[c]*Department of Applied Sciences (Applied Geology), Curtin University, CDT 250, Miri – 98009, Sarawak, Malaysia.*

*Corresponding Author:
E-mail address: ram.geo@gmail.com (R.Ramprasad)

Globally, Archean Au deposits are an important source of gold. They consist of complex and widespread systems of mineral formation in various terrains (Kerrich and Fyfe, 1981; Hagemann and Cassidy, 2000). The potential for gold within the Southern Granulite Terrain (SGT) can be broadly segmented into three distinct provinces: Wynad-Nilgiri, Malappuram, and Attappadi (Krishnamurthi et al., 2010; Krishnamurthi, 2012), as previously documented in the western regions of the SGT. The present study area is situated in the central portion of the SGT, is characterized by Archaean high-grade granulite-gneiss and consists of rocks of various chemical and mineralogical compositions. BIF is banded magnetite-quartzite in these formations. It also includes granulites, amphibolites, metapelites, sillimanite-quartz schists, and pyroxenites (Reddy and Sashidhar, 1989).

A preliminary study has uncovered new insights into the structural and lithological settings of Au mineralization in the Archaean high-grade granulite gneiss terrain. This paper is the first to report gold mineralization in banded magnetite quartzite (BMQ) and pyroxene granulite from the Kattamadavu area of SGT. It consists of highly folded, sheared, and discontinuous bands of BMQ, pyroxene granulite, pyroxenite, granitic gneiss, and eventually quartz veins. All the litho-units are highly sheared and exhibit a dextral sense of shearing. BMQ is dark brown to blackish, marked by alternating quartz-rich and magnetite-rich layers **(Fig. 1a)**. Pyroxene granulite is medium to coarse-grained, greenish-black in colour showing the characteristic salt and pepper texture of basic granulites **(Fig. 1b)**.

Structurally, the area appears to represent the limb part of a regional fold, with an axial plane in the direction of NNE-SSW. The general trend is NE-SW direction. The area has undergone at least three phases of deformation. The entire area primarily suffered ductile deformation followed by brittle, evidenced by pseudotachyllites cutting across the major foliation planes. Ore mineralization exhibits predominantly structural controls. The major mineralization occurs along the prominent foliation plane (S_2) and the event is coeval with the second phase of deformation (D_2). Chip samples were collected using the grooving method across the BMQ banding and foliation planes of the pyroxene granulite.

In thin sections, BMQ is sheared and deformed as evidenced by ribbon-shaped quartz with stretched magnetite crystals; and recrystallized quartz with sutured boundaries. Pyroxene granulite exhibits mainly granulitic texture consisting of clinopyroxene,

orthopyroxene, plagioclase, garnet and hornblende. Ore microscopy reveals the presence of gold, along with the sulphide phases, which are composed of pyrrhotite, pyrite, and chalcopyrite **(Fig. 1c)**. The sulphide phases were quantified by scanning electron microscope (SEM) and electron microprobe analysis (EPMA). The identified sulphide phases are pyrrhotite (Po), pyrite (Py), chalcopyrite (Ccp), pentlandite (Pn) and molybdenite (Mol). Pentlandite and molybdenite occur as inclusions within pyrrhotite. Gold (Au) occurs as native gold, electrum and with telluride phases, which are associated with pyrrhotite or pyrite **(Fig. 1d)** within the BMQ and pyroxene granulite.

It is widely recognized that the brittle-ductile transition zones represent one of the most favourable locales for gold and associated mineralization (Neil Phillips and Powell, 1993). Gold mineralization in the area primarily occurs within the silicified portions of BMQ and is also dispersed within associated pyroxene granulite. This likely represents a hydrothermal system where auriferous fluids reacted with iron in the BMQ and associated litho-units, leading to the precipitation of sulphides. Consequently, gold was liberated and, along with silica, deposited in the silicified zones of BMQ. The shearing event, along with the associated hydrothermal processes, trapped the gold and accompanying sulphide deposits within silica-rich segments of banded magnetite quartzite. This phenomenon is observed in varying degrees, serving as geological hosts for gold mineralization in the Archaean SGT.

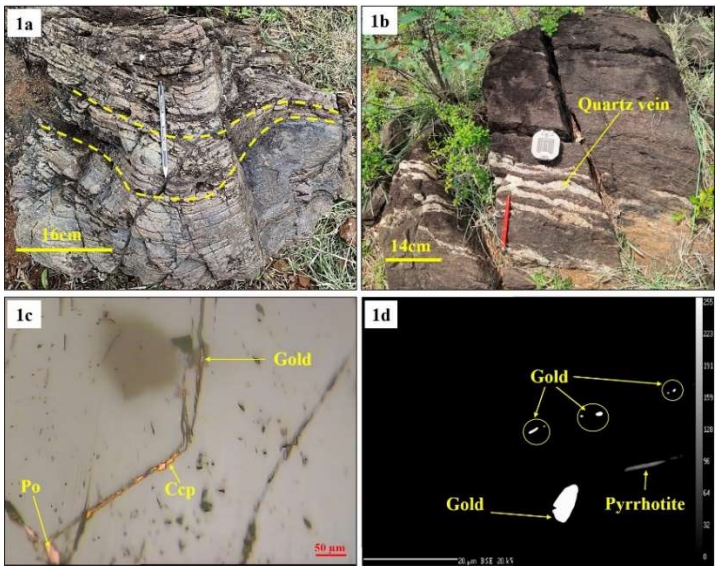

Figure.1. (**a**) Highly sheared and folded BMQ; (**b**) Pyroxene granulite with the intrusion of quartz veins; (**c**) Photomicrograph showing gold grain associated with veins of pyrrhotite (Po) and chalcopyrite (Ccp); (**d**) BSE image (EPMA) showing the presence of gold grains associated with veins of pyrrhotite in BMQ.

Keywords: Southern Granulite Terrain, Pyroxene granulite, BMQ, Silicified, Gold, Archaean, EPMA.

References

Hagemann, S.G., Cassidy, K.F., 2000. Archean Orogenic Lode Gold Deposits. Society of Economic Geologists, 13, 9–60.

Krishnamurthi, R., 2012. Current understanding on the genesis of lode gold mineralization in the Southern granulite Terrain, Peninsular India. Journal of Applied Geochemistry 4, 370–382.

Krishnamurthi, R., Sen, A.K., Pradeepkumar, T., Sharma, R., 2010. Gold mineralization in the Southern Granulite Terrane of Peninsular India. In: Deb, Mihir, Goldfrab, Richard J. (Eds.), Gold Metallogeny. India and Beyond. Narosa Publishing Company House PVT Ltd., pp. 222–233.

Kerrich, R., Fyfe, W.S., 1981. The gold—carbonate association: Source of CO_2, and CO_2 fixation reactions in Archaean lode deposits. Chemical Geology 33(1–4), 265–294.

Neil Phillips, G. Powell, R., 1993. Link between gold provinces. Economic Geology 88(5), 1084–1098.

Reddy, N.S., Sashidhar, A.N., 1989. Mineralogy and chemistry of banded iron formations (BIF) of Tiruvannamalai area, Tamil Nadu. Proceedings of the Indian Academy of Sciences - Earth and Planetary Sciences 98(2), 167–172.

MET 03: Investigation of economic potential of cobalt mineralization in Kalyadi Schist Belt, Dharwar Craton, India

Pratush Kar[a], Abir Banerjee[a], Sakthi Saravanan Chinnasamy[a,*], V.N. Vasudev[b], Prabhakar Sangurmath[c]

[a] *Department of Earth Sciences, Indian Institute of Technology Bombay, Powai, Mumbai - 400076, India*
[b] *Geological Society of India, Bengaluru - 560085, India*
[c] *Hutti Gold Mines Company Limited, Bangalore, Karnataka – 584115, India*

*Corresponding Author:
E-mail address: chinnasamys@iitb.ac.in (C.Sakthi Saravanan)

Cobalt (Co), a critical and strategic metal, is in increasing demand because of its essential role in various fields, most importantly, in creating cobalt-lithium-ion batteries, which are crucial for facilitating the transition from internal combustion engines to electric vehicles, making it vital in fighting against global warming and achieving net zero. The majority of the Co is produced as a by-product of copper (Cu) and nickel (Ni) mining from sediment-hosted Cu-Co deposits (60% of all Cobalt occurrences), magmatic Ni sulphide deposits (23%), laterite-hosted Ni deposits (15%) and hydrothermal vein-type Co deposit (2%). The Democratic Republic of Congo is by far the largest producer of Co worldwide (73% of the production) and the remaining is produced by Indonesia, Australia, The Philippines, Cuba, Morocco etc. This relatively low and sporadic production puts many nations in a risky position with respect to supply chain disruption and foreign dependency. The rising demand has created an urgent need to discover new sources for Co.

The Mesoarchean Kalyadi Schist Belt (KSB), a part of the Western Dharwar Craton located in central Karnataka, India and is a large NW-SE trending amphibolite facies enclave within the Peninsular Gneissic Complex. The greenstone rocks are represented by metaperidotites, serpentinites, amphibolites, cherts and metapelites. Within the mine area, mineralised metachert is the only sedimentary unit, forming a small ridge with a strike length of 900 m. This is interlayered with ultramafic schists, siliceous schists and metapelites. The rock units are undergone at least three phases of deformation. The early isoclinal folds (F1) were involved in a second generation (F2) coaxial open folding and non-coaxial open folding of a third generation (F3). Copper mineralisation is mainly controlled by the F2 folding represented by moderate to steep northerly plunges.

Kalyadi mine is well known for significant copper production in the past and the presence of cobalt has been reported from previous studies. However, there is a research gap on the occurrence of economically valuable Co in the KSB. In this study Cobalt mining potential in the KSB was investigated by petrographic studies, Electron Probe Micro-Analyses (EPMA), Inductively Coupled Plasma Mass Spectrometry (ICP-MS) and Raman spectroscopy using the samples collected from mine dumps and tailings from the now abandoned Kalyadi copper mines area. Metachert is the main host for copper sulphide mineralization. Petrographic studies reveal the presence of sulphide-bearing phases namely pyrite, chalcopyrite, pyrrhotite and the oxide phases such as magnetite and ilmenite. EPMA analysis revealed Co content within pyrite ranging from 0.79–3.29 wt.% (**Table 1**). The negative correlation between Co and Fe suggests that Co is substituting Fe in the pyrite crystal structure. Raman analysis reveals that the cobalt-bearing phases from mineralized zones are to be siegenite (**Fig. 1**).

ICP-MS analysis results on separated sulphide concentrates from the mine tailings show a significant Co content up to 0.31 wt.% as compared to bulk samples (0.01–0.02 wt.%). This study indicates that the Kalyadi schist belt holds significant potential for Co resources. With further studies to assess whether Co can be extracted economically from pyrite and sulphide tailings, the KSB could become a viable Co-bearing mining site, contributing to meeting the increasing demand for Co and achieving global sustainability goals.

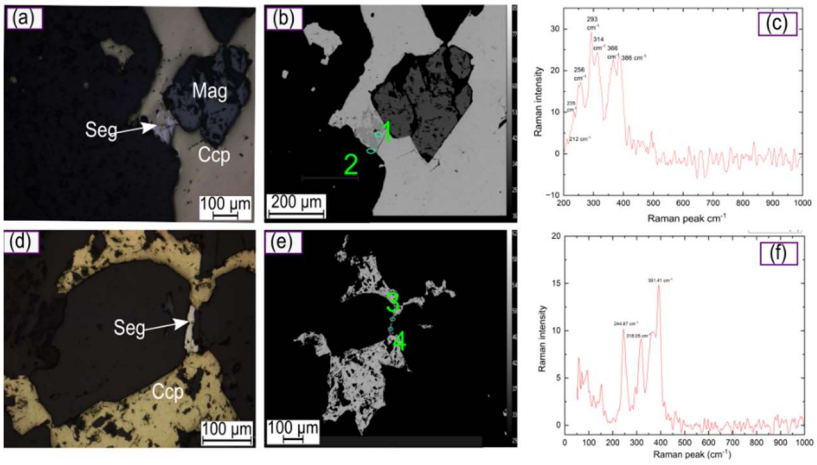

Figure 1. Photomicro-graphs (a, d), Back scattered electron (BSE) (b, e) images and Raman peak (c, f) of the mineral siegenite along with other ore minerals. BSE images showing specific point analysis are presented in

Table. 1. Representative EPMA analytical results (in Wt.%) of pyrite and siegenite from Kalyadi deposit, India.

Point #	Fe	Co	Ni	Cu	Zn	As	S	Mo	Au	Pb	Total	Mineral name
1	2.82	32.89	21.73	0.33	0.04	0.00	42.32	0.10	0.00	0.09	100.34	siegenite
2	2.49	32.75	22.02	0.14	0.00	0.00	42.41	0.02	0.02	0.14	100.01	siegenite
3	0.36	37.56	17.99	0.60	0.00	0.00	41.30	0.14	0.00	0.21	98.19	siegenite
4	0.45	37.70	18.59	0.39	0.00	0.02	41.92	0.06	0.00	0.17	99.32	siegenite
5	44.45	1.30	0.02	0.12	0.00	0.03	52.71	0.01	0.01	0.16	98.81	pyrite
6	43.47	1.80	0.01	0.00	0.00	0.02	53.46	0.00	0.00	0.20	98.99	pyrite
7	44.80	0.86	0.00	0.00	0.00	0.03	53.24	0.05	0.01	0.21	99.20	pyrite
8	43.56	2.28	0.09	0.17	0.04	0.01	53.60	0.00	0.01	0.23	100.00	pyrite
9	43.63	2.30	0.00	0.04	0.00	0.00	53.39	0.12	0.00	0.19	99.69	pyrite
10	43.78	2.45	0.01	0.05	0.00	0.00	53.25	0.00	0.00	0.15	99.68	pyrite
11	43.33	2.70	0.00	0.00	0.00	0.06	52.88	0.09	0.00	0.22	99.32	pyrite
12	42.97	2.91	0.03	0.03	0.07	0.02	53.11	0.05	0.00	0.22	99.42	pyrite
13	42.56	3.29	0.04	0.01	0.00	0.00	52.75	0.00	0.02	0.21	98.86	pyrite
14	44.97	0.79	0.00	0.00	0.00	0.00	53.62	0.00	0.00	0.11	99.50	pyrite
15	44.51	1.13	0.00	0.00	0.00	0.02	53.71	0.04	0.00	0.26	99.69	pyrite
16	43.49	2.06	0.00	0.04	0.01	0.03	52.95	0.05	0.00	0.08	98.71	pyrite
17	44.35	1.45	0.00	0.00	0.00	0.04	53.34	0.12	0.00	0.17	99.47	pyrite

Table 1. Abbreviations: Seg = siegenite, Ccp = chalcopyrite, Mag = magnetite.

MET 04: Critical metal resources in Tibetan geothermal system

Fei Xue[a*], Hongbing Tan[a], Zhiwei Shi[a], Di Wang[a], Weiliang Miao[b]

[a] *School of Earth Sciences and Engineering, Hohai University, Nanjing 210098, China*
[b] *Qinghai Provincial Key Laboratory of Geology and Environment of Salt Lakes, Qinghai Institute of Salt Lakes, Chinese Academy of Sciences, Qinghai 810008, China*

*Corresponding Author:
E-mail address: fei.xue@hhu.edu.cn (Fei Xue)

Tibetan high-temperature geothermal systems are rich in critical metals like lithium (Li), rubidium (Rb), and cesium (Cs), essential for emerging industries and strategic resource security. Geothermal springs facilitate the migration and enrichment of these metals from deep to shallow crustal levels. Our compressive review indicates that Tibetan springs have unusually high concentrations of Li (5.48 mg/L), Rb (0.75 mg/L), and Cs (3.58 mg/L), significantly higher than natural waters. The spatial

distribution of these springs is controlled by the Yarlung Zangbo suture zone and N-S trending rifts, especially in the intersection zone of the two, where the geothermal springs are the most enriched. Based on the spatial distribution, isotopic, and elemental geochemistry, the enriched metals primarily originate from magmatic-hydrothermal fluids from the partial melting of the subducted Indian plate under the Eurasian continent. The enrichment processes involve partial melting, magmatic differentiation, and high-temperature water-rock interactions. Geothermal springs transport RMEs to lake basins, forming salt lake brines under arid conditions, creating a comprehensive model for critical metal enrichment (Fig. 1). This study enhances the understanding of critical metal mineralization and supports exploration and resource assessment in the Qinghai-Tibet Plateau.

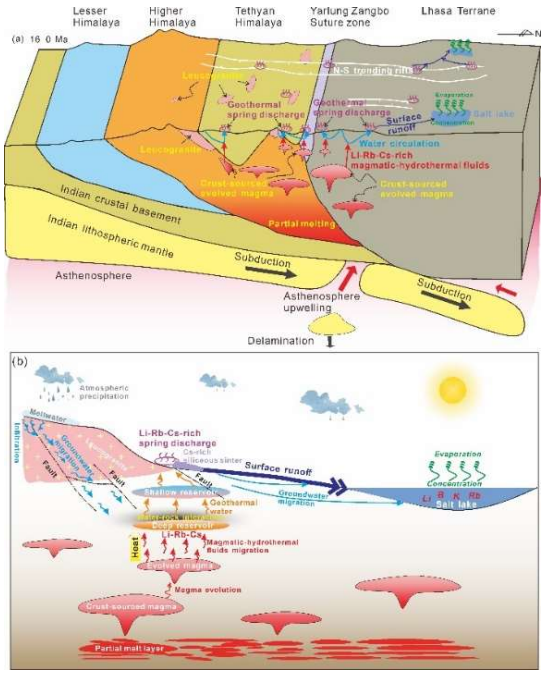

Fig. 1 Schematic diagram for the enrichment process and resource effects of Critical metal elements-riched geothermal springs

Acknowledgements
This work was jointly supported by the Second Tibetan Plateau Scientific Expedition and Research Program (STEP) (Grant No. 2022QZKK0202), the National Natural Science Foundation of China (Grant No. U22A20573), and the Fundamental Research Funds for the Central Universities (Grant No. B230201014), and the Qinghai Provincial Key Laboratory of Geology and Environment of Salt Lakes (Grant No. 2024-KFKT-A07).

MET 05: Identification of Geological Potential and Artisanal Small-Scale Gold Mining Activity in Totopo and the Surrounding Area, Gorontalo Region

Yayu Indriati Arifin[a*], Akram La Kilo[b], Nurfaika[c], Jayanti Rauf[a*]

[a]*Geological Engineering Study Program, State University of Gorontalo, 96119 Gorontalo, Indonesia*
[b]*Chemistry Study Program, State University of Gorontalo, 96119 Gorontalo, Indonesia*
[c]*Medical Study Program, State University of Gorontalo, 96119 Gorontalo, Indonesia*

*Corresponding Authors:
E-mail address: yayu_arifin@ung.ac.id (Yayu Indriati Arifin); jayantirauf11@gmail.com (Jayanti Rauf)

This research examines the geological potential and small-scale gold mining activities in Juria and the surrounding areas of Totopo District, Gorontalo Regency. The methodology encompasses geological field surveys, petrography analysis, and interviews. The petrography data reveal three primary lithologies: andesite, granodiorite, and breccia. Interviews indicate that artisanal mining activities have been ongoing since the 1990s, with 15 gold processing units currently operating. Each unit utilizes 14 to 30 trommels, employing mercury as the primary agent for gold extraction. The mercury usage is approximately 3 ounces per trommel per processing cycle, with up to three cycles conducted daily, resulting in substantial environmental concerns regarding heavy metal pollution, particularly in water sources. The study highlights that the proximity of processing locations to the main river significantly increases the risk of mercury contamination in the water system, which could adversely affect the river ecosystem and local communities that depend on the river for drinking water and fishing. Gold production is estimated at around 3 grams per day per processing unit, offering economic benefits to the local community. However, the environmental impact, particularly regarding mercury use and its consequences for heavy metal contamination, is a critical concern. The amalgamation process, which involves crushing gold-bearing materials, mixing them with mercury, pressing the amalgam, and burning it to separate the gold, is identified as a significant source of environmental and health risks due to mercury exposure. The study underscores the necessity for sustainable and environmentally friendly mining practices to mitigate the negative impacts on water quality and overall environmental health in the region.

Keywords: geological potential, small-scale gold mining, artisanal mining, mercury contamination, environmental impact, Gorontalo Regency

MET 06: Integration of Lineament Analysis, Land Surface Temperature (Lst), and Geology for Geothermal Reservoir Zonation In Kotamobagu, North Sulawesi

Jayanti Rauf[1], Fahira Ramadhani Djibran[1], Dicky Rahmansyah S. Tone[1], Ayub Pratama Aris[1*]

[1]*Program Studi Teknik Geologi, Universitas Negeri Gorontalo, 96119 Gorontalo, Indonesia*

*Corresponding Author:
E-mail address: ayubpratamaaris@ung.ac.id (Ayub Pratama Aris)

Renewable energy (RE) stands as a critical solution to addressing global energy challenges and mitigating climate change. Indonesia, endowed with substantial geothermal potential, particularly in regions like Kotamobagu with its intricate tectonic framework, offers significant opportunities for RE development. This study aims to map the zonation of geothermal reservoir potential in the Kotamobagu area, North Sulawesi. By employing methodologies such as lineament analysis, Land Surface Temperature (LST) measurements, and comprehensive geological analysis, integrated with fuzzy logic, we aim to identify and delineate zones with high geothermal potential. The integration of these methodologies provides a robust framework for assessing geothermal resources, leveraging the unique geological characteristics of the region. Our findings reveal four significant geothermal potential zones. Three of these zones are located in the northwest part of the study area, while one is situated in the south. These zones exhibit promising permeability characteristics and notable LST anomalies, which are conducive to further geothermal exploration and potential development. The presence of such anomalies suggests subsurface heat sources and fluid pathways that are critical for geothermal reservoir

formation. The identification of these potential zones represents a strategic step towards enhancing the contribution of geothermal energy to Indonesia's renewable energy mix. This research not only highlights the geothermal prospects in Kotamobagu but also underscores the importance of integrating advanced analytical techniques in geothermal exploration. The results of this study are expected to support national efforts in achieving renewable energy targets, contributing to a more sustainable and resilient energy future for Indonesia. In conclusion, the study's approach and findings provide valuable insights into geothermal resource assessment and underscore the importance of leveraging Indonesia's geothermal potential. The integration of lineament analysis, LST measurements, and geological analysis with fuzzy logic offers a comprehensive and effective methodology for identifying geothermal reservoirs, paving the way for future exploration and development.

Keywords: Geothermal, Permeability, Land Surface Temperature, Fuzzy Logic, Renewable Energy, Reservoir

Life evolution and paleoenvironment

LE&PE 01: Study on sequence stratigraphy in the Permian sediments of terrestrial sequences within the Chintalapudi sub-basin, Godavari Coal field, Southern India: insight from palynology and geochemistry

Neha Aggarwal[a*], Divya Mishra[a] Bodhisatwa Hazra[b]

[a] *Birbal Sahni Institute of Palaeosciences, 53, University Road, Lucknow-226007, India*
[b] *Central Institute of Mining and Fuel Research, Barwa Road, Dhanbad-826015, India*

*Corresponding Author:
E-mail address: neha_264840@yahoo.co.in (Nega Aggarwal)

The opening of Neo-Tethys within Gondwanaland during the Guadalupian (transition signified a pivotal transgressive event) in the Permian Period. Consequently, an attempt has been undertaken to elucidate the sequence stratigraphy and palaeodepositional settings of fluvial sedimentary deposits encompassing coal and shale sediments within the Godavari Valley Coalfield, South India.

The Total Organic Carbon (TOC) content across the examined samples exhibits a discernable range from 0.07—65.53 wt%, with reactive carbon, measured as Pyrolyzable carbon (PC), displaying variations from 0.02—15.93 wt% and non-reactive carbon, characterized, as Residual Carbon (RC), spans a percentage range of 0—66.86 wt% within the selected samples. The predominant organic matter manifests as type III kerogen, except Sh-47, where type II kerogen is identified.

The combination of Rock-Eval pyrolysis alongside palynofacies analysis facilitates the differentiation of significant system tracts arising from relative sea level fluctuations within the deposited terrestrial sequences. These tracts include swampy and flooded palaeomires settings. Terminologies denoting system tracts within the sequences are indicted as T-*lst*, T-*hst*, T-*tst* and T-*mfs* corresponding to the Low Stand System Tract (LST), High Stand System Tract (HST), Transgressive System Tract (TST) and Maximum Flooding Surface (MFS) respectively. A noteworthy one and half cycles are discerned within the sequence, predicted by Amorphous Organic Matter (AOM), TOC, Hydrogen Index (HI), PC and Gelification Index (GI) values. In the initial cycle, T-*mfs* is identified based on the preponderance of fluorescent AOM, coupled with the highest value of HI and PC. The ratio of opaque/translucent phytoclasts serves as a discriminant in delineating the boundaries of T-*lst,* T-*tst* and T-*hst* within the sequences, corroborating the aforementioned observation. This research serves as a preliminary assessment of the system tracts within fluvial environments. A more intricate, high-resolution exploration of deeper sequences holds the potential to furnish comprehensive insights for subsequent studies.

Keywords: Sequence stratigraphy, terrestrial, Permian, system tracts, Transgression, TOC.

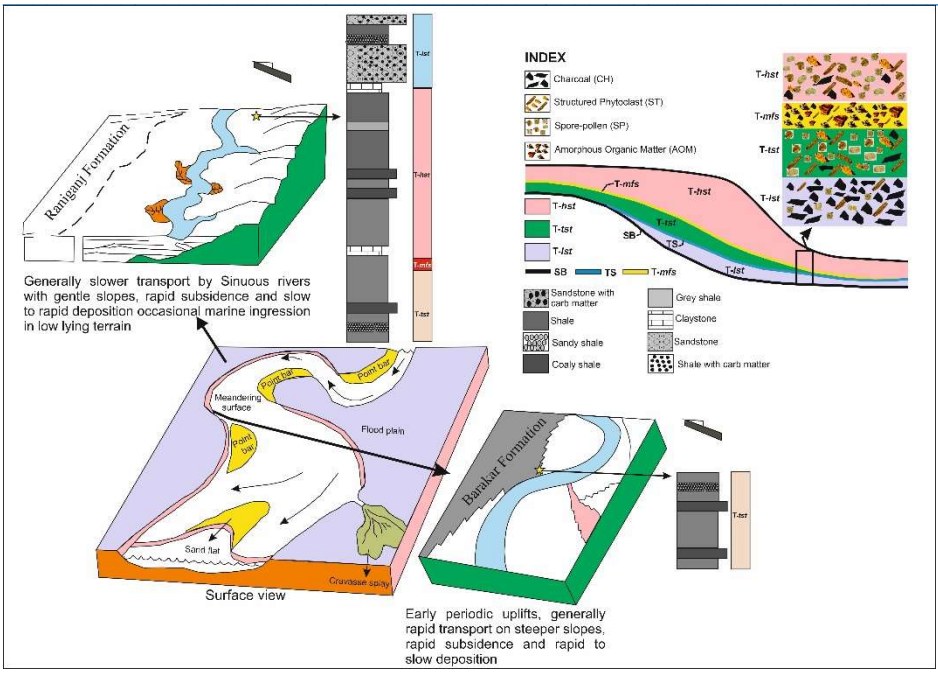

Figure 1. A conceptual model indicating the system tracts in the fluvial Gondwana succession (SB = Sequence Boundary; TS = Transgressive Surface; modified after Li and Zhang, 2017)

References:
Li, J., Zhang, J., 2017. Stratigraphy of fluvial facies: a new type representative from Wenliu Area, Bohai Bay Basin, China. chapter-3. Intech, London, 36–66. http://dx.doi.org/10.5772/intechopen.71149.

LE&PE 02: Nannofossil biostratigraphy of the Jurassic succession from the Langza area, Spiti Valley, Southern Tethys Basin, India

Abha Singh[1*]

[1]*Birbal Sahni Institute of Palaeosciences, 53, University Road, Lucknow, Uttar Pradesh*

*Corresponding Author:
E-mail address: abha.maurya@gmail.com, abha.singh@bsip.res.in (Abha Singh)

For the first time, calcareous nannofossil biostratigraphy has been attempted from the black shales of the Lower Spiti Shale Member of the Spiti Shale Formation exposed in the Langza area, Spiti Valley, Himachal Pradesh. A total of twenty samples were collected for the nannofossil studies from the section exposed along a nala (rivulet cutting) near a small bridge (N 32°16′04″: E 78°04′44″). The section consists of black splintery shales having Belemnites, Brachiopods and Bivalves at various levels. For the qualitative estimation of nannofossils, smear-slides of all 20 samples were prepared. The samples were processed following the conventional method of nannofossil slide preparation. A small fraction of the sample was soaked in neutral distilled water in a clean and dried vial. A homogenous suspension is formed by the fingertip. After the material was allowed to settle for a while, a few drops of the turbid suspension were evenly spread over a clean slide as thin film and allowed to dry over a hot plate. The slides are then mounted in Canada balsam. The calcareous nannofossils were studied using a Leica DM2500P polarizing microscope under a 100X oil immersion objective both under normal (using single polarized) and crossed polarized illumination with gypsum plate.

Based on ammonites and dinoflagellate cysts biostratigraphy, the age of the Spiti Shale Formation was assigned Oxfordian to Tithonian. Here, the present study provides an older, Callovian age (part of NJ12 Nannofossil Zone) to the black shales (*'Belemnites gerardi* beds') belonging to belemnites-rich

Lower Member of Spiti Formation based on the biostratigraphic ranges of *Ansulasphaera helvetica*, *Lotharingius hauffii, Watznaueria contracta and Watznaueria ovata* (**Fig. 1**). In the present study reworking of the *Carinolithus magharensis* (LAD in Bathonian) in samples LK-1 to LK-11 is recorded. The occurrences of *Faviconus multicolumnatus* (FAD in Oxfordian) are noted in the uppermost productive sample (LK-16) indicating the leaking of this taxa from the younger horizons.

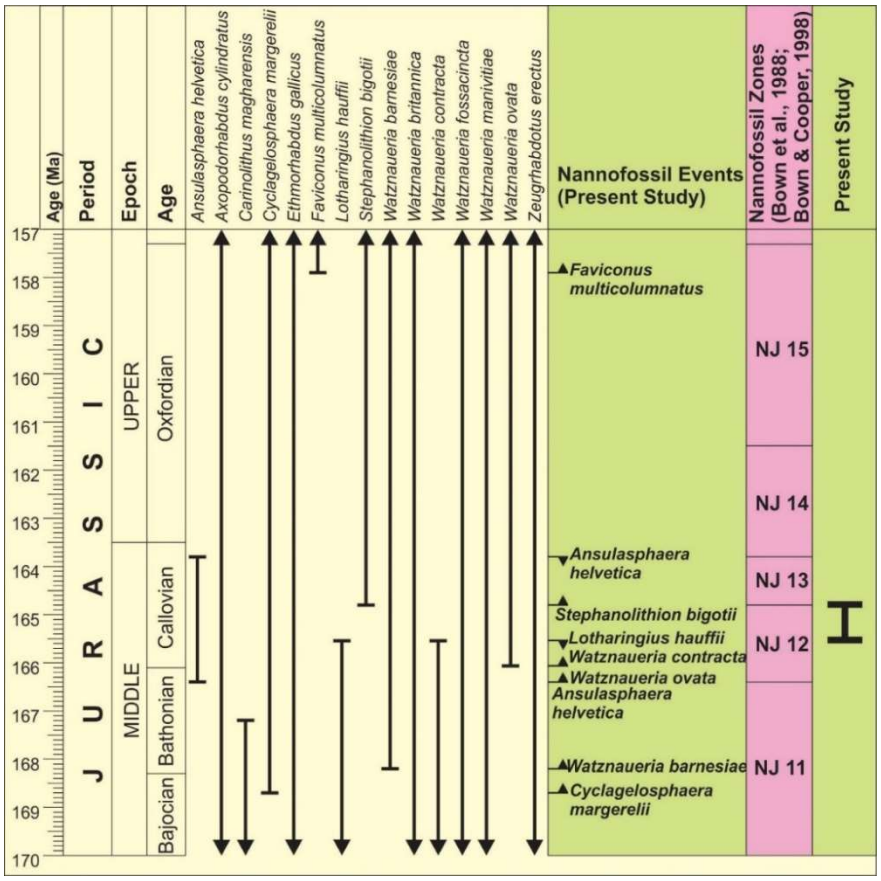

Figure 1. Calcareous nannofossils stratigraphic ranges and events recorded in the present study and its calibration with standard nannofossil zonation scheme for age assignment.

Keywords Calcareous nannofossils, Spiti Shale Formation, Callovian, Langza, Spiti Valley

LE&PE 03: Medical Geology: a burgeoning science

E. Shaji[1*], B.J. Sudhir[2], M. Santosh[3,4]

[1]*Department of Geology, University of Kerala, Kariavattom Campus, Trivandrum 695581, India.*
[2]*Department of Neurosurgery, Sree Chitra Tirunal Institute for Medical Sciences and Technology, Trivandrum 695011, India*
[3]*School of Earth Sciences and Resources, China University of Geosciences Beijing, 29 Xueyuan Road, Beijing 100083, China*
[4]*Department of Earth Science, University of Adelaide, Adelaide SA 5005, Australia*
*Corresponding Author:
E-mail address: shajigeology@gmail.com (E.Shaji)

Medical geology is a multidisciplinary field that investigates the intricate relationship between geological processes, materials, and human health (Finkelmen et al., 2024). This abstract provides an overview of the burgeoning science of medical geology, highlighting its key areas of research and

implications for public health. The study of medical geology encompasses various facets, including the impact of geogenic contaminants on drinking water quality and their associated health risks. Geological factors such as minerals, rocks, soils, and water sources can contain substances like arsenic, fluoride, radon, and heavy metals, which pose significant health hazards when ingested or inhaled by humans (Shaji et al., 2021, 2024). Moyamoya angiopathy (MMA), a rare and enigmatic disease, has intrigued clinicians and researchers for over six decades since its first description (Sudhir et al., 2024). In this past decade, although significant strides have been made in genetic research in MMA, a low penetrance of the phenotype, has led researchers to invoke a geo-environmental agent in its causation. The geographical prevalence of MMA and geospatial maps, food habits, possible sources of industrial pollutant exposure, and groundwater data were examined. The clustering of cases in east Asia, Bangladesh and certain foci in the United States, corresponded with the high levels of arsenic in food and water sources. We propose a hypothesis of an association between arsenic exposure and MMA. Furthermore, we propose to explore the role of geological materials in the occurrence and distribution of diseases, ranging from certain cancers to respiratory illnesses. For instance, exposure to asbestos minerals in geological formations has been linked to elevated risks of lung diseases. Medical geochemistry plays a pivotal role in safeguarding the safety of drinking water by identifying the sources, concentrations, and chemical forms of potentially harmful elements, such as arsenic, mercury, and fluorine, present in natural water sources (Finkelmen et al., 2024). Evolving medical geology into a major interdisciplinary research area holds great promise for advancing our understanding of the complex interplay between the Earth and human health. By fostering collaboration across disciplines, researchers can work towards innovative solutions to address emerging health threats and promote sustainable development for future generations.

Reference:

Finkelman, R.B., Orem, W.H., Plumlee, G.S. and Selinus, O., 2024. Applications of geochemistry to medical geology. In Environmental geochemistry (pp. 619-656). Elsevier.

Shaji, E., Sarath, K.V., Santosh, M., Krishnaprasad, P.K., Arya, B.K. and Babu, M.S., 2024. Fluoride contamination in groundwater: A global review of the status, processes, challenges, and remedial measures. Geoscience Frontiers, 15(2), p.101734.

Shaji, E., Santosh, M., Sarath, K.V., Prakash, P., Deepchand, V. and Divya, B.V., 2021. Arsenic contamination of groundwater: A global synopsis with focus on the Indian Peninsula. Geoscience frontiers, 12(3), p.101079.

Sudhir, B.J., Sreenath, R., Shaji, E., Darshan, H.R., Scaria, S., Easwer, H.V. and Krishnakumar, K., 2024. The quest for a geo-environmental factor in Moyamoya angiopathy: Is arsenic the elusive environmental agent?. Medical Hypotheses, 182, 111233.

LE&PE 04: Inertinite in coal and its geoenvironmental significance

Longyi SHAO[1,*], Fanghui HUA[1], Jiamin ZHOU[1], Tim JONES[2]

[1]*State Key Laboratory for Fine Exploration and Intelligent Development of Coal Resources and College of Geoscience and Surveying Engineering, China University of Mining and Technology (Beijing), Beijing 100083, China*
[2]*School of Earth and Environmental Sciences, Cardiff University, Cardiff, CF10 3YE, Wales, UK*

*Corresponding Author:
E-mail address: shaoL@cumtb.edu.cn (Longyi SHAO)

Inertinite, also called fossil charcoal, is an important and abundant maceral group in coal and coaly mudstone. Inertinite is critical for the study of palaeo-wildfire in deep-time environments, as it provides an insight into the role of fire in reconstructions of the palaeoenvironments. Today wildfires are a common natural phenomenon in different environments with crucial roles in ecosystem destruction and regeneration. It is reasonable to assume that since the evolution of terrestrial plants, wildfires have played similar roles in the geological past. Recently, there has been a significant amount of research on the relationship between palaeo-wildfire, palaeoclimate change and palaeobotany evolution; an understanding of these relations in the geological past is of importance for studying modern ecosystems. This study established positive and negative feedback between inertinite characteristics and

palaeoenvironmental evolution and discussed the role of inertinite in geologic palaeoenvironmental evolution. We argue that palaeo-wildfire events are closely related to terrestrial dynamics, plant evolution, multiple ecosystem changes, and global carbon and phosphorus cycling, and play an irreplaceable role in global ecosystem feedback, acting as "accelerators" during several mass extinction episodes.

Keywords: Inertinite, palaeo-wildfire, atmospheric oxygen, palaeoclimates, terrestrial ecosystems

---

LE&PE 05: Exceptional and extensive Early Ordovician *Cruziana* beds from AlUla, North-West Saudi Arabia

Jan Freedman[1*], Benoit Issautier[2], Yannick Callec[2], Dominique Janjou[3], Olivier Serrano[2], Malick Muhammad Hammad[4], Vicky Rai Chandra[5] and Ahmed Al Shayeb[5]

[1]*Wildlife and Natural Heritage, Royal Commission for AlUla, AlUla, Saudi Arabia*
[2]*BRGM – French Geological Survey, 3 Avenue Claude Guillemin, 45100 Orléans, France*
[3]*Consultant phanerozoic rocks Saudi Arabia. Former BRGM geologist, Olivet, France*
[4]*Department of Geosciences, College of Petroleum Engineering & Geosciences (CPG), King Fahd University of Petroleum & Minerals (KFUPM), Dhahran, Saudi Arabia.*
[5]*Eden Saudi Arabia, 4300 Prince Turkey Street, Al Yarmouk, Khobar, Saudi Arabia*

*Corresponding Author:
E-mail address: j.freedman@rcu.gov.sa (J.Freedman)

AlUla is a county in the North West of Saudi Arabia. The geology of the region is predominantly Early Cambrian and Ordovician sandstone, with Late Precambrian sedimentary, metamorphic and igneous basement rocks found towards the south (Hadley, 1987). The Cambrian and Early Ordovician sandstone formations comprise of the Siq Sandstone (Early Cambrian), Quweira Sandstone (Middle-Late Cambrian) and Saq Sandstone (Early Ordovician) (Whabi, 2014). Historically, there have been a small number of recordings of *Cruziana* trace fossils being found in the north of AlUla (Helal, 1968; Hadley, 1987, Vaslet et al., 1994). However, their extent has not been studied in detail.

Lying unconformably on the Precambrian basement, the reddish Siq Sandstone, known for its higher iron content, is dominated by evidence of fluvial depositional environments. These consist of braided-type to sinuous river and floodplain deposits, with very little evidence of trace fossils (Hadley, 1987; Brown et al., 1989). The Quweira Sandstone, depending on locations within AlUla, lies uncomfortably to para-conformably onto the Siq Sandstone. The sedimentary structures indicate depositional environments passing from braided rivers/alluvial fan deposits to tide and fluvial-dominated shallow marine deposits, with no trace fossils found (Hadley, 1987). From central AlUla to the north, the large Saq Sandstone Formation comprises of the Risha and the Sajir Members (Vaslet et al., 1994). Very small trace fossil trails have been found in most of the Risha Member, which are dominated by braided river-type deposits, however, the uppermost Risha member and the Sajir Member have recently revealed an extremely high concentration of *Cruziana* beds.

The uppermost Risha Member and Sajir Member record several transgressive pulses as well as a significant changes from continental deposits to marine deposits. Sedimentation consists mainly of deltaic deposits with a fluvial-control (Risha Member, lower and middle Sajir Member units) to more mixed upper and lower shoreface deposits in the upper Sajir Member unit. Each of these lithostratigraphic units is associated with great ichnofacies development, with the complexity and

diversity increasing through time, most likely resulting from the life explosion initiated in early Cambrian times and diversifying in Ordovician times.

Several different types of *Cruziana* have now been found and described within the Risha and Sajir members, including *Cruziana pectinate* (Seilacher, 1994), *C. tenella* (Linnarsson, 1871), *C. rugosa* (d'Orbigny, 1842), *C. goldfussi* (Rouault 1850), *C. rusoformis* (Orłowski, 1992), *C. imbricata* (Seilacher, 1970), *C. semiplicata* (Slater, 1853), and *C. almadenensis* (Seilacher, 1970). They are associated with a large diversity of other ichnofacies such *Arthrophycus linearis* (Seilacher, 2000), *A. alleghaniensis* (Harlan, 1831), *Skolithos* (Haldeman, 1840), *Monocraterion* (Torell, 1870), *Rosselia* (Dahmer, 1937), *Zoophycos* (Massalongo, 1855), and *Phycosiphon* (Fischer-Ooster, 1858). Some sites have exceptional preservation of these trace fossils, allowing detailed descriptions of the rich palaeobiodiversity of the Early Ordovician.

A detailed record of the presence of these trace fossils allows the advancement to understanding of previously understudied areas through palaeoenvironmental reconstructions (Brasier and Hewitt, 1979; Bottjer et al., 1988; Aceñolaza and Milana, 2005; Meischner et al., 2020). *Cruziana* beds are also important biostratigraphic markers across regions with similar-aged sedimentary rocks (Crimes, 1969; Crimes, 1987; Aceñolaza and Milana, 2005). In the Arabian Shield, for example, Ordovician African *Cruziana* beds have been correlated with beds in Jordan, providing evidence of the ancient continental processes that shaped Gondwana (Meischner et al., 2020). Further work examining these *Cruziana* fossils from AlUla with specimens across the Arabian Peninsula, and globally, will enable greater, more detailed reconstructions of palaeoenvironments in Gondwana.

References:

Aceñolaza, G.F., Milana, J.P., 2005. Remarkable *Cruziana* beds in the Lower Ordovician of the Corillera Oriental, NW Argentina. Nota Paleontologica 42(3), 633-637.

Bottjer, D.J., Droser, M.L., Joblonski, D., 1988. Palaeonvironmental trends in the history of trace fossils. Nature 333. 252-255.

Brasier, M. D. and Hewitt, R. A., 1979. Environmental setting of fossilifeous rocks from the uppermost Proterozoic - Lower Cambrian of central England. Plaeogeography, Plalaeoclimatology, Palaeoecology 27, 35-37.

Brown, G. F., Schmidt, D. L., and Huffman, A. C., 1989. Geology of the Arabian Peninsula: Shield Area of Western Saudi Arabia. U.S. Geological Survey Professional Paper 560-A.

Crimes, P.T. 1969. Trace fossils from the Cambro-Ordovician rocks of North Wales and their stratigraphic significance. Geological Journal 6, 333-337.

Crimes, P.T. 1987. Trace fossils and correlation of Late Precambrian and Early Cambrian strata. Geological Magazine 124. 97-119.

Hadley, D.G. 1987. Explanatory notes to the geologic map of the Sahl Al Matran quadrangle, sheet 26C, Kingdom of Saudi Arabia. Saudi Arabian Deputy Ministry for Mineral Resources.

Helal, A.H., 1968. Stratigraphy of outcropping Paleozoic rocks around the northern edge of the Arabian Shield (within Saudi Arabia). Zeitschrift der Deutschen geologischen Gesellschaft (band 117, 2. u. 3. teil). 506-543.

Meischner, T., Elicki, O, Masri, A., Moumani, K. A., and Hussein, M. A. A. 2020. Ordovician trace fossils from southern Jordan with particular consideration to the *Cruziana rugose* group: Taxonomy, stratigraphy and trans-regional correlation throughout the Middle East and Northern Africa. Journal of African Earth Sciences 164(10). 103595. https://doi.org/10.1016/j.jafrearsci.2019.103595

Vaslet, D., Janjou, D., Robelin, C., Al Muallem, M.S., Halawani, M.A., Brosse, J.M., Breton, J.P., Courbouleix, S., Roobol, M.J. Dagain, J., 1994.- Geologic map of the Tayma quadrangle (Sheet 27C), Kingdom of Saudi Arabia: Saudi Arabian Deputy Ministry for Mineral Resources, Jeddah, Geoscience Map GM-134.

Whabi A. M. 2014. Sedimentological and Stratigraphic Studies of the Cambro-Ordovician Succession in Northwest Saudi Arabia. (Master thesis). King Fahd University of Petroleum & Minerals, Dhahran – 31261, Saudi Arabia, Dhahran, Saudi Arabia.

LE&PE 06: Fluvial Deposits of the Sai River Basin, Central Ganga Plain: Insights into Morphometry, Depositional Condition and Provenance

S. Kanhaiya[1*], S. K. Yadav[1], S. Tripathi[1], S. Singh[2], M. A. Quasim[3], S. Kumar[5], A. Patra[4]

[1]*Department of Earth and Planetary Sciences, V. B. S. Purvanchal University, Jaunpur 222003, India*
[2]*Department of Geology, Institute of Earth and Environmental Sciences, R. M. L. Awadh University, Ayodhya 224001, India*
[3]*Department of Geology, Aligarh Muslim University, Aligarh 202002, India*
[4]*Department of Geology, Nagaland University, Kohima 797112, India*
[5]*School of Environmental Sciences, Jawaharlal Nehru University 110067, India*

*Corresponding Author:
E-mail address: shyamkanhaiya44@gmail.com (S. Kanhaiya)

River morphology and sedimentological studies of the fluvial sediments play a vital role in deducing the channel dynamics, depositional environment, processes and provenance. In the present study, an attempt is made to describe the regional topography, drainage distribution, depositional processes and provenance of the Sai River Basin, Central Ganga Plain. For the above purpose, a detailed morphometric, lithofacies, textural and heavy mineral analysis were carried out using multi-proxy data sets. Morphometric analysis was done using SRTM data with the help of ArcGIS-10 software, lithofacies association have been identified in the field and the textural analysis was done using a vibratory sieve shaker while the heavy mineral analysis was performed using Bromoform. The area of the basin is 11189.8 km^2 with two sub-basins, which range in area from 1501.15 km^2 to 8105.27 km^2. The drainage pattern of the studied basin is dendritic to sub-dendritic with stream orders ranging from 4^{th} to 5^{th} orders. The drainage density of the basin is 0.41 per km^2, while the bifurcation ratio of the main basin ranges from 2.00 to 6.75 (~ 4.15). A total of five lithofacies i.e. Sp (Planar cross Bedded) [Both Sp1 (Planar Cross bedded foreset inclination < 15°) and Sp2 (Planar Cross bedded foreset inclination > 15°)], Fl (Parallel Lamination), Fc (Convolute lamination), Sr (Ripple Cross Lamination) and Sh (Laminated Horizontal Bedded Sand) were identified in the fluvial deposits of the Sai River. The common lithofacies of the channel bar successions are Sp (Planar cross Bedded) and Sh (Laminated Horizontal Bedded Sand) whereas Sp (Planar cross bedded), Fc (Convolute lamination), Sr (Ripple cross lamination), Fl (Parallel lamination), Fm (Massive sand) and Sh (Laminated horizontal bedded sand) lithofacies are present in point bar succession and Fl (Parallel lamination) and Fm (Massive sand) lithofacies are common in natural levee succession of the river representing varying energy conditions and depositional environment. The mean grain size of the sediments for the channel bar is 2.97 ϕ (ranges from 2.80 - 3.07 ϕ), the point bar is 3.54 ϕ (ranges from 3.05 - 3.28 ϕ) and the natural levee is 3.25 ϕ (ranges from 3.19 - 3.31 ϕ) suggesting that studied sediments are fine sand to very fine sand in nature. The mean standard deviation values for the channel bar sequence is 0.46 ϕ (ranges from 0.45 - 0.50 ϕ), point bar sequences 0.43 ϕ (ranges from 0.39 - 0.51 ϕ) and natural levee sequences 0.56 ϕ (ranges from 0.52 - 0.64 ϕ) suggesting moderate to well-sorted nature of the sediments in all the studied geomorphic units. The mean skewness value of the sediments for the channel bar is 0.01 (ranges from - 0.01 to 0.10), the point bar is -0.14 (ranges from - 0.23 to - 0.03) and natural levee is 0.06 (ranges from 0.17 to - 0.13) suggesting coarse skewed nature of the sediments. The value of kurtosis ranges from 0.83 - 1.06 (mean = 0.91), 0.76 - 1.05 (mean = 0.86) and 0.95 - 1.15 (mean = 1.03) respectively in channel bar, point bar and natural levee sequences suggesting platykurtic to leptokurtic nature of the sediments. The dominant heavy minerals are tourmaline (ranges from 16.3 - 48.8 %), staurolite (ranges from 4.7 - 22.7 %), muscovite (ranges from 3.7 - 18.8 %), epidote (ranges from 6.3 - 13.0 %), zircon (ranges from 2.5 - 12.9 %), brookite (ranges from 1.9 - 12.5 %), chloritoid (ranges from 6.5 - 11.6 %) and kyanite (ranges from 0.3 - 0.6 %) with a few opaque suggesting that the sediments are derived from low to medium grade metamorphic rocks and acid igneous rocks. The ZTR index value ranges from 23.3 - 61.3 % with an average of 37.7 %, which suggests low sediment maturity.

Keywords: Morphometric analysis; Lithofacies; Grain size; Heavy minerals; Provenance

LE&PE 07: Floristic diversity of Gondwana Supergroup and its implications from Nayabazar-Legship Road Section of South Sikkim, India: a multiproxy approach

S Suresh K Pillai[a*], Srikanta Murthy[a], Runcie Paul Mathews[a], Suraj Kumar Sahu[a, b], Anju Saxena[a], Mrutunjay Sahoo[c] and Komal Verma[d]

[a]*Birbal Sahni Institute of Palaeosciences, 53, University Road, Lucknow 226007, India*
[b]*Academy of Scientific and Innovative Research (AcSIR), Ghaziabad 201002, India*
[c]*Department of Geology, Ravenshaw University, Cuttack-753003, Odisha*
[d] *Department of Biochemistry, University of Lucknow, Lucknow-226007, India*

*Corresponding Author:
E-mail address: ssureshk_pillai@bsip.res.in (S Suresh K Pillai)

The present study carried out is based on three proxies i.e. Megafossil, Palynology, and FTIR to determine floral diversity, bio-stratigraphic age and palaeoenviromental conditions that prevailed in the Nayabazar-Legship Road (NLR) Section, of South Sikkim India during Permian Period. Rangit window zone is a fenster allochthonous rock bed situated at Namchi of South Sikkim, India on the Lesser Himalayan sequence. This zone consists of both Precambrian and Permian rock sequences. Lower Permian glacial sediments are very well deposited in this area. It consists of diamictite, glacial boulders and pebbles equivalent to the Lower Permian Talchir Formation. This bed is overlained by the Namchi /Damuda group comprising of sandstone, and carbonaceous shales yielding plant fossil *Glossopteris*. Namchi/Damuda sub-group is not further classified into formations as equivalents Permian sequences are classified in Peninsular India. These sediments are well exposed along the river section. *Glossopteris* leaves are found abundantly along the Rangit River section as it carves out the older Daling rocks to expose the Lower Permian sediments. Leaves are preserved only as impressions on carbonaceous shale and semi-anthracite coal. Compressions of fossils are not found due to tectonic activity along the Lesser Himalayan sequence. These sediments are thermally overmatured leading to the removal of organic compounds. In the present study, six genera and twenty-two species were identified based on macrofloral analysis. The macrofloral assemblage includes *Glossopteris, Gangamopteris, Neogerathioposis*, equisetalean axes, *Vertebraria* and scale leaves. The present palynoassemblage shows the dominance of the non-striate bisaccate pollen *Scheuringipollenites* spp. and the sub-dominance of striate bisaccate pollen *Faunipollenites* spp. This confirms the bio-stratigraphic age to be Lower Barakar palynoflora of Early Permian (Artinskian) affinity and correlates well with the *Scheuringipollenites barakarensis* Assemblage Zone of the Early Permian, Lower Barakar Formation in the Damodar Basin (Tiwari and Tripathi, 1992). Based on the morphological characteristics of leaves - narrow to medium size, narrow midrib and narrow venation patterns fossils, a temperate climate is deduced during the Permian period at the time of deposition of sediments. The abundance of plant megafossils and palynomorphs indicates a high level of vegetation during the deposition of the Barakar Formation sediments. Both the recovered megafloral and palynofloral assemblages indicate an age equivalent to that of the Early Permian Barakar Formation (Artinskian) in the studied section. The present study employs the FTIR technique to characterize the samples (NLR-1 to 6 and NLR- 16) through functional group and inorganic composition. Qualitative analysis of sandstone and shale samples by FTIR spectrometry in a wide wavelength range based on KBr absorbance and attenuated total reflectance shows only inorganic mineral matter peaks, but due to metamorphism, there are no functional group peaks. The FTIR study reveals the presence of carbonate minerals in samples NLR, No.1,2,3,6 and 9 confirms the signature of marine incursion during Lower Permian. This will be the first holistic report of a multiproxy study on megafossil, palynology, and FTIR from South Sikkim. Different authors have denoted the Damuda Formation as a broad bio-stratigraphic age of Permian sediments in Sikkim, but the present study reveals the precise biostratigraphic age of the sediments.

Key Words: North Sikkim, Rangit Formation, *Glossopteris*, Palynology, Permian, FTIR

LE&PE 08: Single-crystal x-ray characterization of heavy minerals in clastic sediments for provenance determination and its implications on basin analysis and landscape evolution

R.Shreelakshminarasimhan[a*], M.Ramkumar[b], R.Nagarajan[c,d], K.J.Juni[b], AL Fathima[b], P. Athira[b], M.Santosh[e,f], P.D.Roy[g], V.Thirukumaran[h], K.Balasubramani[i], D.Menier[j], N.A.Siddiqui[k], M.J.Mathew[l]

[a]*Department of Geology, National College, Tiruchirappalli-620001, India.*
[b]*Department of Geology, Periyar University, Salem-636011, India.*
[c]*Department of Applied Sciences (Applied Geology), Curtin University Malaysia, Miri, Malaysia.*
[d]*Curtin Malaysia Research Institute, Curtin University Malaysia, Miri, Malaysia.*
[e] *chool of Earth Sciences and Resources, China University of Geosciences Beijing, Beijing, China.*
[f] *epartment of Earth Sciences, University of Adelaide, Adelaide, SA, Australia.*
[g]*Instituto de Geología, Universidad NacionalAutónomade México, Ciudad de México, México.*
[h] *Department of Geology, Government Arts College (Autonomous), Salem, India.*
[I] *epartment of Geography, Central University of Tamil Nadu, Thiruvarur- 610005, India.*
[j] *eo-Ocean, Univ Bretagne Sud, Univ Brest, CNRS, Ifremer, UMR6538, Vannes, France.*
[k] *epartment of Geosciences, UniversitiTeknologi PETRONAS, Seri Iskandar, Malaysia*
[l] *epartment of Geography, Geology and the Environment, Kingston University, Kingston Upon Thames KT1 2EE, United Kingdom.*

*Corresponding Author:
E-mail address: shreelakshminarasimhan.r@gmail.com (R.Shreelakshminarasimhan)

On a temporal scale of a few thousands to millions of years of time, sediments, soils, and rocks exposed on the surface of the earth undergo weathering that includes physical, chemical and mineralogical disintegration, which are then transported along the river course. Nevertheless, not all of these segments complete the journey; some are deposited along the way due to differences in their densities and other factors involved in transportation and deposition. The transported materials travel slowly yet towards the confluence and from thereon, to the abyss. Rocks/parent materials of the past, which are completely gone now would have left their remnants behind from which the past can be deciphered.

Deciphering the provenances with the help of heavy mineral occurrences, and associations of types of heavy minerals in placer and/or clastic sediments and sedimentary rocks is a time–tested technique employed in sedimentary basin analysis (Joshi et al., 2021). It is based on the premise that the lithologies that occur in the source area, namely, the igneous, metamorphic, volcanic or sedimentary rocks and soils might have unique combinations of mineral assemblages that can be discriminated to identify, even after a considerable lapse of time between erosion and deposition. The mineral assemblages and each mineral type might have required specific P-T conditions of crystallization that might have also been unique to the formation of specific rock types. The prevalence and sustenance of those specific P-T conditions play a role in the formation and occurrence of stoichiometric and non-stoichiometric mineral/crystal grains, a trait we in this paper attempt to exploit to accurately characterize/discriminate geochemically-mineralogically-crystallographically fingerprint the **a)** source areas, **b)** conditions of crystallization and discriminate source rock types more precisely than genetically generalist assumptions, and **c)** demonstrate the utility of a new technique in basin analysis.

In this study, we generated data on “Single-crystal diffraction” which uses only a single crystal. This technique involves measuring directions and intensities of diffraction when a collimated X-ray beam strikes a carefully oriented small crystal (Alexander and Smith, 1962; Li et al., 2014). The crystal size used in this method is 50 to 250 microns in longest dimensions. This analytical technique documents crystal structure including unit cell dimensions, bond-lengths, bond-angles and site-ordering

information. As the crystal-chemical controls on mineral chemistry, data are acquired in terms of structures of high-pressure and high-temperature phases and powder patterns from a single crystal. These data are then processed for generating crystal – atomic structure of the material under study and interpreted for the geological provenances and other requirements, as the case may be.

As a case study, three major river basins draining the southern part of Peninsular India, namely, the Cauvery (**Fig.1 A (b)**, the Vaigai (**Fig.1A (c)** and the Thamirabarani (**Fig.1A (d)** are chosen to examine these premises. Systematic fieldwork, documenting geology, structure, geomorphology, landuse, soil, vegetation and other characteristics was conducted. In addition, sediment samples (n: Cauvery 60; Vaigai 60; Thamirabarani 52) were collected from the middle of the trunk channel and heavy minerals were separated from these samples following standard laboratory protocols. Tabulation, quantification, and reflective light microscopic examination were conducted to characterize the heavy mineral occurrence. Three samples from each of the basins, covering upper, middle and lower stream sections were chosen for single crystal X-Ray study. From the heavy mineral separates of these chosen samples, individual heavy mineral grains such as zircon, garnet, magnetite, rutile, etc. among others, were examined under single crystal X-ray diffraction.

Though these three rivers drain over Precambrian basement rocks and other myriad varieties of lithologies, there are many commonalities, but have diverse accessory minerals in them (Fig.1A (e), a trait, we intend to exploit towards the objectives of this study. We hypothesize that though the river transport brings and delivers unique heavy mineral assemblages toward downstream and ultimately to the coastal regions, they may get mixed, and the unique signature might have been overprinted by marine overprinting, especially through sorting, littoral and tidal currents and waves. In order to discriminate this mixing/overprinting related agglomeration of coastal heavy mineral assemblage, if specific signatures in terms of bonding characteristics of heavy minerals are ascribed/ascribable to each basin, it would be useful to discriminate the relative contribution of each of the basin, pinpoint the provenance regions of within each of the basin, as well as directional movement of sediments in the coastal realm, i.e., north, south, offshore, onshore, etc.

Examination of the occurrences of heavy minerals in each of the chosen river channels, as well as that, occur along the Tamil Nadu coastal region (Fig.1A (e) reveals the following: **a)** A complete list of possible heavy minerals that occur along the coastal zone of Tamil Nadu, that might have been invariably brought in by the east flowing rivers including the Cauvery, Vaigai and Thamirabarani. **b)** The Venn diagram of heavy mineral distribution among the studied river basins indicates certain uniqueness for each of the basins **c)** Nevertheless, each of the unique association/occurrence in the specific basin(s) suggest plausible meta-igneous/meta-sedimentary and basic-igneous source/provenances, that were not geographically extensive and or not exposed currently anywhere in the basin and **d)** this peculiarity necessitates enlisting and/or fingerprinting the heavy minerals and their unique characteristics through specific traits, a factor that influenced the authors to examine single crystal x-ray of chosen heavy mineral grains.

Occurrences of perfect stoichiometric zircon (**Fig.1A C, D**) in all the river basins studied, together with altered mineral phases of zircon, rutile, magnetite, and garnet, are recognized during the initial part of the study and we are confident of gathering convincing evidence and demonstrating the utility of atomic crystal structure for provenance studies.

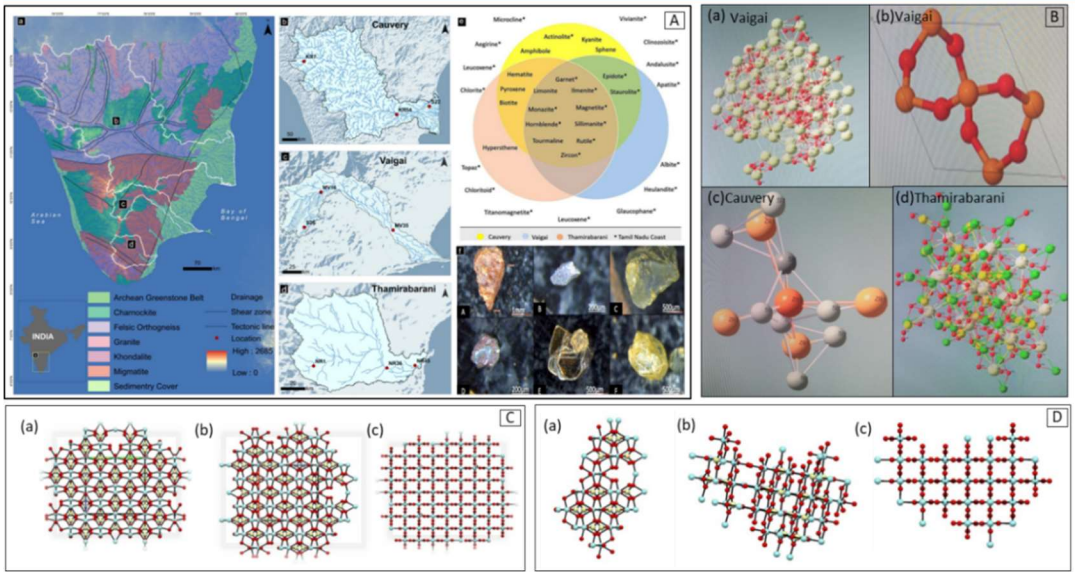

Figure 1. A: Location of the study area, and distribution data of heavy minerals of the river basins and the single-crystal X-ray data pattern of the selected sample(s); **B:** The atomic crystal structure of garnet **a)**, Monazite **b)** from Vaigai River Basin, Zircon **c)** from Cauvery River Basin, and Garnet **d)** from Thamirabarani River Basin; **C:** Represents the Packing of molecules along a, b and c axis of the selected zircon grain showing **a)**, **b)**, **c)** respectively; **D:** The molecular structure viewed in ORTEP software in different directions showing **a)**, **b)** and **c)**; Table 1 shows crystal data and the Bond length (Å) for the selected zircon grain in the Vaigai River Basin.

Table 1. Results of Single crystal XRD for the selected grains of Zircon

Atomic coordinates and equivalent isotropic atomic displacement parameters (Å²)

$U(eq)$ is defined as one third of the trace of the orthogonalized U_{ij} tensor.

	x/a	y/b	z/c	U(eq)
Zr1	0.000000	0.500000	0.49992(8)	0.0200(17)
Zr2	0.25032(8)	0.99996(8)	0.62529(9)	0.041(3)
Zr3	0.75002(5)	0.75003(5)	0.25053(5)	0.0210(17)
Zr4	0.50006(8)	0.74985(8)	0.37454(9)	0.041(3)
Zr5	0.500000	0.500000	0.500000	0.0209(17)
Zr6	0.500000	0.500000	0.000000	0.0210(17)
Si1	0.500000	0.000000	0.750000	0.081(7)
Si2	0.500000	0.500000	0.2476(4)	0.074(6)
Si3	0.74997(17)	0.49994(16)	0.37562(19)	0.014(4)
Si4	0.49988(15)	0.74981(16)	0.12431(19)	0.013(4)
Si5	0.2510(3)	0.7499(3)	0.5038(4)	0.084(6)
Si6	0.500000	0.000000	0.250000	0.077(8)
O1	0.4988(7)	0.8403(7)	0.0359(10)	0.022(2)
O2	0.4980(8)	0.9090(7)	0.3410(10)	0.027(3)
O3	0.4074(7)	0.0025(9)	0.6581(11)	0.025(3)
O4	0.2480(8)	0.6585(7)	0.5927(11)	0.027(3)
O5	0.5013(9)	0.5942(8)	0.3420(11)	0.025(3)
O6	0.6605(7)	0.4994(7)	0.4650(10)	0.022(2)
O7	0.8417(7)	0.5000(8)	0.4621(10)	0.022(3)
O8	0.7504(8)	0.4096(7)	0.2882(10)	0.023(3)
O9	0.5917(7)	0.4968(8)	0.1589(10)	0.026(3)
O10	0.5009(8)	0.6588(7)	0.0378(10)	0.023(3)
O11	0.5922(7)	0.7509(7)	0.2146(10)	0.022(2)
O12	0.4107(7)	0.7490(7)	0.2153(10)	0.022(2)
O13	0.7496(8)	0.5918(7)	0.2887(10)	0.021(3)
O14	0.2523(8)	0.8432(7)	0.5907(10)	0.024(3)
O15	0.1572(7)	0.7521(8)	0.4083(10)	0.023(3)
O16	0.3433(7)	0.7475(8)	0.4087(11)	0.025(3)

Crystallographic properties

Chemical formula	$O_{16}Si_4Zr_4$	
Formula weight	733.24 g/mol	
Temperature	296(2) K	
Wavelength	0.71073 Å	
Crystal system	tetragonal	
Space group	I -4	
Unit cell dimensions	a = 13.2322(4) Å	α = 90°
	b = 13.2322(4) Å	β = 90°
	c = 11.9979(6) Å	γ = 90°
Volume	2100.73(16) Å^3	
Z	8	
Density (calculated)	4.637 g/cm^3	
Absorption coefficient	4.433 mm^{-1}	
F(000)	2752	

Bond lengths (Å)

Zr1-O7#9	2.143(9)	Zr1-O7	2.143(9)
Zr1-O1#18	2.157(9)	Zr1-O1#12	2.157(9)
Zr1-O3#6	2.257(12)	Zr1-O3#2	2.257(12)
Zr1-O2#6	2.257(12)	Zr1-O2#2	2.257(12)
Zr1-Si1#11	2.9985(10)	Zr1-Si6#12	3.0005(10)
Zr1-Zr2#6	3.6292(11)	Zr1-Zr2#2	3.6292(11)
Zr2-O14	2.115(10)	Zr2-O15#5	2.120(10)
Zr2-O3	2.116(10)	Zr2-O9#10	2.137(10)
Zr2-O1#13	2.271(11)	Zr2-O8#10	2.292(12)
Zr2-O10#13	2.302(12)	Zr2-O13#10	2.307(11)
Zr2-Si4#13	2.995(3)	Zr2-Si3#10	3.003(3)
Zr2-Zr3#4	3.6275(12)	Zr3-O11	2.133(9)
Zr3-O13	2.143(10)	Zr3-O8#15	2.162(9)
Zr3-O12#16	2.165(9)	Zr3-O4#2	2.237(12)
Zr3-O15#16	2.267(11)	Zr3-O14#2	2.269(12)
Zr3-O16#16	2.275(12)	Zr3-Si5#2	2.948(5)
Zr3-Si5#16	3.051(5)	Zr3-Zr4	3.6267(13)
Zr4-O5	2.097(10)	Zr4-O16	2.115(10)
Zr4-O4#2	2.134(10)	Zr4-O2	2.144(10)
Zr4-O12	2.247(11)	Zr4-O6#4	2.259(11)
Zr4-O11	2.273(11)	Zr4-O7#4	2.306(12)
Zr4-Si3#4	2.998(3)	Zr4-Si4	3.002(3)
Zr4-Zr5	3.6326(10)	Zr5-O6	2.164(10)
Zr5-O6#7	2.164(10)	Zr5-O6#4	2.164(10)
Zr5-O6#2	2.164(10)	Zr5-O5	2.268(12)
Zr5-O5#7	2.268(12)	Zr5-O5#2	2.268(12)
Zr5-O5#4	2.268(12)	Zr5-Si2#2	3.028(5)
Zr5-Si2	3.028(5)	Zr6-O10	2.149(10)
Zr6-O10#3	2.149(10)	Zr6-O10#7	2.149(10)
Zr6-O10#1	2.149(10)	Zr6-O9	2.260(12)
Zr6-O9#1	2.260(12)	Zr6-O9#7	2.260(12)
Zr6-O9#3	2.260(12)	Zr6-Si2	2.971(5)
Zr6-Si2#1	2.971(5)	Si1-O3	1.648(11)
Si1-O3#14	1.648(11)	Si1-O3#8	1.648(11)
Si1-O3#17	1.648(11)	Si2-O9	1.615(11)
Si2-O9#7	1.615(11)	Si2-O5#7	1.684(12)
Si2-O5	1.684(12)	Si3-O8	1.590(11)
Si3-O6	1.598(11)	Si3-O7	1.597(11)
Si3-O13	1.602(10)	Si4-O10	1.590(11)
Si4-O1	1.599(10)	Si4-O12	1.607(11)
Si4-O11	1.633(10)	Si5-O4	1.613(12)
Si5-O14	1.617(11)	Si5-O16	1.671(12)
Si5-O15	1.688(12)	Si6-O2	1.626(11)
Si6-O2#8	1.626(11)	Si6-O2#13	1.626(11)
Si6-O2#16	1.626(11)		

Anisotropic atomic displacement parameters (Å²)

The anisotropic atomic displacement factor exponent takes the form: $-2\pi^2[h^2a^{*2}U_{11} + \ldots + 2hka^*b^*U_{12}]$

	U_{11}	U_{22}	U_{33}	U_{23}	U_{13}	U_{12}
Zr1	0.016(2)	0.016(2)	0.028(3)	0.000000	0.000000	0.0000(4)
Zr2	0.038(4)	0.018(4)	0.047(5)	0.0003(5)	0.0001(5)	0.0001(5)
Zr3	0.018(2)	0.018(2)	0.027(2)	-0.0002(3)	0.0002(3)	0.0000(3)
Zr4	0.037(4)	0.018(4)	0.047(5)	-0.0003(5)	0.0004(5)	0.0000(5)
Zr5	0.018(2)	0.018(2)	0.027(3)	0.000000	0.000000	0.000000
Zr6	0.018(2)	0.018(2)	0.027(3)	0.000000	0.000000	0.000000
Si1	0.072(10)	0.072(10)	0.098(11)	0.000000	0.000000	0.000000
Si2	0.055(8)	0.049(8)	0.116(14)	0.000000	0.000000	0.002(2)
Si3	0.006(5)	0.007(5)	0.027(7)	0.0002(9)	-0.0009(9)	0.0006(7)
Si4	0.006(3)	0.007(5)	0.027(7)	-0.0007(9)	-0.0008(9)	0.0002(7)
Si5	0.073(10)	0.072(10)	0.107(10)	0.0007(19)	0.001(2)	0.000(2)
Si6	0.067(10)	0.067(10)	0.099(12)	0.000000	0.000000	0.000000
O1	0.019(4)	0.027(5)	0.021(5)	0.001(3)	0.007(5)	0.000(4)
O2	0.033(6)	0.022(5)	0.025(6)	-0.003(4)	-0.003(6)	0.000(4)
O3	0.022(5)	0.030(6)	0.024(6)	-0.002(4)	-0.002(4)	-0.001(4)
O4	0.031(6)	0.023(5)	0.026(6)	-0.001(4)	-0.001(6)	0.001(4)
O5	0.029(6)	0.020(5)	0.025(6)	-0.002(4)	0.000(6)	-0.002(4)
O6	0.024(5)	0.020(4)	0.023(5)	-0.008(3)	0.001(5)	-0.001(4)
O7	0.022(5)	0.022(5)	0.023(7)	0.006(6)	0.000(4)	-0.001(4)
O8	0.022(5)	0.023(5)	0.024(8)	-0.004(4)	-0.006(6)	0.000(4)
O9	0.025(5)	0.030(6)	0.023(6)	0.004(6)	-0.001(4)	-0.002(4)
O10	0.022(5)	0.026(6)	0.022(7)	0.002(4)	-0.006(6)	0.000(4)
O11	0.023(5)	0.020(4)	0.023(5)	0.006(5)	-0.003(3)	-0.001(4)
O12	0.024(5)	0.021(4)	0.021(5)	-0.005(5)	0.001(3)	-0.001(4)
O13	0.019(5)	0.023(5)	0.020(7)	0.005(4)	0.007(6)	0.000(4)
O14	0.029(6)	0.022(5)	0.022(8)	0.000(4)	0.002(6)	0.000(4)
O15	0.018(5)	0.029(6)	0.023(5)	-0.002(6)	0.002(4)	0.000(4)
O16	0.023(5)	0.029(6)	0.023(7)	0.001(6)	-0.001(4)	0.001(4)

References:

Alexander, L.T., Smith, G.S., 1962. Single crystal intensity measurements with the three-circle counter-diffractometer. Acta Crystallographica 15, 983-1004.

Joshi, K.B., Banerji, U.S., Dubey, C.P. and Oliveira, E.P., 2021. Heavy minerals in provenance studies:An overview. Arabian Journal of Geosciences 14, 1-16.

Li, S., Wu, X., Pan, Q., Cheng, Q., Li, H., 2014 Comparison of the accuracy of powder and single-crystal X-ray diffraction techniques in determining organic crystal structure. Chinese Science Bulletin 59, 497-501.

LE&PE 09: Palynofloristics and evidence for wildfire from Permian deposits of the Satpura Gondwana Basin, India: a multiproxy approach

Anju Saxena[a*], Srikanta Murthy[a], S Suresh K Pillai[a], Ranjit Khnagar[b], Dieter Uhl[c], Vikram Pratap Singh[a], Suyash Gupta[a] and Nandeshwar Borkar[d]

[a]*Birbal Sahni Institute of Palaeosciences, 53, University Road, Lucknow 226007, India*
[b]*Geological Survey of India, State Unit: Manipur and Nagaland, Northeastern Region, Circular Road, Dimapur–797112, India*
[c]*Senckenberg Forschungsinstitut und Naturmuseum Frankfurt, Senckenberganlage 25, 60325 Frankfurt am Main, Germany*
[d]*Geological Survey of India, Central Region, Seminary Hills, Nagpur–440006, India*

*Corresponding Author:
E-mail address: anju_saxena@bsip.res.in (Anju Saxena)

The Permian deposits in peninsular India are confined to five major Gondwana sedimentary basins namely, Damodar, Son, Mahanadi, Satpura and Wardha-Godavari, and these sequences are characterized by five distinct formations namely Talchir, Karharbari, Barakar, Barren Measures and Raniganj in stratigraphical order. The deposition in these basins commenced with Permo-Carboniferous deglaciation, predominantly in fluvio-lacustrine settings with occasional incidences of marine incursions. In the present study, palynological and fossil charcoal analyses of the Barakar and Motur sediments (equivalent to Barren Measures Formation) procured from bore-core PKK-2B (445.5 m thick), located in the Pench-Valley Coalfield, Satpura Basin (India) were carried out to assess the palaeofloral diversity, palynostartigraphic status, age and evidence for palaeowildfire. The procured bore-core intersected through Barakar Formation (between 595.40- 513.96 m depth) comprising sandstones, shales, clay and coal; Motur Formation (between 512.10- 149.65 m depth) comprising medium- coarse reddish-brown sandstone, grey-chocolate clay and mudstones; Jabalpur Formation (between 149.35- 143.85 m depth) comprising medium-grained sandstone and siltstone and Deccan traps (between 142.85- 2.40 m depth) consisting of dark grey-greenish basalt. Eighteen samples were collected at different intervals from the core of which 5 samples were from the Barakar Formation, and 13 samples were from the Motur Formation The core sediments belonging to the Barakar Formation exhibit typical cyclic sedimentation, deposited in a fluvial environment. The palynological study reveals the identification of two distinct palynoassemblages namely Palynoassemblage-I (Barakar) and Palynoassemblage –II (Motur). Palynoassemblage -I is *Faunipollenites varius* palynoassemblage and dated as Kungurian (late Early Permian) and Palynoassemblage II is *Gondisporites raniganjensis* palynoassemblage dated as Lopingian (Late Permian) in age. These assemblages show the dominance of pollens having affinities with Glossopteridales followed by Cordaitales and Coniferales.

In this sedimentary sequence, the occurrence of macroscopic charcoal is also reported at two levels suggesting the incidents of repeated wildfires in the surrounding area. These macroscopic charcoal fragments revealed anatomical features such as bordered pitting, rays with varying heights with tapering ends, and helical thickenings on the cell walls of tracheids. These features suggest a gymnospermous wood affinity. Frequent occurrences of large-sized charcoal fragments are encountered in some layers and most of the specimens exhibit rounded edges suggesting an allochthonous origin. In addition, the fusinite reflectance study of these charcoal/inertinite fragments indicates that they were formed in the temperature range of~ 305-962°C. This suggests that incidents of palaeowildfire occurred at two levels, one is of high-temperature crown fires, together with other medium- and low-temperature surface- and ground fires respectively.

Keywords: Charcoal; Fusinite; Late Permian; Palaeowildfire; Palynotaxa

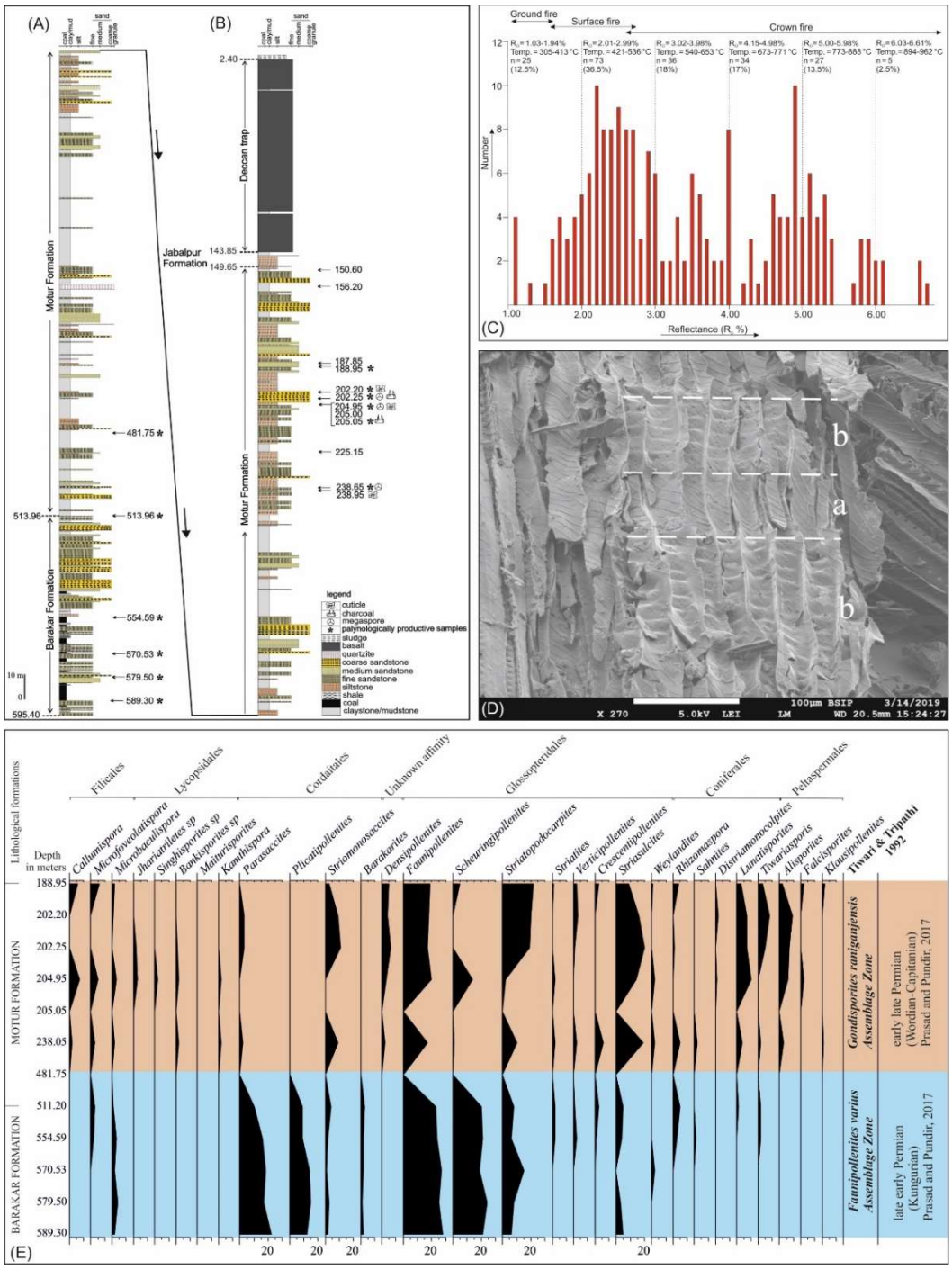

Figure 1. (A, B) Lithocolumn of the bore-core PKK-2B (Satpura Gondwana Basin) showing the position of samples, different formations and lithofacies. (C) The histogram of cumulative fusinite reflectance values shows calculated combustion temperatures and reconstructed fire types. (D) Tangential view of charred wood showing cross-field pitting of rays (b). (E) Frequency chart showing the vertical distribution of different palynomorphs recovered in the bore-core along with their botanical affinities and palynological assemblage zones.

LE&PE 10: Using Biogeochemical Indices to Assess Water and Sediment Quality: Insights from Kavaratti Island, Lakshadweep Archipelago

Euniksha Mohapatra[a], Babu Nallusamy[a*], Rakhil Dev[b], Krishnakumar Subbiah[c], Vijay Anand S[d]

[a]*Department of Geology, Central University of Karnataka, Kalaburagi, 585367, India*
[b]*Department of Marine Geology and Geophysics, Cochin University of Science and Technology, Kochi, 682016, India*
[c]*Department of Geology, Malankara Catholic College, Mariagiri, Kanyakumari, 629153, Tamil Nadu, India*
[a]*Department of Applied Sciences (Applied Geology), Curtin University, Miri, Sarawak, Malaysia*

*Corresponding Author:
E-mail address: babun@cuk.ac.in (Babu Nallusamy)

Reef-associated sediments were collected from 9 locations around densely populated Kavaratti Island (2396 persons/Sq.km) of the Lakshadweep archipelago in the north-western Indian Ocean. Since recent advancements in modernization and developmental activities on the island might have affected the reefs, the FoRAM Index (FI) and ecological indices were used to understand the current status of reef health. The quality of water and sediments from the intertidal zone of Kavaratti Island were studied for this purpose. This study recorded eight benthic foraminiferal species corresponding to seven foraminiferal genera in diverse abundance. Out of these, *Amphistegina*, *Neorotalia*, and *Sorites* genera belong to the symbiont-bearing functional group (**Fig.1**). At the same time, *Ammonia* belongs to Opportunistic and *Quinqueloculina*, *Planorbulinella*, *Cornuspira*, and *Uvigerina*, belonging to the Heterotrophic functional group, respectively. The FI>4 in all stations indicates the healthy nature of water and reefs; moreover, the proximity of FI values to 10 indicates the virtually contaminant-free nature of water. On the other hand, trace metal concentrations were measured from sediment, and ecological indices were calculated. The decreasing order of heavy metal concentrations in the sediments is ranked as Fe> Mn> Zn> Cr> Nd> Cu> Ni> Rb> Pb> Th> Sm> As> Co> Cd> Ag. The Contamination factor (*CF*) shows values <1, which indicates that the area is at a low level of contamination. The pollution load index (*PLI*) values (<1) also point to the fact that the study area is not currently polluted. Similarly, the potential ecological risk coefficient (E^i_r) shows values <40, and the potential ecological risk index (*RI*) shows values <150 also indicates lower contamination (**Table 1**). Based on these biogeochemical indices, Kavaratti Island is classified as highly conducive to reef growth. The developmental and tourism activities have not yet had any impact on the quality of water, sediment, or reef health. These parameters indicate that the water, sediment, and reefs surrounding Kavaratti Island exhibit favourable conditions.

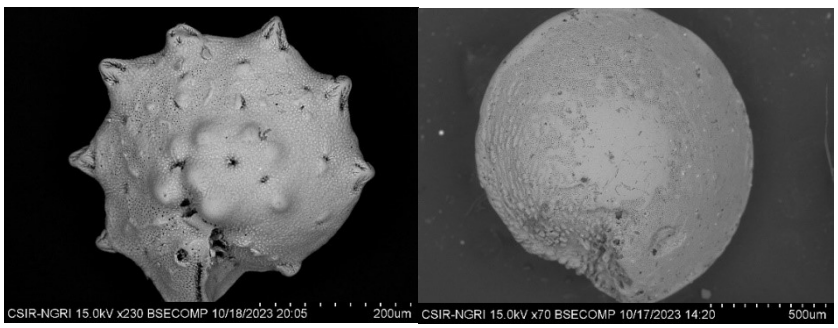

Fig. 1. Scanning electron micrographs of the dominant foramnifers from Kavaratti Island. *Neorotalia calcar* on the left and *Amphistegina lessonii* on the right.

Table 1. The values of Foram Index **(FI)**, Potential ecological risk coefficients (E^i_r), Conatmination factor (C_F), Potential ecological risk index **(*RI*)**, Pollution Load Index **(*PLI*)** from the intertidal zones of Kavaratti Island, Lakshadweep Archipelago.

St. No	FI	Potential ecological risk coefficients (E^i_r) and Contamination factor (C_F) for single heavy metals.												(*RI*)	*LI*)
		Cd		Pb		Cu		Ni		Zn		Cr			
		E^i_r	C_F	E^i_r	C_F	E^i_r	C_F	E^i_r	C_F	E^i_r	C_F	E^i_r	C_F		
KV 1	9.93	0.26	0.21	0.05	0.04	1.20	0.05	0.64	0.03	0.13	0.05	0.72	0.06	2.99	0.08
KV 2	9.97	0.13	0.11	0.03	0.03	1.02	0.04	0.97	0.05	0.25	0.09	1.00	0.09	3.40	0.07
KV 3	9.93	0.15	0.12	0.01	0.08	1.50	0.07	0.39	0.02	0.36	0.14	0.52	0.05	2.93	0.08
KV 5	9.89	0.14	0.11	0.05	0.04	0.99	0.04	0.24	0.01	0.21	0.08	0.35	0.03	1.97	0.05
KV 6	9.97	0.19	0.16	0.25	0.19	1.68	0.07	0.34	0.02	0.28	0.11	0.46	0.04	3.21	0.10
KV 7	9.95	0.14	0.11	0.10	0.06	2.39	0.10	0.43	0.02	0.59	0.22	0.72	0.06	4.40	0.10
KV 8	10	0.18	0.15	0.05	0.04	0.99	0.04	0.45	0.02	0.33	0.13	0.53	0.05	2.53	0.07
KV 9	9.99	0.16	0.13	0.05	0.04	1.04	0.05	0.37	0.02	0.24	0.09	0.43	0.04	2.30	0.06
KV 10	10	0.20	0.17	0.05	0.05	1.58	0.07	0.59	0.03	0.32	0.12	0.58	0.05	3.33	0.08

Keywords: Benthic Foraminifera, Lakshadweep Reefs, FORAM Index, Ecological Indices, Heavy Metal Contamination

---

LE&PE 11: Palaeobotanical and Geochemical Evidences for Permian-Triassic Transition from Talcher Coalfield, Son-Mahanadi Basin, India: Insights into the Age, Palaeovegetation and Palaeoclimate

Srikanta Murthy[1*], Deveshwar P. Mishra[1,3], Dieter Uhl[2], Anju Saxena[1] Vikram P. Singh[1], Runcie P. Mathews[1], Anurag Kumar[1], Bindhyachal Pandey[3]

[1]*Birbal Sahni Institute of Palaeosciences, Lucknow 226007, India*
[2]*Senckenberg Forschungsinstitut und Naturmuseum Frankfurt, Senckenberganlage 25, 60325 Frankfurt am Main, Germany*
[3]*CAS Dept. of Geology, Banaras Hindu University, Varanasi- 221005, India*

*Corresponding Author:
E-mail address: srikanta_murthy@bsip.res.in (Srikanta Murthy)

The Talcher Coalfield is located in the southeastern corner of the Mahanadi Basin, India. This study provides a combined analysis of the palynology, fossil charcoal, isotopes and biomarkers of the subsurface deposits from borehole TTB-7, attempting to establish the chronology of sedimentation and to propose palaeobotanical and geochemical evidence for the occurrence of wildfires during deposition.

Two distinct palynoassemblages have been identified. Palynoassemblage I is characterized by the dominance of *Striatopodocarpites* and sub-dominance of *Densipollenites* confirming a Lopingian age. Palynoassemblage II exhibits mixed palynomorphs of the Late Permian-Early Triassic age, denoting the possibility of Permian-Triassic transition. The palynoassemblages reveal the dominance of Glossopteridales and Coniferales along with Filicales, Lycopsids, Equisetales, Cordaitales and Peltaspermales. Further, a bimodal *n*-alkane distribution pattern indicates the contribution of terrigenous and microbial sources. Although, the occurrences of long-chain alkanes indicate higher plants, the low P_{wax} values (< 0.26) suggest relatively less input. The P_{aq} values (≅ 1) and amorphous organic matter (av. 33.24%) suggest a high macrophyte input in the samples pointing to the occurrence of moderate aquatic conditions in the basin. Furthermore, the hopanoid distributions and degraded

organic matter (av. 29.96%) reflect the bacterial degradation of organic matter. Also, the $\delta^{13}C$ values of the section varied from -31.2‰ to -21.8‰ (**Fig.1**). The large carbon isotopic offset of 9.4‰ across the (assumed) Permian-Triassic transition, Pr/Ph ratio (0.3-1.3) and distribution of palynofacies composition of the studied section apparently indicate a significant change in climatic conditions. Moreover, the structured macroscopic charcoal fragments with homogenized cell walls, uniseriate to biseriate pitting and rays point to the contribution of gymnospermous wood with severe fungal infection before charring.

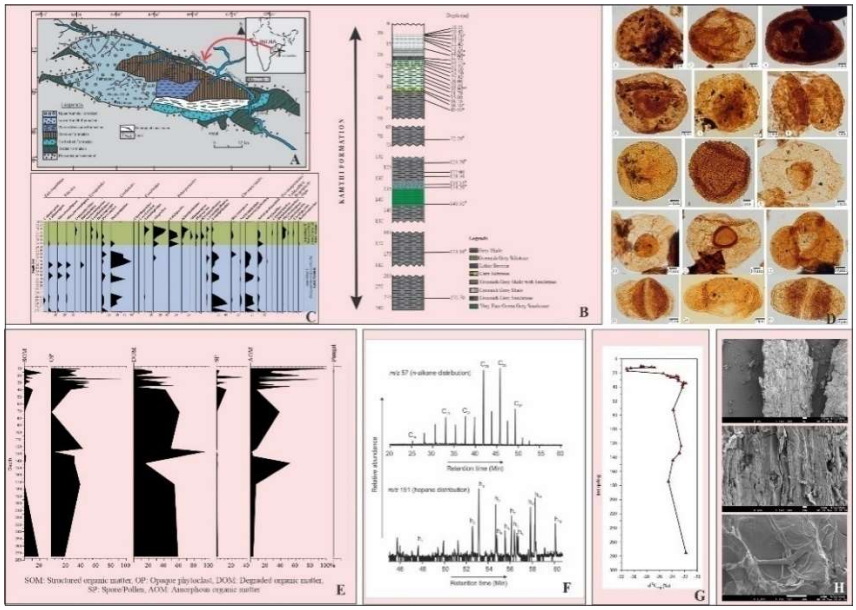

Figure 1. The composite figure shows A. showing the location of the borehole TTB-7, B. position of samples in the litholog, C. frequency chart showing the vertical distribution of palynotaxa, D. marker palynotaxa from Permian and early Triassic, E. frequency chart of palynofacies study, F. distribution of *n*-alkanes and hopanes, G. Bulk organic carbon in per mil (δ^{13}Corg ‰), H. SEM images of charred wood showing anatomical details and Fungal hyphae.

Keywords: Glossopteridales, Palynology, Palynofacies, Bulk carbon isotope, Palaeowildfire, Biomarkers

LE&PE 12: Palynological and palynofacies analysis for age estimation and depositional setting of Lower Gondwana sequence, Korba region, Mahanadi Basin, India

Deveshwar P. Mishra*[1], Pooja Tiwari[1], Srikanta Murthy[1], Biswajeet Thakur[1]

[1]*Birbal Sahni Institute of Palaeosciences, Lucknow, 226007*

*Corresponding Author:
E-mail address: dpmishra@bsip.res.in (Deveshwar P. Mishra)

The Korba Coalfield occupies the south-central part of Son-Mahanadi basin and is situated in the Korba and Bilaspur districts of Chhattisgarh Indian State. The Lower Gondwana deposits of the Korba Coalfield are exposed along the Devpahri road section Korba region (22°36′25.1″ N and 82°43′40.8″ E). The eight outcrop samples of coaly shale were collected and analyzed for palynological and palynofacies studies. The palynological assemblage is dominated by monosaccate pollen mainly *Parasaccites* and sub-dominated by trilete spore *Callumispora* along with other monosaccate pollen *Plicatipollenites*, *Barakarites*, as well as striate bisaccate pollen viz. *Scheuringipollenites*, *Faunipollenites* and *Chordasporites*. Palynology is indicative of *Crucisaccites monoletus* assemblage

zone (*Parasaccites-Callumispora* Zone) from the Upper Karharbari Formation, dated as an Early Permian (Artinskian) age for the studied section. The palynofacies association reveals varying proportions of brown degraded organic matter (OM), opaque phytoclasts, structured OM, and palynomorphs, with very low levels of amorphous OM (AOM). Based on the kerogen component, four distinct palynofacies assemblages are identified viz. Assemblage I is dominated by palynomorphs, followed by brown degraded OM and opaque phytoclasts, with low AOM, Assemblage II is Characterized by a dominance of brown degraded OM, with a fair representation of opaque phytoclasts, palynomorphs, and structured OM, and sporadic AOM. The Assemblage III is marked by a co-dominance of opaque phytoclasts and brown degraded OM, with fewer structured OM and palynomorphs, and limited AOM. Alternately, the Assemblage IV features highly structured OM, moderate amounts of opaque OM and brown degraded OM, and very low AOM. Based on the palynofacies data ternary plot was prepared for establishing a depositional environment. The palaeoenvironment inferred based on the plot suggests a proximal shelf, indicated by the high contribution of phytoclasts, with significant terrestrial influx. The presence of opaque phytoclasts with internal structure indicates long-distance transport and evidence of palaeo-fires. The high abundance of palynomorphs in samples shows areas of high biodiversity under moderately oxidizing conditions.

Graphical Abstract:

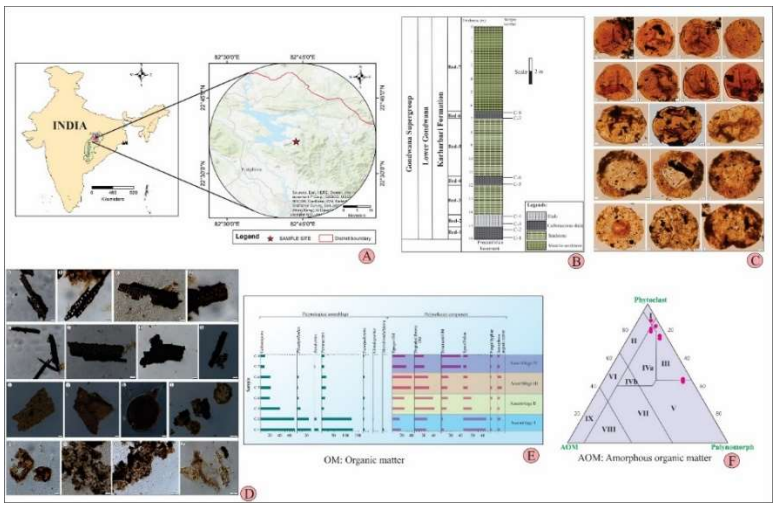

Figure 1 shows: A.Location map of the study area; B.Litholog of the study area; C. Palynomorphs recovered from Korba region; D.Organic matter recovered from Korba region; E.Frequency chart showing the distribution of palynomorphs and palynofacies component and F.Ternary plot showing the distribution of organic matter

Key words: Palynology, Palynofacies, Palaeo-fire, Biodiversity, Artinskian, Karharbari

LE&PE 13: Early Permian palynofloristics from Son-Mahanadi Basin, Chhattisgarh: Implications for age assessment and palaeoenvironment

Suyash Gupta[a*], Anju Saxena[a], Srikanta Murthy[a], Neha Aggarwal[a], Husain Shabbar[b], S Suresh Kumar Pillai[a]

[a]*Birbal Sahni Institute of Palaeosciences, 53, University Road, Lucknow 226007, India*
[b]*Department of Geology, Parul University, Vadodara, Gujarat- 391760, India.*

*Corresponding Author:
E-mail address: suyashgupta2007@gmail.com (Suyash Gupta)

The Gondwana sediments in Peninsular India are mostly of terrestrial origin and preserved generally in half-graben structures, bounded on their southern boundary by normal faults. These Gondwana sediments were commenced during the Permo-Carboniferous Period after a long hiatus since Proterozoic and chiefly distributed in the five major basins of peninsular India viz. Damodar-Koel, Son-Mahanadi, Satpura, Rajmahal and Wardha-Godavari Basin. It covers approximately 200Ma time span from the Latest Carboniferous to the Early Cretaceous Period. In this time span, lower and upper Gondwana sedimentations were occurred and studied as the Gondwana Supergroup. Lower Gondwana is more economically important due to the vast preservation of coal, it contains approximately 99% reserves of the country. The complete Lower Gondwana succession comprises the Talchir, Barakar, Barren Measures and Raniganj formations respectively.

The present work elucidates the palynofloral and palynofacies studies from two outcrop sections of the Talchir Formation, located in the Chirimiri area, Chhattisgarh, Son- Mahanadi Basin, India. The first outcrop section named 'CTF-1' is characterised by the dominance *Plicatipollenites* and sub-dominance of *Parasaccites* monosaccate pollen grains. The assemblage also contains other monosaccate pollen grains such as *Potonieisporites Caheniasaccites*, *Divarisaccus*, *Gondwanpollis, Striomonosaccites* and bisaccate pollen grains namely *Circumstraitites*, *Limitisporites*, *Faunipollenites*, *Crescentipollenites*, *Rhizomaspora*, *Striatopodocarpites*, *Lunatisporites* along with rare occurrence of trilete spores namely *Calamospora*, *Callumispora and Verrucosisporites*. Therefore, based on dominant and sub-dominant pollen grains recovered palynoassemblage of the CTF-1 section is correlated with Lower Talchir palynoassemblage "*Plicatipollenites gondwanensis* Assemblage Zone" and Asselian age is assigned.

The second section 'CTF-2' has a dominance of monosaccate pollen grains mainly *Parasaccites*, and followed by a sub-dominance of *Plicatipollenites* pollen grains. The assemblage also contains the other pollen grains namely *Potonieisporites*, *Tuberisaccites* and bisaccate pollen grains *Limitisporites, Faunipollenites, Crescentipollenites*, *Striatopodocarpites*, *Scheuringipollenites* along with trilete spores namely *Callumispora* and *Calamospora.* This recovered palynoassemblage is correlated with the upper Talchir palynoassemblage "*Parasaccites korbaensis* Palynoassemblage Zone" and assigned to be of Asselian-Sakmarian in age.

In addition, palynofacies analysis of both sections revealed that these sediments were deposited in lake lake-dominated environment with a cool climate, in proximal, in very low energy hydrodynamics and oxic settings.

Keywords: Chirimiri**,** Gondwana, Palynology, Permian, Talchir.

LE&PE 15: Foraminifera as A Proxy for Monitoring Heavy Metal Pollution in Ennore Creek, South India

Sivaraj K[a,*], Priyanka V[a], Subadharani R[a], Gopal V[b]

[a]*Department of Geology, Anna University, Chennai 600 025, India*
[b]*CEAS, Sathyabama Institute of Science and Technology, Chennai 600 119, India*

*Corresponding Author:
E-mail address: kasivaraj@gmail.com (K Sivaraj)

The Ennore Creek is a crucial estuarine system in Tamil Nadu state of South India, which faces significant ecological threats due to escalating anthropogenic activities. This work demonstrates the presence of foraminifera in the sediments of the creek environment and geochemical investigation of the 12 surface sediments and 1 short core sample collected within the creek to assess the extent and

impact of human-induced contamination. Sediment samples were analyzed for a range of heavy metals, including Iron (Fe), Manganese (Mn), Copper (Cu), Zinc (Zn), Lead (Pb), Cadmium (Cd) and Chromium (Cr), using Atomic Absorption Spectrometry (AAS). The results reveal elevated concentrations of these metals, exceeding natural background levels given by Wedepohl (1995) for the respective heavy elements, indicating substantial anthropogenic input. Observed the overall decreasing order of mean concentration of Heavy metals in the creek sediments as Fe>Ni>Pb>Cr>Mn>Zn>Cu. Spatial distribution patterns of heavy metals were mapped to identify hotspots of contamination, closely associated with industrial discharges, urban runoff, and port activities. Enrichment factor (EF), Contamination Factor (CF) and geo-accumulation index (Igeo) calculations were employed to quantify the degree of pollution and assess the potential ecological risk. The study also incorporates multivariate statistical analyses, such as Principal Component Analysis (PCA) and Cluster Analysis (CA), to distinguish between natural and anthropogenic sources of contamination. Foraminifera were separated from the sediments by the wet sieving method and were examined under the microscope (Green, 2001). All the surface sediments and subsamples of the short core sediments were investigated for foraminifera analysis. In which 25 genera/species were identified and Fourier Transform Infrared Spectroscopy (FT-IR) was used to study the variations in organic matters of dominant benthic foraminiferal species *(Ammonia beccarii)*. The most common functional group obtained in the samples were carbonyl compounds ranging from 1800-1000 cm^{-1} wave number which is due to the carbonate content of the foraminifera test and hydroxyl compounds ranging from 4000-3300 cm^{-1} which is due to the water content present and aliphatic hydrocarbons ranging from 3000-2800 cm^{-1} is due to the presence of fats and waxes. The presence of aromatic ring (C-H Monosubstitution (phenyl)) at the range of 770-730 cm^{-1} wave number which might be due to the macromolecular thermal alteration. It was found that the benthic foraminifera respond to elevated concentrations of certain heavy metals by changes in their test morphology and size. Findings highlight a severe impact on the creek's sediment quality, likelihood of aquatic life and human health. The elevated levels of heavy metals pose a risk of bioaccumulation in the food chain, warranting immediate remediation measures.

Key words: India, Tamil Nadu, Ennore Creek, Benthic Foraminifera, FT-IR analysis, Heavy metals

References:
Green, O.R., 2001. *A manual of practical laboratory and field techniques in palaeobiology*. Springer Science & Business Media. 538p.
Wedepohl, K.H. (1995) The Composition of the Continental Crust. Geochimica et Cosmochimica Acta, 59, 1217-1232.

LE&PE 16: Paleomagnetism, and Geochemistry of Gondwana sediments of South Indian region, and their implications on paleoclimate, and source area characteristics

R. Subin Prakash[a,b]*, S. Ramasamy[b]

[a]*Department of Geology, Farook College (Autonomous), Kozhikode, Kerala- 673 632, India*
[b]*School of Earth Sciences, Department of Geology, University of Madras, Guindy campus, Chennai- 600 025, India*

*Corresponding Author:
E-mail address: suban5geo@gmail.com (R. Subin Prakash)

The breakup between India and East Antarctica from the Gondwana assembly generated several pericratonic rift basins in India. This research results from an integrated paleomagnetic and geochemical study on the Palar Basin of Tamil Nadu from southern India with a view to constrain the sediment provenance, paleoweathering, tectonic setting and drift history of the Indian subcontinent. A total of 68 oriented samples were used for NRM, Thermal and AF-Demagnetization (AF). To resolve the direction of individual components of the demagnetization results,

principle Component Analysis (PCA) has been applied. A mean ChRM is recovered from the Ongur (D/I=57/32º, palaeopole at 118.84ºE, 30.32 N (Permian) and Satyavedu Formations (D/I=76.65/-5.85º; palaeopole at 176.30ºE, 12.25ºN (Early Cretaceous). The Ongur Formation exhibits a normal polarity during the Permo Carboniferous Superchron (i.e. prior to ~250Ma). The absence of overprint from the Satyavedu Formation suggests the corresponding age of the Early Cretaceous (i.e. prior to ~125Ma). A grand mean incorporating the recent results from the Indian Gondwana blocks defines a dual polarity axis for the Ongur Formation (D/I=121.69º/23.25º) and a pole position at 91.2ºE, 23.25ºS, which is similar to the Talchir formation of the Gondwana Supergroup. Our reconstruction also confirms that the Ongur Formation was earlier part of the present Talchir Formation of the Gondwana Supergroup and that during the Gondwana period, the Palar Basin was situated near East Antarctica. The Ongur Formation witnessed intense glacial activity when the Talchir sediments were deposited.

The weathering indices such as the Chemical Index of Alteration (CIA), Plagioclase Index of Alteration (PIA), Chemical Index of Weathering (CIW) and A-CN-K ($A=Al_2O_3$, $CN=CaO^*+Na_2O$, $K=K_2O$) plots indicate that the source area experienced moderate to intense weathering reflecting hot and humid climatic conditions. The geochemical discriminations and elemental ratios of Eu/Eu*, La/Sc, La/CO, Th/Sc, La/Th, Th/CO, Cr/Th as well as chondrite normalized REE patterns with flat HREE, LREE enriched and negative Eu anomalies for the Palar Basin are suggestive of dominantly felsic and intermediate rocks in the source area. A comparative study of the REE pattern and its Eu anomalies suggests that the sediment input might have come from the Dharwar Craton.

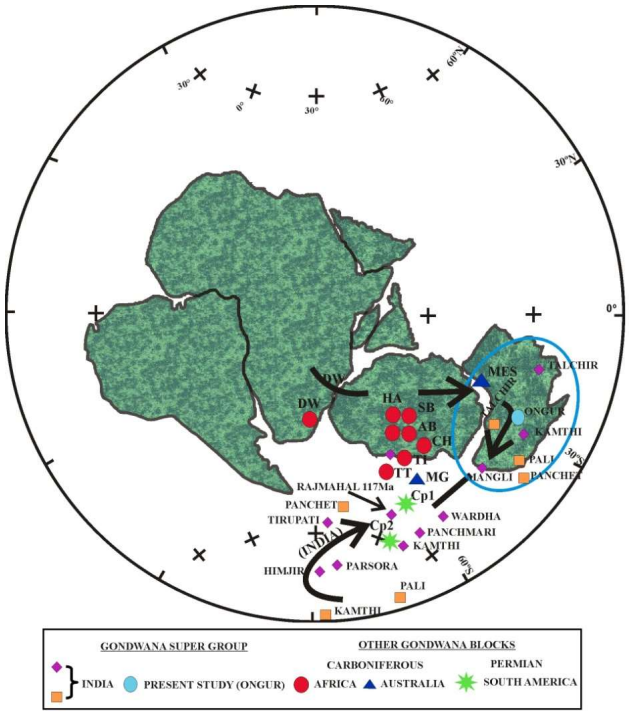

Figure 1. The reconstruction diagram of the Gondwana sediments of Palar Basin. The reconstruction follows the Gondwana supercontinent configuration after Smith and Hallam (1970) with Africa retained in present study day co-ordinates and showing pole positions interpreted to be primary from rocks of Carboniferous to Permian age. Pole positions derived from the Gondwana Supergroup are shown as rectangular orange colour (Wensink, 1968), a diamond with a purple colour (Basu Mallik et al., 1999) and the present study (Ongur) circles with sky blue colour. The summary of the pole from Smith et al. (1993), which may be consulted for full referencing Poles coded as follows. **AFRICA: SB -** Saida and Bechar Limestone (Cm-U); **HA** - Hassi Bachi and Ain Ech Chebbi Redbeds (Cu); **IL**- Illizi sediments (C); **DW**- Dwyka varves (Cu?); **TI** - Tiguentourine redbeds (C-P); **AB** - Abadla redbeds (PI); **CH**- Chougrane redbeds (PI); **TT** - Taztot Trachyandesite (PI). **SOUTH AMERICA: CP1** and **CP2** - La Collina rocks (PI, 266Ma). **AUSTRALIA: MES** - Mount Eclipse Sandstone (Cm) and **MG** - Main Glacial Stage (Cu).

Keywords: Paleomagnetism; Geochemistry; Palar Basin; Tectonic reconstruction; Provenance

References:

Basu Mallik, B., Piper, J.D.A., Das, A.K., Bandyopadhyay, G., Sherwood, G.J., 1999. Paleomagnetic and rock magnetic studies in the Gondwana Supergroup (Carboniferous to Cretaceous), Northeast India. Geological Society of India Memoir, 44, 87-116.

Smith, A.G., Hallam, A., 1970. The fit of the southern continents. Nature 225, 139-144.

Smith, B., Moussine-Pouchkine, A., Kaci Ahmed, A.A., 1993. Paleomagnetic investigation of Middle Devonian limestones of Algeria and the Gondwana reconstruction. Geophysics Journal International 119, 166-186.

Wensink, H., 1968. Paleomagnetism of some a Gondwana red beds from Central India, Paleogeography Palaeoclimate Palaeoecology 5:323-343.

LE&PE 17: Report on the Occurrences of Gondwana Palynofossils in and around Dambuk, Lower Dibang Valley District, Arunachal Pradesh, India

Diganta Bhuyan[a]*, Devojit Bezbaruah[a], Pradip Borgohain[b], Yadav Krishna Gogoi[a], Dipanjal Chutia[a]

[a]*Department of Applied Geology, Dibrugarh University, Dibrugarh 786004, Assam, India*
[b]*Department of Petroleum Technology, Dibrugarh University, Dibrugarh 786004, Assam, India*

*Corresponding Author:
E-mail address: diganta.bhuyan@dibru.ac.in (Diganta Bhuyan)

The present palynological study has been carried out to confirm the presence of Gondwana rocks in the eastern side of the Siang River, Siluk-Dambuk area, East Siang and Lower Dibang Valley, Arunachal Pradesh. By observing the similarity of lithological associations of established Gondwana sediments in other parts of the Arunachal Himalayas and the study area, this attempt has been made to establish the age of these sediments. Geological mapping was carried out and the area is mainly comprised of sandstone, shale, carbonaceous shale, gray shale, and purple shale with minor limestone bands and volcanics (**Fig. 1**). The studied samples did not yield any macrofossil. Seven samples have been processed for palynological study and productive samples produced 18 palynofossil. They include the following typical Upper Permian palynotaxa -*Undulatisporites* sp, *Microbaculispora tentula, Alisporites oblongus*, *Monosaccate* sp, *Horriditriletes bulbosus*, *Parasaccites obscurus*, *Plicatipollenites gondwanensis*, *Parasccites radialis*, *Triletes* sp., *Microbaculispora* sp., *Verrucosisporites* sp., *Brevitriletes unicus, Densipollenites indicus, Microbaculispora tentula, Tetraporina* sp., etc. The above fossil assemblage suggests the presence of Gondwana sediment of the Early Permian Age deposited dominantly under fluvial conditions, which was periodically influenced by marine incursions. These Gondwana sediments of Easternmost Arunachal Pradesh are exposed in an NW-SE trending linear and narrow belt in front of the Mishmi Hills.

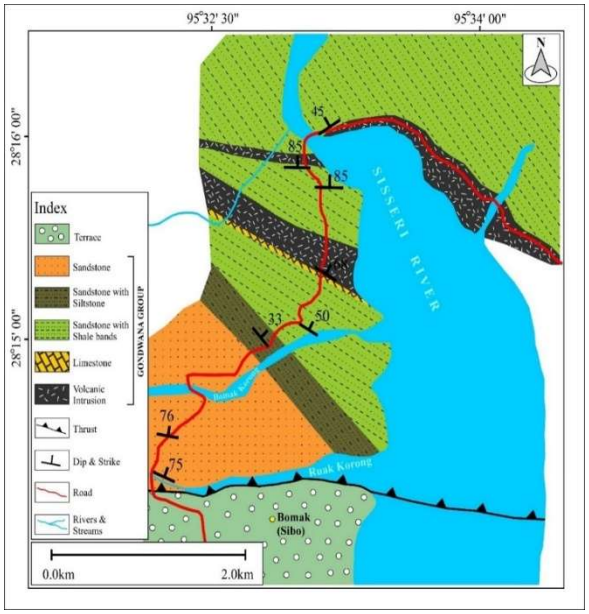

Figure 1 Geological map along Siluk-Dambuk area, East Siang and Lower Dibang Valley, Arunachal Pradesh.

Keywords: Gondwana, palynofossil, Dambuk, Lower Dibang Valley, Arunachal Pradesh, India

LE&PE 18: Paleoclimatic conditions and depositional environment investigation of Barail shale in and around Leimatak area, Noney, Northeast Manipur (India)

W. Ajoykumar Singh[1*] and Y. Raghumani Singh[1]

[1]*Department of Earth Sciences, Manipur University, Imphal-795003 (India)*

*Corresponding Author:
E-mail address: wahengbamajoykumar@gmail.com (Ajoykumar Singh)

The Barail shale is well exposed in and around the Leimatak area of Noney district, Manipur, North East (India) (**Figure 1; A & B**). These sequences are from the Indo-Myanmar Ranges (IMR) and comprise the syn-collisional flysch and post-collisional molasses sediments. The flysch sediments include the Barail Group (Late Eocene to Late Oligocene), composed of thick sandstone, siltstone, and thin shale. Previous studies on the Barail Group of Manipur have primarily focused on the petrography of sandstone and trace fossils, suggesting a shallow marine depositional environment and tropical to subtropical climatic conditions during sedimentation. However, no record of palynological work has been conducted in this area. This study aims to investigate the palaeoclimatic conditions and depositional environment of Barail shales exposed in and around the Leimatak area. The investigation is based on a palynological analysis of ten representative outcrop samples and a trace element analysis of four representative samples.

Ten outcrop shale samples from the Barail Group were collected from two sections, NL9 and NL10, which comprise the alteration of shale or silty-shale sandstone and siltstone (**Figures 1; D, E, F & G**). All ten samples were palynologically, productive. Standard techniques were used to extract the palynomorphs: HF to remove silicates, HCl to remove carbonates, and HNO_3 to remove humic organic matter. Organic fossils and residues were separated with a heavy liquid ($ZnCl_2$ and HCl solution) at Manipur University's Palynological Laboratory. The samples were then prepared on slides using Canada balsam and analyzed with a Nikon Eclipse E200 microscope. Four representative shale samples for trace element analysis were selected from these two sections. These samples were finely powdered manually by agate mortar to avoid contamination. Trace elements were determined by X-ray fluorescence spectrometry (XRF) analysis at Central Chemical Laboratory, Geological Survey of India, Kolkata, India.

The palynomorphs recovered from the study area mainly comprise *Hammenisporis multicostatus, Hammenisporis susannae*, *Hammenisporis* sp., *Monolites* sp., *Palaeogigaspora excellensa*, *Proxapertites assamicus* etc. *Hemmeniposri*s sp. is the most abundant palynomorphs present in this area. The palynomorphs present in the area indicate that the deposition environment of the collected samples is a freshwater and mixed terrestrial environment with tropical to subtropical climatic conditions during an episode of sedimentation. *Phragmothyrites eocaenica* and fungal remains also suggest the prevalence of warm and humid climates during the sedimentation of this Barail shale. It further supports the paleodepositional environments presented from the palynotaxa of the Barail shale based on the trace element analysis data. The trace element ratios of Rb/Sr and Sr/Cu show the region had warm, humid weather during its deposition (**Fig. 1C**). The ratio of Sr/Ba and the V/Ni-Sr/Ba plot also support that the deposition occurred in freshwater or continental environments (**Figs. 1; C & I**). The ratio of V/Cr, U/Th, Ni/Co, V/(Ni+V) and V(V+Ni) verses Ni/Co also suggest the paleo-redox environmental conditions of the Barail shale of the study area have ranged from oxic to dyoxic conditions (**Figs. 1; C & J**).

In conclusion, the palynological and trace element analyses of the Barail shale in and around the Leimatak area indicate that sedimentation occurred in a freshwater and mixed terrestrial environment with a warm, humid, and tropical to subtropical climate. The study also suggests that the

paleoenvironment ranged from oxic to dyoxic conditions. These findings provide a palynological assemblage of Barail shale and valuable insights into this region's paleoclimatic and environmental conditions during the Late Eocene to Late Oligocene period.

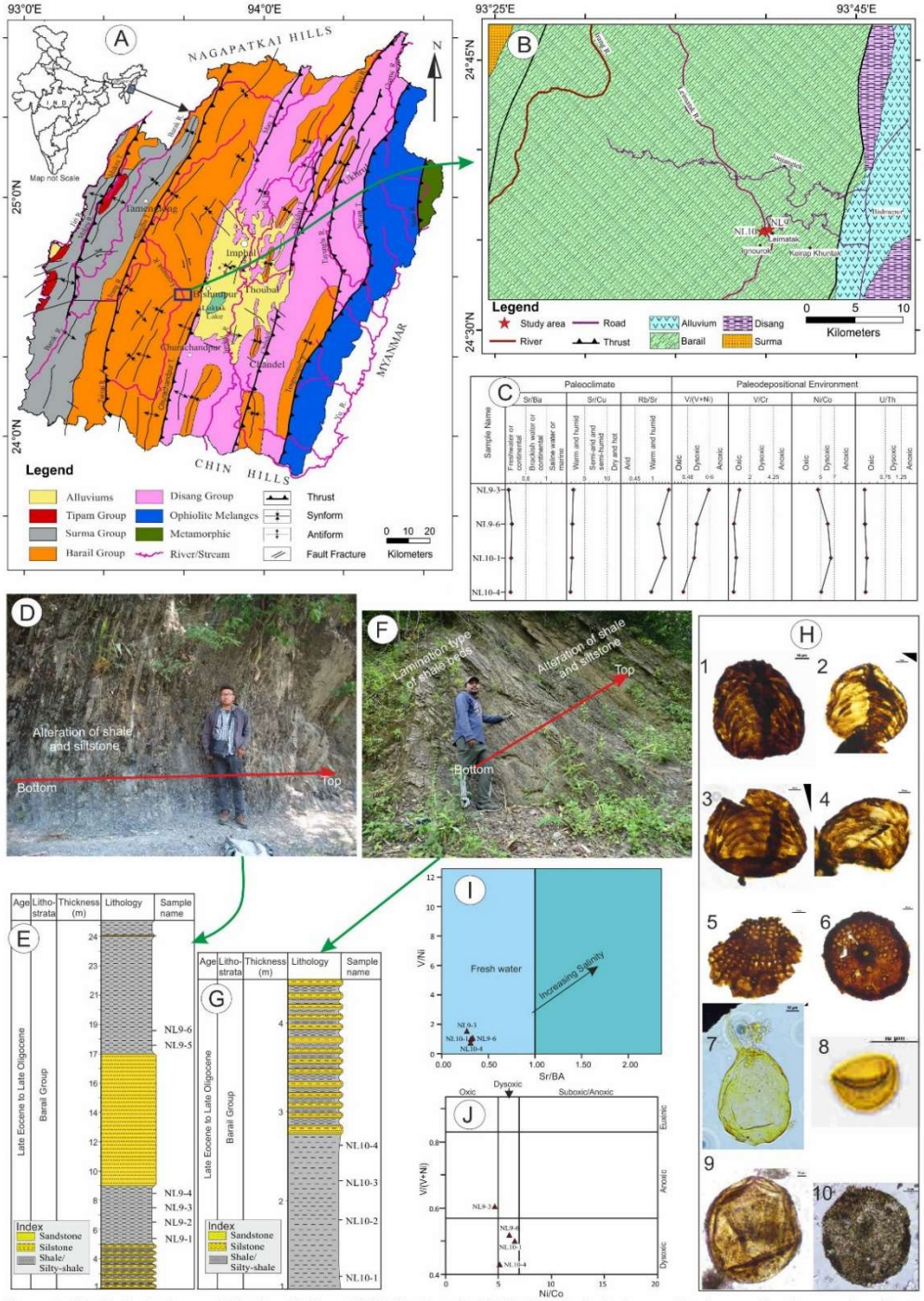

Figure 1: **(A)**: Geological map of Manipur (Soibam, 2000; Singh et al., 2015); **(B)**: Geological map of study area showing sample collection site; **(C), (I)** & **(J)**: Interpretation of trace elements data; **(D)** & **(F)**: Field photograph of section NL9 and NL10 respectively; **(E)** & **(G)** Lithologs of the sample collection site showing thickness and sample details of section NL9 & NL10 respectively; **(H)**: Palynology assemblage of the study areas; 1&2: *Hemmenisporis multicostatus*; 3&4:*Hemmenisporis sussanae*; 5: *Phrarmothyrites eocenicus*; 6 & 7: Fungal remains; 8: *Monolites*; 9: *Palaeogigaspora excellensa*; 10: *Proxapertites assamicus.*

Keywords: Barail, palynotaxa, trace element, Manipur, India

LE&PE 19: Salt Clock: An Innovative Indirect Method to Estimate the Age of Terrestrial Endorheic Hypersaline Astroblemes

V.R. Rani[1,2*] and R.B. Binoj Kumar[2]

[1]*Central Ground Water Board, Southern Region, Hyderabad 500068, India*
[2]*Department of Geology, University of Kerala, Thiruvananthapuram 695581, Kerala, India*

*Corresponding Author:
E-mail address: ranisajin@gmail.com (V.R. Rani)

Our planet Earth was bombarded with millions of cosmic bodies in the early past, which was very crucial in shaping the planet's surface and in the development of the geological environment. When large meteorites competent to exceed the atmospheric resistance, plunge into the earth's surface and create impact craters leaving signatures to understand our planet's history of cosmic collision and planetary evolution. Despite the extensive surficial geological activities that obscure the original features of impact craters on Earth, only 211 confirmed craters are preserved currently. This relatively small number of confirmed craters is valuable for the planetary science group as it represents terrestrial analogs on other planetary bodies, especially Mars and Moon. Rarely, these large depressions formed by impact are filled with water, either recharged from springs, groundwater, or inflow from streams and precipitation, and are called astroblemes. One of the major challenges faced by the scientific community is the non-availability of the age of meteoritic craters/astroblemes. Currently, there are 31 astroblemes, of which five astroblemes are endorheic in nature, namely Bosumtwi and Tswaing in South Africa, Karakul in Tajikistan, Pingaluit in Canada and Lonar in India. As endorheic lakes sans outlet, usually referred to as sinks, they lose water by means of percolation or evapotranspiration resulting in the accumulation of salts that eventually result in hypersaline lakes. Earlier, the salinity parameter was utilized in the concept of the salt clock, wherein the age of the earth was proposed. Though the determination of the age of the Earth has uncertainties due to longer age and diversified climatic zones, endorheic lakes of younger age like Lonar are feasible for such study. Thus, this study proposes a novel approach and utilizes the progressive accumulation of salts in endorheic basins over time that is influenced by geology, climate and hydrologic factors for age determination of endorheic astroblemes using salinity as a proxy. By analyzing the salinity trend in the lake and correlating it with the geology and paleoclimate, a relationship between salinity and age can be established. Thus, by establishing the trend of salinity with paleoclimate, age determination of astroblemes becomes a less time-consuming approach.

In the present study, the only astrobleme reported in the Indian sub-continent, the Lonar astrobleme (N 19°58′35″ and E 76°30′30″), located in the Buldhana district of Maharashtra (**Fig. 1**), is selected. This near circular lake of about 1 km^2 is fed by two perennial springs and precipitation. Previous studies reveal that the Lonar Lake is not only saline but also shows high alkalinity. Rainfall being the main contributor, a detailed rainfall distribution pattern analysis carried out over the years reveals that either low or high rainfall occurs about 8-10 years cycle and estimated the evaporation rate as 0.3 cm/day from the fluctuation in water level in the lake and the average annual rainfall is 759 mm. The salinity as well as NaCl variation over a long year also confirms the influence of the cyclic nature of rainfall (**Fig. 2**). Furthermore, the present study reaffirms that the dominant cation is sodium and anions are carbonate + bicarbonate, followed by chloride. The high salinity when compared to the dug wells in the near vicinity of lake indicates the accumulation of sodium bicarbonate and chloride is due to the disintegration of country rock. The conductivity of groundwater samples collected from dug wells is in the range of 1000 -1200 µs/cm while in the case of lake water samples the value is so high in the range of 8800 -9200 µs/cm. Even though a lot of research have been done on various aspects of Lonar lake hydrochemistry, usually with a single temporal data, a continuous monitoring of water quality has not

been done earlier. Thus, a systematic long-time data revealing the hydrochemistry would shed light on the age of formation of Lonar crater, which is this study aims at. As part of the 5-year long monitoring project, where our study completed two successful years, we have observed that the salinity of Lonar astrobleme is increasing in a linear way (**Fig. 2**). Hence, with the available data and with the upcoming results, we would able to derive an indirect age for Lonar, which has now contradictory views with ages, with suggestions spanning from 15±13 Ka to 52±6 Ka has been suggested.

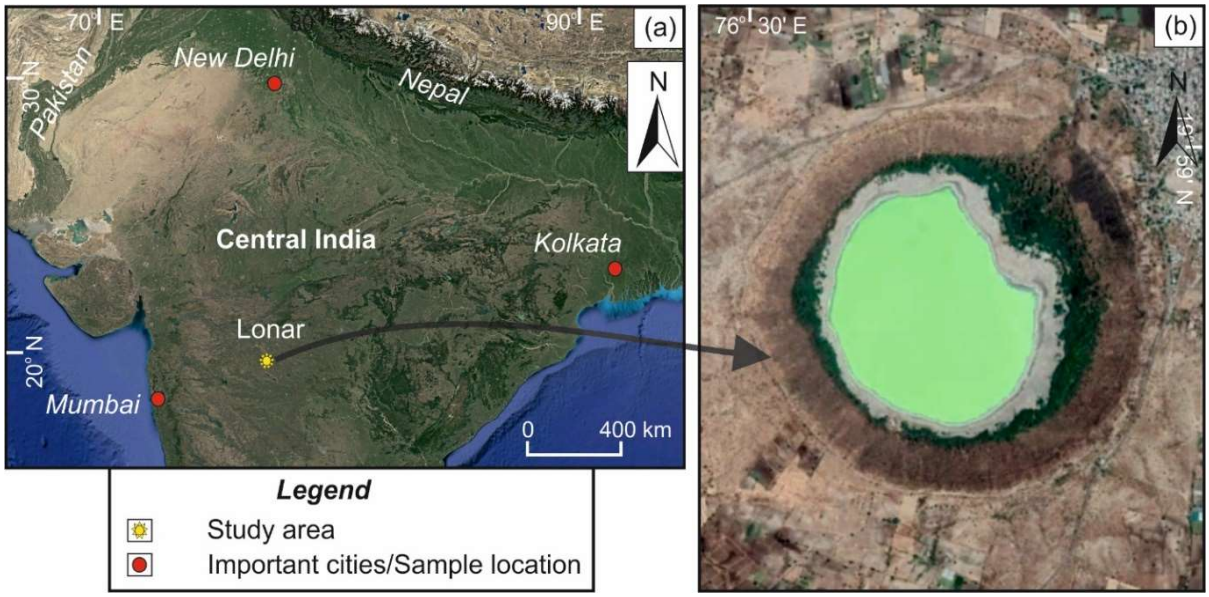

Figure 1 Location of Lonar astrobleme

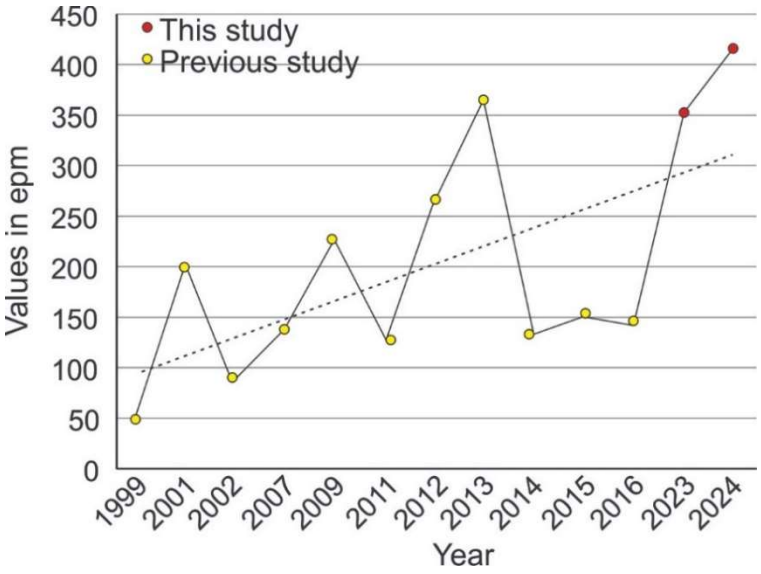

Figure 2 Variation of Sodium Chloride concentration (Note that the fluctuating values from the previous studies could be due to sampling in different seasons)

Keywords: Salinity, Astroblemes, Endorheic, Lonar, Impact crater

LE&PE 20: Net primary productivity of paleo-peatlands linked to deep-time glacial periods in the late Carboniferous and early Permian icehouse interval

Yanwen Shao[1*], Fenghua Zhao[1], Longyi Shao[1]

[1]*College of Geoscience and Surveying Engineering, China University of Mining and Technology (Beijing), Beijing 100083, China*

*Corresponding Author:
E-mail address: shao-yw@qq.com (Yanwen Shao)

Peatlands, an important organic carbon reservoir, play a crucial role in the global carbon cycle. The carbon accumulation of peatlands, reflected by net primary productivity (NPP), can have an impact on global carbon cycling and climate change. The late Carboniferous – early Permian is an icehouse period, during which numerous thick coal beds were accumulated in the North China Block (NCB) located within a low-latitude area, providing an opportunity for studying the carbon cycling under the glacial and interglacial climates. In this study, spectral analysis was performed on the natural gamma-ray (GR) logs of the Benxi, Taiyuan and Shanxi formations of the late Carboniferous to early Permian in a borehole section located within the Ordos Basin in western NCB. Cyclic signals related to astronomical orbital parameters were identified, including long eccentricity (~405 kyr), short eccentricity (~125 kyr and ~95 kyr), and obliquity (~35.5kyr). A floating astronomical time scale was established by using the long eccentricity signal, and this time scale was further used to constrain the durations of the accumulation of coal-forming paleo-peatlands. The paleo-peatland for the C8+9 coal seam (9 m thick) of the Taiyuan Formation lasted approximately 203 kyr, and the paleo-peatland for the C5 coal seam (4 m thick) of the Shanxi Formation lasted approximately 46 kyr. Using this timeframe and an estimation of carbon loss during coalification, the carbon accumulation rates of the late Carboniferous – early Permian low-latitude peatlands are calculated to be 104.7±14.9 $g{\cdot}C{\cdot}m^{-2}{\cdot}a^{-1}$for the C_{8+9} coal seam and 192.6±11.6 $g{\cdot}C{\cdot}m^{-2}{\cdot}a^{-1}$for the C_5 coal seam. The NPP of the paleo-peatlands, which deducts a part of the carbon loss caused by the loss of CO_2 and CH_4, can be calculated from the carbon accumulation rates. The calculated average NPP of the paleo-peatlands for the C_{8+9} seam was 199±28 $g{\cdot}C{\cdot}m^{-2}{\cdot}a^{-1}$, and that of the C_5 seam was 366±22 $g{\cdot}C{\cdot}m^{-2}{\cdot}a^{-1}$. In combination with the absolute time scale calibrated by high-precision U-Pb dates from the Palougou section in western NCB, the depositional time of the investigated strata was constrained to be from 300.1±0.5 Ma to 294.3±0.5 Ma. The coal seams of the late Carboniferous to early Permian in the NCB correspond to interglacial interval around ~298Ma. The peatland with a lower NPP corresponds to the warming stage and the peatland with a higher NPP corresponds to the cooling stage (**Fig. 1**). This implies that a lower NPP of paleo-peatland tends to be less efficient in carbon storage, and cannot reduce the atmospheric CO_2 substantially. In contrast, a higher NPP of paleo-peatland tends to accelerate carbon fixation, leading to temperature decrease and the termination of interglacial interval in early Permian. The results of this study could provide insights into the relationship between the development of paleo-peatlands and the record of the paleoclimates during the same period and could be helpful for the prediction of future climate change.

Keywords: Ordos Basin, coal-bearing series, cyclostratigraphy, carbon accumulation rate, astronomical time scale, paleoclimate

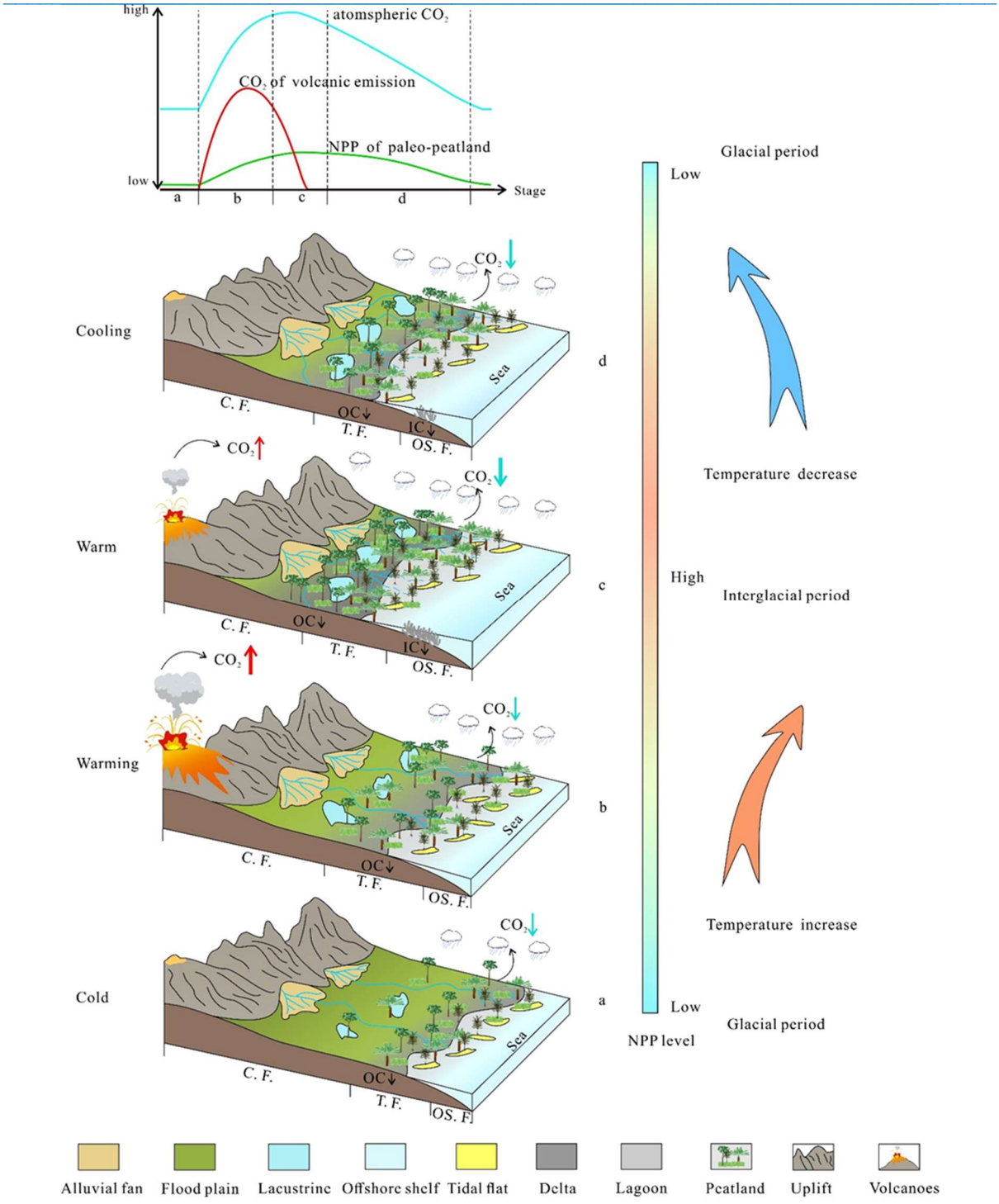

Figure 1. The responding model of paleo-peatlands NPP to interglacial period during the transition of late Carboniferous and early Permian, (a) the cold stage, (b) the warming stage, (c) the warm stage, (d) the cooling stage, (the grey area represents the paleo-peatland distribution, OC: Organic carbon, IC: Inorganic carbon, C. F.: Continental facies, T. F.: Transitional facies, O.S. F.: Offshore shelf facies).

LE&PE 21: Biostratigraphic significance of plant mega and microfossils: Evidence from the Bhareli Formation, Arunachal Pradesh, India

Deepa Agnihotri*[a], Srikanta Murthy[a], Alok Kumar Mishra[a] and Rajni Tewari[b]

[a]*Birbal Sahni Institute of Palaeosciences, 53, University Road, Lucknow-226007, India*
[b]*C-38, Alkapuri, Sector-C, Aliganj, Lucknow-226020, India*

*Corresponding Author:
E-mail address: deepa_agnihotri@bsip.res.in (D. Agnihotri)

The lower Gondwana group in Arunachal Pradesh is characterized by the presence of Miri, Bichom, Bhareli formations, and Abor volcanics. The plant fossils have mainly been recovered from the Bichom and Bhareli formations of the area. The Bhareli Formation, characterized by grey to dark grey feldspathic sandstone, grey shale, and intermittent coal layers, lies above the Bichom Formation and represents continental facies. Outcrops of the Bhareli Formation are well exposed near Pinjoli Nala, Elephant Flat, Supari Kemp, and Sessa Village on Balukhpong-Bomdila road in West Kameng District of Arunachal Pradesh. The plant mega and micro-fossil records from the Bhareli Formation of Arunachal Pradesh, India are sporadic (Srivastava et al., 1988; Datta et al., 1988; Bhushan et al., 1989, 1990; Singh and Bajpai, 1990; Tewari and Srivastava, 2000; Maithy et al., 2006).

In the present study, qualitatively and qualitatively rich floral assemblages have been recovered from the Bhareli Formation of Arunachal Pradesh. A comprehensive systematic study of plant mega and micro-fossils has been carried out to discuss the past vegetation and biostratigraphic correlation in detail.

The mega floral assemblage of the Bhareli Formation of Arunachal Pradesh comprises the order Equisetales (6%) of pteridophytes and, the orders Glossopteridales (92%), Cordaitales (1%), Pinales (1%) of gymnosperms and simple axis of unknown affinity. Order equisetales including Equisetalean axes and Cordaitales are known by two species of Genus *Noeggerathiopsis*. Order Glossopteridales dominates the assemblage and contains four species of the genus *Gangamopteris*; thirty-six species of *Glossopteris*, one species of Genus *Vertebraria*, and three types of sterile scale leaves. Order Pinales is represented by one species of Genus *Buriadia.* Dispersed Gymnospermous seeds are known by the species of two genera *Cardaicarpus* and *Samaropsis*.

Well-preserved palynomorphs have also been recovered from the Bhareli Formation. The statistical analysis of the miofloral assemblage reveals that pollen grains predominate over spores and the palyno-assemblage shows the occurrence of stratigraphically marker palynotaxa such as *Indotriradites korbaensis, Indotriradites* sp., *Maculatisporites* sp.*, Barakarites indicus, Scheurangipollenites* Spp. (S. *barakarensis*, S. *maximus*, S. *tentulus*), *Faunipollenites varius*, *Primuspollenites levis.* Thus, this palynoassemblage can be correlated with *Scheuringipollenites barakarensis* assemblage Zone of the lower Barakar Formation in the Raniganj Coalfield, Damodar Basin, India.

The presence of *Noeggerathiopsis-Gangamopteris* association along with the taxon *Buriadia heterophylla* in the present assemblage suggests that the flora of the Bhareli Formation may be correlated with the flora of Karharbari Formation of peninsular India as also suggested by the earlier workers. However, Genus *Glossopteris* is dominant in the assemblage and represented by thirty-five species. Therefore, the floral assemblage of the present study can broadly be correlated with the Barakar flora of Damodar, Mahanadi, Wardha, Godavari, Rajmahal, South Rewa, and Satpura basins of the peninsular region, and Nishatbagh Formation of the extra peninsular region of India. The flora of the Bhareli Formation of Arunachal Pradesh has modest similarities to the Early Permian floras of South

Africa, Argentina, Brazil and Antarctica. The mega and micro-floral studies suggest the Artinskian age for the Bhareli Formation.

Figure 1. Graphical Summary

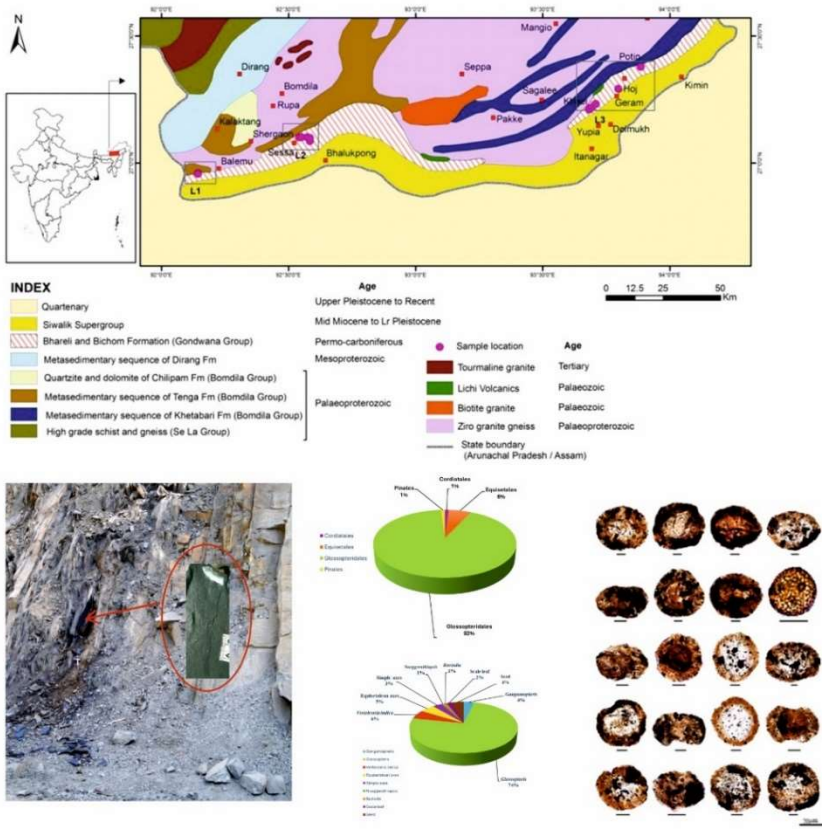

References

Bhushan, S.K., Sharma, S.K., Banerjee, D.C., Bindal, C.M. 1989. Geology along Bhalukpong - Bomdila and Foot Hill - Tenga, Amatullah - Kalaktrang roads, West Kameng district, Arunachal Pradesh. Records of Geological Survey of India 122(4), 7–8.

Dutta, S.K., Srivastava, S.C., Gogoi, D., 1988. Palynology of the Permian sediments in Kameng district, Arunachal Pradesh. Geophytology 18(1), 53–61.

Maithy, P.K., Bindal, C.M., Bhushan, S.K., Sharma, S., Banerji, D.C., Kumar, G., 2006. Lower Gondwana plant fossils from Arunachal Pradesh, Lesser Himalaya and their age. Journal of the Geological Soceity of India 68, 316–326.

Singh, T., Bajpai, U. 1990. On some plant fossils from Gondwana equivalent sediments of eastern Himalaya. Palaeobotanist 37. 284–291.

Srivastava, S.C., Anand Prakash, Singh, T. 1988. Permian palynofossils from the eastern Himalaya and their genetic relationship. Palaeobotanist 36, 326–338.

Tewari, R., Srivastava, A.K., 2000. Plant fossils from Bhareli Formation of Arunachal Pradesh, North East Himalaya, India. Palaeobotanist 49, 209–217.

LE&PE 22: Astronomical driving of the permo-carboniferous transitional facies coal-bearing cycles in Qinshui basin of China

Chu Jiangman[1*], Shao Longyi[1], Zhou Jiamin[1]

[1]*College of Geoscience and Surveying Engineering, China University of Mining and Technology (Beijing), Beijing 100083*

*Corresponding Author:
E-mail address: chujman@163.com (Chu Jiangman)

The Permo-Carboniferous marine-continental transitional facies coal-bearing series in Qinshui Basin(35°40'-37°20'N, 111°10'112°45'E) was developed with obvious cyclicities which shows a good correspon-dence with the astronomical periodic signals. Based on the natural gamma (GR) logging data which have been regarded as paleoclimate proxy, we used the Acycle software to perform the time series analysis on the coal-bearing series. The astronomical period signals were identified and the floating astronomical timescales were established. According to the spectral analysis, the 405 ka long eccentricity period, 92.4-128.7 ka short eccentricity period, 33.5-48.1 ka obliquity period, and 19.7-23.2 ka precession period of the late Carboniferous-early Permian were determined. These periods are similar to the Permo-Carboniferous astronomical orbital cycles proposed by previous researchers, indicating that the relevant sedimentary records were driven by the Earth's orbital periods. According to the floating astronomical timescales constrained by astronomical orbital periods, the sedimentary time range of the coal-bearing series in the Qinshui Basin were constrained to 6.9 Ma. By combination of the sequence stratigraphic framework and the astronomical timescale, the age of the top boundary of Benxi Formation in Qinshui Basin was constrained as 300.00 Ma, the age range of Taiyuan Formation was 300.00 -295.28 Ma, and the age range of Shanxi Formation was 295.28-293.95 Ma. The calculated time duration for sequence 1 (Benxi formation and lower part of Taiyuan Formation) was 1500 ka, with the sedimentation rate being about 2.7 cm/ka, and the lagoon and offshore carbonate continental shelf facies were mainly developed during this period. The calculated time duration for sequence 2 (middle and upper Taiyuan Formation) was 4070 ka, with the sedimentation rate being about 3.0 cm/ka, and the sedimentary facies during this period were mainly tidal flats, lagoons and offshore carbonate shelf, being transitioned to delta facies. The calculated time duration for sequence 3 (Shanxi Formation) was 1330 ka, with the sedimentation rate being 3.7 cm/ka, and the delta facies was developed. The sedimentation rate showed a trend of gradual increasing, and the sedimentation rate of the marine-continental transitional facies was faster than that of the marine-dominated facies. The results of this paper can provide a high-resolution chronostratigraphic framework for the analysis of the paleoenvironmental evolution of the coal-bearing series in this area.

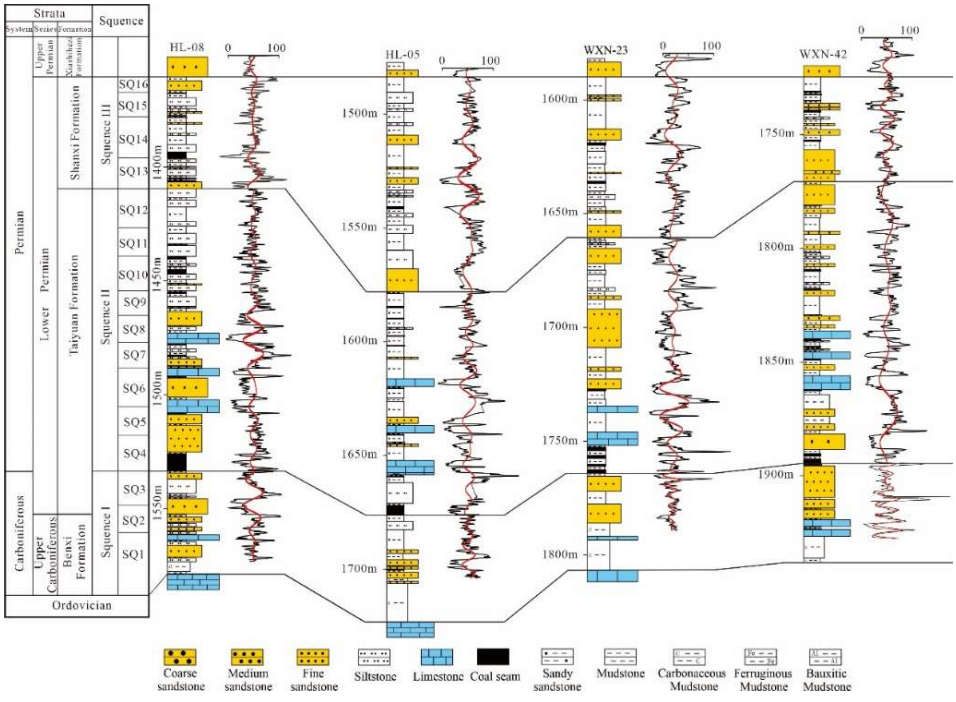

Figure 1. High-resolution sequence stratigraphic framework of the Permo-Carboniferous coal-bearing rocks in the Qinshui Basin constrained by long eccentricity

Keywords: Permo-Carboniferous; marine-continental transitional facies; high-resolution sequence stratigraphy; astronomical time scale; rate of sedimentation

LE&PE 23: Study of Paleogene carbonate sequences of Jaisalmer basin, Rajasthan, India to determine depositional environment and paleoclimate

A. Patra[a*], A. D. Shukla[b], B. P. Singh[c]

[a]*Nagaland University, Kohima, Nagaland, India- 797004*
[b]*Geosciences Division, Physical Research Laboratory, Ahmadabad, India- 380009*
[c] *CAS in Geology, Banaras Hindu University, Varanasi, India-221005*

*Corresponding Author:
E-mail address: amitava.geol@gmail.com (A. Patra)

The Paleogene carbonate sequences of the Jaisalmer basin, Rajasthan are studied on the basis of field, petrography and geochemical analysis to determine the depositional environment and paleoclimate. Field study identified three different lithofacies those are chalky limestone, fossiliferous limestone and nodular limestone. Petrography reveals that the studied limestones contain ooids, peloids and diverse genera of larger foraminifera which demonstrate that the deposition of limestones took place in a tropical climatic condition. The geochemical analysis of these limestones especially the REE pattern indicates deposition took place in a coastal environment with some contribution from freshwater also. Isotopic studies (stable carbon and oxygen) of these studied limestones are carried out to find the signatures of climatic fluctuation during that time. The $\delta^{13}C$ values of the limestones in the studied sequences are depleted and there are two prominent shifts in the $\delta^{13}C$ curve towards the more depleted side, one in the lower part and another in the middle of the succession. The lower one represents the Paleocene–Eocene Thermal Maximum and the middle one represents the Early Eocene Climatic Optimum (**Fig.1**). These two peaks are interpreted as the addition of carbon from the atmosphere or land as a result of the regional tectonics which could be connected with India-Asia collision. Also, the shift in the $\delta^{18}O$ (−6.38 to −9.84‰), values can be linked with the Eocene warming events that are coeval with the carbon isotopic stages I and II.

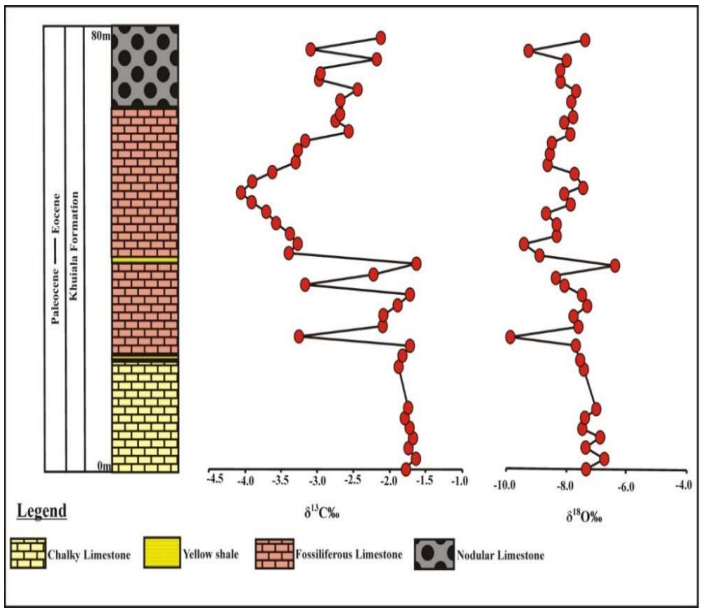

Figure 1. Stable isotopic variations in limestones against the depth show the climatic fluctuation over time.

LE&PE 24: Metal Enrichments in a Natural Protected Coastal Lagoon: A case study from Boca Paila lagoon system, Quintana Roo, Mexico

P. Guadarrama-Guzmán[1], S.B. Sujitha[2], Nagarajan Ramasamy[3,4], P. F. Rodríguez-Espinosa[1], M.P. Jonathan[1*]

[1]*Centro Interdisciplinario de Investigaciones y Estudios sobre Medio Ambiente y Desarrollo (CIIEMAD), Instituto Politécnico Nacional (IPN), Calle 30 de junio de 1520, Barrio la Laguna Ticomán, C.P.07340, Ciudad de México, México.*
[2]*Escuela Superior de Ingeniería y Arquitectura (ESIA), Unidad Ticomán, Instituto Politécnico Nacional (IPN), Calz. Ticomán 600, Delg. Gustavo A. Madero, C.P. 07340, Ciudad de México (CDMX), México*
[3]*Department of Applied Sciences (Applied Geology), Curtin University, Miri, Sarawak 98009, Malaysia*
[3]*Curtin Malaysia Research Institute, Curtin University, Miri, Sarawak 98009, Malaysia*

*Corresponding Author:
E-mail address: mpjonathan7@yahoo.com (M.P. Jonathan)

In 41 surface sediment samples from three coastal lagoons: Caapechén (CH), Boca Paila (BP) and San Martín (SM) in Quintana Roo, Mexico, the concentration of heavy metals such as Cd, Co, Cr, Cu, Fe, Mn, Ni, Pb and Zn, grain size, and carbonate content were analyzed, and enrichment factor (EF), contamination factor (CF), modified hazard quotient (mHQ), pollution load index (PLI), potential ecological risk index (PERI) and toxic risk index (TRI) as well as geoaccumulation index (Igeo) were calculated to evaluate the natural and anthropogenic contamination processes in the area. The results show high values of EF, Igeo, PERI, TRI and mHQ for metals such as Cd, Zn and Pb; likewise, there is a positive correlation between these metals (Cd and Zn, $r = 0.55$; Cd and Pb = 0.66, $p < 0.05$) indicating a similar origin. Among the main sources of Cd, Zn and Pb in the area are landfills, wastewater discharges, agriculture, tourism, as well as the characteristics of the terrain itself that can transport contaminants from other sites to the study site. The results found in this study indicate that anthropogenic activities in the area increase the concentration of metals such as Cd, Zn and Pb and could represent a problem for the ecosystem.

Keywords: Geochemical process, metals, enrichment, Boca Paila, México

LE&PE 26: Sediment Texture and Geochemistry of Veeranam Lake sediments, Tamil Nadu, India: Implications for Paleoweathering, Provenance and Ecological Risk Assessment

S.R. Singarasubramanian[1*], Venkatesan Selvaraj[1], Ajin Bejino Aloysius[1], Bobby Jones Ambrose[1], and Zuvairiya Saleem[1]

[1]*Department of Earth Sciences, Annamalai University, Annamalai Nagar, Chidambaram-608002, Tamilnadu, India*

*Corresponding Author:
E-mail address: singara67@gmail.com (S.R.Singarasubramanian)

The present study was carried out to identify the textural and geochemistry characteristics of sediments from Veeranam Lake, Tamil Nadu, India. Totally 50 surface samples were collected in the grid pattern from the study area using a van Veen grab sampler. The main aim of this study is to analyze the weathering history, provenance and ecological risk assessment of the area. The textural characteristics of the sediments are dominated by clay and silt fractions. The geochemical classification diagram of the Herron graph indicates that the sediments are Fe-shale in nature. The Chemical Index of Alteration (CIA) and Chemical Index of Weathering (CIW) and Plagioclase Index of Alteration suggest an intense chemical weathering of the source rock. The A-CN-K triangle plot also confirms the same. The average SiO_2/Al_2O_3 in sediment samples suggests that most of the sediments are derived from acidic rocks (Granite and Granodiorite). The discriminant diagram indicates that the sediments fall under intermediate to felsic igneous source rock. The bivariate SiO_2 versus (Al_2O_3 + K_2O + Na_2O) plot demonstrates humid paleoclimatic condition. The rocks present in the study area are predominantly felsic rocks with a meager amount of Cr/V ratio and abundance presence of Y/Ni. Environmental pollution indices, CF (Contamination Factor) indicate low to moderate contamination EF (Enrichment Factor). The Igeo Index (Geoaccumulation index) shows a moderately polluted category. The resulting sediments from PLI (Pollution Load Index) and SPI (Sediment Pollution Index) signify that they are falling under, low to moderate polluted and low ecological risk category.

Keywords: Texture, CIA, Provenance, Weathering, Pollution, Veeranam Lake

LE&PE 27: Formation of the Molucca Sea microplate in SE Asia

Yanhui Suo[a,b]*, Tao Chen[a,b], Zeji Chen[a,b], Jie Liu[a,b], Li Sanzhong[a,b]

[a.] *Frontiers Science Center for Deep Ocean Multispheres and Earth System, Key Lab of Submarine Geosciences and Prospecting Techniques, MOE, College of Marine Geosciences, Ocean University of China, Qingdao 266100, China*
[b.] *Laboratory for Marine Mineral Resources, Qingdao Marine Science and Technology Center, Qingdao 266237, China*
[c.] *Bureau of Economic Geology, Jackson School of Geosciences, University of Texas at Austin, Austin, TX, USA*

*Corresponding Author:
E-mail address: suoyh@ouc.edu.cn (Sue Yanhui)

The Molucca Sea microplate (MSM) in SE Asia is located at the convergent junction of the Eurasian, Philippine Sea and Australian plates. It is proposed to be a remnant of the North Australian Ocean, which has been consumed to the north of the Australian continent due to the complex subduction of the Neo-Tethys Ocean. It is currently subducting westward along the Sangihe trench and subducting eastward under Western Pacific along the Halmahera trench, exhibiting an asymmetric divergent double subduction geometry. Therefore, the MSM serves as an ideal setting to study dynamic interactions between the Pacific and Tethys tectonic domains. However, which subducting plate plays a key role in governing the regional geodynamics is not well understood.

The open-source software *LaMEM* (Lithosphere and Mantle Evolution Model), is a parallel 3D numerical code that can be used to simulate various thermo-mechanical geodynamical processes, via solving the fundamental equations of momentum, mass, and energy conservation under the Boussinesq approximation. Using this approach, we aimed to reproduce the geodynamic process shaping the asymmetric slab geometry of the MSM under the complex convergent context.

It concluded that: 1) the Sangihe subduction initiated along a transform plate boundary at ~25 Ma, due to the stability of triple junctions. 2) The Halmahera subduction on the east side occurred at ~15 Ma, jointly controlled by westward motion of the Philippine Sea Plate, the existence of the pre-existing stagnant slab, and the advancement of the Sangihe Trench. 3) The westward moving Philippine Sea Plate broadly influences the dynamic interactions between the Pacific and Tethys domains.

Keywords: Molucca Sea microplate, Double subduction, Sangihe trench, Halmahera trench, the Philippine Sea Plate.

LE&PE 28: Characterization of Tide-Dominated Sedimentary Facies from Outcrop Gamma Ray Logs in the Miqrat Formation, Central Oman

Sohag Ali[1], Numair Ahmed Siddiqui[1], Mohamed A.K. EL-Ghali[2], AKM Eahsanul Haque[1*], Md. Yeasin Arafath[1], Nisar Ahmed[1], Alidu Rashid[1]

[1]*Department of Geoscience, Universiti Teknologi PETRONAS, Perak, Malaysia*
[2]*Department of Earth Sciences, College of Science, Sultan Qaboos University, Muscat, Sultanate of Oman*

*Corresponding Author:
E-mail address: eahsanul.haque@utp.edu.my (AKM Eahsanul Haque)

Outcrop gamma-ray spectrometric logging is a useful tool to interpret lithology, depositional environment, paleogeography, weathering processes, and stratigraphic correlation with the subsurface where the core is not available. The aim of this study is to investigate the influence of lithological variation on gamma ray trends, identify exposed sequences along with their associated sedimentological characteristics, and reconstruct the paleodepositional environment of the Miqrat Formation. The study area is situated in the Wadi Sumaynah region of Central Oman, where the formation is well-exposed, allowing for detailed analysis of the outcrops. A portable gamma-ray spectrometer (Model: RS-230 Super Spec) was used to acquire high-resolution gamma-ray profiles at 5-10 cm intervals, and a sedimentological log of a 311.8-meter-thick outcrop was re-logged to describe the sedimentary facies and depositional environment. Based on the sedimentary structures, textures, trace fossils, bed thickness grain size, and lithology, the formation was deposited in a marginal marine environment, with tidal influence (supratidal to intertidal). The gamma-ray logs show different shapes/trends in tide dominated environments such as cylindrical or box shaped, bell shaped, funnel shaped, and serrated or irregular shaped. They can only differentiate sandstones from mudstone or siltstone but cannot distinguish sandstone-dominated lithofacies. They cannot determine thin beds (less than 5cm), and small-scale sedimentary structures, which are crucial for interpreting depositional systems and reservoir properties. Comparing outcrop spectral gamma-ray data with nearby outcrops or core data can improve the interpretation of sub-surface architectural elements.

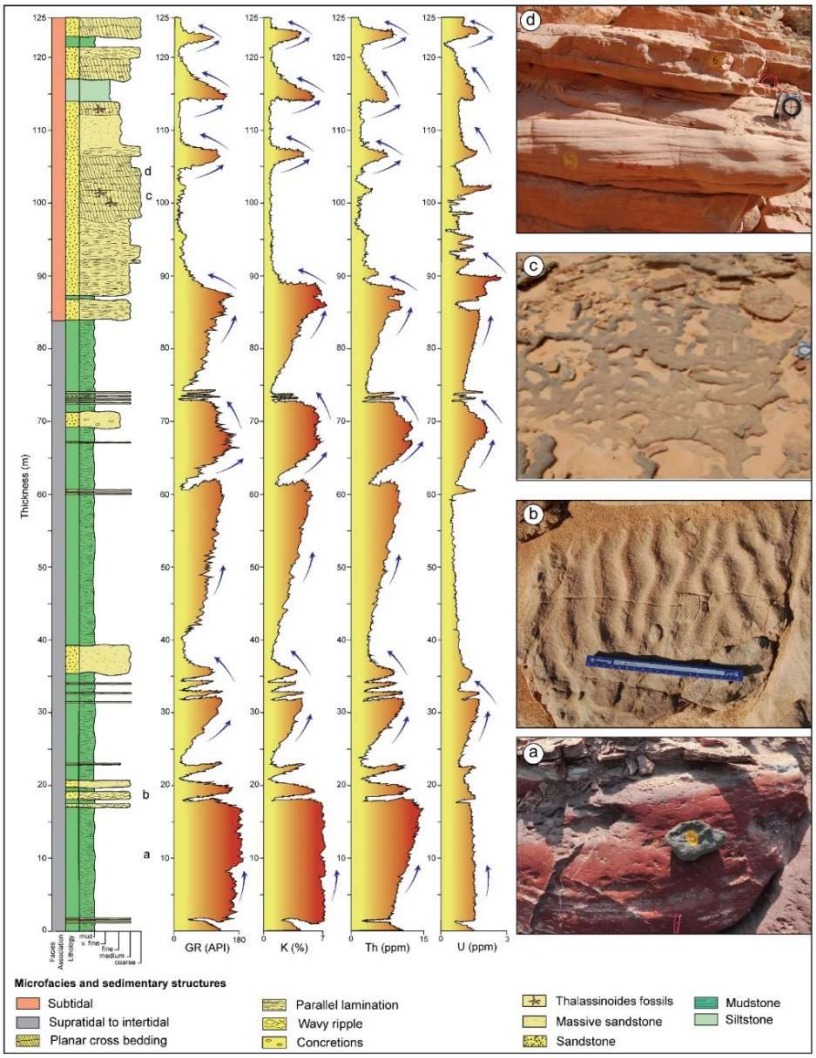

Figure1: Composite sedimentary log showing lithofacies, depositional environment and gamma ray logs of the exposed rock sequence of the Miqrat Formation: (a) mudstone, (b) wavy ripples, (c) Thalassinoides - like trace fossil and (d) planar cross bedding and parallel laminated sandstone.

Keywords: Tide-Dominated, Sedimentary Facies, Gamma-ray, Miqrat Formation, Central Oman

---

LE&PE 29: Lower Eocene (Ypresian) Selachian fauna from the Kapurdi Lignite Mine, Barmer (Rajasthan)

Priyadarshini Rajkumari[a*], Vaibhav Miglani[b], Prasad GVR[c]

[a]*Earth Sciences Department, Manipur University, Canchipur-795003, India*
[b]*G-46, Upper Ground Floor, Kirti Nagar, New Delhi, India*
[c]*Department of Geology, University of Delhi, Delhi-110007, India*

*Corresponding Author:
E-mail address: priyadarshini.rajkumari@gmail.com (Priyadarshini Rajkumari)

For the past few years, various researchers have made significant contributions to mammalian fauna from the Early Eocene Cambay Shale Formation of Vastan Lignite Mine, Surat (Gujarat), Middle Eocene Harudi Formation, Kutch (Gujarat) and Subathu Formation of NW Himalaya, which suggested that India hosted disparate groups of mammals during the early Palaeogene. The search for mammals

in other sedimentary basins of northwestern India led to the recovery of rich assemblages of elasmobranch and bony fish remains from the Eocene of Akli and Kapurdi Formations of Barmer district (Rajasthan) and Khuiala Formation of Jaisalmer district (Rajasthan). These ichthyofaunas played an important role in understanding the transition of biota from Cretaceous to Eocene in the Indian subcontinent and the environmental constraints on such transitions. As an integral part of such studies, fieldwork was carried out in the Kapurdi Lignite Mine, situated 20 km north of Barmer Town (25° 56′ 56′′N 71°21′30 ′′E). Bulk sampling of the bottom bench of the greenish clay from the Kapurdi Lignite Mine led to the recovery of an ichthyofauna represented by *Ginglymostoma angolense, Brachycarcharias* sp.*, Abdounia reticona, Coupatezia boujoi, Coupatezia* sp. *Dasyatis* sp. *Dasyatis ponsi, Dasyatis margarita, Physogaleus secundus, Galeocerdo* sp.*, Diodon* sp.*, Rhinobatos* sp.*, Arechia arambourgi, Heterotorpedo* sp.*, Osteoglossidae* indet., *Pycnodus, Rhizoprionodon* sp.*, Eogaleus* sp.*, Cybium* sp.*, Trichiurus* sp. and *Paralbula*. The majority of the fauna is dominated by the marine Myliobatiformes and Carcharhiniformes with an admixture of freshwater and brackish water forms. Most of the taxa recovered from the Kapurdi Lignite Mine are known from the Lower Eocene (Ypresian) deposits, but some have also extended into the Lutetian. The present assemblages show close taxonomic affinity with the assemblages reported from the Lower Eocene Kapurdi Formation, Barmer Basin and the Lower Eocene Khuiala Formation of Rajasthan. The present faunal assemblage bears striking similarities with the fauna found in the Palaeogene deposits of Morocco, Cabinda, Niger, Togo, Egypt, Belgium, and southeastern North America implying that the fauna may have utilized the Tethys seaway as a dispersal route between these regions.

Keywords: Eocene, Selachian, Kapurdi Lignite Mine, Barmer, India, Tethys

---

LE&PE 30: Hyperthermal and global cooling events in the Paleogene: Evidence from the sedimentary sequences of western India

B. P. Singh[a*] and A. Patra[b]

[a]*Department of Geology, Institute of Science, Banaras Hindu University, Varanasi-221005, India.*
[b]*Department of Geology, Nagaland University, Kohima Campus, Nagaland-797004, India.*

*Corresponding Author:
E-mail address: drbpsingh1960@gmail.com (B.P.Singh)

Cenozoic era was the turning point in the geological history of the Indian subcontinent when India experienced maximum isolation before it collided with Asia and there occurred a great mountain building activity shaping the Himalaya. In the Cenozoic era, the sedimentation commenced in the late Paleocene (~57.9 Ma) in the pericratonic basins of western India as well as the foreland basin of the western Himalayas those mark the beginning of a major transgression on the Indian subcontinent. We studied Paleogene sequences of the Jaisalmer basin and Jammu Himalaya to recognize the evidence of major transgressions and regressions that are forced by hyperthermal and cooling events. For this purpose, we recorded various sedimentary facies based on field and laboratory investigations and analysed $\delta^{13}C$ and $\delta^{18}O$ on an Isotope Ratio Mass Spectrometer. In the Jaisalmer area, the Cretaceous limestone is directly overlain by the late Paleocene sandstone, whereas the late Paleocene succession occurs unconformably above the Precambrian limestone in the Jammu area. This suggests the occurrence of a major transgression during the late Paleocene in the Jaisalmer basin as well as the Jammu area. This is supported by a $\delta^{13}C$ and $\delta^{18}O$ excursion at this interval in both areas (**Fig. 1**). Another transgression occurred at the Paleocene–Eocene boundary with the accumulation of the fossiliferous limestones in many studied sections. We, further, recorded a $\delta^{13}C$ and $\delta^{18}O$ excursion at the Paleocene-Eocene boundary that marks another hyperthermal event in both basins. It is interpreted

that the primary driver for the late Paleocene transgression was the regional tectonics that marked the beginning of the India-Asia convergence. The second transgression has been global and influenced by global warming at the Paleocene-Eocene Thermal Maximum (PETM). This transgression has been noticed even in the Paleogene sequences of the other continents. During the latest Middle Eocene, the Jammu Himalaya reveals the presence of red-beds and pedogenic horizons, including pedogenic calcretes. This succession possesses freshwater fauna, including mammals suggesting a change from marine conditions to freshwater conditions. Thus, a major regression occurred during the latest middle Eocene (41.3-38.0 Ma) that corresponds to global sea-level fall. This regression is global and can be identified even in the Cenozoic basins developed within the African plate. It is interpreted that this regression was driven by the global cooling during the latest middle Eocene/late Eocene possibly associated with the nucleation of the Antarctica ice sheets coupled with the uplift of the Himalaya.

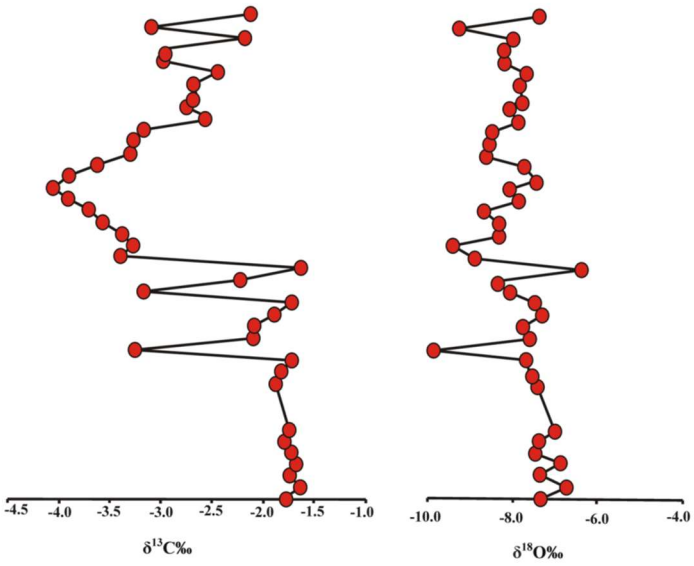

Figure 1. Stable isotopic variations in limestones against the depth show the climatic fluctuation over time.

LE&PE 31: Stratigraphic features and paleogeographic evaluation of Cisangkal area in Pamutuan Formation, Pangandaran, Indonesia: uncovering the secrets of Megalodon tooth fossils

Mohamad Sapari Dwi Hadian[a*], Luthfia Tahir[a], Cecep Yandri Sunarie[a], Lia Jurnaliah[a], Mochamad Nursiyam Barkah[a] , Winantris[a]

[a] *Faculty of Engineering Geology,Universitas Padjadjaran,Jatinangor 45363, Indonesia*

*Corresponding Author:
E-mail address: sapari@unpad.ac.id (H. Mohamad Sapari Dwi)

The Pamutuan Formation's stratigraphic and paleogeographic characteristics were formed during the Middle to Late Miocene period. This formation comprises limestone, sandstone, volcanic rocks, and sandy claystone, deposited in a shallow marine environment, offering valuable insights into historical life and organism characteristics. This study aims to explore the environmental products of shallow marine deposition, particularly focusing on the discovery of Megalodon tooth fossils (-7°36'22; 108°30'45). The exploration intends to examine a geological model that presents the distribution and characteristics of rock deposits containing Megalodon fossils within a specific geological context. The

main goal is to establish a reference for determining geological conservation areas as heritage sites and the development of aspiring geoparks. Methods used to identify and map the distribution of fossil-containing rocks in the study area included direct field observations, stratigraphic measurements, lithology identification, and sample collection for further laboratory analysis. Microscopic analysis using a polarizing microscope examined the mineral composition and rock structure. The information obtained was correlated with the relative age of rocks on the geological time scale and compared with other fossil data. Results indicate that the Pamutuan Formation is predominantly found in the Pangandaran area, West Java, containing significant fossils crucial for studying land formation history and rock facies, especially in paleontology and paleoclimatology. Fossils discovered in this formation serve as essential indicators of past living environments and paleoclimatic conditions, with notable finds including Megalodon teeth (**Fig. 1**), commonly found worldwide. These findings are expected to contribute valuable data on the initial discovery locations of Megalodon teeth, aiding in the precise determination of the relative age and depositional environment. he findings are anticipated to enhance our understanding of the Miocene paleoenvironment through the lens of marine paleontology and paleoclimatology. The discovery and analysis of Megalodon teeth and other significant fossils will provide crucial insights into the marine biodiversity and climatic conditions of the past, offering a more detailed picture of the evolutionary history and geological transitions of the area. This will not only enrich scientific knowledge but also foster a greater appreciation and awareness of geological heritage among the public and academic communities. Ultimately, this research is expected to contribute to global paleontological databases, enriching current understanding and sparking further investigations into similar formations worldwide.

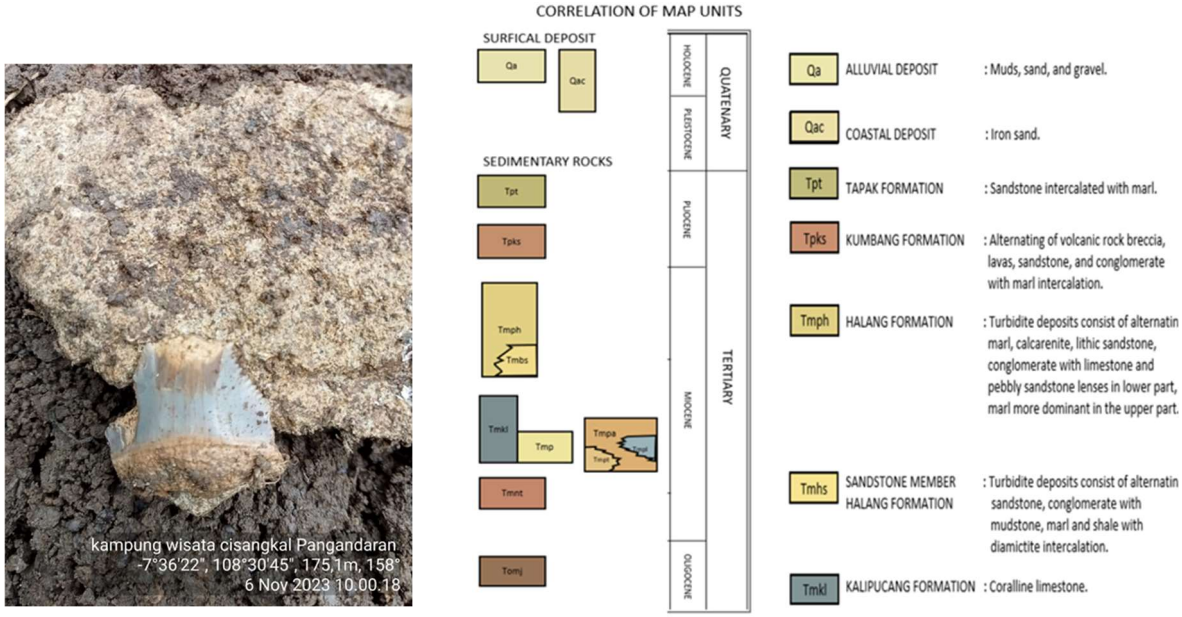

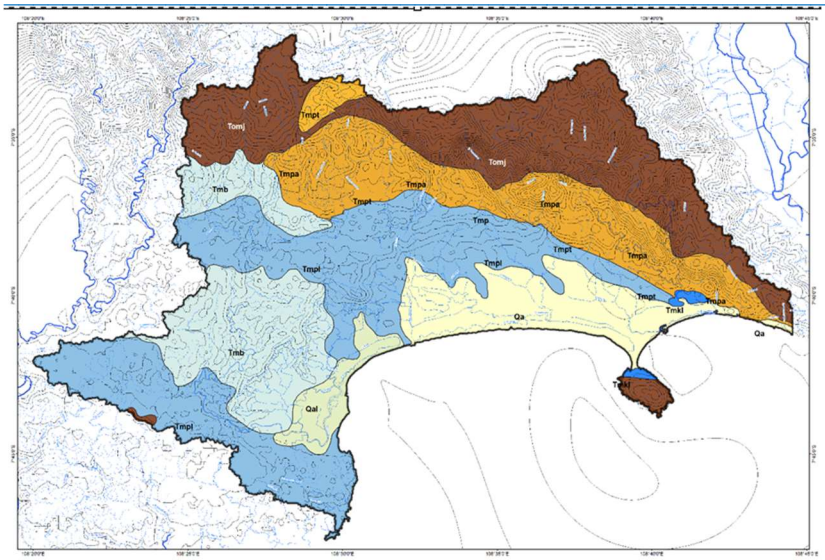

Figure 1 shows the location map and the teeth of Megalodon

Keywords: Conservation, geopark, geological heritage, geological model, Megalodon tooth

Acknowledgments
We thank the members of PPM-KKN DRPMI Unpad for their support, the Paleontology Laboratory, We thank all parties who have supported this activity, for their assistance in determining the taxonomy of shark species. We thank The Ria, for her help in the preparation.

LE&PE 32: Unveiling the First *Fictovichnus* Trace Fossils in India: A Landmark Discovery from the Fatehgarh Formation, Barmer Basin, Western Rajasthan, India.

Pawan Kumar[1*]

[1]*Department of Geology, Jai Narain Vyas University, Jodhpur, Rajasthan, India.*

*Corresponding Author:
E-mail address: pawanvaishnav932@gmail.com (Pawan Kumar)

This study deals with the well-preserved *Fictovichnus* trace fossils from the Cretaceous Fatehgarh Formation of the Barmer Basin in western Rajasthan, India. The study area is located near Sandha village, which lies about 22 km from Fatehgarh. Through systematic field surveys to identify potential fossil-bearing strata, followed by careful extraction of rock samples, the fossils were documented and compared with existing *Fictovichnus* records. This discovery marks the first documentation of *Fictovichnus* fossils in India, providing significant insights into the paleoenvironment of the Cretaceous period in this region. The Fatehgarh Formation is mainly composed of medium to fine-grained, calcareous to ferruginous sandstone, wherein three distinct ichnospecies of insect trace fossils have been found, viz. *Fictovichnus gobiensis*, *Fictovichnus aragon* and *Fictovichnus sciuttoi*. The *Fictovichnus gobiensis* are 18-30 mm in length and 8-10 mm in width, presenting ellipsoid casts with a smooth surface (**Fig. 1**). One end is rounded to spherical, whereas a truncated tunnel protrudes from the opposite end. The *Fictovichnus aragon* exhibits a rounded end on one side and a pointed end on the other, with dimensions of 9-20 mm in length and 6-10 mm in width, and *Fictovichnus sciuttoi* fossils are 25-30 mm long and 11-17 mm wide, having an ovoidal to ellipsoidal, capsule-shaped structure that shows fine lobed textures with helically arranged ridges. These trace fossils are found in two stratigraphic horizons,

forming a typical firmground ichnoassemblage with all species gregariously deposited parallel to the horizon and well-preserved in yellowish to brownish, medium to fine-grained ferruginous sandstone from the Sandha village section. The possible producers of *F. gobiensis* are coleopterans, whereas *F. aragon* and *F. sciuttoi* are probably produced by pompilid or sphecid wasps cacoons. In contact with the matrix, specimens show micritic layers, interpreted as the remains of the original silky wall constructed by the wasp larva. Based on the presence of *F. gobiensis*, *F. aragon* and *F. sciuttoi* as well as previously recorded fossil assemblages, this study proposes continental shallow marine environments for the Sandha Section of the Fatehgarh Formation.

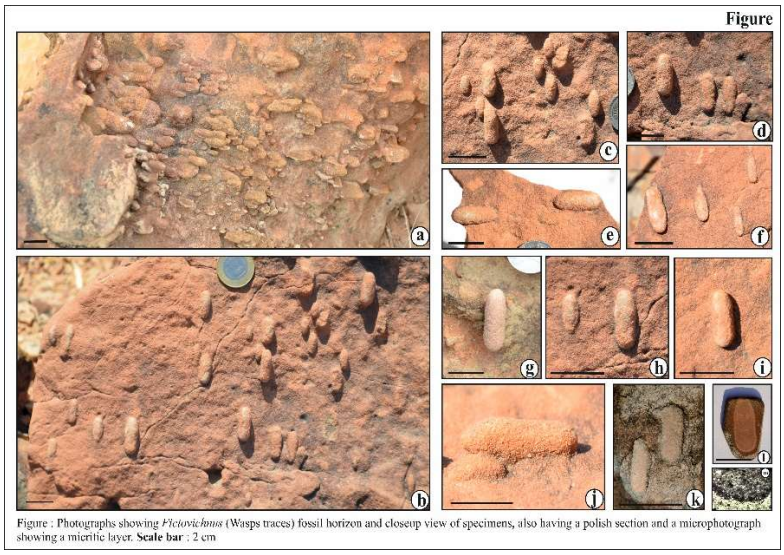

Figure : Photographs showing *Fictovichnus* (Wasps traces) fossil horizon and closeup view of specimens, also having a polish section and a microphotograph showing a micritic layer. **Scale bar** : 2 cm

Figure 1 shows photographs of *Fictovichnus* (Wasps Traces) fossil horizon and a closeup view of the specimens, also the polished section and microphotograph show a micritic layer.

Keywords: *Fictovichnus*, Trace-fossil, Wasp-Larva, Fatehgarh Formation, India.

LE&PE 33: Characterization of Paleocene-Eocene Transition (PET) in the Shillong Plateau, Meghalaya (India)

Y. Raghumani Singh[a*], A. Bijayalaxmi Devi[a,b], Mark Abbott Bunkar[c]

[a]*Department of Earth Sciences, Manipur University, Canchipur-795003, India*
[b]*Department of Geology, Pravabati College, Mayang Imphal-795132, India*
[c]*University of Pittsburgh, Department of Geology and Environmental Science, Pittsburgh, PA, USA*

*Corresponding Author:
E-mail address: yengmani@gmail.com (Y. Raghumani Singh)

The remarkable transition of the PET has been presented in this paper concerning dinoflagellate cysts and carbon isotope excursion in the Lakadong Sandstone of the East Khasi Hills of Meghalaya, India. Palynological assemblage is rich in the three sections such as Mawsmai BT, Mawmluh limestone querry ML, and Amlarem AR and presented by seventeen species of dinoflagellate cysts and rare abundant pollen grains with rare foraminiferal linings and fungal remains. Among the palynological assemblage are *Apectodinium* spp., *Polysphaeridium* spp., *Cordosphaeridium* spp., *Adnatosphaeridum* spp., *Glaphyrocysta* spp., *Lingulodinium machaerophorum. Homotryblium* spp., *Achilleodinium biformoides; Cleistosphaeridium diversispinosum Proxapertites spp., Baculatisporites crenulatus, Neucouperipollis kutchensis.* The PET has been identified BT1 of the BT, ML23 of ML and AR5 sections using the

stratigraphic marker of *Apectodinium* spp., such as *A. homomorphum, A. parvum, A. quinquelatum, A. paniculatum, A. hyperacanthum, A. augustum*. Among this *Apectodinium*, PET is highly marked by stratigraphic markers of dinoflagellate cysts (taxa of *Apectodinium augustum, now Axiodinium augustum)* with negative carbon isotope excursion (CIE). The palynofloral assemblage indicates the sequence represents warm, humid tropical to subtropical conditions with heavy rainfall. The depositional environment of the Lakadong Sandstone Member is interpreted to be neritic.

Keywords: *Apectodinium*, Carbon stable isotope, Meghalaya, Lakadong Sandstone, Palynology, Paleocene-Eocene transition (PET)

LE&PE 34: Sequence stratigraphy of Permian fluvio-marine successions in riftogenic Gondwana basin, Peninsular India: A sedimentological-ichnological approach

Biplab Bhattacharya[1*]

[1]*Department of Earth Sciences, Indian Institute of Technology (I.I.T.) Roorkee, Roorkee, Uttarakhand, India – 247667*

*Corresponding Author:
E-mail address: biplab.bhattacharya@es.iitr.ac.in (Biplab Bhattacharya)

Application of sequence stratigraphy to discern the cause and effect of net accommodation creation has remained challenging for craton-interior fault-bound rift basins. In such basinal settings, sedimentological studies, complemented with ichnofabric and ichnofacies analysis, help effectively in the demarcation of the stratal stacking patterns, favouring a better understanding of the paleoenvironmental forcings. Integrated sedimentological-ichnological-sequence stratigraphic analysis of the Permian fluvio-marine Lower Gondwana successions from the craton-interior riftogenic Gondwana Basin in Peninsular India depicts a transgressive, fluvio-tidal interactive estuarine depositional setting with minor wave influences. The fluvial deposits in the upstream-controlled settings, lying landward beyond the zone of tidal encroachments, record the absence of trace fossils attributed to a low colonization window caused by high fluvial discharge and frequent channel migrations. In the downstream-controlled settings near the river-mouth area, the tidal interactions with varied fluvial discharge led to – (i) a higher-energy bay-head delta in the inner-middle estuary with the dominance of suspension-feeding and deposit-feeding ichnotaxa, suggesting a mixed Skolithos–Cruziana ichnofacies, followed by (ii) a low-energy central estuarine area allowing opportunistic colonizers and deposit feeders of the Cruziana-Zoophycos ichnofacies, and (iii) an outer estuary with increasing wave-dominance, inhabited by suspension-feeding, domicile ichnotaxa of the Skolithos ichnofacies inter-mixed with the Cruziana ichnofacies. The recurrent juxtapositions of the Seilacherian marginal marine ichnofacies with characteristic lithofacies architecture attributed to complex sediment–organism interaction patterns in response to varied energy conditions, sediment discharge and substrate conditions in different zones of the fluvio-tidal estuarine setting. Characteristic startal stacking patterns identified from the lithofacies and ichnofacies distributions, delineate the key sequence elements. These signify shifting accommodation conditions in the upstream-controlled and the downstream-controlled part of the riftogenic Gondwana Basin, in response to varied allogenic (tectonic and/or climatic) factors. The approach epitomizes the scopes of sequence stratigraphy in reconstructing the paleogeographic changes in the craton-interior rift basins in deep time.

Keywords: Sedimentary facies architecture, Ichnofabric and ichnofacies, Transgressive estuary, Fluvial-tidal-wave inter-action, Gondwana paleogeography.

LE&PE 35: *Beaconites*: Tracing the Subterranean Ancient Ecosystems Artistry ingenuity from the Baisakhi Formation of Jaisalmer basin, Rajasthan, India

Anshul Harsh[1*]

[1]*Department of Geology, Jai Narain Vyas University, Jodhpur, 342005, Rajasthan, India.*

*Corresponding Author:
E-mail address: anshulharsh11295@gmail.com (Anshul Harsh)

A ichnospecies *Beaconites* (Vialov, 1962) is described from the coastal distributary deposition of the upper Jurassic sedimentary sequence of the Lanela Member of the Baisakhi Formation, Jaisalmer basin, India. Baisakhi is a distinctive sequence of Upper Jurassic sedimentary rock found in western India, which has been the most fertile source of trace fossils. The aim of the study is to mark the horizon of *Beaconites* (Vialov, 1962) and stabilize the relation of *Beaconites* (Vialov, 1962) ichnospecies with other trace fossils as well as possible producer of these *Beaconites* (Vialov, 1962) traces. This study also tries to find out the paleo-environment and the opening of this sea from the west Gondwana continent in the late Jurassic juxtaposition (Seton et al., 2012). Methodology includes the Field work and collection-fieldwork this includes noting the geological context (stratigraphy, lithology) of the site where the fossil was found, as well as recording measurements, dimensions, and morphological features of the *Beaconites* (Vialov, 1962). The Treatise on Invertebrate Paleontology Part-W Miscellanea Trace Fossils and Problematica (Hantzschel, 1962) as well as ICZN rules are followed in this study. This trace fossil is found from two stratigraphic horizons and constitutes a typical firmground ichnoassemblage of the *Beaconites* (Vialov, 1962). Well-preserved specimens have been recovered from the pinkish to yellowish (brownish some part) fine-grained silty sandstone of Lanela scarp section. This abstract delves into the allure of *Beaconites* (Vialov, 1962), exploring its significance as a trace fossil and bioglyphs the valuable insights it provides into the behaviors of long-extinct organisms. The *Beaconites antarcticus* (Vialov, 1962), *Beaconites caprouns* (Howard and Frey, 1984), and *Beaconites coronus* (Frey et al, 1984) trace fossils bearing Lanela Member is located near Lanela village about 60 km away from Jaisalmer city. Our research highlights that *Beaconites antarcticus* plays a critical role in the opening sea (Antarctic and Indian Sea opening about 140 Ma ago) marine ecosystem by influencing food web dynamics, *Beaconites caprouns* affect social structures and competition in temperate zones, and *Beaconites coronus* impacts pelagic community organization through its light-based behaviors. Each species demonstrates unique bioluminescent adaptations that reflect their respective ecological niches and environmental conditions with the help of this straight or gently curved meniscate cells (meniscate packet and cup segments) and back-filled burrows with heterogeneous packed meniscate backfill and homogeneous segmented meniscate backfill (Keighley and Pickerill, 1994). The *Beaconites* (Vialov, 1962) provide a way to distinguish bioturbation by marine-recruited fauna which is produced in long-range sedimentary deposition environment lacustrine to outer-shelf depositions in the rock records. Based on the *Beaconites antarcticus* (lacustrine to mouth bar), *Beaconites caprouns* (inner-shelf), *Beaconites coronus* (inter-tidal) and associated trace fossils assemblages, this study suggests intertidal shallow marine environments for the Lanela Member of the Baisakhi Formation. Modern meniscate burrows are produced by a wide range of organisms including arthropods, insect larvae, bivalves, gastropods, soft-bodied worm-like organisms, and some vertebrate's endobenthically (Melchor et al., 2012; Neto de Carvalho et al., 2015; Boyd and McIlroy, 2017). The generally broad meandering pattern (up to 10°), wide turning radius, and few relatively tight bends of the burrows

suggest the flexible body design of the producers. Along with further lines of evidence, the circular burrow suggests that the vermiforms are probably the producers of the Beaconites.

Keywords : *Beaconites*; Jurassic; Jaisalmer Basin; Baisakhi Formation

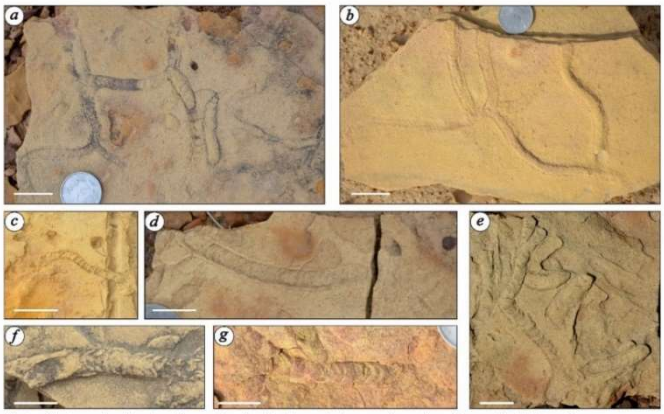

Plate : Photographs showing *Beaconites* fossil slabs and closeup view of specimens. **Scale bar** : 2 cm

References

Boyd, C., McIlroy, D., 2017. Three-Dimensional Morphology of Beaconites capronus from Northeast England. Ichnos 24(4): 250-258. http://dx.doi.org/10.1080/10420940.2017.1282862.

Frey, R. W., Pemberton, S. G., Fagerstrom, J.A. 1984. Morphological, ethological, and environmental significance of the ichnogenera Scoyenia and Ancorichnus. Journal of Paleontology 58,511-528.

Hantzschel, W., 1962. Trace fossils and problematica. In Treatise on Invertebrate Paleontology, Part W, Moore R (ed.). Geological Society of America and University of Kansas Press; W177–W245.

Howard, J. D., Frey, R. W. 1984. Characteristic trace fossils in nearshore to offshore sequences, Upper Cretaceous of east-central Utah. Canadian Journal of Earth Sciences 21, 200-219.

Keighley, D. G., and Pickerill, R. K. 1994. The ichnogenus Beaconites and its distinction from Ancorichnus and Taenidium. Palaeontology 37, 305-338.

Melchor, R. N., Genise, J. F., Umazano, A. M., Superina, M. 2012. Pink fairy armadillo meniscate burrows and ichnofabrics from Miocene and Holocene interdune deposits of Argentina: Palaeoenvironmental and palaeoecological significance. Palaeogeography, Palaeoclimatology, Palaeoecology, 350, 149-170.

Neto de Carvalho, C., Baucon, A., and Canilho, S. 2015. "Meniscate burrow" ichnoguild from the alluvial fan deposits of Sarzedas Basin (Upper Miocene, Portugal). In McIlroy, D. (ed.). Ichnology: Papers from Ichnia III Geological Association of Canada, Miscellaneous Publication 9, 51-61.

Seton, M., Müller, R.D., Zahirovic, S., Gaina, C., Torsvik, T., Shephard, G., Talsma, A., Gurnis, M., Turner, M., Maus, S., Chandler, M., 2012. Global continental and ocean basin reconstructions since 200 Ma. Earth Science Review 113, 212–270. https://doi.org/10.1016/j.ears cire2012.03.002.

Vialov, O.S., 1962. Problematica of the Beacon Sandstone at Beacon Height West, Antarctica. New Zealand Iournal of Geology and Geophysics 5, 718-732.

Theme 4: Geoenergy and Future Sustainability

GEFS 01: Energy Trilemma: Ecological sustainability and economic goals: What are the challenges and solutions for top emitting countries?

Irfan Khan[1*]

[1]*Beijing Institute of Technology, Beijing, China*

*Corresponding Author:
E-mail address: Khan.Irfan4032@yahoo.com (Irfan Khan)

The paper aims to explore the various dimensions of the energy trilemma, which refers to the complex relationship between energy security, environmental sustainability, and affordability. The paper discusses the concept of energy trilemma and its significance in the energy sector, focusing on the challenges the top emitting countries face in balancing these three goals. The paper begins by defining the energy trilemma and explaining its origins. It highlights the importance of energy security, environmental sustainability, and affordability in the context of global energy transition. The paper discusses the trade-offs and compromises those countries often face when trying to address all three dimensions of the energy trilemma simultaneously. Furthermore, the paper delves into the approaches and strategies that top emitting countries have adopted to address the energy trilemma. It explores various policy measures, technological advancements, and international cooperation initiatives that can contribute to resolving the energy trilemma. The paper also highlights the importance of stakeholder engagement and public consultation in formulating effective energy policies. Lastly, the paper concludes with an analysis of the current state of the energy trilemma and a discussion of the future challenges and opportunities. It highlights the need for continued research, innovation, and international cooperation to ensure a sustainable and equitable energy future.

Keywords: Energy Trilemma; Economic Growth; Environmental Sustainability; Energy Security; Energy Access; Energy Supply; Top Emitting Countries

GEFS 02: A Comparative Study on the Geochemical Characteristics of Estuaries in northern Sarawak Coastal ecosystem

Prasanna Mohan Viswanathan[1*]

[1]*Department of Applied Sciences, Curtin University, Malaysia, CDT 250, 98009 Miri, Sarawak, Malaysia*

*Corresponding Author:
E-mail address: prasanna@curtin.edu.my (M.V.Prasanna)

Estuaries are intricate, dynamic riverine zones that are essential to the ecosystem's physicochemical and ecological processes. Estuaries of three major rivers (Baram River, Miri River, and Sibuti River) in the Miri coastal region are noticeable for growing urbanization, high sedimentation rate, industries and tourism, which makes this ecosystem highly contaminated. Hence, an attempt was made to study the geochemical processes in these estuaries to understand the ecological risk due to natural and

anthropogenic impacts. Selected water samples and bed load sediments were collected in these three estuaries and analyzed for various geochemical parameters (major ions/oxides, nutrients, metals and isotopes). For the data analysis, statistics and geochemical modelling were mainly used. Stable isotopes were used to trace the sources of estuary waters. Pollution indices were also applied to the data to understand the vulnerability to metal pollution due to various activities that occurred in the estuaries. Nutrient concentrations were higher in the Miri estuary, which indicate various anthropogenic activities in this region. The higher total suspended solids (TSS) were observed in the Baram estuary, which indicates a high sediment load, and also supports the mobility of metals. Interpretation of results reveals that the estuaries are highly stressed due to natural and anthropogenic activities. Through this study, it is suggested to implement sustainable management plans to safeguard these estuaries for the ideal habitat for the aquatic animals.

GEFS 03: Sediment texture, Provenance and Ecological Risk assessment of sediments from Kodiyampalayam to Cuddalore Coast, Tamil Nadu, India

Venkatesan Selvaraj[a]*, Singarasubramanian S.R.[a], Parthasarathy Pandu[b] and Ajin Bejino Aloysius[a]

[a]*Department of Earth Sciences, Annamalai University, Annamalai Nagar - 608002, Tamil Nadu, India*
[b]*Department of Applied Geology, University of Madras, Guindy Campus, Chennai, Tamil Nadu 600025, India*

*Corresponding Author:
E-mail address: csvenkatg@gmail.com (V.Selvaraj)

The primary objective is to depict the sediment's texture, heavy minerals, microtextures and heavy metals from the coastal regions of Kodiyampalayam to Cuddalore, Tamilnadu, India. The textural characteristics are determined by adopting the dry sieving method ASTM using measures viz., Mean (Mz), Standard Deviation (σ_1), Skewness (Sk_I) and Kurtosis (K_G). The result implies that the Sediments are medium to fine sand, well-sorted sediment grains, leptokurtic, mesokurtic, highly platykurtic, symmetrical and coarsely and finely skewed. CM pattern indicates that the sediments are in the bottom suspension field. The beach environment and turbidity actions were represented by the sediment's linear discriminant function (LDF). Surface microtextures were examined with a Quartz grain using Scanning Electron Microscopy (SEM) with mechanical, chemical and morphological properties. Conchoidal cracks and arcuate steps in sand grain show their crystalline formation. The opaque and non-opaque properties of the heavy minerals are identified and it indicates that the heavy minerals are derived from igneous and metamorphic rocks. Minerals such as quartz, feldspar, clay minerals, carbonate minerals and organic carbon are identified from the samples using FTIR techniques. The trace metal (EDXRF) concentration is decreasing in the order: Fe >Mn >Ni >Cr >Cu >Pb >Zn. The pollution assessment indices viz., the EF (Enrichment Factor), the SPI (Sediment Pollution Index), Igeo (Geoaccumulation Index), CF (Contamination Factor), and PLI (Pollution Load Index) of the sediments suggest that the Sediments exhibit low to moderate polluted and Ecological Risk assessment indicates low to medium category risk.

Keywords: Texture, Provenance, Heavy Metal, Pollution, Coastal Sediments.

GEFS 05: Temporal Factor Analysis and Decision Tree for Interpreting Paleo Depositional Environments from Geochemical Data for CO_2 Storage

B. Venkateshwaran[1, 2*], AKM Eahsanul Haque[1], Numair Ahmed Siddiqui[1], Mu. Ramkumar[3], Mohamed Elsaadany[1], Hariharan Ramachandran[4], A. Manobalaji[5]

[1]*Department of Geoscience, Universiti Teknologi PETRONAS, Bandar Seri Iskandar 32610, Perak, Malaysia.*
[2]*Centre for Subsurface Imaging, Institute of Hydrocarbon Recovery, Universiti Teknologi PETRONAS, Seri Iskandar 32610, Malaysia.*
[3]*Department of Geology, Periyar University, Salem 636011, India.*
[4]*Institute of GeoEnergy Engineering (IGE), School of Energy, Geoscience, Infrastructure & Society, Heriot-Watt University, Edinburgh, UK.*
[5]*Department of Applied Sciences (Applied Geology), Faculty of Engineering and Science, Curtin University Malaysia, Miri, Malaysia.*

*Corresponding Author:
E-mail address: venkateshwa_22011656@utp.edu.my; venkateshwarangeo@gmail.com (B. Venkateshwaran)

Carbon Capture, Utilization, and Storage (CCUS) encompasses various techniques for capturing and storing carbon dioxide (CO_2) generated from fossil fuel combustion, either temporarily or permanently. A primary focus lies on underground geological formations as potential storage sites due to their substantial capacity and favourable fluid flow characteristics influenced by their respective depositional environments (Okwen et al., 2013; Raza et al., 2019; Rasool et al., 2023). The potential storage efficiency, determined through basin analysis to modelling phenomena from micro scale to macro scale, involves determining the depositional environments as one of the initial screenings of site selection. Evaluating depositional environments involves analysing the hydraulic sorting effects and mineralogical heterogeneity of coarse- and fine-grained sediments, as these factors influence the depositional processes (Kimura et al., 2004; Ohta, 2004). Depositional environments, based on their burial depth, are classified into three diagenetic mechanisms that might affect porosity: mechanical compaction, chemical compaction, and cementation (Houseknecht, 1987; Rahman et al., 2022). These diagenetic mechanisms, grain size distribution, and porosity evolution are typically examined through petrographic analysis, core sample analysis (which includes geochemical studies), well-log analysis, and other methods; these are applicable to all types of depositional environments. The determination of storage efficiency from different depositional environments is an important consideration, which includes deltaic, shelf clastic, shelf carbonate, fluvial deltaic, strand plain, reef, fluvial and alluvial, and turbidite settings (Okwen et al., 2013). This study selected the turbidite sequence as a target site and utilized geochemical data from core plug samples from the Bengal Fan in the central Indian Ocean. These were classified into seven facies types (Crowley et al., 1990). This study focused on the first facies across eight sequence depth zones. Building on prior work, this study interprets the depositional environments of subsurface core samples using major element geochemical data (SiO_2, Al_2O_3, TiO_2, Fe_2O_3, MgO, CaO, Na_2O, K_2O, MnO, P_2O_5, LOI) across eight depth levels in a temporal sequence from younger to older strata depths (14.20 to 694.30 m).

Factor analysis helps identify the relative contributions of geochemical signals, aiding in the understanding of diagenetic processes, dissolution, and precipitation mechanisms (Ohta, 2004; Venkateshwaran, 2021). It leverages the lithofacies-geochemistry relationship through temporal factor analysis of the geochemical data, examining samples in order of increasing depth and corresponding geologic age (Ramkumar, 2015). Factor scores are obtained for each element, which can be interpreted individually or collectively, contingent upon the user's expertise. While professionals may approach this interpretation differently, machine learning (ML) algorithms can provide a consistent and objective approach (Venkateshwaran et al., 2024). One powerful ML algorithm that can be employed is the decision tree, a non-parametric supervised learning method suitable for both classification and regression tasks. Decision trees operate based on algorithms like CART (Classification And Regression

Trees), Chi-square, ID3, and Reduction in Variance. The CART algorithm, specifically, utilizes the Gini Index as a metric to create decision points for classification tasks, considering both Gini Impurity and Gini Gain (Belousova et al., 2002; Itano and Sawada, 2024). To apply the Gini Index, factor scores are labelled and categorized into classes such as "Very High," "High," "Medium," "Low," and "Very Low." The Gini Index is subsequently calculated for each class and depth, resulting in three Gini Index values (one for each factor). The Gini Index is applicable only for individual variables in the trees and is not associated with other variables, whereas the factor scores need to be determined with three factor scores concurrently. In this case, a novel metric termed the paleo affinity index (PAI) is introduced to combine all variables' Gini measures to derive a new value. This study presents an innovative approach to characterizing potential CO_2 storage reservoirs by analysing paleo-depositional environments through the integration of temporal factor analysis and decision tree ML model.

Our integrated approach provides insights into the complex interplay of geological processes such as hydraulic sorting, weathering, and diagenesis that reorganize sediment chemical composition. Factor analysis factor scores elucidated the dominant processes that occurred during diagenesis based on the major element relationships. In the overall factor scores interpretation, the inverse relationship between carbonate and siliciclastic components suggests that carbonate minerals inhibit the presence of non-carbonate minerals, a common feature in mixed carbonate-siliciclastic systems. This relationship has implications for understanding the depositional environment and subsequent diagenetic processes. The contrasting behaviour of Fe and Mn provides insights into the redox conditions during deposition. Our results indicate that Mn migrated to oxidizing environments, precipitating as MnO_2, while Fe moved to reducing environments, forming FeS_2 or its precursors (Calvert and Pedersen, 1993). Our results reveal that despite belonging to single facies, samples from different depths exhibit three distinct depositional signatures based on the PAI values, leading to variable mineralogical characteristics. PAI values close to 1 represent the equal contribution of the elements, while values close to 0 represent the unequal proportion of the major elements, indicating that specific elements dominate while others contribute minimally. Factor analysis of major elements in the sedimentary formations identified three sample groups based on their PAI values. Group 1 (D1, D5) exhibited PAI values of ~0.35 to ~0.38, Group 2 (D2-D4) showed values of ~0.18 to ~0.22, and Group 3 (D6-D8) had values of ~0.09 to ~0.11 (**Table-1**). These groups corresponded to specific stratigraphic units: Group 1 to Units 2, 4, and 5; Group 2 to Units 2 and 4; and Group 3 to Unit 5. Key findings from this study include the identification of distinct depositional environments based on PAI groupings, reflecting variations in facies characteristics (Cochran and Stow, 1989). The geochemical groupings in our study reflect these facies variations, with higher PAI values corresponding to coarser-grain alteration. This separation is crucial for assessing the mineralogical alteration that affects the porosity, as redox conditions influence mineral reactivity and long-term stability. It is important to note that the Bengal fan location chosen for the pilot study, which available for core geochemical data while it lacks the typical features of a hydrocarbon reservoir, not a promising site for CO_2 storage options. The application of this geochemical approach to turbidite sequences demonstrates its utility in characterizing potential CO_2 storage sites. While our study provides valuable insights into the depositional and diagenetic processes, it also highlights the need for integrated analysis. Future work should incorporate trace element and isotope geochemistry to refine our understanding of fluid-rock interactions and long-term storage capacity based on the reservoir characterization and fluid flow simulations.

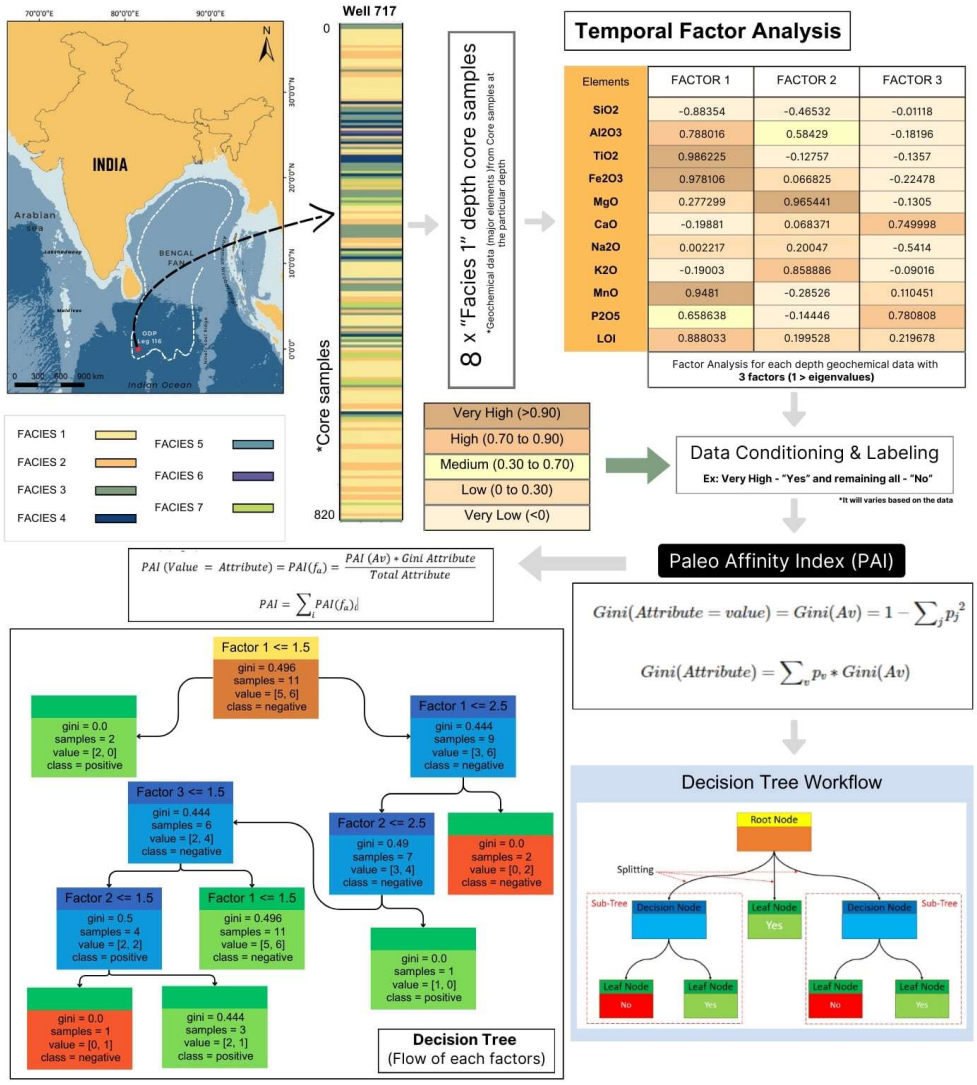

Figure 1 shows the summary of the graphical abstract of the research.

Table 1. Factor analysis of major elements in the sedimentary formations identified three sample groups based on their PAI values.

Depths	Range (m)	Total depth/ samples	GI(Factor1)	GI(Factor2)	GI(Factor3)	PAI
D1	14.20 - 38.18	6	0.242424242	0.43030303	0.354545455	0.359231762
D2	114.21 - 151.30	8	0.236363636	0.236363636	0.242424242	0.181737374
D3	312.84 - 332.90	6	0.121212121	0.43030303	0.121212121	0.240228956
D4	446.83 - 465.04	4	0.136363636	0.242424242	0.402597403	0.221704615
D5	534.05 - 559.53	6	0.212121212	0.272727273	0.493506494	0.380035372
D6	597.49 - 607.69	5	0	0.136363636	0.309090909	0.118015152
D7	654.53 - 664.30	5	0.090909091	0.145454545	0.339393939	0.135250281
D8	683.03 - 694.30	5	0.145454545	0.145454545	0.272727273	0.096686869

References

Belousova, E.A., Griffin, W.L., O'Reilly, S.Y., Fisher, N.I., 2002. Igneous zircon: Trace element composition as an indicator of source rock type. Contributions to Mineralogy and Petrology 143(5), 602–622. https://doi.org/10.1007/s00410-002-0364-7

Calvert, S. E., Pedersen, T.F., 1993. Geochemistry of Recent oxic and anoxic marine sediments: Implications for the geological record. Marine Geology 113(1–2), 67–88. https://doi.org/10.1016/0025-3227(93)90150-T

Cochran, J.R., Stow, D.A.V., 1989. Site 717 Summary. Proceedings of the Ocean Drilling Program, 116 Initial Reports, July 1987. https://doi.org/10.2973/odp.proc.ir.116.105.1989

Crowley, S.F., Stow, D.A.V., Bouquillon, A., Tiercelin, J.-J., 1990. Major-Element Geochemistry and Clay Mineralogy and Their Relationship to Facies Discrimination in Distal Bengal Fan Sediments: Leg 116. Proceedings of the Ocean Drilling Program, 116 Scientific Results. https://doi.org/10.2973/odp.proc.sr.116.200.1990

Houseknecht, D. W. 1987. Assessing the relative importance of compaction processes and cementation to reduction of porosity in sandstones. American Association of Petroleum Geologists Bulletin 71(6), 633–642. https://doi.org/10.1306/9488787f-1704-11d7-8645000102c1865d

Itano, K., Sawada, H. 2024. Revisiting the Geochemical Classification of Zircon Source Rocks Using a Machine Learning Approach. Mathematical Geosciences. https://doi.org/10.1007/s11004-023-10128-z

Kimura, S., Shikazono, N., Kashiwagi, H., Nohara, M. 2004. Middle Miocene-early Pliocene paleo-oceanic environment of Japan Sea deduced from geochemical features of sedimentary rocks. Sedimentary Geology, 164(1–2), 105–129. https://doi.org/10.1016/j.sedgeo.2003.08.003

Ohta, T., 2004. Geochemistry of Jurassic to earliest Cretaceous deposits in the Nagato Basin, SW Japan: Implication of factor analysis to sorting effects and provenance signatures. Sedimentary Geology, 171(1–4), 159–180. https://doi.org/10.1016/j.sedgeo.2004.05.014

Okwen, R., Frailey, S., Leetaru, H., 2013. Assessing Reservoir Depositional Environments to Develop and Quantify Improvements in CO_2 Storage Efficiency: A Reservoir Simulation Approach Project Number: DE-FE0009612.

Rahman, M.J., Fawad, M., Jahren, J., Mondol, N.H., 2022. Influence of Depositional and Diagenetic Processes on Caprock Properties of CO_2 Storage Sites in the Northern North Sea, Offshore Norway. Geosciences (Switzerland), 12(5). https://doi.org/10.3390/geosciences12050181

Ramkumar, M. (2015). Chemostratigraphy: Concepts, Techniques, and Applications. Chemostratigraphy: Concepts, Techniques, and Applications, 1–515. https://doi.org/10.1016/C2013-0-09872-6

Rasool, M. H., Ahmad, M., Ayoub, M., 2023. Selecting Geological Formations for CO_2 Storage: A Comparative Rating System. Sustainability (Switzerland), 15(8), 1–39. https://doi.org/10.3390/su15086599

Raza, A., Gholami, R., Rezaee, R., Rasouli, V., Rabiei, M., 2019) Significant aspects of carbon capture and storage – A review. Petroleum, 5(4), 335–340. https://doi.org/10.1016/j.petlm.2018.12.007

Venkateshwaran, B., 2021. The Geochemical and Geostatistical Analysis of Iron Ore Groups in Northern Tamilnadu, India. Periyar University.

Venkateshwaran, B., Ramkumar, M., Siddiqui, N. A., Haque, A. E., Sugavanam, G., Manobalaji, A. 2024. A Graph Convolutional Network Approach to Qualitative Classification of Hydrocarbon Zones Using Petrophysical Properties in Well Logs. Natural Resources Research, 33(2), 637–664. https://doi.org/10.1007/s11053-024-10311-x.

GEFS 06: Importance of geoscientific information in forming new public policies for exploitation of groundwater around the World

P. F. Rodriguez-Espinosa[a*], Jose Jorge Caracheo Gonzalez[a], K. M. Ochoa-Guerrero[a], E. Martinez-Tavera[b],

[a]*Centro Interdisciplinario de Investigaciones y Estudios sobre Medio Ambiente y Desarrollo (CIIEMAD), Instituto Politécnico Nacional (IPN), Calle 30 de Junio de 1520, Barrio La Laguna Ticomán, Municipio Gustavo A. Madero, C.P. 07340 Ciudad de México, México.*
[b]*UPAEP Universidad. 21 Sur 1103, Barrio de Santiago, Puebla, C.P. 72410, México.*

*Corresponding Author:
E-mail address: pedrof44@hotmail.com (P. F. Rodriguez-Espinosa)

Recent scientific research published in the field of geohydrology shows that there is a considerable decrease in our global groundwater reserves. Hydrology results presented from 170,000 wells in 1,693 aquifer systems around the world, represents 75% of the world's groundwater reserves. The decline in the groundwater level is present in different parts of the world as hotspots indicate an acceleration in the decrease of the water table of the world's aquifers, quantified as such, since 1950s. On the other hand, recent scientific publications integrated isotopic information of the world's groundwaters in which they refer to the importance that fossil waters represent the groundwater reserves. Isotopic results carried out with radiocarbon refer that our underground reserves contain water from millennial infiltration. The information quantifies the depth of 250 meters preferred for exploitation, which contains between 40 and 80% of fossil water. The results are clear in that agricultural areas, arid and

semi-arid climates are those that show the greatest decline. Isotopic results indicate that they refer to tritium as a tracer isotope of recent intrusions from the 1950s to the present that are possibly contaminating the world's aquifers. However, recent scientific publications indicate that current rainfall may not be recharging deep aquifers in a time of sustainable units. This is also well supported by scientific evidence in Mexico that the data radiocarbons already published indicate direct relationships with stable isotopic relationships with prevailing paleoclimates in the paleo infiltration that gives rise to the aquifer of a metropolitan area of more than 4 million people in central Mexico. The scientific in the present study indicates the evidence of a recent georisk associated with the intense extraction of groundwater in non-karstic agricultural areas that develops sinkholes. The depletion of our global groundwater reserves must be considered in the reformulation of our national public policies and form part of new international guidelines that should be adopted by other countries. Finally, the results presents a proposal for an underground blue bond that would allow the development of sustainable programs for better exploitation and reuse of global groundwater.

GEFS 07: Comparative approach on the adsorptive potential of native and NaOH-activated hybrid biochar from *Prosopis Juliflora* and Crustacean residue for the removal of Cango Red from wastewater

Karthikeyan Asaithambi[1], Sugumaran Karuppiah[1] and Mahalakshmi Mathivanan[1*]

[1]*School of Civil Engineering, SASTRA Deemed University, Thanjavur, Tamil Nadu, India*

*Corresponding Author:
E-mail address: mahalakshmi@civil.sastra.edu (M.Mahalakshmi)

The synthetic dyes released from industries are one of the most influential factors in water pollution. These dyes can affect biotic resources on a large scale. So far, various methods have been introduced to remove these dyes. Among those methods, adsorption is the most frequently used due to its low cost and high efficiency. Crustacean waste, Crab shell, an abundant marine waste, and *Prosopis juliflora*, an invasive plant species, are adsorbents. These two materials were mixed in the weight ratio 1:1 and converted to composite biochar (CB). This composite biochar was activated by two chemicals, namely Hydrochloric acid (ACB) and Zinc Chloride (ZCB) (**Fig. 1**). This study takes into consideration the elimination of Congo Red (CR). One of the most soluble and stable anionic diazo dyes, Congo Red (CR), is utilized in various industries, including textile, plastic, cosmetics, and pharmaceutical. Furthermore, the aquatic ecosystem and human health are impacted by this dye, which is dangerous and carcinogenic. Batch adsorption experiments were conducted to optimize the various adsorption parameters, to obtain the maximum biosorption potential and the removal rate of Congo Red (CR) dye. Based on the conventional optimization studies, the essential adsorption parameters for removing CR were the maximum removal efficiency of 74.57% at pH 2(ACB) and 64.17% at pH 4(ZCB). The optimum dosage for both ACB and ZCB is 0.18 g. The maximum adsorption capacity of ACB and ZCB were obtained at 66.22 and 15.38 mg/g at 50°C, respectively. The spontaneous and endothermic adsorption of CR was confirmed by thermodynamic analysis. Experimental data fitting on various kinetic models was examined for CR adsorption onto ACB and ZCB. Among that, the pseudo-second-order kinetic model best suited the data. Finally, the structural and functional characteristics of the activated adsorbents were examined using Scanning Electron Microscope (SEM) and Fourier Transform Infrared (FTIR) Spectroscopy. Consequently, ACB and ZCB exhibit great potential as an adsorbent with a strong affinity for hazardous CR dye molecules in wastewater. All these results

highlight the efficiency of the composite biochar chemically treated for the adsorption of CR dye molecules from the wastewater.

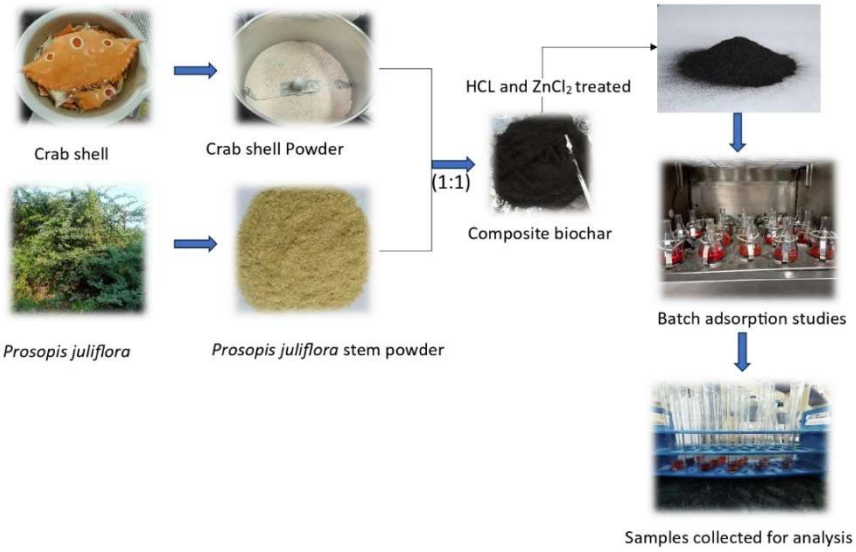

Figure 1. Graphical summary of the research methodology

Theme 5: Sustainable Resources & Geo-Engineering

SRGE 02: Physical Properties & Tensile Performance of Short Fibers/ Particles Reinforced Thermoset Composites

Dominick Wong[1], Anshuman Mishra[2], Sujan Debnath[1,*], Mahmood Anwar[3], Ian J. Davies[4], Moola Reddy[1], Abdul Hamid[1], Amin Razali, Alokesh Pramanik[4], Chithirai Pon Selvan[5]

[1]*Department of Mechanical Engineering, Curtin University, Malaysia, CDT 250, Miri 98009, Sarawak, Malaysia*
[2]*Department of Applied Science, Curtin University, Malaysia, CDT 250, Miri 98009, Sarawak, Malaysia*
[3]*Department of Mechanical Engineering, School of Computing, Engineering and Built Environment, Glasgow Caledonian University, Cowcaddens Road, Glasgow, G4 0BA, Scotland, United Kingdom*
[4]*School of Civil and Mechanical Engineering, Curtin University, GPO Box U1987, Perth, WA 6845, Australia*
[5]*Science and Engineering, Curtin University, Dubai International Academic City, Block 11, Fourth Floor, P. O. Box 345031, Dubai, UAE*

*Corresponding Author:
E-mail address: d.sujan@curtin.edu.my (Sujan Debnath)

Recent advancements in the development of materials with low emissions have become a global priority in the effort to limit the effects of climate change and achieve net-zero emissions. Natural fiber composites have received attention from both the commercial and research communities because of their inherent eco-friendliness, lower cost, and lower energy consumption during processing compared to their synthetic counterparts. Despite the absence of physical comparisons for locally available natural fiber composites in the Borneo region, this study has attempted to address this gap by examining various natural fibers, including oil palm empty fruit bunch fiber, water hyacinth, and coir, in both short fiber and particle forms. The developed composites were assessed through colorimetric assessment, fractographic analysis, and tensile tests. It was revealed that particle composites exhibited lower luminance values, by up to 19.05 L* as compared to short fiber composites, implying better dispersion of fillers. Additionally, it was established that the utilization of particle forms displayed greater tensile performance than short fiber forms where it on average outperformed by up to 19.17 MPa and offers higher ductility. The findings of this research will be beneficial in advancing the production of composites through the incorporation of natural fibers in the wet hand layup/open-casting fabrication technique.

Keywords: Natural Fiber, Short Fiber, Particle, Biomass Valorization

SRGE 03: Thermal characteristics of sustainable concrete incorporating eggshell powder and fish bone ash

Ying Ze Soo[1], Yeong Huei Lee[1,2*], Yee Yong Lee[3], Tina Chui Huon Ting[1], Timothy Zhi Hong Ting[1,2], Yie Hua Tan[4], Paran Gani[1], Ai Chen Tay[1]

[1] *Department of Civil and Construction Engineering, Faculty of Engineering and Science, Curtin University, Sarawak Malaysia, CDT 250, 98009 Miri, Sarawak, Malaysia.*

[2] *Curtin Highway Infrastructure Research & Innovation Hub (CHIRI), Faculty of Engineering and Science, Curtin University, Sarawak Malaysia, CDT 250, 98009 Miri, Sarawak, Malaysia.*
[3] *Department of Civil Engineering, Faculty of Engineering, University Malaysia Sarawak, 94300 Kota Samarahan Sarawak, Malaysia.*
[4] *Petroleum and Chemical Engineering, Faculty of Engineering, Universiti Teknologi Brunei, Gadong, BE1410, Brunei Darussalam*

*Corresponding Author:
E-mail address: yeong.huei@curtin.edu.my (Yeong Huei Lee)

This study aims to investigate the thermal performance of sustainable concrete incorporating food-processing waste as a partial cement replacement material, thereby assessing the potential and reliability of this sustainable concrete for real-life construction applications. After examining various food-processing wastes based on their chemical components and properties, eggshell powder (ESP) and fish bone ash (FBA) were selected as partial cement replacements at 5% and 10%, respectively. Structural strength tests were also conducted to ensure that the food-processing waste concrete meets the minimum industrial compression strength requirement of 17 MPa, as the American Concrete Institute (ACI) specified. The study found that the food-processing waste concrete's compression and splitting tensile strength achieved satisfactory structural strength on the 28th curing day. The structural strength of the food-processing waste concrete exhibited an insignificant decrease compared to conventional concrete. Furthermore, a scaled-wall test was performed to determine the decrement factor and time lag of the concrete wall. This involves placing a scaled concrete wall in a polystyrene box wrapped with aluminium foil and heated with a 100-watt light bulb. The temperatures of the wall's interior and exterior surfaces were measured using thermocouples connected to a data logger. The time lag was recorded as the time required for the heat source to propagate through the concrete wall completely. At the same time, the decrement factor was the ratio of the interior wall's maximum temperature to the exterior wall's maximum temperature. The results indicate that food-processing waste concrete has a lower decrement factor and higher time lag than conventional concrete. In conclusion, the food-processing waste concrete meets the minimum required strength specified by the ACI and demonstrates better thermal performance than conventional concrete.

SRGE 04: Polymer Stack Design for Thermoacoustic Effect of a Renewable Energy Based Desktop Green Refrigerator

Clara Rutendo Mutsakanyi[1], Mahmood Anwar[2], Sujan Debnath[1,*], Dominick Wong[1], Muditha Kulatunga[2]

[1] *Department of Mechanical Engineering, Curtin University, Malaysia, CDT 250, Miri 98009, Sarawak, Malaysia*
[2]*Department of Mechanical Engineering, School of Computing, Engineering and Built Environment, Glasgow Caledonian University, Cowcaddens Road, Glasgow, G4 0BA, Scotland, United Kingdom*

*Corresponding Author:
E-mail address: d.sujan@curtin.edu.my (Sujan Debnath)

Recent climate change issues have led to striving for green refrigeration technology moving away from convectional Vapour compression refrigerant cycles, which impose an environmental threat due to the usage of carbon-based working fluids commonly known as refrigerants. Interestingly, a Thermoacoustic refrigerator is a potential alternative to overcome such negative influence refrigerants impose on natural

ecosystems since thermoacoustic refrigerators use environmentally friendly renewable sources, i.e. air as a working fluid. However, appropriate stack design which is the core part of this green technology is crucial in order to harness the challenging thermoacoustic effect, particularly through 3D-printed stack fabrication. Hence, in this research, the influence of the stack geometry design with stack material influence on the cooling effect of a desktop thermoacoustic refrigerator was investigated. Three stack geometries: parallel plate, circular pored and triangular pored stack geometries with three stack materials i.e. ABS, PETG and PLA were fabricated through 3D printing. A desktop-based test setup was built with a stacked sample, which was mounted in the resonator with 260 Hz as the designed frequency, and the resonator was coupled with the acoustic driver where temperature data was collected at the stack ends to identify the thermoacoustic effect at ambient pressure with air as working fluid. It is revealed that the parallel plated stack design showed better performance in terms of thermoacoustic effect among the three geometric designs. Interestingly, ABS material showed a higher influence on thermoacoustic effect i.e. $\Delta T_{max} = 1.07°$ although possessing a higher Coefficient of thermal expansion properties. It is expected that such findings would pave the way towards further development of green refrigerators through thermoacoustic technology.

Keywords: Climate change, sustainability, thermoacoustic cooling, CTE, refrigeration technology and acoustic material.

SRGE 05: Environmental Green-collar Crime: A Focus on Illegal Transfer of Hazardous Waste

Mohammad Belayet Hossain[1*], Dhanuskodi Rengasamy[1], Mohammad Abdul Matin Chowdhury[1]

Faculty of Business, Curtin University, Malaysia, CDT 250, Miri 98009, Sarawak, Malaysia

*Corresponding Author:
E-mail address: belayet.hossain@curtin.edu.my (Mohammad Belayet Hossain)

Illegal transfer of hazardous waste is a pressing form of environmental crime, with limited research on the effectiveness of international conventions and the socioeconomic factors fueling this problem. This study delves into the impact of international legal frameworks like the Basel Convention on curbing illegal hazardous waste movements and the socioeconomic factors contributing to these crimes, especially in developing nations. Employing a doctrinal methodology, this study scrutinizes a set of case studies selected based on criteria including the frequency and scale of illegal waste transfers, as well as the regulatory landscapes of the impacted nations. The case studies are evaluated through qualitative analysis, focusing on key indicators like enforcement effectiveness, the impact of socioeconomic factors, and the outcomes of international agreements. The study also evaluates the role of developed countries in promoting these practices and the vulnerabilities within the legal systems of developing nations. The findings underscore the deficiency of enforcement mechanisms in international instruments, leading to inconsistent application across regions and impacting global policy. Case studies demonstrate that weak governance, economic pressures, and inadequate regulatory frameworks in developing countries significantly contribute to illegal waste dumping. Furthermore, the research pinpoints particular socioeconomic factors like poverty, corruption, and the absence of alternative waste management infrastructure, elucidating their roles in exacerbating the problem. The study suggests specific measures for international organizations and policymakers: enhancing transparency through stricter enforcement of reporting obligations, ensuring uniform application of legal frameworks across regions, and fostering the development of local waste management solutions in affected countries. The

circular economy approach in Amsterdam, the decentralized waste management model in Curitiba, and the zero waste initiatives in San Francisco serve as exemplary models that have effectively addressed waste management challenges, offering insights for improving global governance. Addressing these issues is crucial due to the extensive implications of illegal hazardous waste transfers on global health, ecosystems, and the integrity of international governance. This research enriches the current knowledge by delving into the intricate relationship between legal frameworks and socioeconomic drivers in environmental green-collar crime, presenting actionable recommendations that can enhance global waste management practices.

Keywords: Hazardous waste, disposal, Basel Convention, environmental green collar crime, industry.

SRGE 06: Stormwater Management and Treatment with Adsorbent Pervious Concrete: A Comprehensive Review

Ehsan Teymouri[1] and Wong Kwong Soon[1,2,*]

[1]*Department of Civil and Construction Engineering, Faculty of Engineering and Science, Curtin University, Malaysia, 98009, Miri, Sarawak, Malaysia*
[2]*Peatland Research, Faculty of Engineering and Science, Curtin University, Malaysia, 98009, Miri, Sarawak, Malaysia*

*Corresponding Author:
E-mail address: wongkwongsoon@curtin.edu.my (Wong Kwong Soon)

Adsorbent Pervious Concrete (APC) represents an innovative approach to stormwater management and treatment, integrating low-cost adsorbents into conventional pervious concrete to enhance its pollutant removal capabilities. This advanced material offers a sustainable solution with numerous environmental benefits, effectively mitigating stormwater contamination. This review paper delves into both the performance of APC in stormwater management and its potential to reduce the risk of flash flooding through optimized flow efficiency. In addition to reviewing the mechanical properties and mixture designs of APC, the paper critically examines its hydraulic performance, permeability, and capacity to manage stormwater flow, ensuring efficient drainage. Laboratory findings related to the compressive strength, porosity, and permeability of APC, along with their interdependencies, are comprehensively analyzed. The influence of diverse low-cost adsorbents, such as minerals, industrial byproducts, and nanoparticles, on the engineering properties and efficacy of APC in pollutant removal is critically assessed. Building on the state-of-the-art review, the paper emphasizes the need for further research into the application of APC in stormwater treatment, highlighting the importance of understanding its engineering properties and long-term environmental performance.

Keywords: Pervious Concrete; Adsorbents; Stormwater Management and Treatment, Engineering Properties; Environmental Impacts

---

Theme 6: Natural Hazards

NH 01: Geospatial Analysis of Landslide Susceptibility in Pulwama, Jammu and Kashmir, India: A Multi-Criteria Decision-Making Approach

Mahalingam Bose[1*] and Indrakant Behera[1]

[1]*Department of Geography, Central University of Karnataka, Karnataka- 585311, India*

*Corresponding Author:
E-mail address: mahabose@gmail.com (Mahalingam Bose)

Landslides are common, frequent, and abrupt natural disasters that negatively impact people, their livelihoods, their homes, and the environment. It is one of the most devastating and ruinous natural disasters (Chingkhei et al., 2013), which can cause massive losses and damages directly or indirectly over time (Parkash, 2011). A landslide is a descent down a slope of a mass composed of fragments, stones, or soil propelled solely by gravitational force. Different landslides move at different rates; in hilly areas, some move quickly, causing destruction and casualties, while others move more slowly, posing a threat but not immediately causing harm (Shah et al., 2021). Thousands of people die each year worldwide due to landslides (Froude and Petley, 2018); especially developing countries bear the brunt of the consequences, as they experience about 95% of these calamities (Enigda and Suryanarayana, 2021).

India is especially susceptible to landslides due to its distinct geographic and geological features, including unstable soil and rock formations, heavy rains, and seismic activity (Bhandari et al., 2023). The rough terrain and slope instability events are prone in the Northern Himalayas, and this has gotten worse because of growing anthropogenic activity throughout time (Panikkar & Subramanyan, 1996). Indian Himalayas are vulnerable to multiple hazards and have experienced numerous devastating calamities that have caused significant loss of life and property. According to the Jammu and Kashmir State Disaster Management Plan 2017, the state has been designated as a multi-hazard zone under Seismic Zones IV and V, with intensity MSK of VIII to IX or more.

Pulwama District of Jammu & Kashmir, India, faces significant risks due to its rugged topography, intense rainfall, and anthropogenic activities such as deforestation, unplanned construction, mining, and road building (**Fig. 1**). This study employs Multi Criteria Decision Making (MCDM) and Analytical Hierarchical Process (AHP) proposed by (Saaty, 1977) in Geographic Information System (GIS) to identify landslide susceptibility zones in Pulwama, Jammu & Kashmir, India. Ten factors, such as elevation, slope, lithology, rainfall, soil, geology, geomorphology, and distance from lineament, streams, and vegetation cover, are evaluated through pairwise comparisons using AHP. Weighted Overlay Analysis (WOA) has been applied in ArcGIS Pro to obtain the landslide susceptibility zones.

The analysis results indicate three main susceptibility zones: high, moderate, and less (**Fig. 2**). Assessing the spatial extension reveals 227.33 sq. km. as highly susceptible, constituting 25.49 percent of the total area, primarily concentrated in Pulwama's northeastern and northern regions. This is due to towering mountains, steep slopes, loose and young soils, and minimal vegetation cover with significant precipitation. Apart from these regions, highly susceptible areas are also in the other parts of districts in a linear shape, associated with the presence of streams and lineaments, which are the major influencing factors for landslides.

Additionally, 661.77 sq. km. are identified as moderately susceptible, covering 74.19 percent of the area. Pulwama's central and southern parts exhibit moderate susceptibility due to less elevated land with a gentle slope, stable soil, and rock structure than highly susceptible areas. Notably, certain regions in the central part of the district are less vulnerable due to an almost flat surface with a fair amount of

vegetation at a certain distance from lineaments and streams. An area of about 2.90 sq. km. falls into the category of low susceptibility, accounting for 0.32 percent of the total area. The result is overlaid using ArcGIS Pro 3.2.0 base map and Google Earth Pro, through which it is identified that high susceptibility areas are associated with high terrain with steep slopes or with streams and lineaments.

The result of this study can help local authorities with risk mitigation, the development of appropriate policies, the implementation of early warning systems, and the enhancement of community awareness in high-risk areas.

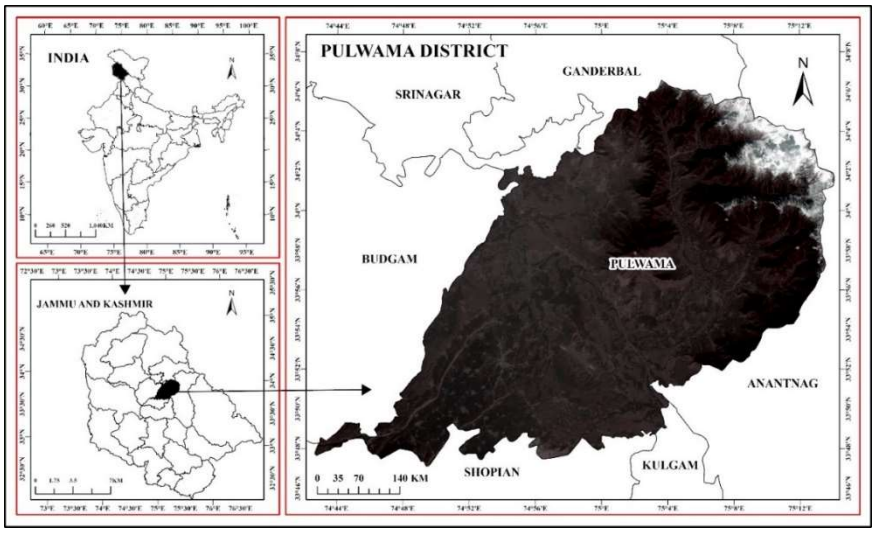

Figure 1: Study Area

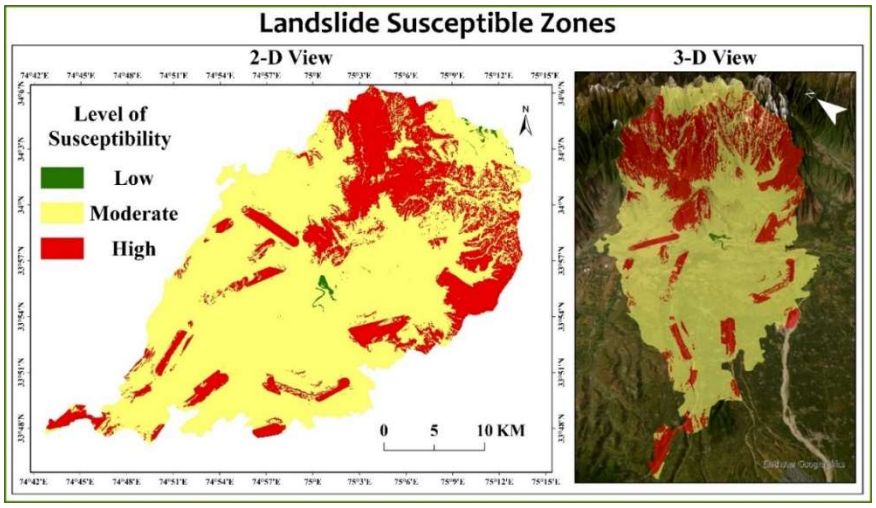

Figure 2: Zones of Landslide Susceptibility in Pulwama, Jammu & Kashmir, India

Keywords: Landslide, Susceptibility, GIS, Weighted Overlay Analysis, Analytical Hierarchical Process

Reference

Bhandari, K., Acharya, M., Dhital, M. R., Shrestha, S., 2023. Landslide Susceptibility Mapping of West Central Nepal Lesser Himalaya Baglung Municipality, Baglung, Nepal. American Journal of Applied Scientific Research 7(1), 163-173.

Chingkhei, R. K., Shiroyleima, A., Singh, L. R., Kumar, A., 2013. Landslide Hazard Zonation in NH-1A in Kashmir Himalaya, India. International Journal of Geosciences 4(10), 1501–1508. https://doi.org/10.4236/ijg.2013.410147

Enigda, E. A., Suryanarayana, T. 2021. Landslide evaluation in parts of Tarmaber District (Debresina), Central Ethiopia; an expert evaluation approach. International Journal of Geoinformatics Geological Science 8(1), 15-26.

Froude, M. J., Petley, D.N., 2018. Global fatal landslide occurrence from 2004 to 2016. Natural Hazards and Earth System Sciences, 18, 2161–2181. https://doi.org/10.5194/nhess-18-2161-2018

Panikkar, S. V., Subramanyan, V., 1996. A geomorphic evaluation of the landslides around Dehradun and Mussoorie, Uttar Pradesh, India. Geomorphology 15(2), 169-181.

Parkash, S. 2011. Historical records of socio-economically significant landslides in India. Journal of South Asia Disaster Studies 4(2), 177–204.

Saaty, T.L., 1977. A scaling method for priorities in hierarchical structures. Journal of Mathematical Psychology 15(3), 234–281.

State Disaster Management Plan, Government of Jammu and Kashmir, Department of Disaster Management, Relief, Rehabilitation and Reconstruction. Notified vide SRO No. 218, Dated 22.5.2017.

NH 02: Microscale evaluation of vulnerability and resilience to natural hazards in the Coastal Region of Tamil Nadu, Southern India: Implications at Local and Regional Scales

K. Balasubramani[a*], S. Leo George[a], Mu. Ramkumar[b]

[a]*Department of Geography, Central University of Tamil Nadu, Thiruvarur, India*
[b]*Department of Geology, Periyar University, Salem, India*

*Corresponding Author:
E-mail address: geobalas@cutn.ac.in (K. Balasubramani)

The coastal plain region of Tamil Nadu (TN), defined by the coastal watershed boundaries and the contours of 40 m, is a unique physiographic region of the State in India comprising 16 districts and 75 sub-districts with 5,008 villages/wards. Although this plain region is densely populated (~2,000/km^2) and extremely sensitive to multiple natural hazards, the disaster risks of this region are not being assessed at a micro-level concerning all key risk elements. The present study is attempted for the entire coastal stretch of TN with the micro-administrative units through a systematic multi-hazard risk framework. The study used all the key risk elements (hazard, exposure, vulnerability, and lack of coping capacity) with 34 components to evaluate disaster risks in the coastal plains of TN. Each component was prepared as a thematic layer using the datasets obtained/generated from multiple sources (satellite images, published reports, and ground surveys) and was used to determine an integrated index through spatial multi-criteria approaches such as the Analytical Hierarchy Process (AHP) and Technique for Order of Preference by Similarity to Ideal Solution (TOPSIS). The findings indicate that ~95 % of micro administrative units with very high vulnerability to disaster risks are observed in the northern coastal plains of TN, stretching from Nagapattinam to the north of Chennai, with hot spots around Cuddalore and Chennai. The micro-level approach adopted in the study is comprehensive and necessary to prepare a disaster-resilient society. The paper also highlights the importance of integrating vulnerability and coping capacity parameters when assessing natural hazards and provides recommendations for future research at different scales.

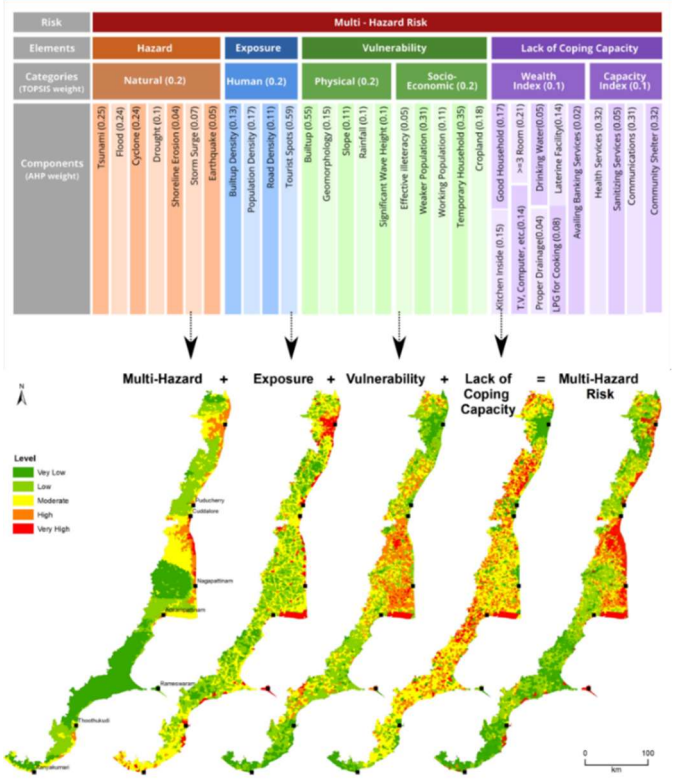

Figure 1. Graphical Abstract

Keywords: Multi-hazard, Coastal Hazards, Vulnerability, Exposure, Disaster Risk

---

NH 03: Geotourism Development Around Geohazard Prone Area of Pangandaran Aspiring Geopark, West Java, Indonesia

Dicky Muslim[1*], Zufialdi Zakaria[2], Ghazi O Muslim[1], Irvan Sophian[2], Fauzan N Muslim[1], Winantris[2]

[1]*Laboratory of Engineering Geology, Universitas Padjadjaran, Bandung, Indonesia*
[2]*Postgraduate Program of Geology, Universitas Padjadjaran, Bandung, Indonesia*

*Corresponding Author:
E-mail address: d.muslim@unpad.ac.id (Dicky Muslim)

Pangandaran is one of the popular beach destinations in the West Java Province. The local government of Pangandaran Regency is currently proposing an aspiring Geopark to accommodate the economic development while maintaining natural conservation on geotourism through the pillars of Geodiversity, Biodiversity and Cultural Diversity. Meanwhile, Pangandaran beaches had also experienced a major tsunami event on July 17, 2006, causing more than 600 fatalities and major economic loss in the area after an offshore earthquake with 6.8 Magnitude struck near the Indian Ocean at a depth of 10 km. This paper is aimed to reveal the importance of disaster resilience for the community toward a safe geotourism environment. The methodology in this study consists of fieldwork for analyzing the potential of geological hazards and mapping the communities' distribution in the built environment related to geotourism in the study area. The result of the study shows that the proposed aspiring geopark

assignment has attracted more tourists and visitors to this area than before. Some locations of geosites along the coastline of the Indian Ocean are found vulnerable to geological disasters such as earthquakes and tsunamis. It is relatively unsafe for the inhabitants and visitors when this geological event occurs. Though several beaches such as Pananjung, Batuhiu and Parigi have developed activities based on disaster resilience parameters through education for stakeholders as well as disaster awareness for the public. Due to the geological condition of this study area, it is important to note that behind the natural beauty, there are several potential disasters that might occur in the future. Earthquakes and collateral damages such as tsunamis, landslides and liquefaction are indispensable for the population and infrastructures. It can be concluded that the ideas of disaster resilience for the community have already started to be implemented even though there is still a lot of work to do to support a safe geotourism environment in the study area.

Keywords: Pangandaran, geohazard, geotourism, environment, disaster resilience

NH 04: The collaboration between bivariate and multivariate statistical methods in determining landslide Vulnerability zones in Garut Regency, West Java Province, Indonesia

Dean Saptadi[a] , Twin H.W. Kristyanto[a,b*], Urwatul Wusqa[a], Zufialdi Zakaria[b], Dicky Muslim[b]

[a] *Geology Study Program, Faculty of Mathematics and Natural Sciences, Universitas Indonesia, Depok, 16424, Indonesia*
[b] *Doctoral Program in Geology, Faculty of Geological Engineering, Universitas Padjadjaran, Jatinangor, Sumedang District, 45363*
*Corresponding Author:
E-mail address: twin.hosea@sci.ui.ac.id (Twin Hosea W.K)

Landslides are among the most frequent natural disasters in Indonesia, with 1,152 events recorded in 2020 alone, according to the National Agency for Disaster Countermeasures (BNPB). Garut Regency, located in West Java Province, is particularly vulnerable, having experienced 407 landslide events in 2020 and 161 events from 2000 to 2020. This study aims to develop a monthly landslide susceptibility map for Garut Regency using the Weight of Evidence (WoE) and Logistic Regression (LR) methods and to compare the performance of these two approaches.

The research employs WoE and LR methods to identify and classify landslide susceptibility zones. WoE evaluates the influence of individual parameter classes on landslide occurrence, while LR analyzes the correlation between various parameters. Key parameters considered include elevation, slope, slope aspect, curvature, NDVI, proximity to rivers, roads, and lineaments, land use, lithology, and monthly rainfall. A dataset of 104 landslide events from 2000 to 2020 was divided into a training set (70%) for model validation and a test set (30%) for prediction validation, with performance measured using the Area Under Curve (AUC) metric.

The study produced landslide susceptibility maps that categorize the region into four risk zones: very low, low, medium, and high (**Figs. 1-2**). Results show that the WoE model achieves an AUC success rate ranging from 0.76 to 0.80 and a predictive rate between 0.81 and 0.86. In contrast, the LR model yields an AUC success rate of 0.74 to 0.81 and a predictive rate of 0.82 to 0.87. These findings suggest that while the WoE method offers slightly better success rate accuracy, the LR method excels in predictive rate accuracy, indicating that both methods can be complementary in landslide susceptibility analysis.

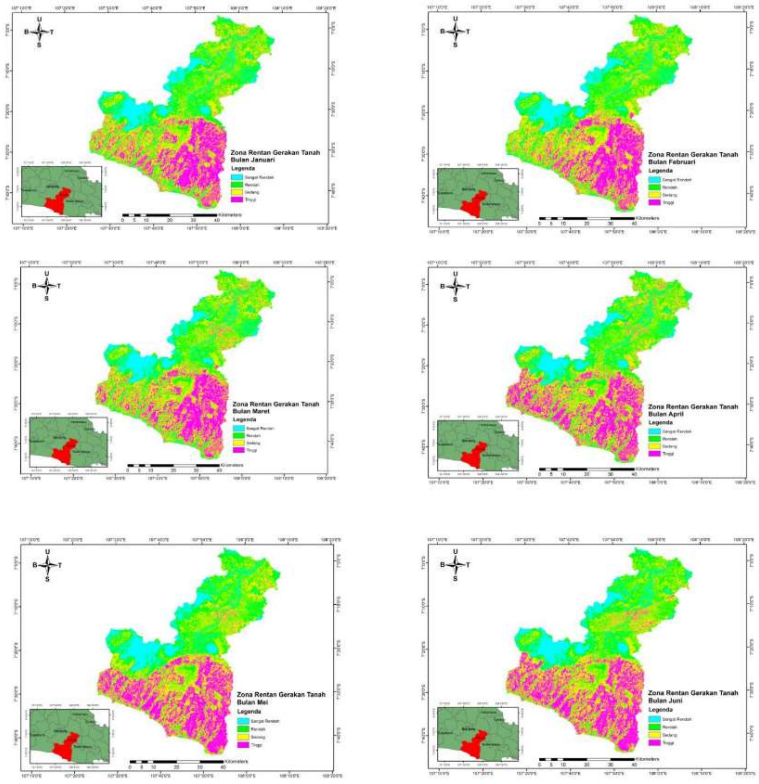

Figure 1a. Landslide Susceptibility Maps using WoE From January to December

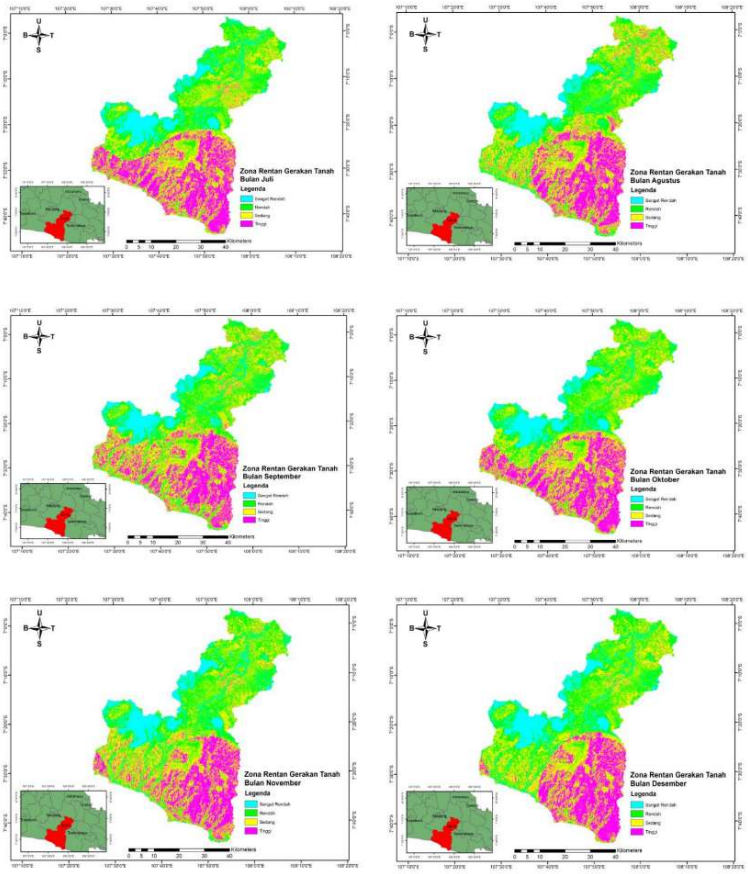

Figure 1b. Landslide Susceptibility Maps using WoE From January to December

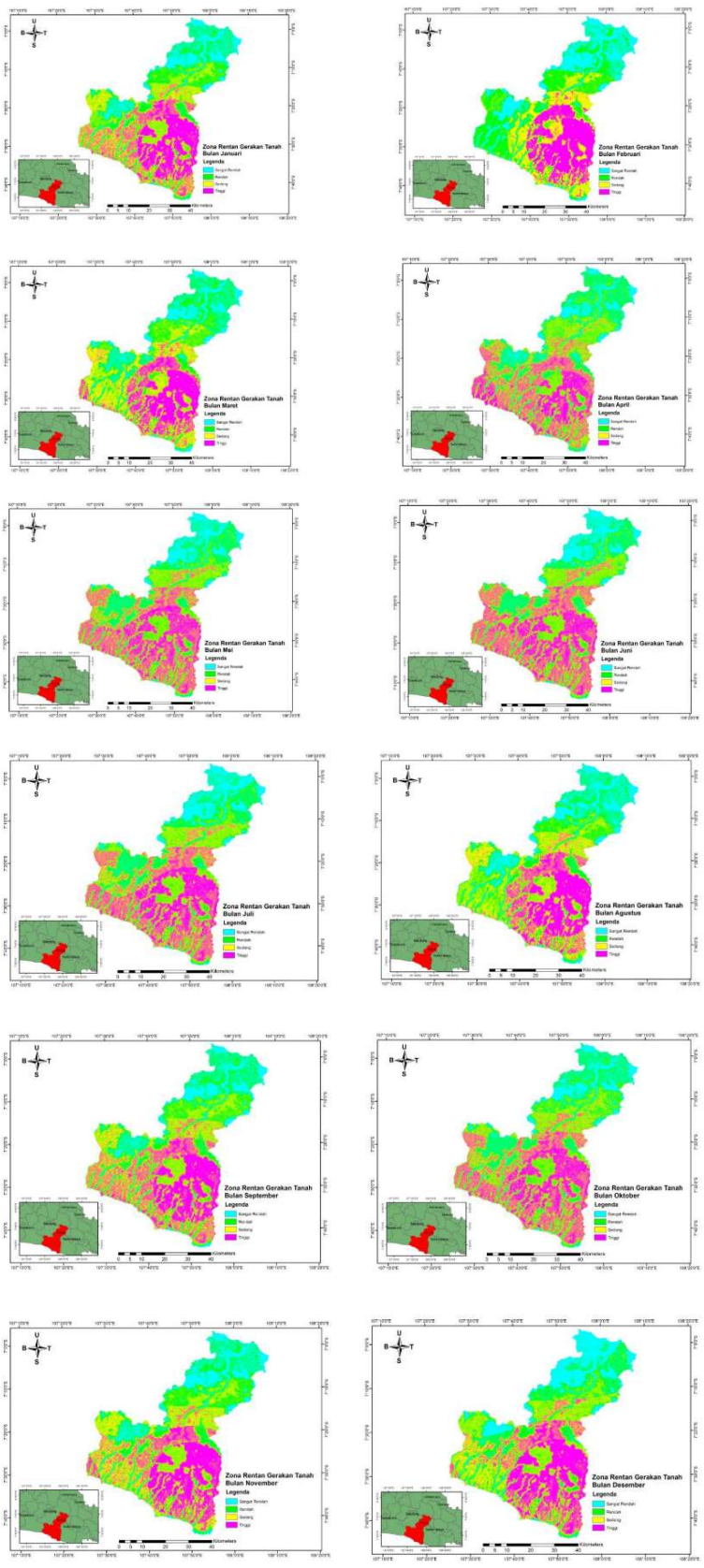

Figure 2b Landslide Susceptibility Maps using LR From January to December

Figure 2a.Landslide Susceptibility Maps using LR From January to December

NH 05: Optimum cell size selection on landslide susceptibility model of Tasikmalaya, West Java Province, Indonesia

Agus Lingga[a] , Twin H.W. Kristyanto[a,b*], Urwatul Wusqa[a], Zufialdi Zakaria[b], Dicky Muslim[b]

[a] *Geology Study Program, Faculty of Mathematics and Natural Sciences, Universitas Indonesia, Depok, 16424, Indonesia*
[b] *Doctoral Program in Geology, Faculty of Geological Engineering, Universitas Padjadjaran, Jatinangor, Sumedang District, 45363*

*Corresponding Author:
E-mail address: twin.hosea@sci.ui.ac.id (Twin Hosea W.K)

Landslides are the most frequent natural disaster in Indonesia, particularly in Tasikmalaya Regency, West Java. Data from the Tasikmalaya Disaster Prevention Agency indicates that 260 hazardous events occurred from January to September 2021, with 51% (133 incidents) being landslides. This study aims to determine the optimum cell size for the landslide susceptibility model using Frequency Ratio (FR) and Logistic Regression (LR) methods. Both methods were employed to create landslide susceptibility maps for Tasikmalaya. The frequency ratio method is a fairly common method used to identify landslide-prone zones. The Frequency Ratio (FR) method is a widely used statistical approach in landslide susceptibility modeling. It involves the calculation of the ratio between the occurrence of landslides and the distribution of contributing factors, such as slope, elevation, rainfall, and land use efforts (Lee and Pradhan, 2007). By comparing the spatial relationship between landslide events and these factors, the FR method quantifies the influence of each factor on landslide susceptibility. This method is advantageous due to its simplicity and the ease with which it can integrate various data types. The resulting frequency ratio values are used to generate a landslide susceptibility map, which helps identify areas at higher risk, supporting land-use planning and disaster mitigation efforts (Lee & Sambath, 2006). This model can provide an overview of factors that have a high correlation with landslide events at each location. The advantage of this model is that it has a high correlation that can be calculated using basic statistical calculations (Soma and Kubota, 2017). The FR method assessed the significance level of each factor class, while LR calculated landslide probability values and the effectiveness of each landslide factor (Lee and Pradhan, 2007). The probability values range from 0 to 1, with values closer to 1 indicating higher susceptibility zones (Hosmer and Lemeshow, 1989). The landslide susceptibility map then be validated to determine whether the model has been carried out well or not. This validation is helpful in predicting how well the modeling has been made in the danger of landslides and will produce a prediction accuracy value based on AUC (Area Under Curve). The study used data from 125 filtered landslide events, divided into 80% training data and 20% validation data (Mezughi et al., 2011). Factors considered included lithology, slope aspect, slope, elevation, land use, rainfall, distance from the fault, distance from the river, curvature, and Normalized Differential Vegetation Index (NDVI). The sources of each factor are shown in **Table 1**. The NDVI was used to identify the vegetation cover of the area. The model testing showed that the accuracy of the FR model increased with cell size, reaching optimum accuracy at a cell size of 35, with an AUC of 0.75 for the success rate and 0.81 for the predictive rate. Conversely, the LR model's accuracy varied with cell size, achieving optimum accuracy at a cell size of 25, with an AUC of 0.84 for the success rate and 0.85 for the predictive rate (**Fig 1-3**). In conclusion, both FR and LR methods effectively model landslide susceptibility in Tasikmalaya. The optimum cell sizes for the FR and LR models are 35 and 25, respectively.

Table 1. Data collection

No.	Factors	Resources
1.	Digital Elevation Model (DEM)	Indonesian Geospatial Agency (https://tanahair.indonesia.go.id/demnas/#/)
2.	Lithology	Regional Geological Map published by Geological Agency (https://geologi.esdm.go.id/geomap)
3.	Slope	Derived from DEM
4.	Elevation	Derived from DEM
5.	Land use map	Indonesian Geospatial Agency (https://tanahair.indonesia.go.id/demnas/#/)
6.	Rainfall (year 2000-20220)	NASA Power (https://power.larc.nasa.gov/)
7.	Distance from fault	Derived from geological structure data provided Regional Geological Map published by Geological Agency (https://geologi.esdm.go.id/geomap)
8.	Distance from river	Derived from Indonesian Geospatial Agency (https://tanahair.indonesia.go.id/demnas/#/)
9.	NDVI	Landsat 8 (OLI)
10.	Landslide inventory	National Disaster Relief Agency (https://gis.bnpb.go.id/)

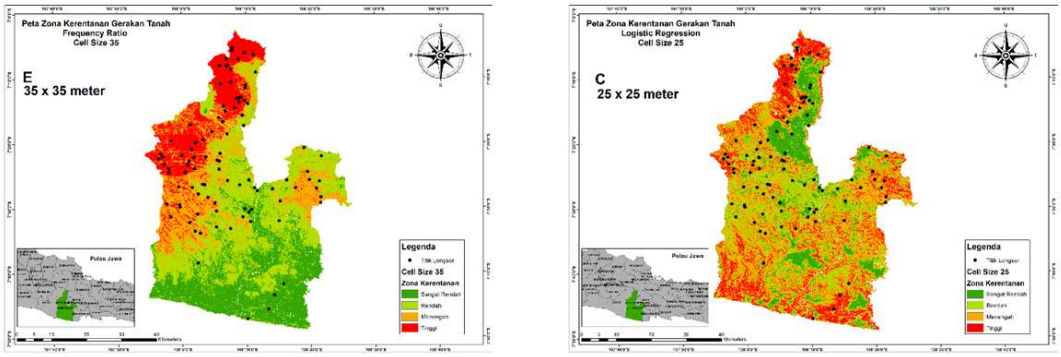

Figure 1. Landslide susceptibility maps Frequency Ratio with cell size 35x35 (left hand side) and Logistic Regression with cell size 25x25 (right hand side)

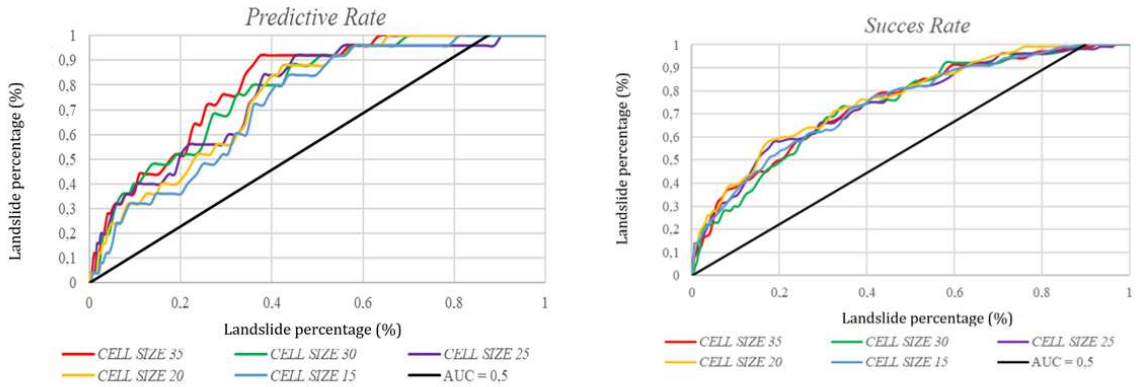

Figure 2. AUC of success rate (left-hand side) and predictive rate (right-hand side) for FR model in various cell size

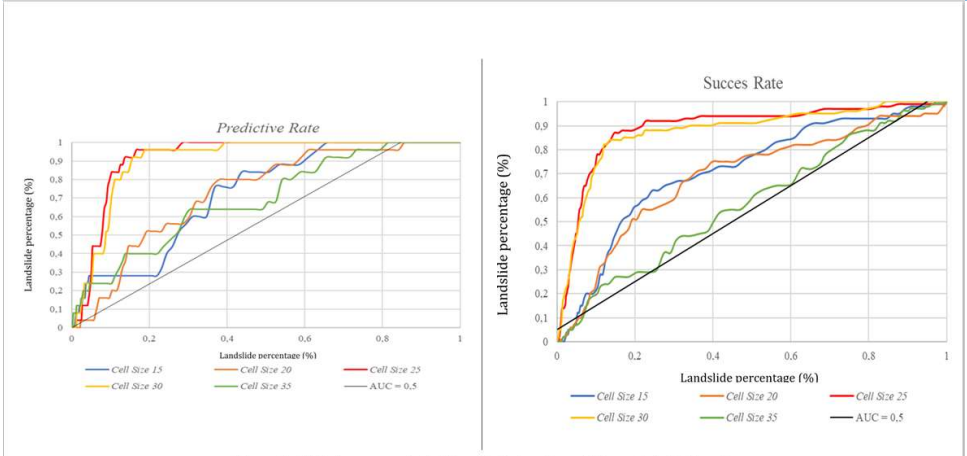

Figure 3. AUC of success rate (left-hand side) and predictive rate (right-hand side) for LR model in various cell size

Keywords: Landslide susceptibility, Frequency Ratio, Logistic Regression, Optimum cell size

References:

Hosmer, D. W., Lemeshow, S., 1989. Applied Logistic Regression. New York: Wiley.

Lee, S., Pradhan, B., 2007. Landslide hazard mapping at Selangor, Malaysia using frequency ratio and logistic regression models. Landslides, 4(1), 33–41. https://doi.org/10.1007/s10346-006-0047-y

Lee, S., Sambath, T., 2006. Landslide susceptibility mapping in the Damrei Romel area, Cambodia using frequency ratio and logistic regression models. Environmental Geology, 50(6), 847–855. https://doi.org/10.1007/s00254-006-0256-7

Mezughi, T., Akhir, J. M., Rafek, A. G., Abdullah, I., 2011. A multi-class weight of evidence approach for landslide susceptibility mapping applied to an area along the EW Highway (Gerik–Jeli), Malaysia. Electronic Journal of Geotechnical Engineering 16, 1259–1273.

Soma, A. S., Kubota, T., 2017. The Performance of Land Use Change Causative Factor on Landslide Susceptibility Map in Upper Ujung-Loe Watersheds South Sulawesi, Indonesia. Geoplanning: Journal of Geomatics and Planning, 4(2), 157. https://doi.org/10.14710/geoplanning.4.2.157-170.

NH 06: Data-driven bivariate statistical modelling for landslide susceptibility zonation in Khazwal district in Mizoram, India

Jonmenjoy Barman[1*]

[1]*Department of Geography and Resource Management, Mizoram University, Aizawl, 796004, India.*

*Corresponding Author:
E-mail address: jonmenjoybarman07@gmail.com (J.Barman)

Landslides are a serious issue in tropical mountain regions like the Khazawl district of Mizoram. It accounting a large number of life losses, environmental degradation and other related issues. The Khazawl district is one of the newly forming districts among the eleven districts of Mizoram. The objective of the study is to preparation of landslide susceptibility zones by utilizing three data-driven statistical models namely information value (IOV), frequency ratio (FR), and weight of evidence (WOE) and their comparative performance in landslide susceptibility mapping under similar geo-environmental condition. In this regard, twelve landslide conditioning factors including slope, elevation, aspect, curvature, roughness, TPI (Topographic Position Index), TWI (Topographic Wetness Index), NDVI (Normalized Difference Index), DTL (Distance to Lineament), DTR (Distance to Roads), Geom (Geomorphology), and lithology. In addition, 146 landslide locations are collected from the GSI website (Geological Society of India). Further, the landslide points are randomly classified into training landslides (70%) and testing landslides (30%) for running models and validation of models respectively. The output of the three models is grouped into five consequent hierarchical zones, such as very low,

low, moderate, high, and very high susceptibility zones. As the spatial distribution, the study area has contributed more than 332.30 Km^2 (0.03%) as very high landslide susceptibility zones. The predictive precisions are 0.900, 0.888, 0.883 and success precision are 0.878, 0.867, and 0.861 for IOV, FR, and WOE models respectively. The models used in the current study reflected higher accuracy than the existing literature based on the spatial distribution of landslides and triggering factors. The generated landslide susceptibility zones will be helpful for the decision-makers in reducing landslide risk.

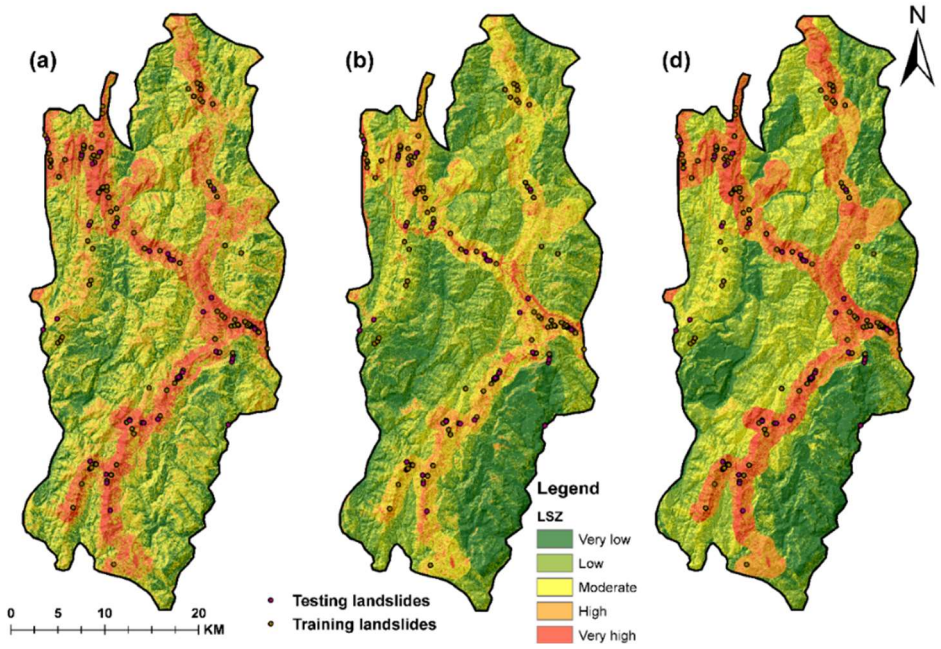

Figure 1: Landslide susceptibility zones, (a) LSZ using the Information value method, (b) LSZ using the Frequency ratio method, (c) LSZ using the Weight of Evidence method.

Table 1: Area of landslide susceptibility zones

Models	Area	Low	Very low	Moderate	High	Very high
IV	Km^2	1493.97	2783.25	3516.40	2272.27	1575.58
	%	0.13	0.24	0.30	0.20	0.14
FR	Km^2	2723.14	4458.93	2602.23	1524.84	332.30
	%	0.23	0.38	0.22	0.13	0.03
WOE	Km^2	2487.11	3726.33	2268.34	1821.22	1338.44
	%	0.21	0.32	0.19	0.16	0.11

Keywords: Landslide, bivariate statistical modelling, susceptibility zonation, Mizoram

NH 07: Impact of climate change on agriculture in India Emerging evidence and issues

R. R. Biradar[1*] and Babu Nallusamy[1]

[1]Central University of Karnataka, Karnataka, India

*Corresponding Author:
E-mail address: rrbiradar@kud.ac.in (R. R. Biradar)

The impact of climate change on the Indian economy, particularly in agriculture, has emerged as a significant environmental challenge, mirroring issues faced globally. The Earth's climate is undergoing

rapid changes, largely due to human-caused increases in greenhouse gas (GHG) emissions. These emissions have led to a rise in global temperatures by 0.11°C every ten years since 1850, with projections for further increases in the future due to historical emissions. The Intergovernmental Panel on Climate Change (IPCC) estimates that global average temperatures could increase by 1.7°C to 2.4°C by 2100. The relationship between GHG concentrations and their impact on global warming suggests that temperatures could exceed 2.1°C to 2.9°C by the same year, according to a report by McKinsey's Global Energy Perspective. The effects of climate change include the melting of glaciers, rising sea levels, more frequent rainfall, severe weather events, altered seasons, and the potential for heat stress to affect one billion people.

A study by NGML, US Department of Commerce (2023), on CO_2 emissions notes a rise from 338.80 ppm to 414.57 ppm over the past forty years, attributed to human activities as per IPCC (Summary for Policymakers, 2023). India ranked third globally in GHG emissions in 2021, following China and the US, contributing 45% of global fuel combustion emissions (Yona et al., 2020). Emissions are projected to decrease 30-70% by 2050, with a peak expected around 2023 following IPCC recommendations. India aims to reduce carbon emissions per unit of economic activity by 45% by 2030, and half of its energy from non-fossil fuels, and achieve carbon neutrality by 2070.

From 1986 to 2023, India experienced a significant warming trend, with annual mean, maximum, and minimum temperatures increasing by 0.15°C, 0.15°C, and 0.13°C per decade, respectively. India's average annual temperature is estimated at 24.64°C. Studies revealed that India's warmest year on record in 2016 was the hottest at 0.71°C above average, followed by 2023 at 0.65°C. The impacts of climate change in the country, largely due to its reliance on natural resources, are particularly pronounced and noticeable. Climate change adversely affects the agricultural sector, water resources, forestry, wildlife, and, most importantly, human health. A significant proportion of India's rural population depends on climate-sensitive sectors like agriculture and forestry for their livelihoods, and most are poorly equipped to cope with the challenges posed by climate change due to weak institutional mechanisms.

India's agriculture is highly vulnerable to climate change. Droughts, floods, tropical cyclones, heavy precipitation events, hot extremes, and heat waves adversely affect agricultural production and farmers' livelihoods. The melting of Himalayan glaciers will reduce irrigation availability, particularly in the Indo-Gangetic plains, significantly impacting food production. In the short term, climate change is likely to favor agricultural production in temperate regions (predominantly northern Europe and North America), while negatively affecting tropical crop production (South Asia, Africa). Although some regions may see gains in certain crops, the overall impact of climate change on agriculture is anticipated to be negative, posing a threat to food security and farmers' livelihoods.

In this context, the current study aims to assess the magnitude of climate change through temperature trends and rainfall variability, evaluate its impact on cropping patterns and agricultural production (yields of significant crops), and identify potential climate change mitigation and adaptation measures in India. The study will also provide policy recommendations for addressing climate change challenges. The study is based on secondary data to be collected from the Statistical Abstract of India, Agricultural Statistics at a Glance, and Annual Reports of the Meteorological Department, etc. The multiple linear regression model will be employed to examine the impact of variability in rainfall on agricultural production in India.

Keywords: Climate Change, greenhouse gas (GHG) emissions, Carbon Emission, Impact of Agriculture and Multiple linear regression.

References:

Yona, L., Cashore, B., Jackson, R. B., Ometto, J., Bradford, M.A. 2020. Refining national greenhouse gas inventories. Ambio, 49(10) 1581-1586. https://doi.org/10.1007/s13280-019-01312-9

NH 08: Comparison of GIS-Based Landslide Susceptibility Map Distribution Using Frequency Ratio and Weight of Evidence Method in Sumedang Regency, West Java

Putri M. H. Aulia[a], Urwatul Wusqa[a*], Rezky Aditiyo[a]

[a]*Geoscience Department, Faculty of Mathematics and Natural Sciences, Universitas Indonesia, Depok, 16424, Indonesia*

*Corresponding author:
E-mail address: urwatulwusqa@sci.ui.ac.id (Urwatul Wusqa)

Landslides are frequent natural disasters in West Java, particularly in regions with complex geological and geomorphological settings. Van Bemmelen (1949) regionally divides West Java into five distinct zones: the Jakarta Coastal Plain Zone, the Bogor Zone, the Bandung Zone, the Bayah Mountains Zone, and the South Mountain Zone. The study area, Sumedang Regency, is part of the Bandung Zone and is characterized by a diverse geological structure. Based on the Geological Map of the Bandung Sheet (Silitonga, 1973), the research area comprises tertiary to quaternary-aged rocks, including intrusive rocks, sedimentary rocks, and volcanic rocks. Landslide occurrences in this region are often driven by multiple factors such as intense rainfall, geological conditions, land use changes, and human activities that disregard surrounding geological and slope stability conditions. The massive Sumedang landslide in early 2021, caused by slope failure in a catchment area, highlights the critical need for detailed landslide susceptibility mapping.

This study aims to assess and map the landslide susceptibility distribution in Sumedang Regency by comparing the Weight of Evidence (WoE) and Frequency Ratio (FR) methods in a GIS-based environment. The data used include Sentinel-2 imagery, DEMNAS (Digital Elevation Model Nasional), the Rupabumi Indonesia map for topographic data, CHIRPS rainfall data (2012-2021), a geological map from the Geological Agency of Indonesia, and landslide occurrence data from the Center for Volcanology and Geological Hazard Mitigation, the Regional Disaster Management Agency of Sumedang, the National Disaster Management Agency, as well as visual interpretation of Google Earth imagery.

A total of 100 landslide points were identified and randomly divided into 70% training data to develop the landslide potential distribution model and 30% test data for model validation. Ten factors were used in the analysis, including elevation, slope, aspect, distance to roads, distance to rivers, distance to lineaments, Normalized Difference Vegetation Index (NDVI), lithology, land use, and rainfall data from 2012 to 2021. The resulting landslide susceptibility zones were classified into five categories and validated using the Area Under the Curve (AUC) metric to determine model accuracy (**Fig.1-4**).

Both the WoE and FR models yielded 12-month AUC values, with the FR model achieving averages of 74% (training data) and 62% (test data), and the WoE model yielding averages of 76.5% (training data) and 63.5% (test data) (**Fig.5-6**). These results indicate that while both models demonstrate high predictive quality, their accuracy remains moderate for creating detailed susceptibility maps. Nevertheless, both methods are considered applicable for landslide susceptibility mapping in the study area.

Keywords: Landslide, Weight of Evidence, Logistic Regression, Landslide Susceptibility, Hazard

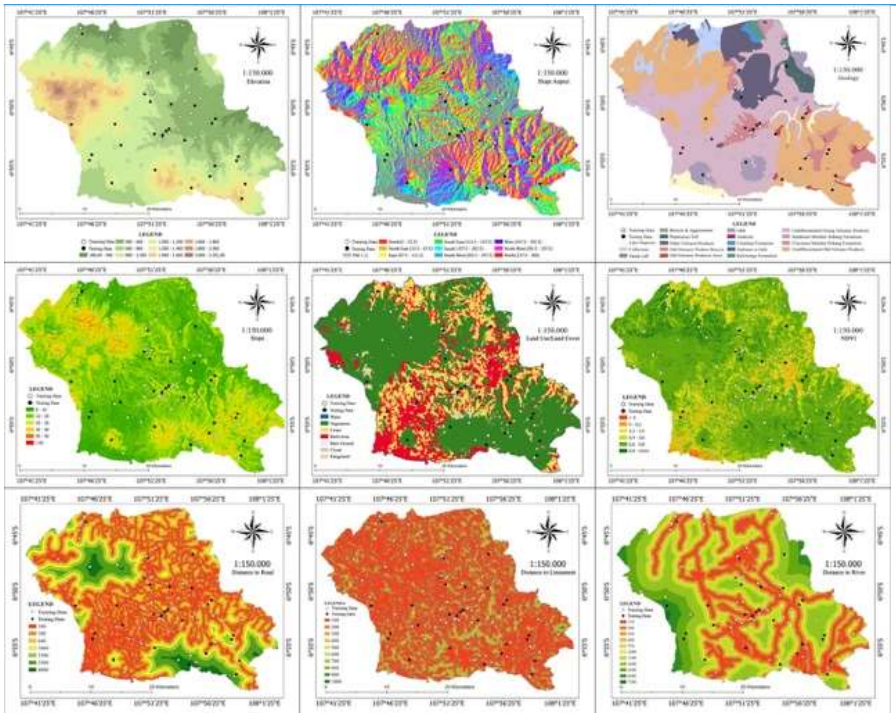

Figure 1. Landslide Causative Factor and Landslide Susceptibility Map; Landslide causative factor: a) elevation, b) slope aspect, c) geology, d) slope, e) land use/land cover, f) NDVI, g) distance to road, h) distance to lineament, i) distance to the river

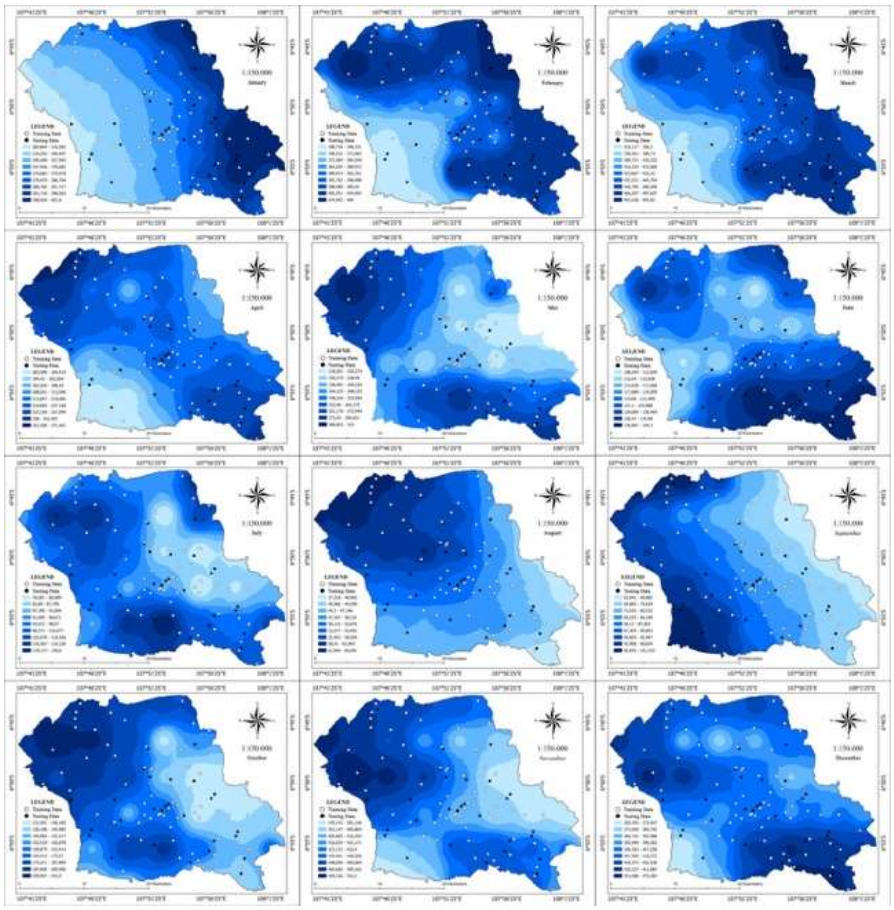

Figure 2. Landslide causative factor rainfall map from January to December

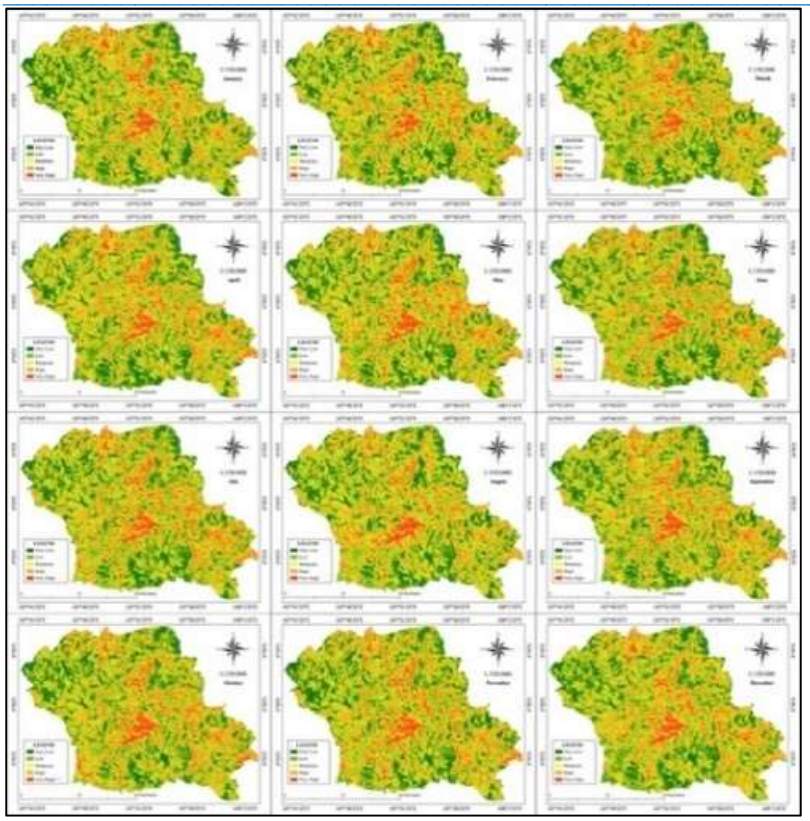

Figure 3. Landslide susceptibility map using frequency ratio model

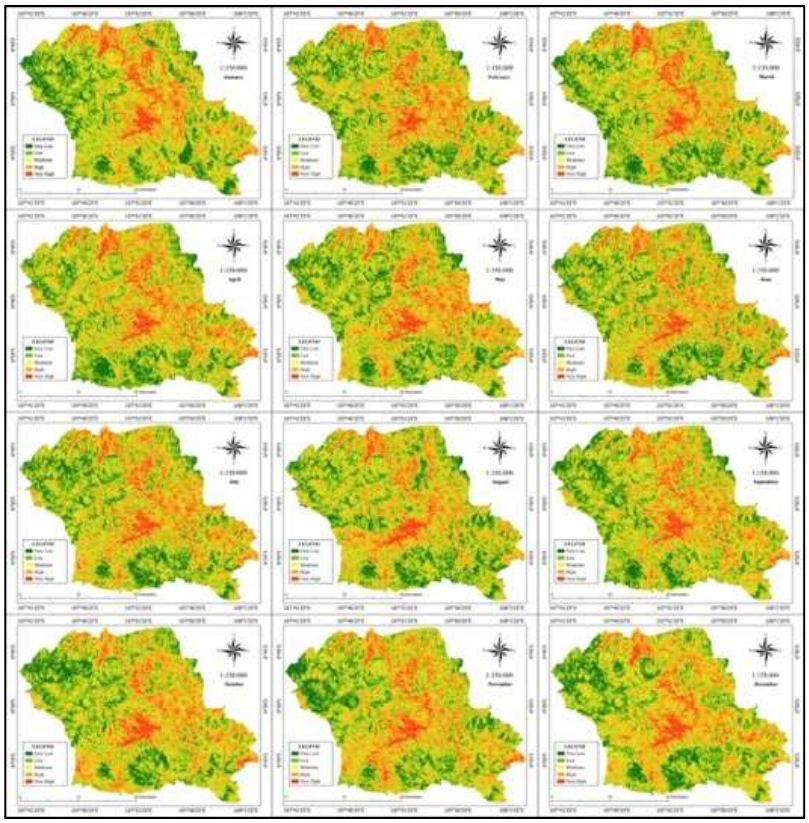

Figure 4. Landslide susceptibility map using weight of evidence model

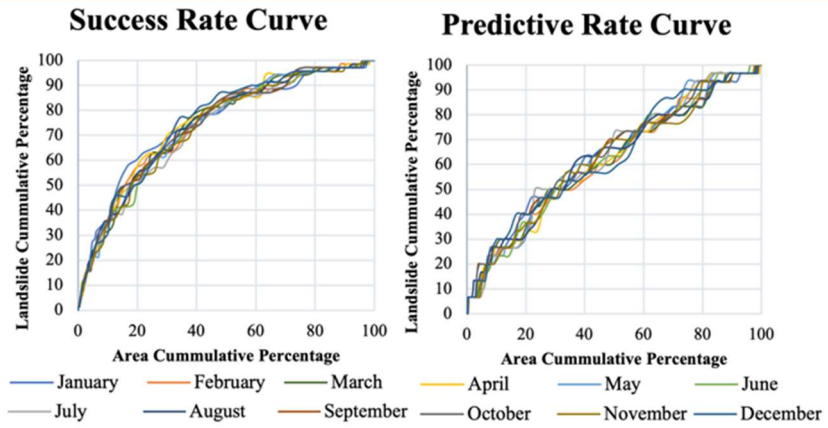

Figure 5. AUC Graph for FR Model

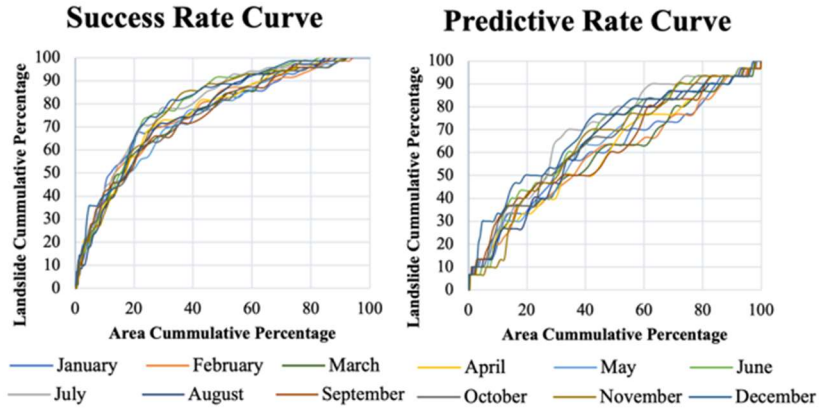

Figure 6. AUC Graph for WoE Model

References

Kementrian Energi dan Sumber Daya Mineral. (2021). Laporan dan rekomendasi Gerakan tanah kec. Cimanggung, kabupaten sumedang provinsi jawa barat. Accesed on April 4th, 2022. (https://vsi.esdm.go.id/index.php/gerakan-tanah/kejadian gerakan-tanah/3390-laporan-dan-rekomendasi-gerakan-tanah-kec-cimanggung-kabupaten-sumedang-provinsi-jawa-barat.)

Silitonga. 1973). Peta geologi indonesia, lembar bandung, jawa barat. Bandung: Pusat Penelitian dan Pengembangan Geologi

Van Bemmelen, R. W. (1949). The geology of Indonesia. General Geology of Indonesia and Adjacent Archipelagoes. In Government Printing Office, The Hague (pp. 545 547; 561–562).

NH 09: The occurrence of a sinkhole its causes and methods of study, A case study from Puebla México

J.J. Caracheo-Gonzalez[a], P.F. Rodriguez-Espinosa[a*], E. Martínez-Tavera[b]

[a]*Centro Interdisciplinario de Investigaciones y Estudios sobre Medio Ambiente y Desarrollo (CIIEMAD), Instituto Politécnico Nacional (IPN), Calle 30 de Junio de 1520, Barrio La Laguna Ticomán, Municipio Gustavo A. Madero, C.P. 07340 Ciudad de México (CDMX).*
[b]*UPAEP Universidad, 21 sur no. 1103 Barrio de Santiago, Puebla, Puebla, Mexico C.P. 72410, 18 Mexico.*

*Corresponding author:
E-mail address: pedrof44@hotmail.com (P.F. Rodriguez-Espinosa)

The relationship between anthropogenic activity and the environment implies a delicate balance of both subjects of study, when that balance is disturbed, harmful phenomena are likely to happen, an example

of this is the formation of sinkholes, a geomorphological depression caused by the sinking of the overlying layers of soil (Salem, 2020), occurring on a sudden way, sinkholes are phenomena involving the interaction of water and soil. From a general definition, sinkholes are divided into two main branches, those produced naturally and those created by anthropogenic activity (Newton, 1987). Human activities accelerate sinkholes' occurrence tend to be frequent and are also associated with the lowering of the groundwater level (Galloway et al., 1999), sinkholes associated with this formation mechanism usually occur on soils made up of unconsolidated sediment deposits where voids naturally exist and where a phenomenon known as piping takes place where the voids in the soil interconnect and due to the loss of sediments the natural support of the soil is lost (Jones, 2010) this naturally leads to the loss of the soil's capacity to support itself and as a consequence, it collapses. The causes and mechanisms of karstic sinkholes are highly discussed in literature while the mechanisms causing non-karstic sinkholes related to groundwater depletion due to agriculture are still in need of a wider discussion, thus, this study aims to analyze and explain some of the factors contributing to the occurrence of a non-karstic sinkhole located in the Puebla-Tlaxcala valley in the middle of an agricultural land (**Fig. 1**).

Sinkholes represent a huge risk for the human population because they can engulf houses or entire buildings, in the actual case study of the Juan C. Bonilla sinkhole in Puebla, Mexico, which occurred in 2021; swallowed a house almost entirely, likewise, sinkholes are also associated with climate change, due to the intensity of rainy days caused by global warming (Guarino and Nisio, 2012; Xiao et al., 2018). In the last few years, places all over the world have experienced the occurrence of sinkholes of anthropogenic origin (Hermosilla, 2012; Parise, 2015; Rahardjo et al., 2019; Rodriguez-Espinosa et al., 2023; Tang, 2017).

The methodology started by the analysis of satellite data from Sentinel-1 and GRACE satellites, by the analysis of these data it is possible see how the ground water is fluctuating in the whole *Rio Balsas* basin, the subsidence can be monitored through the processing of sentinel-1 images. Additionally, a geochemical analysis was done on the sediments collected from the study area to exlore further correlations between the mechanical erosion of the sediments and the fluctuating groundwater level. The geochemical analysis was done by partially digesting the sediments taking 1 g of sample with the three acid mixture at a ratio of 2 ml HNO_3, 0.5 ml HCL 5 ml H_2O_2. The soil samples (1 g) were placed in a Teflon digestion vessel and then were heated on a hot plate, later they were analyzed using an using a persing Elmers ICP-OES 8300.

It was found that the whole Rio Balsas basin had experienced a water shortage in the last 5 years before the sinkhole's occurrence (**Fig. 2**), it was also found that most of the sediment chemistry is controlled by the granulometry, specifically in its fine fraction, likewise, as the fluctuation of the underground water level (**Fig. 3**). In non-karst environments, the most important actions to be taken for its prevention are, in the first instance, the identification of risks and geological and geotechnical characteristics of the soil, as well as the correct management of water resources and planning of the available land.

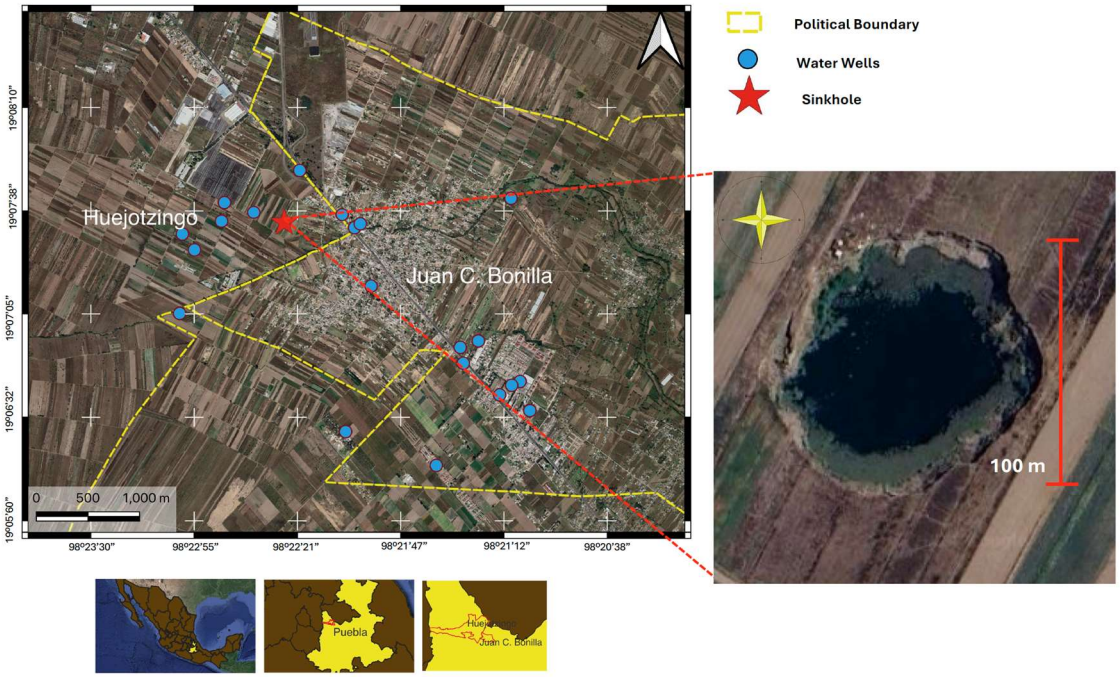

Figure 1. Location map of the study area

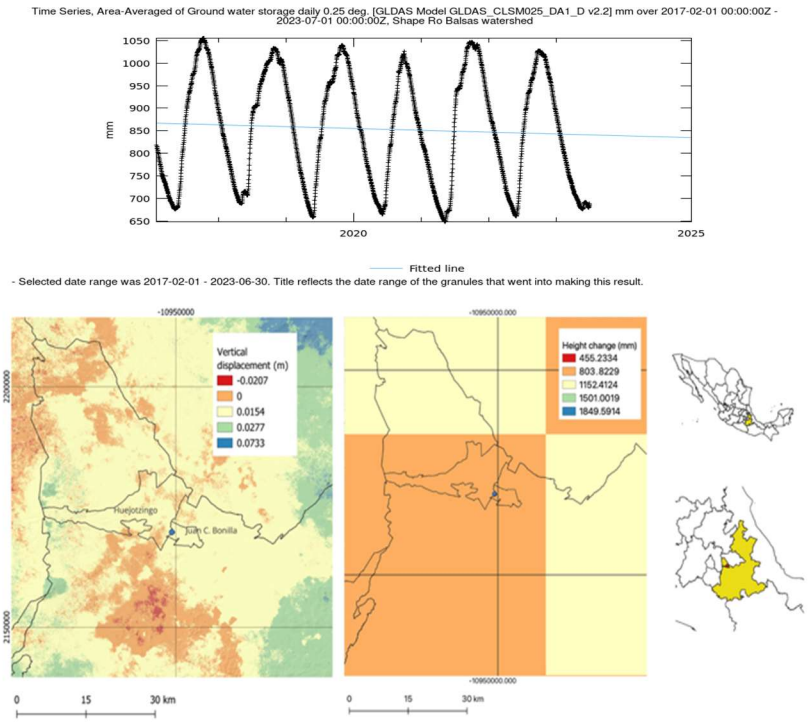

Figure 2. a.Time series of groundwater depletion during the five years prior to the collapse. Made with data from GRACE satellite obtained trough Giovanni platform by NASA
b.Comparison between the sentinel-1 map showing subsidence (left) and the groundwater depletion map from GRACE (right).

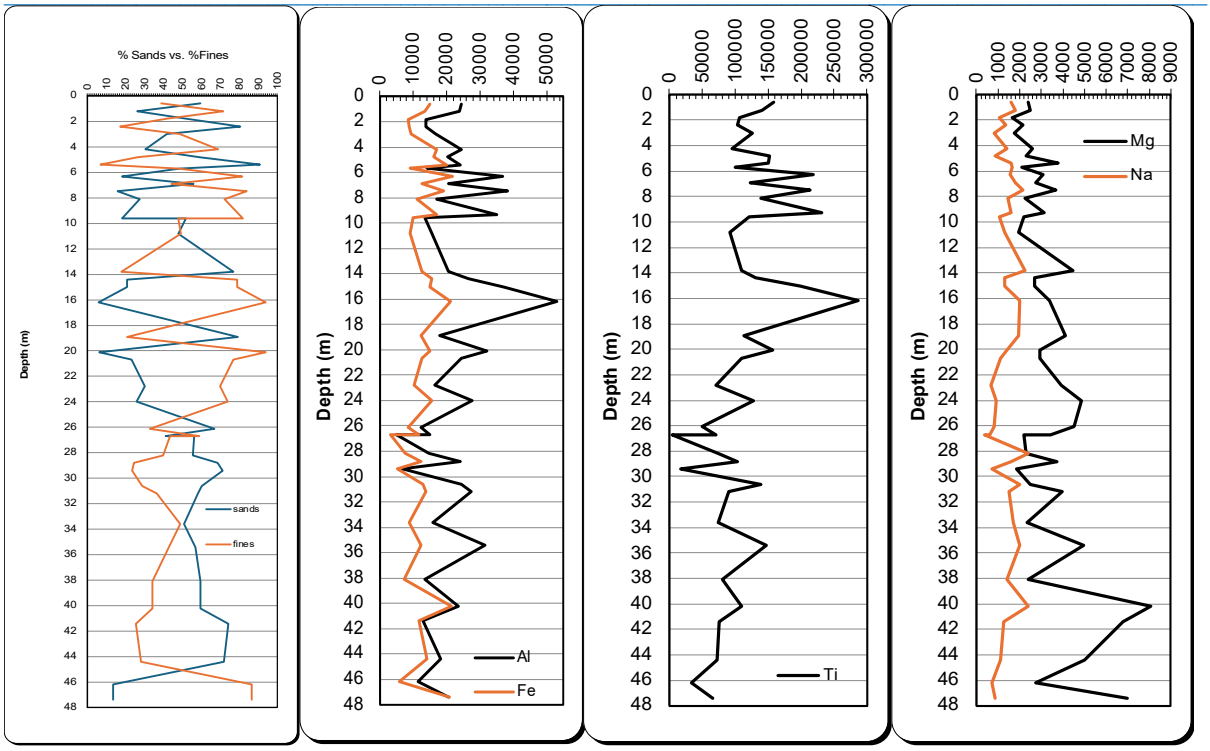
% Sands vs. %Fines
Depth (m)
sands
fines
Al
Fe
Ti
Mg
Na

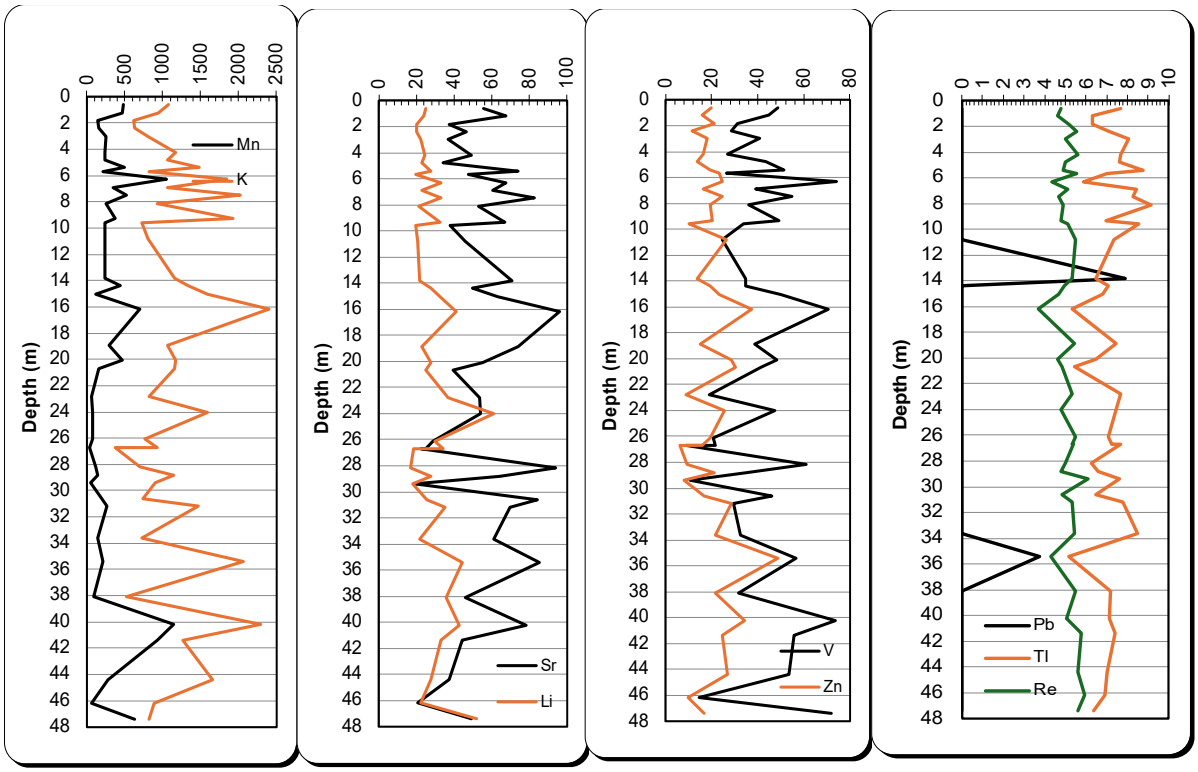
Depth (m)
Mn
K
Sr
Li
V
Zn
Pb
Tl
Re

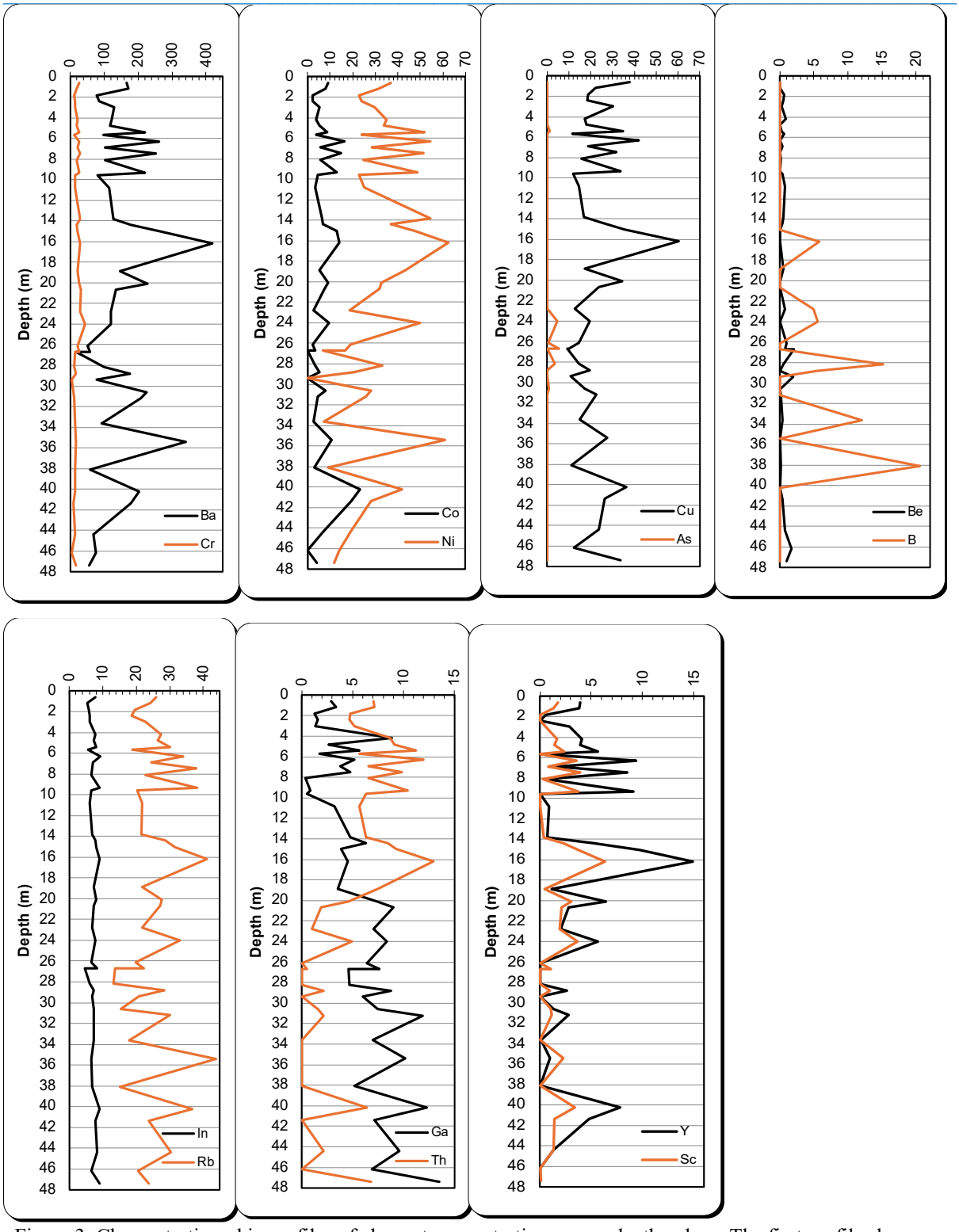

Figure 3. Chemostratigraphic profiles of element concentration versus depth values. The first profile shows the grain size distribution versus depth.

References:

Galloway, D.L., Jones, D.R., Ingebritsen, S.E., Survey, U.S.G. 1999. Land subsidence in the United States. In *Circular*. https://doi.org/10.3133/cir1182

Guarino, P. M., Nisio, S., 2012. Anthropogenic sinkholes in the territory of the city of Naples (Southern Italy). Physics and Chemistry of the Earth, Parts A/B/C, 49, 92–102. https://doi.org/https://doi.org/10.1016/j.pce.2011.10.023

Hermosilla, R.G., 2012. The Guatemala City sinkhole collapses. Carbonates and Evaporites 27(2), 103–107. https://doi.org/10.1007/s13146-011-0074-1
Jones, J.A.A. 2010. Soil piping and catchment response. Hydrological Processes 24(12), 1548–1566. https://doi.org/10.1002/HYP.7634
Newton, J. G. 1987. Development of sinkholes resulting from man's activities in the eastern United States. US Geological Survey 968–969.
Parise, M., 2015. A procedure for evaluating the susceptibility to natural and anthropogenic sinkholes. Georisk 9(4), 272–285. https://doi.org/10.1080/17499518.2015.1045002
Rodriguez-Espinosa, P. F., Ochoa-Guerrero, K. M., Milan-Valdes, S., Teran-Cuevas, A. R., Hernandez-Silva, M. G., San Miguel-Gutierrez, J. C., Caracheo-Gonzalez, J. J., Creuheras Diaz, S. 2023. Impacts on groundwater-related anthropogenic activities on the development of sinkhole hazards: a case study from Central Mexico. Environmental Earth Sciences 82(14), 1–12.
Salem, H.S. 2020. Multi-and inter-disciplinary approaches towards understanding the sinkholes' phenomenon in the Dead Sea Basin. SN Applied Sciences 2(4), 667.
Tang, Y., 2017. Mechanisms of Soil Erosion due to Defective Sewer Pipes. https://doi.org/10.7939/R32N4ZX83
Xiao, H., Li, H., Tang, Y., 2018., Assessing the effects of rainfall, groundwater downward leakage, and groundwater head differences on the development of cover-collapse and cover-suffosion sinkholes in central Florida (USA). Science of The Total Environment 644, 274–286.

NH 10: Depositional Environment, Provenance, and Ecological Risk Assessment of Sediments from Kaliveli Lagoon, Villupuram District, Tamilnadu, India

Pandu Parthasarathy[1*], Jayagopal Madhavaraju[2], Sooriamuthu Ramasamy[1], Venkatesan Selvaraj[3]

[1]*Department of Geology, University of Madras, Guindy Campus, Chennai 600025, Tamilnadu, India*
[2]*Estacion Regional del Noroeste, Instituto de Geología, Universidad Nacional Autónoma de México, Hermosillo, Sonora, Mexico*
[3]*Department of Earth Sciences, Annamalai University, Annamalai Nagar, Chidambaram-608002, Tamilnadu, India*

*Corresponding author:
E-mail address: petrosarathy@gmail.com (P.Parthasarathy)

Kaliveli Lagoon ecosystem (seasonal wetland) is situated in Villupuram District, Tamil Nadu, East coast of India. Two core samples (MKM-C1 and MKM-C2) were collected from the study area in order to assess the textural characteristics, clay mineralogy and geochemistry. The length of the cores is 135 cm for C1 and 126 cm for C2. Both of the core sediments are silty sand and sandy silt nature. The calcium carbonate is chiefly derived from terrestrial and coastal input into the Kaliveli lagoon and the rapid increase of calcium carbonate percentage at certain levels of the cores is due to the enrichment of shell fragments. The organic matter content of the sediments is mostly derived from continental wash and partially mangrove humus. The microtexture of the sediments shows rounded, with grooves and evidence of conchoidal fracture. The observed microtextural features point to combined mechanical and chemical weathering processes. The identified clay minerals such as illite, kaolinite and chlorite suggest their source granite and charnockitic provenances, which were subjected to a moderate physical and chemical weathering process under semiarid to semihumid climate. The studied heavy metals are depleted in the core sediments compared to UCC except Zn and Pb. The Cr/V vs Y/Ni ratio of the samples in the present study also reiterates the felsic source rocks. Elemental ratios such as Cr/Th, Th/Sr, Th/Co, and Th/Cr are mostly related felsic to intermediate source rocks rather than a mafic source. The other elemental ratios such as Ni/Co, Cu/Zn, Ni/Co vs V/Cr and Ni/Co vs V/(V+Ni), suggest oxic to suboxic depositional environment. Environmental pollution indices such as EF, CF, Igeo Index, PLI, SPI, MPI, and PERI have collectively labeled the sediment as under unpolluted to moderate polluted type.

Keywords: Texture, Geochemistry, Depositional environment, Pollution, Kaliveli Lagoon

Theme 7: Geoheritage

GH 01: The limited "life span" of crayback stalagmites: geoheritage conservation and long-term geological preservation

Dominique Dodge-Wan[1*]

[1]*Department of Applied Sciences, Curtin University, Malaysia, CDT 250, 980009 Miri, Sarawak, Malaysia*

*Corresponding author:
E-mail address: dominique@curtin.edu.my (Dominique Dodge-Wan)

Crayback stalagmites are bio-mineral structures that develop in some cave entrances with specific microenvironmental characteristics i.e. they have narrow tolerance for certain environmental parameters particularly light, dripping cave water and air circulation. Hence, they are rare and have been found in only a limited number of locations worldwide. Furthermore, they are still under-researched and their mode of formation is not fully understood. It involves cyanobacterial colonisation of "classic" dark zone, entirely mineral stalagmites and passive trapping of wind-borne mineral particles on the slimy outer coating of cyanobacteria and/ or more active precipitation of $CaCO_3$ mineral sheaths on filamentous cyanobacteria. As a result, they are considered to be subaerial stromatolitic stalagmites. The Niah caves, in particular the Painted Cave entrance and the Gan Kira passage and entrance, are host to a relatively large cluster of unusual crayback-like stalagmites. Observation of their features and the surrounding cave entrance environment leads to inferences regarding their mode of formation, their "life span" and their low potential for long-term geological preservation. In addition, their rarity and high potential to provide paleoenvironmental records indicate the need for geoheritage conservation.

GH 02: Utilizing guide led tours at heritage sites as a method for geoscience communication: a case study in AlUla, Saudi Arabia

Jan Freedman[1*]

[1]*Geologist, Royal Commission for AlUla, AlUla, Saudi Arabia*

*Corresponding author:
E-mail address: j.freedman@rcu.gov.sa (Jan Freedman)

Geology as a science is relatively unknown to the general public, with the 'big hitters' such as dinosaurs and volcanoes often being the only focus in the media (Stewart and Neild, 2013). Rocks and minerals do not appear to have any relevance to everyday lives, and it is that relevance that is key to enabling the science of our planet being more understandable and accessible to all (Walsby, 2008). Studies have shown that children being in an outside, natural environment are more likely to ask more questions about the nature around them (Waters and Maynard, 2010; Skalstad, 2020; Skalstad and Munkebye, 2021). Adults, and perhaps even more strongly, older adults, also feel more curious and connected to nature when they are in the natural environment (Harlow et al., 1950), which also contributes to improving their well-being (Gottlieb and Oudeyer, 2018; Talmage and Knopf, 2018). Being in nature,

within a landscape, is something that creates a curiosity to discover more about what is around us (Hartmeyer and Mygind, 2016).

AlUla, a 22,000 km^2 county in north-western Saudi Arabia, covers a richness of geological diversity that is seldom found in a relatively small area. The south of the region lies on the northern part of the Arabian Shield, composed of Precambrian basement igneous and metamorphic rocks, and towards the north, large expanses of Palaeozoic sedimentary rocks, and Tertiary volcanic rocks cover the landscape (Hadley, 1987; Brown et al., 1989). The geodiversity in AlUla has not only led to a richness in biodiversity, with 5 nature reserves protecting over 50% of land, but also a plethora of internationally important, active archaeological sites.

The rifting of the Red Sea, which began around 30 million years ago, created uplift and fracturing of the Palaeozoic sedimentary rocks, which aided erosion in creating valleys and open plains. The erosion of the Cambrian and Early Ordovician sandstones in central and northern AlUla has created a spectacular natural landscape of buttes, mesas, fault scarps, pinnacles, yardangs, and many other wind-sculpted formations that all showcase the strong geoheritage of the area. These open expanses within the large sandstone mesas and other formations, created a clear route through Arabia for humans for around 250,000 years.

With it's globally significant heritage sites and stunning geoheritage, AlUla is being developed as a major tourist destination as a part of the Saudi Vision 2023, under the Royal Commission for AlUla (RCU) (Vision2030, 2023). Key to the development is sustainable tourism, which includes new eco-lodges and eco-friendly hotels, and the increasing opportunities to raise awareness of the wildlife and the heritage sites in the area through educational experiences. This presents a unique opportunity to disseminate the geology narrative through the growing tourism offers in the region.

AlUla was a strategic part of the Incense Trade Route, utilizing the large valleys and the rich supplies of water for traders passing through. Here, the first major city in AlUla was built: the capital of the ancient Kingdom of Dadan. This was one of the most important sites for trade in Arabia, dating around 3,000 years ago (MacDonald, 2018). Fracturing in the Saq sandstone from the opening of the Red Sea caused jointing on the rock face, which allowed relatively easy quarrying of the well-compacted braided river deposits of the Upper Saq (Beni et al., 2023). The softer marine delta deposits of the Middle Saq were predominantly used for tombs, dug directly into the rocks, with tombs for wealthier individuals being dug into the harder Upper Saq deposits.

Shortly after the fall of Dadan, the Nabataeans built their second largest city outside of Petra, called Al-Hijir (also known as Mada'in Salih, and now called Hegra). Hegra was the first site in Saudi Arabia that was designated a UNESCO World Heritage Site (MacDonald, 1997; Ansary and Abu Al Hassān, 2001; Hausleiter, 2012). The site, and the landscape, of Hegra are very different from Dadan. The city was built in the north of AlUla, with tombs carved into the younger Siq sandstone landforms (**Fig. 1**). The same formation was utilized at Petra in Jordan; the Nabataeans knew they could carve monumental structures into the Siq sandstone.

Today, both of these internationally important heritage sites have welcome centers with interpretation and guided tours for local and international visitors. Detailed information about each site has been provided by archaeologists and researchers for the guides (locally known as a *rawi*, which translates to storyteller). Since they first opened, the tours and the information, has focused on the archaeology. However, many of the rawis have fed back that visitors want to learn more about the landscape these historic sites are set in, with common questions asked, such as how did the rocks form? How did the landscape form? Why did these civilizations build their homes *here*?

During 2022 and 2023, there were over 140,000 visitors to the heritage sites in AlUla, and this presents a unique opportunity to include the geological history into the narrative. The story not only demonstrates that the geology and the heritage are intimately entwined but also allows the story of Gondwana to be told to a non-specialist audience in a different and engaging way. The rawis have undertaken training and workshops to introduce them to geology concepts, giving them that basic fundamental background knowledge to understand geological processes. Additional workshops were provided, which focuses on the geological history of AlUla and how the landscape formed. Field trips at the heritage sites supplemented the workshops, for real onsite examples.

Some of this new information is included as a part of the narrative for the tours, but the main aim was for the guides to have the knowledge, and the confidence, to talk to visitors about the geological history of the heritage sites. These sessions have enabled both local and international visitors to have their questions answered, resulting in an enriched experience. The geology is relevant to the visitors in AlUla; it is a part of the experience. And with the relevance, the story can be told.

Figure 1. One of the tombs at Hegra. Carved into the Siq sandstones, the tombs show features of the ancient environments as well as more recent erosional features, that all add to the story for tourists.

References:

Ansary, A.R., Al Hassān, A. 2001. The civilization of two cities: Al-'Ula and Mada 'in Sahil. Riyadh: Dar Al-Qawafil.

Brown, G.F., Schmidt, D.L., Huffman, A.C., 1989. Geology of the Arabian Peninsula: Shield area of Western Saudi Arabia. U.S. Geological Survey Professional Paper. 560-A.

Beni, T., Boldini, D., Crosta, G., Frodella, W., Gallego, J., Lusini, E., Margottini, C., Spizzichino, D., 2023. Rock instabilities at the archaeological site of Dadan (Kingdom of Saudi Arabia). Landslides. https://doi.org/10.1007/s10346-023-02122-7

Gottlieb, J., Oudeyer, P.Y. 2018. Towards a neuroscience of active sampling and curiosity. Nature Reviews. Neuroscience 19, 7580-770.

Hadley, D.G. 1987. Explanatory notes to the geological map of the Sahl Al Matran quadrangle, sheet 26C, Kingdom of Saudi Arabia. Saudi Arabian Deputy Ministry for Mineral Resources.

Harlow, H.F., Harlow, M.K., Meyer, D.R. 1950. Learning motivated by a manipulation drive. Journal of Experimental Psychology 40, 228-234.

Hartmeyer, R. Mygind, E. 2016. A retrospective study of social relations in a Danish primary school class taught in 'udeskole'. Journal of Adventure Education and Outdoor Learning 16(1),78-89.

Hausleiter, A., 2012. North Arabian Kingdoms. In: Potts, D.T., (ed) A companion to the Archaeology of the Ancient Near East. 2, 816-832, Wiley-Blackwell.

MacDonald, M. C. A. 1997. Trade routes and trade goods at the northern end of the 'Incense Road' in the First Millennium B.C. In: Avanzini., A. (ed) Profumi d'Arabia: Atti del Convegno Rome: 'L'Erma" di Bretschneider. 333-349.

MacDonald, M. C. A. 2018. Towards a Re-assessment of the Ancient North Arabian Alphabets Used in the Oasis of al-ʿUlā. In: MacDonald, M. C. A. (ed.). Languages, Scripts and Their Uses in Ancient North Arabia. Archaeopress. pp. 1–19.

Skalstad, I., 2020. Oi! Sjå på den! – Funn av naturelement som utgangspunkt for utforskande naturfaglege samtalar mellom barn (5-6 år) og pedagogar. [Wow! Look at this! – Findings of nature elements as starting points for exploratory scientific dialogues between children (5-6 years) and teachers]. Nordic Studies in Science Education 16(2), 199–214.

Skalstad, I., Munkebye, E., 2021. Young children's questions about science topics when situated in a natural outdoor environment: a qualitative study from kindergarten and primary school. International Journal of Science Education 43(7), 1017-1035.

Talmage, C.A., Knopf, R.C. 2018. Wisdom and Curiosity Among Older Learners: Elucidating Themes of Well-Being from Beautiful Questions in Older Adulthood. OBM Geriatrics 2(4), 1804025. https://doi.org/10.21926/obm.geriatr.1804025

Walsby, J.C. 2008. GeoSure; a bridge between geology and decision-makers. In: LIverman, D.G.E., Pereira, C., Marker, B., (Eds) Communicating Environmental Geoscience. Geological Society London, Special Publications 305, 81–87.

Waters, J., Maynard, T., 2010. What's so interesting outside? A study of child-initiated interaction with teachers in the natural outdoor environment. European Early Childhood Education Research Journal 18(4), 473–483.

Vision2030. 2023. Vision 2030 a story of transformation. Viewed on 6th March 2023. Accessed: https://www.vision2030.gov.sa

GH 03: Student Himalayan Field Exercise Program 12 years

Yoshida Masaru[1*] and Student Himalayan Field Exercise Project[2]

[1]*Gondwana Institute for Geology and Environment, 147-2 Hashiramoto, Hashimoto, Japan 648-0091, and Tribhuvan University, Kathmandu, Nepal*
[2]*c/o Faculty of Multi-Disciplinary Science and Technology, Shimane University, Matsue, Japan*

*Corresponding Author:
E-mail address: gondwana@oregano.ocn.ne.jp (M.Yoshida)

The Himalayas are the highest and the youngest mountain range on the globe. This mountain range is still rising today and will continue to rise in the future for a long time to come. The Cenozoic Himalayan Orogeny is the result of the collision of Indian and Eurasian plates. The Indian plate is still moving northward by 9 cm per year and the mountain is still uplifting by 5 cm per year. The still-growing mountain range formed steep mountain slopes, which resulted in various natural hazards including various mass movements and floods.

The geologic structures of the Himalayas reflect the collisional tectonics of the plates. All the original geologic units of the Himalayan Orogen ranging from early Proterozoic to late Mesozoic ages were formed at the northern margin of the Indian subcontinent and the Tethys Sea north of the subcontinent and were squeezed, disrupted and uplifted by thrusting, forming four geologic zones running parallel to the mountain range (**Fig. 1**).

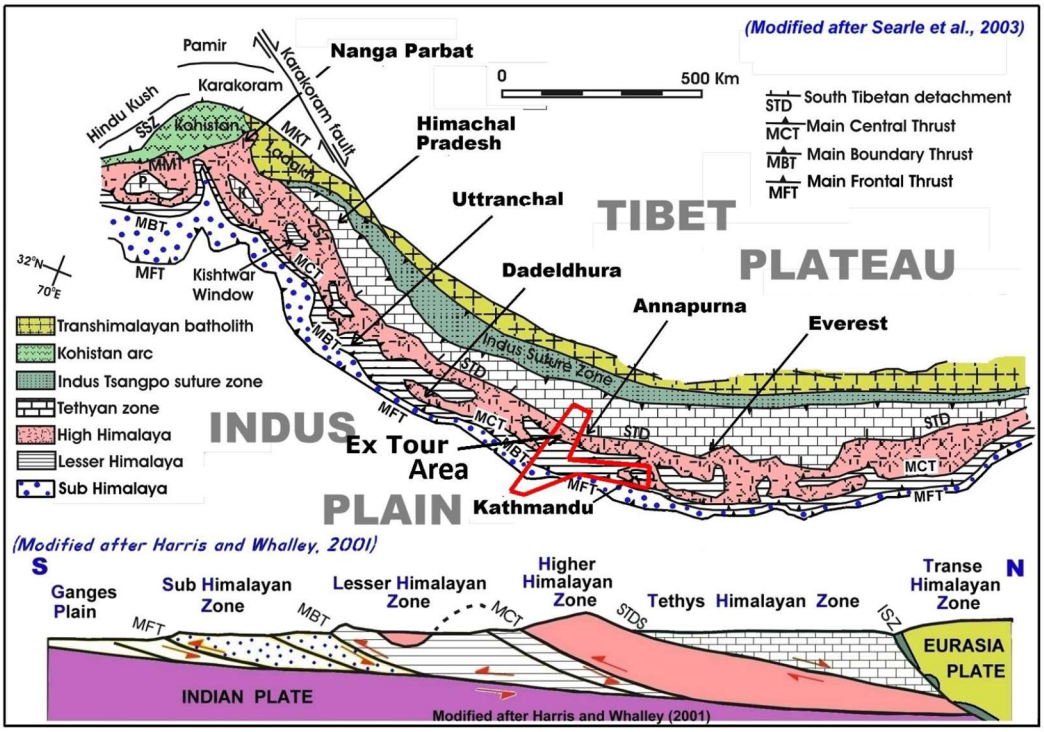

Figure 1. Himalayan geologic outline and the exercise tour area (red frame)

A climatic zonation from tundra in the high mountain range to the subtropical in the Alluvial plain develops along the mountain range reflecting its altitudinal difference. The climatic zonation results in zonations of vegetation, human settlements, as well as natural hazards. The Himalaya is thus the best natural museum to study the nature of the earth.

The Kaligandaki River of west-central Nepal Himalaya is an ancient river, which flowed southward through the area even before the rise of the Himalayas. It cuts through the deepest valley on the earth, with over 8000m high peaks on both sides exhibiting the relief of 6000m with very steep slopes. As one moves from north to south, an amazing change in geology, topography, climate, vegetation and culture can be clearly noticed. Because of this, the Kaligandaki River valley has been one of the most favored trekking routes in the Himalayas.

The Student Himalayan Field Exercise Tour (SHET) has aimed to show students the full N-S section of the Himalayan Orogen mostly along the Kaligandaki Valley. The SHET started in 2012 to let students see natural processes related to the orogeny, as well as to feel the dynamic crustal processes in the field and to have an interest in geology. Since then, the SHET has been conducted every year (except in 2021 due to the Covid-19 pandemic). The details of the SHET program are given on the SHET home page (SHET-HP, 2024). The geo-tour of the Himalayas should give a strong impact on students, who walk there. We have expected that the impact will spread to students and teachers in Japan, although a small step by step, and finally will begin to work as a brake on the recent trend of university curriculums that are giving little weight to or even neglecting the field study of natural sciences.

The field tour of SHET covers a 250 km traverse from the north to the south of the Himalayan Orogen, covering the Tethys Himalayan, Higher Himalayan, Lesser Himalayan, Sub Himalayan and the Gangetic Alluvial zones, observing important geologies of all the geologic zones and boundary major faults. The tour starts from the northernmost Muktinath (3800m asl), where the world's most holy temple of Hinduism is situated, passing through Pokhara city, the central of the Himalayan sightseeing, and Tansen city, a traditional capital town of old Palpa kingdom, and ends at Lumbini (150m asl), the world's most holy place of Buddhism as the birthplace of Buddha, traversing from the tundra zone to subtropical zone within its 250km length of the tour route. The changing climatic zones reflect dramatic changes in vegetation as well as the living styles of human beings. Thus the tour includes a variety of interests apart from geology as well.

Before the start and after the field tour, a pre-tour seminar and a summary seminar were organized, which held at the Department of Geology, Tri-Chandra Campus, Tribhuvan University (DGTU), Kathmandu, and after the seminars, the participants of the SHET are escorted to city tours by students of the DGTU. Participants of the SHET submit a report of the tour and the tour chief leader edits all the reports and tour data and forms a book titled Traversing the Himalayan Orogen 2012 (2013 and so on), and the project has been published the book every year (e.g., Yoshida, 2024). All 182 participants of the tour of 12 years evaluated not only the great geology and beauty of the Himalayas (**Fig. 2**) but also friendship interaction among participants as well as with students of the DGTU.

Figure 2. The SHET-4 team with the Dhaulagiri range on the backsight (March 2015)

The voluntary leaders-teachers of the exercise tours have included retired and/or active university teachers and office/company engineers who are experienced in Himalayan geology as well as field

geology. The Gondwana Institute for Geology and Environment (Hashimoto, Japan) has mainly been conducting the organization of the exercise tour, in collaboration with the DGTU.

The total number of Participants of the 1st to 12th SHET included 143 students from 27 Japanese universities and 22 students of DGTU, 4 students from Indian and Chinese universities, and 13 citizens of Japan and Nepal. Participation fees for a Japanese student including airfare ranged from 139,000-215,000 JPY with an average of ca. 172,500 JPY, which is the lessened amount due to the support by the SHET project, which collected donations from organizations and individuals and from crowdfunding (SHET-CF, 2023), of the average of 30,500 JPY per student.

At the poster presentation, highlights of the exercise tours of the past 12 years will be displayed. A recruit for the 13th SHET to be held next March will also be delivered.

References

SHET-HP., 2024. www.gondwanainst.org/geotours/Studentfieldex_index.htm
SHET-CF., 2023. www.gondwanainst.org/cf
Yoshida, M., (Ed.), 2024. Traversing the Himalayan Orogen 2024 - A Record of the twelfth Student Himalayan Field Exercise Tour in March 2024. Field Science Publishers, Hashimoto, PDF version 391p.

Posters – Abstracts

Poster 01: Controls on the formation of porphyry Mo, Cu and Au deposits in the Qinling Orogenic Belt, central China

Li Tang[1*]

[1]*School of Earth Sciences and Resources, China University of Geosciences, Beijing 100083, China*

*Corresponding author:
E-mail address: ltang@cugb.edu.cn (Li Tang)

The Qinling Orogenic Belt (QOB) hosts one of the world-class porphyry Mo belts (proven Mo resource of 8.43 Mt), several porphyry-skarn Cu and Au deposits, and abundant barren granitoids. The Late Jurassic to Early Cretaceous mineralized and barren porphyry systems are broadly coeval and distributed in the eastern part of the QOB. The key factors controlling the porphyry fertility and diversity are not well understood, with magma source, magmatic water content, magma oxidation state, sulfur and halogen values, and nature of magma chamber, among other aspects. The fertile porphyries of Mo and Au deposits are characterized by enriched Sr-Nd-Hf isotopes, relatively low $\delta^{18}O$ values of 4.58 to 8.65‰, abundant Neoarchean to Paleozoic inherited zircons and high apatite MnO contents, indicating a mixed magma sources from partial melting of the Neoarchean to Paleoproterozoic lower crust, subducted continental crust of the Yangtze Block and the metasomatized lithospheric mantle. The ore-forming porphyries of Cu (-Mo) deposits have depleted isotopic features and distinct magma source from partial melting of the Triassic juvenile lower crust with significant contribution of mantle derived mafic magma. We suggest that the lithospheric architecture and magma source are the primary controlling factors for the diverse Cu (-Mo), Mo (-W) and Au mineralization in Qinling. Chlorine and fluorine contents also show contrast between Cu-related and Mo-related porphyries, with the former being Cl-rich which is favorable for extraction and transportation of Cu, and the latter is F-rich which is crucial for porphyry Mo mineralization through lowering viscosity, promoting crystal fractionation and partitioning of Mo into fluid. The fertile porphyries in the Cu (-Mo) deposits have adakite-like Sr/Y ratios and high magmatic water content involving early amphibole fractionation and suppression of plagioclase fractionation. The less evolved porphyry Mo (-W) magma share similar geochemical features with the porphyry Cu (-Mo) and Au magmas, whereas the highly evolved porphyry Mo (-W)

magma shows moderately high water content that cannot suppress plagioclase fractionation. The diverse porphyry Mo (-W) and Au mineralization with comparable magma source are controlled by the higher magmatic water content and oxidation state of the porphyry Au magma. The barren suites show overlapped Sr-Nd-Hf-O isotopes, whole-rock Fe_2O_3/FeO ratios, zircon ΔFMQ and Ce^{4+}/Ce^{3+} values, and apatite SO_3 contents with the different types of fertile porphyries. The flat roof of the barren batholiths resulting in lack of fluid flow and focusing into a small volume could account for the barren porphyries, whereas the highly evolved late phase with favorable geometry would have higher potential for porphyry mineralization.

Poster 02: Multi-field intelligent monitoring technology in landslide model test

Fang Kun[1*]

[1]*Faculty of Engineering, China University of Geosciences, Wuhan 430074, China*

*Corresponding author:
E-mail address: kunfang@cug.edu.cn (Fang Kun)

Physical model testing stands as a cornerstone of investigative methodologies within the spheres of geotechnical and geological engineering. The role of monitoring technology in the context of landslide model testing is paramount. This paper delineates the creation and refinement of an innovative multi-smartphone-based three-dimensional deformation measurement system, alongside a principal stress measurement system and a profound displacement measurement system, all of which harness the capabilities of multi-field intelligent monitoring technology. At its core, the manuscript offers a detailed exposition on multi-field intelligent monitoring technology, shedding lighton the sophisticated methodologies, intricate system architecture, and meticulous accuracy analysis associated with the trio of measurement systems. The narrative progresses to display the application of these three avant-garde monitoring technologies across a variety of landslide model experiments. Culminating in the employment of multi-field intelligent monitoring technology, the research embarks on conducting a nuanced inverted slope valley downcutting experiment as well as a meticulous bedding slope excavation experiment, showcasing the depth and breadth of potential applications in geotechnical and geological study.

Poster 03: Signatures of Metamorphic Evolution of Banded Iron Formation from the Attappadi Valley, Kerala, Southern India

Y. Anilkumar[1*], R. Radhika[1], A.P. Pradeepkumar[1]

[1]*Department of Geology, University of Kerala, Thiruvananthapuram 695 581, India*

*Corresponding author:
E-mail address: anilgeol@keralauniversity.ac.in (Y.Anilkumar)

The chemical sedimentary rock, characterised by alternate bands of iron and silica-rich minerals, is called the Banded Iron Formations (BIFs), which were predominantly formed in the Precambrian. The Attappadi Valley (study area) in the Palakkad district of Kerala falls within the western termination of the Bhavani Shear Zone within the Southern Granulite Terrane (SGT) of Peninsular India. It preserves

the Archean Supracrustal complex of rocks. Metamorphosed BIF are among the significant rock types in the area, together with TTG (tonalite-trondhjemite-granodiorite) gneisses, charnockites, meta-ultramafics, amphibolites, felsic volcanics, and metapelites. BIFs in the study area occur as narrow, isolated bands in association with ultramafic rocks, and they are characterised by the presence of oxide (magnetite, hematite), silicate (grunerite, pyroxene, garnet amphibole) and sulphide (pyrite, chalcopyrite, arsenopyrite) minerals. Presence of the ferromagnesian minerals like pyroxenes, amphibole and biotite is the result of metamorphism. The whole-rock major element data of BIFs are analysed using X-ray Fluorescence (XRF) spectrometry. The samples are enriched in SiO_2 (35-91 wt.%) and Fe_2O_3 (4-55 wt.%). Since BIFs are pure chemical sediments, the amount of TiO_2 and Al_2O_3 are relatively less, but the enrichment of Al_2O_3 (1.19-6.3 wt.%) in the sample with the presence of garnet indicates the influence of continental input in proximity to the BIF deposition. The SiO_2 vs Al_2O_3 plot falls within the hydrothermal field. The Fe/Ti Vs Al/(Al+Fe+Mn) and the ternary diagram of Fe, Al and Mn also suggest the relative contribution of hydrothermal components in the sediments. The marine environment for the deposition of BIFs is evidenced by the lower ratio (0.21) of CaO/(CaO+MgO) in the samples compared to freshwater (>0.70). The ternary diagram using SiO_2, Al_2O_3, and Fe_2O_3 depicts the Precambrian origin of the BIF. Another ternary diagram consists of (CaO+MgO), Fe_T, and SiO_2 and also represents the time of deposition of BIF as Precambrian. The presence of coexisting silicate mineral phases such as two-pyroxenes, garnet-orthopyroxene, and garnet-amphibole; and their mineral chemistry are important for understanding the evolutionary history of BIFs. The mineral chemistry of the samples has been extracted using EPMA analysis. The two-pyroxene geothermobarometers of Wood and Banno (1973), Wells (1977), Kretz (1982), Brey and Kohler (1990) and Putirka (2008), based on the Mg-Fe distribution between coexisting opx (orthopyroxene) and cpx (clinopyroxene), yielded a temperature range of 857-652˚C. Based on the garnet-orthopyroxene geothermometer, the temperature obtained is between 532-629˚C at 9.6 kb. Magnetite-ilmenite pairs are also present in the same sample, which yielded a temperature of 475-256˚C with an oxygen fugacity range of -25 to -45. The composition of amphiboles in the BIFs range from anthophyllite to pargasite. The common garnet-hornblende thermometry is used for the amphibole bearing assemblages and the temperature obtained in the range of 495-438˚C and 731-608˚C. Garnet-biotite assemblage is also used for the temperature determination, which yielded a range of 703-659˚C. Among all geothermobarometers, the maximum temperature obtained from the two-pyroxene assemblage is 857˚C, which is characteristic of the granulite facies metamorphism and represents the prograde stage for the BIF's of the Attappadi Valley. After the peak metamorphism, the BIF has also undergone a retrograde stage, which is marked by the temperature from the garnet-hornblende geothermometer. In addition, the low temperature obtained from the magnetite-ilmenite pair and the corresponding oxygen fugacity indicate cooling in the later stages of metamorphism. Field observation, petrography and major element geochemistry of BIFs in the study area revealed a Precambrian Algoma-type origin; formed in a marine environment with significant input from hydrothermal sources. Various parameters including texture, mineral chemistry, petrography, and geothermometry affirmed that the BIF of Attappadi Valley has originated in a marine environment, and has undergone a prograde metamorphic path up to granulite facies and followed a retrograde metamorphic path due to the exhumation of the terrain.

Keywords: Banded iron Formations (BIFs), Bhavani Shear Zone, Southern Granulite Terrane (SGT), mineral chemistry, geothermometry, Algoma.

References

Brey, G.P., Köhler, T., 1990. Geothermobarometry in four-phase lherzolites II. New thermobarometers, and practical assessment of existing thermobarometers. Journal of Petrology 31(6), 1353–1378. https://doi.org/10.1093/petrology/31.6.1353.

Kretz, R., 1982. Transfer and exchange equilibria in a portion of the pyroxene quadrilateral as deducted from natural and experimental data; Geochimica et Cosmochimica Acta 46, 411-421.

Putirka, K., 2008. Thermometers and Barometers for Volcanic Systems. In: Putirka, K., Tepley, F. (Eds.), Minerals, Inclusions and Volcanic Processes, Reviews in Mineralogy and Geochemistry. Mineralogical Society of America 69, 61-120.

Wells, P. R. A. 1977. Pyroxene thermometry in simple and complex systems. Contributions to Mineralogy and Petrology 62, 129-139.

Wood, J., Banno, S., 1973. Garnet-orthopyroxene and orthopyroxene- clinopyroxene- relationships in simple and complex systems. Contributions to Mineralogy and Petrology 42, 109- 124.

Poster 04: Magmatic-hydrothermal transition in highly fractionated granites: evidence from biotite

Zhiqiang Wang[1,2*], Haoxiang Da[1,2], Feng Yuan[1,2], Xiaoxia Duan[1,2], Yufeng Deng[1,2], Xiaohui Li[1,2]

[1] *Ore Deposit and Exploration Centre (ODEC), School of Resources and Environmental Engineering, Hefei University of Technology, Hefei 230009, China*
[2] *Anhui Province Engineering Research Center for Mineral Resources and Mine Environments, Hefei 230009, Anhui, China*

*Corresponding author:
E-mail address: wangzq@hfut.edu.cn (Zhiqiang Wang)

The highly fractionated granites are closely related to the rare-metal mineralization, but the mechanisms for their unusual geochemical features (e.g., low Nb/Ta ratios) and extreme enrichment of rare metals remain contentious. The existence and role of exsolved fluids are key issues of debate. In this study, we employ biotite to trace the magmatic-hydrothermal transition in the Mesozoic Fuling pluton in the eastern part of the Jiangnan orogenic belt. The Fuling pluton consists of coarse-grained biotite monzogranite-syenogranite, medium-fine-grained porphyritic biotite syenogranite and fine-grained biotite syenogranite, in which biotites are classified as BT-I, BT-II and BT-III, respectively. BT-I show high TiO_2, MgO, Cl, V and Ba and low rare-metal contents. Petrography, geochemistry and numerical modeling indicate that fractional crystallization is the main controlling factor for compositional variations of BT-I. In contrast, BT-III show very low TiO_2, MgO, Cl, V and Ba and extremely high rare-metal contents, which cannot be explained by fractional crystallization because the required crystallinity is too high (>95%). Furthermore, we use the difference in fluid mobility of compatible elements (Sc and Mn versus V and Ba) to distinguish hydrothermal from magmatic processes, which unequivocally indicate that BT-III was formed mainly from the entrapped exsolved fluids. This hypothesis is supported by the near solidus formation temperature, abrupt increase of F/Cl ratios, and the characteristics of BT-III distributing along the cracks of granites. BT-II show transitional compositional features, but with magmatic petrography characteristics, suggesting that they probably form from a fluid-rich residual melt. Given the very low Nb/Ta ratios and extremely high rare-metal contents of BT-III, we believe that the exsolved hydrothermal fluid is an essential ingredient in making the highly fractionated granites, although magmatic processes like fractional crystallization also play an important role.

Poster 05: Investigating *Saccharomyces cerevisiae's* potential for biosorption in native and treated forms for the removal of toxic pollutants

Baranikumaar, V[1], Karthikeyan Asaithambi[1*] and Mahalakshmi Mathivanan[1]

[1]*School of Civil Engineering, SASTRA Deemed to be University, Thanjavur, 613401, Tamil Nadu, India*

*Corresponding author:
E-mail address: karthikeyan_a@civil.sastra.ac.in (A.Karthikeyan)

The textile industry is one of the largest in the world, contributing significantly to the economies of many nations and offering work opportunities without the need for specialized training. Approximately 1,000–3,000 m^3 of water leaked out during the processing of 12–20 tons of textiles every day. Because of the actual ecological problems associated with the dyestuffs and the consequences of their breakdown, the release of these pollutants into the environment is disgusting. Water usage in the textile industry is high, mostly because of plant colouring and completion processes. This study's primary goals are to treat the hazardous pollutant using *Saccharomyces cerevisiae* (SAC) and look into SAC's potential for biosorption in both its treated and native forms. The SAC was grown in yeast, peptone, and dextrose (YPD) medium and is employed in both native and treated methods. SAC is treated by placing it in a microwave and named as TSAC. The pH, dose, concentration, duration, and temperature tests are used to determine the ideal conditions for achieving maximal Methylene blue (MB) removal. Maximum MB removal efficiency % was observed at pH 9 (84.80%) for SAC and at pH 8 (90.20%) for TSAC. Maximum MB removal efficiency % was observed at a dosage of 2 g/L (83.50% & 92.80%) for both SAC and TSAC. Removal efficiency % becomes constant after 100 minutes of contact time for SAC and as well as for TSAC. The biosorbent was characterized using, SEM (Scanning Electron Microscope) analysis, and FTIR (Fourier Transform Infrared Spectroscopy) test. From Langmuir model, the maximum adsorption capacity was found to be 7.2 mg/g for SAC and 11.2 mg/g for TSAC. The biosorption kinetics was best explained by the pseudo second-order model through high R^2 values which confirms the adsorption of MB on both biosorbents was chemisorption. The TSAC exhibits more significant and varied shifts in the FTIR spectra, suggesting that the treatment process enhanced the reactivity and availability of functional groups for adsorption. This enhancement likely improves the TSAC capacity to interact with and adsorb methylene blue dye, compared to untreated SAC. These changes underscore the importance of treatment in modifying biosorbents to optimize their performance in dye removal processes.

Poster 06: Structural geometry and tectonic implications of the Seosan-Taean area in the western Gyeonggi Massif: Insight into the Korean Collision Belt and East Asian continental evolution

Seongjae Park[1*], Minho Kang[1], Yirang Jang[1], Sanghoon Kwon[2], Vinod O. Samuel[2]

[1]*Department of Geological and Environmental Sciences, Chonnam National University, Gwangju 61186, Republic of Korea*
[2]*Department of Earth System Sciences, Yonsei University, Seoul 03722, Republic of Korea*

*Corresponding author:
E-mail address: star980518@jnu.ac.kr (Seongjae Park)

Since the extension of the Qinling-Dabie-Sulu Belt between North China Craton (NCC) and South China Craton (SCC) to the Korean Peninsula has been suggested (e.g., Yin and Nie, 1993; Zhang, 1997; Oh et al., 2005; Kwon et al., 2009), the western Gyeonggi Massif, part of the recently suggested as the Hongseong-Imjingang Belt (Kee et al., 2019), is tectonically correlated with the Qinling-Dabie-Sulu Belt, and the micro-continents in between (e.g., Kwon et al., 2009; Park et al., 2014).

In this context, the Seosan-Taean area within the western Gyeonggi Massif is critical for understanding the structural evolution related to the subduction to collisional events, as it preserves evidence of contractional orogenic events. The Paleoproterozoic Seosan Group, which forms the basement beneath the Paleozoic Taean Formation, displays distinct NE-SW trending repeated map

patterns in the Seosan-Taean area. To decipher these structural patterns, we have conducted detailed field mapping and realistic structural geometric interpretations using down-plunge projections (Marshak and Mitra, 1988). The results indicate that the overall structural geometry in the Seosan-Taean area consists of the NE-SW trending overturned synform-antiform-synform pairs. These structures plunge SW in the northern, southern, and eastern parts, and NE in the central part. This fold geometry is interpreted as a second-order fold within the hanging wall of a regional-scale fault, specifically the Dangjin fault, located in the eastern part of the study area. These fault-related folds in the Seosan-Taean area were formed by basement-involved deformation following the sedimentation of the Paleozoic Taean Formation, in relation to the Permo-Triassic collisional event in the Korean Peninsula.

The spatial and temporal structural changes of these structures will provide fundamental insights into a prominent mountain belt in the Seosan-Taean area, and will eventually enhance our understanding on the role of the western Gyeonggi Massif during the tectonic evolution of the East Asian continent.

Keywords: Western Gyeonggi Massif, Seosan-Taean area, Down-plunge projection, Synform-antiform-synform pair, Permo-Triassic Collisional event

References

Kee, W.-S., Kim, S.W., Kim, H., Hong., P., Kwon, C.W., Lee, H.-J., Cho, D.-L., Koh, H.J., Song, K.-Y., Byun, U.H., Jang, Y., Lee, B.C., 2019. Geologic map of Korea. KIGAM, scale 1:1,000,000.

Kwon, S., Sajeev, K., Mitra, G., Park, Y., Kim, S.W., Ryu, I.-C., 2009. Evidence for Permo-Triassic collision in Far East Asia: The Korean collisional orogen. Earth and Planetary Science Letters 279, 340-349.

Marshak, S., Mitra G., 1988. Basic Method of Structural Geology: Prentice Hall, 446p.

Oh, C.W., Kim, S.W., Choi, S.G., Zhai, M., Guo, J., Krishana, S., 2005. First finding of eclogite facies metamorphic event in South Korea and its correlation with the Dabie-Sulu Collision Belt in China. The Journal of Geology 113, 226-232.

Park, S.-I., Kim, S.W., Kwon, S., Thanh, N.X., Yi, K., Santosh, M., 2014. Paleozoic tectonics of the southwestern Gyeonggi massif, South Korea: insight from geochemistry, chromian-spinel chemistry and SHRIMP U-Pb geochronology. Gondwana Research, 26, 684–698

Yin, A. Nie, S., 1993. An indentation model for the north and south China collision and the development of the TanLu and Honam fault systems, eastern Asia. Tectonics 12, 801-813.

Zhang, K.J., 1997. North and South China collision along the eastern and southern North China margins. Tectonophysics 270, 145-156.

Poster 07: Indosinian Orogeny recorded in sedimentary rocks of the Indochina Block, central Thailand

Hidetoshi Hara[a, *], Thasinee Charoentitirat[b], Tetsuya Tokiwa[c], Toshiyuki Kurihara[d], Keisuke Suzuki[a], Apsorn Sardsud[e]

[a] *Geological Survey of Japan, AIST, 1-1-1 Higashi, Tsukuba, Ibaraki 305-8567, Japan*
[b] *M.Sc. in Petroleum Geoscience Program, Department of Geology, Faculty of Science, Chulalongkorn University, Bangkok 10330, Thailand*
[c] *Faculty of Science, Shinshu University, Matsumoto, Nagano 390-8621, Japan*
[d] *Graduate School of Science and Technology, Niigata University, Niigata 950-2181, Japan*
[e] *Department of Mineral Resources, Bangkok 10400, Thailand*

*Corresponding author:
E-mail address: hara-hide@aist.go.jp (Hidetoshi Hara)

The Indosinian Orogeny was a major event that contributed to the build-up of the Asian mainland and took place over most of southeastern to eastern Asia during the Permian to Triassic. The provenance of conglomerates and associated sedimentary rocks are expected to have preserved sedimentary and erosional events related to the Indosinian Orogeny. In the present study, we investigated the Indosinian Orogeny as recorded in the Indochina Block by conglomerates and associated sedimentary rocks using geochemistry and detrital zircon U–Pb ages, central Thailand.

The Indosinian I Event is recorded in Type-1 limestone conglomerates, whose formation was a result of the collapse of the Permian carbonate platform. This event was triggered by a collision between the Indochina and South China blocks during the Late Triassic (Norian). The Indosinian II Event is represented by Type-2 conglomerates, which are composed of various clasts and basaltic sandstones derived from the collapse of the Sukhothai Arc, the Nan Back-arc Basin, the Phetchabun Volcanic Belt, and basement rocks of the Indochina Block. This event was caused by the closure of the Paleo-Tethys and the commencement of collision between the Sibumasu Block, the Sukhothai Arc, and the Indochina Block at the latest Triassic (Rhaetian). The Indosinian III Event is preserved in Type-3 conglomerates, which comprise volcaniclastic rocks and volcanic breccias composed of andesite and dacite. This event was associated with post-collision magmatism that occurred between the Sibumasu and Indochina blocks after the late Early Jurassic (Toarcian or younger).

We provided new insights into the Indosinian I, II, and III events based on conglomerates and associated sedimentary rocks, and concluded the triggers and timing of these events. The Indosinian Orogeny within the Indochina Block was associated with tectonics involving continental collision and Paleo-Tethyan subduction during the Middle Triassic to Early Jurassic.

Keywords: Indosinian Orogeny, Indochina Block, unconformity, conglomerate, U–Pb age

Poster 08: Establishment of Local Rainfall Thresholds Values for Landslide Early Warning

L.A.L. Kithmini[a *], A.D.H.J.Perera[a]

[a]*National Building Research Organisation, Sri Lanka*

*Corresponding author:
E-mail address: kithminiliyanaarachchi@gmail.com (L.A.L. Kithmini)

Landslides are natural and potentially hazardous phenomena that mainly occur in a variety of geologic settings in the Sri Lanka every year causing a significant hazard to human lives and infrastructure. Landslides naturally occur because of several factors, which can act alone or in combination, including geologic, geomorphologic, hydrologic, and land-use factors and mainly triggered by rainfall leading to potentially destructive landslides. Landslides triggered by rainfall are caused by the buildup of water pressure into the ground. Groundwater conditions responsible for slope failures are related to rainfall through infiltration, soil characteristics, antecedent moisture content, and rainfall history. Therefore, high intensity of rainfall in hilly areas plays a major role in landslide occurrences in Sri Lanka during the periods of heavy monsoons and unusual heavy inter monsoon events. Thus, forecasting and measuring the rainfall is the best approach to predict landslide disaster in Sri Lanka.
National Building Research Organization (NBRO) has been designated as the National Focal Point for landslide risk management and is the authorized body for landslide Early Warning (EW) in Sri Lanka. Regional Landslide Early Warning (RLEW) based on the rainfall thresholds plays a significant role as a non-structural risk reduction method on rainfall-induced landslides. The warning on a regional scale goes off based on predefined rainfall threshold limits under three levels, i.e., watch, alert, and evacuation respectively at 75 mm/day, 100 mm/day, and 150 mm/day or 75 mm/h. The NBRO uses an automated network of rain gauges established in the landslide-prone areas of the country to obtain real-time rainfall data, based on which the early warnings are issued.

However, because of climatic changes, the usual rainfall pattern has been significantly altered resulting in more erratic rainfall. The effect of precipitation for the landslide initiation will differ locally and therefore, it is problematic and misleading to predict for local areas using a regional or country wise

rainfall threshold value. So, this study was focused on the requirement of locally defined rainfall thresholds for effective early warning and the study was focused in the Badulla District of Uva province in Sri Lanka. Fifteen major landslides activated within the Northeast monsoon period (November-December) of Sri Lanka 2023, were selected for the study. Rainfall data associated with landslide events were extracted from NBRO automated rain gauges (**Table 1)** and the most effective nearby rain gauges were selected by considering the morphology of the area.

The value of cumulative rainfall for each landslide was plotted and then the average cumulative rainfalls were obtained considering all the landslides studied (**Fig. 1**). According to the study, all the landslides in the study area have been triggered by the rainfall but it is depicted that the 1hr rainfall has low influence in triggering landslides. Further, it seems that landslide activation occurred prior to the rainfall of 75 mm/day in the Badulla District and hence, a "watch" alert should be issued around 50-60 mm/day. The study verified that not only does the daily rainfall affect the landslide initiation but also the antecedent rainfall also contributes to the initiation of landslides. It is considered that large-scale landslides were initiated with landslide symptoms within the study period, they were not progressive as the rainfall gradually decreased over a short period of time.

Therefore, further studies are required with the monitoring of how these landslides are progressive in extreme rainy events to establish threshold values for "alert" and "evacuation" level warnings.

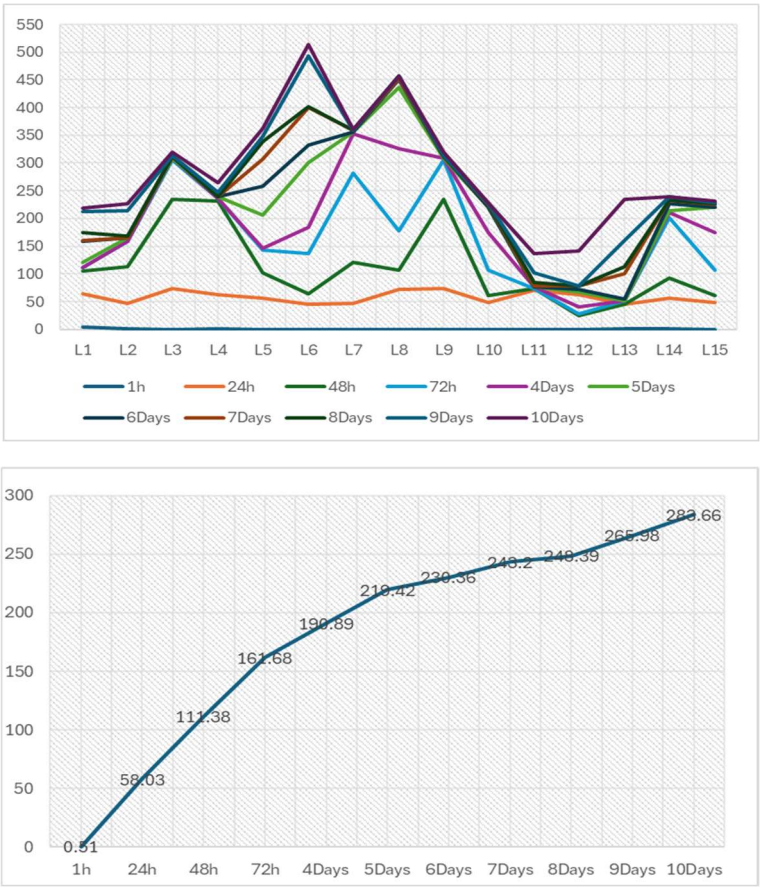

Figure 1. The cumulative rainfall value for each landslide area (top) and the average cumulative rainfall value obtained considering all the landslides studied (bottom)

Table 1. Rainfall data associated with landslide events were extracted from NBRO automated rain gauges

Landslide Index	Rainfall (mm)										
	1h	24h	48h	72h	4Days	5Days	6Days	7Days	8Days	9Days	10Days
L1	4.5	63.5	104.5	111	111.5	121	158.5	160.5	174.5	212	219
L2	0.6	46.2	113.4	159.2	159.2	164.4	165.4	165.4	168	213.8	226.8
L3	0	73.2	235.2	305.2	309	309	312.4	312.4	312.4	313	319.8
L4	1.8	62	232	235.8	235.8	239.2	239.2	239.2	239.8	246.6	264.6
L5	0	57	101.5	143.5	146.5	205.5	258	307	338.5	348	362
L6	0	45.4	63.4	136.2	184.8	301.2	332.4	400	401.4	492.8	513.2
L7	0	47.2	120.4	282.4	352.4	356.2	356.2	359.6	359.6	359.6	360.2
L8	0	72	107	178.5	325.5	436.5	451	453	457.5	457.5	457.5
L9	0	73.2	235.2	305.2	309	309	312.4	312.4	312.4	313	319.8
L10	0	48	60.6	106.8	174	219.8	219.8	225	226	226	228.6
L11	0	70	73.8	73.8	77.2	77.2	77.2	77.8	84.6	102.6	136.2
L12	0	62	24.4	28.2	41	67	71.6	77.8	77.8	77.8	141.4
L13	0.39	45.8	45.8	51	52	52	54.6	100.4	113.4	160.6	233.8
L14	0.5	56	92	201.5	210.5	213.5	227	232.5	233	238.5	240
L15	0	49	61.6	107	175	219.9	219.8	225	227	228	232
Average	0.51	58.03	111.38	161.69	190.89	219.43	230.37	243.2	248.39	265.99	283.66

Poster 09: Age and radiolarian fauna of pelagic siliceous rocks within the Akiyoshi belt in the Hashidate area, Itoigawa City, Niigata Prefecture, central Japan

Toshiyuki Kurihara[a*], Keisuke Suzuki[b], Ryo Urushiyama[c]

[a] *Department of Geology, Faculty of Science, Niigata University, Niigata 950–2181, Japan*
[b] *Geological Survey of Japan, AIST, 1–1–1 Higashi, Tsukuba, Ibaraki 305–8567, Japan*
[c] *Murao Giken Co. Ltd, Niigata 950–0948, Japan*

*Corresponding author:
E-mail address: kurihara@geo.sc.niigata-u.ac.jp (Toshiyuki Kurihara)

The Akiyoshi belt, a late Permian accretionary complex in Southwestern Japan, contains early Carboniferous to middle Permian pelagic rocks constituting ocean plate stratigraphy and atoll-type limestones developed in the Panthalassa (Kanmera et al., 1990). These limestones, with their abundant fossils, well preserve records from the Visean (early Carboniferous) to the middle Permian, enabling detailed reconstructions (Sano, 2006). On the other hand, pelagic siliceous rocks of the same age as the limestones, which were deposited in abyssal plains, have been less reported than the limestones. These rocks are expected to preserve the environmental conditions of the Panthalassa and are crucial for reconstructing the Earth's environment during the Carboniferous to Permian period.

The present study reports early Permian radiolarians from chert distributed in Itoigawa, Niigata Prefecture, central Japan. The Permian siliceous and clastic rocks belonging to the Akiyohi belt in Itoigawa have been recognized as the Himekawa Complex (Nagamori et al., 2010). This geologic unit is distributed in the east of the Omi Complex which is composed mainly of Carboniferous to Permian limestone with minor basalts. In the Himekawa Complex, a stratigraphy has been reconstructed as follows: red mudstone and chert, alternating red chert and green acidic tuff, alternating green and black siliceous mudstone, mudstone, and sandstone. However, no fossils suitable for age determination have been reported from the cherts, and the full extent of radiolarian assemblages remains unclear. In

addition, the Himekawa Complex has been correlated with Nishiki and Yoshii groups of the Akiyoshi belt in the Chugoku region based on information from acidic tuffs and siliceous mudstones. However, due to the lack of age-diagnostic radiolarians from the cherts, the correlations with the cherts of the Nishiki and Yoshii groups have yet to be conducted.

The chert from which we obtained Permian radiolarians is exposed in the Hashidate area, western Itoigawa City. The apparent total thickness of this chert is c.a. 30 m, although several layer-parallel faults are observed. Red-colored bedded cherts predominate in the outcrop, and minor pale green-colored cherts also occur. Using the standard HF etching technique, we obtained well-preserved radiolarians from red cherts. The radiolarian fauna is dominated by Latentefistularia and Entactinaria, with minor albaillellarians. The following species are identified: *Albaillella sinuata* Ishiga and Imoto, *Pseudoalbaillella scalparata* Holdsworth and Jones, and *Albaillella* sp. Based on the unitary association zone (Xiao et al., 2018), these species indicate the Kungurian age of late early Permian. The Kungurian age of chert has been commonly reported from the Akiyoshi belt (Kanmera et al., 1990).

Upon examining the previously reported ages of cherts in the Akiyoshi belt, it is evident that most cherts indicate a Kungurian age. The cherts dated by radiolarians in this study also indicate this age. One aspect to consider is that the cold climate induced by the Late Paleozoic Ice Age (LPIA; Isbell et al., 2021) might have reduced the productivity of radiolarians, which prefer warmer seawater, resulting in less chert deposition and more deep-sea clay accumulation during the Kasimovian (late Carboniferous) to the early Artinskian (early Permian). This scenario might explain the stacking of layers with different physical properties, such as clay and chert, in the ocean floor sedimentary sequence, potentially creating a décollement layer during accretion. In other words, the hypothesis is that siliceous rocks older than Kungurian were subducted along with the plate and are not well preserved in the Akiyoshi belt. The relationship between the LPIA, pelagic siliceous rock sedimentation, and the interaction between climate and plankton productivity during the Carboniferous to early Permian needs to be better understood.

References

Isbell, J. L., Vesely, F. F., Rosa, E. L. M., Pauls, K. N., Fedorchuk, N. D., Ives, L. R. W., Mcnall, N. B., Litwin, S. A., Borucki, M. K., Malone, J. E., Kusick, A. R., 2021. Evaluation of physical and chemical proxies used to interpret past glaciations with a focus on the late Paleozoic Ice age. Earth-Science Reviews 221, 103756. https://doi.org/10.1016/j.earscirev.2021.103756.

Kanmera, K., Sano, H., Isozaki, Y., 1990. Akiyoshi Terrane. In Ichikawa, K., Mizutani, S., Hara, I., Hada, S. and Yao, A., eds., Pre-Cretaceous Terranes of Japan, Nippon Insatsu Shuppan, no. 224, 49–62.

Nagamori, H., Takeuchi, M., Furukawa, R., Nakazawa, T., Nakano, S., 2010. Geology of the Kotaki district. Quadrangle Series, 1:50,000, Geological Survey of Japan AIST, 130p. (in Japanese with English abstract 4p.).

Sano, H., 2006. Impact of long-term climate change and sea-level fluctuation on Mississippian to Permian mid-oceanic atoll sedimentation (Akiyoshi Limestone Group, Japan). Palaeogeography, Palaeoclimatology, Palaeoecology 236, 169–189. https://doi.org/10.1016/j.palaeo.2005.11.009.

Xiao, Y., Suzuki, N., He, W., 2018. Low-latitudinal standard Permian radiolarian biostratigraphy for multiple purposes with Unitary Association, Graphic Correlation, and Bayesian inference methods. Earth-Science Reviews 179, 168–206. https://doi.org/10.1016/j.earscirev.2018.02.011.

Poster 10: Palynological and Biostratigraphical Investigations on Borehole Samples Retrieved from Brunei Bay, Brunei Darussalam

Nafisah Mardhiah Munawar[1*], Amajida Roslim[1], Muqri Ahmad[1], László Kocsis[2], and Christa-Ch Hofmann[3]

[1] *Faculty of Science, Geology Group, Universiti Brunei Darussalam, Jalan Tungku Link Gadong, BE1410, Brunei Darussalam*
[2] *Institute of Earth Surface Dynamics, University of Lausanne, Rue de la Mouline, 1015 Lausanne, Switzerland*
[3] *University of Vienna, Department of Palaeontology, A-1090, Vienna, Austria*

*Corresponding author:
E-mail address: nafisah.munawar@gmail.com (Nafisah Mardhiah Munawar)

Palynology is the study of organic wall structures, such as pollen, spores, and other microscopic organisms, that have been preserved in rock records. In geology, this study is often used to interpret ecology, past environment and ages of terrestrial, coastal, and marine rocks. Such an environment is seen in the Brunei Bay area in Brunei. Brunei Bay represents an area where terrestrial and marine waters coexist, at the same time, surrounded by untouched mixed rainforest systems, including mangroves, swamps, peat swamps, and the Dipterocarpaceae forest existed since the late Miocene. Despite successful analyses, however, there were still missing biostratigraphical data and detailed palaeoenvironmental discoveries, potentially due to the sediments being thoroughly checked with limited sampling intervals throughout the boreholes. In this study, a palynological investigation was conducted on 44 borehole samples from an 88-meter core retrieved from the Brunei Bay area with the aim of interpreting the past environment and attempting biostratigraphical analysis.

Samples underwent standard palynological preparation procedures, including chemical analyses such as chlorination and acetolysis in the laboratory. Then, treated samples were observed directly under a light microscope, where the palynomorphs were identified and quantified. Results revealed a total of 2,495 specimens from 26 families and 40 taxa, with the most abundant taxa including Rhizophoraceae (*Rhizophora* sp.) with 371 specimens found across all samples, followed by Sapotaceae (*Palaquium* sp.) and ferns Polypodiaceae (*Verrucatosporites usmensis*) with 321 and 316 specimens, respectively. Six forest types were identified, including mixed dipterocarp, mangrove, peat swamps, freshwater swamps, hill forests and hinterland vegetation, indicating possible transportation through river runoffs at that time. Our findings illustrate the environmental shifts in the past; mangrove forests thrived in the upper section (10m to 34m) due to the high presence of *Rhizophora* sp., and potentially located in a brackish environment, specifically within a lower delta plain area (Morley and Morley, 2013). Then the environment transitioned to a peat swamp in the middle section (40m to 55m) due to the occurrence of *Palaquium* sp. A barren section with sandy well-sorted units and the absence of pollen in the deeper section (58m to 64m) suggests a change to a riverbed environment that could possibly be caused by local events such as the Brunei Bay faulting. Mangrove taxa (*Sonneratia caseolaris*) and other swamp forest assemblages reappeared in the lower strata (67m to 88m), indicating a low-salinity swampy environment with a significant tidal influence.

Biostratigraphic analysis revealed that the samples are no older than the middle Miocene due to the presence of the extinct taxon Florschuetzia meridionalis in the deepest section of the core. The appearance of *Podocarpus* sp. in the middle section indicates the middle Pliocene age (Morley, 1991), and the upper section of the core is likely to be from the Holocene.

Figure 1: Light microscopy (LM) micrograph of palynomorph *Florschuetzia meridionalis* from Brunei Bay.

Keywords: Palynology, Brunei Bay, Palaeoenvironment, biostratigraphy, Mangrove

References

Morley, R.J., 1991. Tertiary stratigraphic palynology in Southeast Asia: Current status and new directions. Geological Society of Malaysia, Bulletin, 28, 1–36.

Morley, R.J., Morley, H.P., 2013. Mid-Cenozoic freshwater wetlands of the Sunda region. Journal of Limnology 72(s2). https://doi.org/10.4081/jlimnol.2013.s2.e2

Poster 11: Metamorphism in the Prydz Belt, East Antarctica constraints the evolution of the East Kuunga orogen

Wei-(RZ) Wang[1*]

[1]*Institute of Geomechanics, Chinese Academy of Geological Sciences, Beijing 100081, China*

*Corresponding author:
E-mail address: atwangwei@163.com (Wei-(RZ) Wang)

The Prydz Belt in East Antarctica preserves diverse rock types with a complex metamorphic history and thus is critical to understanding the tectono-metamorphic evolution of the east section of the Kuunga Orogen in East Antarctica. We investigated different types of metamorphic rocks by integrating petrological analysis, thermodynamic modeling, and in situ zircon and monazite geochronology. Phase equilibrium modeling and mineral thermometry based on detailed petrological and mineralogical analyses indicate that some granulites in the Larsemann Hills underwent extreme metamorphism with peak conditions to ultrahigh temperatures (UHT). The UHT metamorphism features extremely high dT/dP values along a clockwise path with evident decompression at high temperatures and subsequent near isobaric cooling. Textural relationships, *in situ* NanoSIMS zircon U–Pb analysis, and LA-ICP-MS zircon and monazite dating and trace element analysis indicate protracted tectono-thermal evolution from the latest Neoproterozoic to early Palaeozoic (*c.* 570–500 Ma), with a peak stage likely from *c.* 550 to *c.* 540 Ma, and a retrograde stage from *c.* 540 to *c.* 500 Ma. We further compile the existing age and composition data of zircon and monazite from the region's metamorphic rocks and link their critical characteristics to the metamorphic evolution of the Prydz Belt. The frequency of zircon U–Pb ages increases noticeably from ~555 Ma, peaking between 530 Ma and 520 Ma, followed by a dramatic decline after 520 Ma. High Th/U values (> 0.1) of zircon are observed from ~545 Ma, displaying a noticeable increasing trend in Th/U values before a rapid decline from ~520 Ma. The frequency of monazite ages progressively increases from ~540 Ma, reaching its peak at 515 Ma, and subsequently decreases dramatically after 490 Ma. Combined with the crystallization behaviors of zircon and monazite, the systematic changes in Th/U values of zircon after 545 Ma should indicate a transition in the thermal regime of the Prydz Belt towards the cooling stage. Abundant growth of zircon and monazite corresponds to the post-peak cooling process. In contrast, the crystallization peak of monazite lags behind that of zircon by ~5–15 Ma, which indicates a relatively low cooling rate. The compiled data suggest that the Pan-African event likely peaked at ~555–545 Ma and gradually cooled to near-solidus conditions at ~520–510 Ma, with a relatively slow average cooling process. The results provide constraints on the evolution of the East Kuunga orogen.

Poster 12: Archean banded iron formations (BIFs) in the Bundelkhand Craton, Indian Shield: a review

Ajay Kumar[1*], Pradip Kumar Singh[1], Balaram Sahoo[1]

[1]*Department of Geology, Banaras Hindu University (BHU), Varanasi, India.*

*Corresponding author:
E-mail address: ajaykumar.geo@bhu.ac.in (Ajay Kumar)

Banded iron formations (BIFs) are typically thin-bedded or laminated chemical sedimentary rocks comprising layers of iron- and silica-rich minerals and are important worldwide repositories of major environmental transitions and biological innovations in early Earth's history. Thus, the BIFs provide vital constraints on the geochemical evolution of the ancient crust of the Earth.

In Bundelkhand Craton, BIFs occur as alternating iron-rich and silica-rich layers. BIFs occur in several places as dismembered bodies, mainly in Mahoba, Mauranipur, and Babina of the central part and in the Girar, Baraitha, and Khurrat locations of the southern part of the Bundelkhand Craton. They are associated with ultramafic-mafic and felsic volcanic rocks as supracrustal remnants along the E–W trending Bundelkhand Tectonic Zone in the central part of the craton. In fact, in the Girar belt BIFs are interspersed with volcaniclastic sediments, mafic rocks, calc-silicates and quartzites. These BIFs commonly experienced multiple episodes of deformations and metamorphic overprints, making it difficult to identify the origin, relevant precipitation mechanism and tectonic settings. However, opinions are varied regarding the origin, tectonic setting and geochemical characteristics of BIF in this terrane.

Bundelkhand BIFs can be classified into three different types: (1) Least altered BIF (with well-defined bands); (2) Moderately altered BIF and (3) Strongly altered BIF. Moreover, it is important to highlight that the BIF samples from the Girar belt show well-defined bands of iron-rich and quartz-rich layers. Such kinds of bandings are similar to other Indian cratons and different parts of the world. In contrast, comparatively less defined bands are seen in the Babina and Mauranipur greenstone belts.

Since there is not much information available in the literature on the mechanism of precipitation and formation, the impact of metamorphism, and the direct radiometric data of age in Bundelkhand BIFs. Integrated petrological, geochemical and geochronological investigations could be very helpful in understanding the formation mechanism of the banded iron formations in the Bundelkhand Craton.

Poster 13: Late Silurian HT-LP metamorphism and anatexis of Kuhai Group in the southern East Kunlun Orogen: Implications for tectonothermal regime in the Proto- to Paleo-Tethys realm transition

Xiang Ren[1,2*], Yunpeng Dong[2], Christoph A. Hauzenberger[3], Dengfeng He[2], Inna Safonova[1]

[1] *Faculty of Geosciences and Engineering, Southwest Jiaotong University, Chengdu 611756, China*
[2] *State Key Laboratory of Continental Dynamics, Department of Geology, Northwest University, Northern Taibai Str. 229, Xi'an 710069, China*
[3] *Institute of Earth Sciences - NAWI Graz Geocenter, University of Graz, Universitaestplatz 2, Graz 8010, Austria*

*Corresponding author:
E-mail address: xiang.r@outlook.com (Xiang Ren)

A forearc environment is usually characterized by a relatively low geothermal gradient with little magmatism and a low degree of metamorphism unless the geodynamic setting beneath the subduction zone has changed. Thus, recognition of thermal anomaly in the forearc setting is critical to understanding the change of geodynamics in the suprasubduction zone. The East Kunlun Orogen (EKO) lays along the northern margin of the Tibetan Plateau, sandwiched between the Proto-Tethys and Paleo-Tethys domains, and is a typical accretionary orogen. The southern EKO was considered as a forearc accreted terrane formed during long-term tectonics of the Proto-Tethys and Paleo-Tethys oceans. Here, we report metamorphic timing and P-T condition of migmatitic paragneiss of the Kuhai Group, as well

as geochronology and geochemistry of anatectic S-type granites to determine tectonothermal events that occurred in southern EKO, shedding light on change in geodynamics in the subduction zone. The paragneiss of the Kuhai Group contains a phase assemblage of garnet + biotite + plagioclase + K-feldspar + quartz + muscovite + melt ± sillimanite ± ilmenite, typical of amphibolite-facies metamorphism. Garnet porphyroblasts are free of mineral inclusions and show homogeneous chemical zoning revealed by mineral chemistry, suggesting garnets probably preserve only the final peak metamorphic P-T condition. According to geothermobarometers and thermodynamic modelling, the P-T of peak metamorphism was estimated at 690–740 °C and 5.5–7.4 kbar. The *in-situ* U-Pb isotopic dating of monazites in thin sections of paragneiss constrained the metamorphic time at ca. 430 Ma. The migmatitic paragneiss of the Kuhai Group is characterized by intrusion of leucocratic granitic sills parallel to the foliation, which contains typical aluminous minerals of muscovite and garnet, representative of S-type granites. Integrated monazite Th-U-Pb_{total} and zircon U-Pb dating estimated the formation time of S-type granites at ca. 440 Ma. Based on geochemical features, S-type granites can be divided into two groups. One group is composed of muscovite granites with strongly peraluminous signature (ASI > 1.1), low Sr content (63–126 ppm) and CaO/Na_2O ratio (0.08–0.20), whereas high Rb/Sr ratios (0.56–2.53). The other is dominated by two-mica granites showing opposing geochemical features, for example, moderately peraluminous nature (ASI = 1.02–1.09), higher CaO/Na_2O ratios (0.47–0.96) and Sr contents (207–324 ppm), as well as exceptionally lower K_2O contents (0.74–1.46 wt.%) and Rb/Sr ratios (0.04–0.32) relative to muscovite granites. By compared with experimental results of partial melting of metasedimentary rocks, muscovite granites were more likely produced by dehydration melting of metapelites, and conversely, the two-mica granites were derived from partial melting of metagreywackes at excess water contents. Our results suggest that the Kuhai Group experienced upper amphibolite-facies metamorphism in the Late Silurian, accompanied by local anatexis of sedimentary rocks to produce S-type granitic melts. Such low metamorphic T/P ratio (ca. 1000 °C/GPa) of the Kuhai Group implies heat anomaly in the forearc accreted terrane of southern EKO, possibly due to upwelling of mantle magmas related to the breakup of subducting slab or subduction of oceanic ridge beneath southern margin of EKO. Therefore, we argue the subduction in the southern margin of EKO still continued in the Late Silurian, and argued against the closure of the Proto-Tethys Ocean in the Late Silurian, and subsequent evolution into the Paleo-Tethys domain in late Paleozoic time in the southern end of EKO.

Poster 14: Assessing the risks and identifying highly vulnerable regions from lahars around Mount Rainier Volcano, USA

Kitty Murtha[1*], Manoj Mathew[1,*], David Kidd[1]

[1]*Department of Geography, Geology and the Environment, Kingston University London, Kingston upon Thames KT1 2EE, United Kingdom*

*Corresponding author:
E-mail address: Kittymurtha@gmail.com (Kitty Murtha); m.mathew@kingston.ac.uk (Manoj Mathew)

A consequential and profound deleterious ramification of climate change-driven physiographic change is the conspicuous amplification in the frequency and magnitude of geohazards affecting global communities. Despite not receiving the deserved attention relative to other more commonly investigated geohazards, ostensibly due to its occurrence being confined to very specific and distinct geographic and geological settings (i.e., volcanic landscapes), lahars or water-saturated volcanic mass-mudflows are a catastrophic geohazard that is gravity-driven, discrete, rapidly mobile (between 10–100 km/h) and far-reaching (>100 km downstream of volcanoes) (Pierson et al., 2014; Thouret et al., 2020). In the absence

of robust and reliable warning systems, lahars are very difficult to predict and account for 26% of total volcano-related fatalities since 1500 AD around the world (Brown et al., 2017). A pertinent case in point for this devastating geohazard that significantly threatens the security, economic well-being, and resources of communities in the vicinity of volcanoes is Mount Rainier, a stratovolcano in Washington State, USA, nestled in the Cascade Range (**Fig. 1**). Inasmuch as Mount Rainier hosts a formidable glacial cover, substantial surface water, and hillslopes with hydrothermally weakened rocks and clay minerals, which collectively contributed to significant prehistoric lahars and increase susceptibility to future incidents (Vinnell et al., 2021), there remains a paucity of information in regard to specific regions that could be impacted if a lahar were to descend downstream from Mount Rainier. Here we show the locations at greatest risk from lahars within a 100 km radius of Mount Rainier through a mechanistic and comprehensive multi-criteria assessment that utilises datasets pertaining to population density, Land Use Land Cover, Normalized Difference Vegetation Index, Topographic Wetness Index, geology/surficial sediments, precipitation, slope, elevation, distance to rivers and roads, and drainage density that was organised and analysed within a GIS environment to identify and prioritise vulnerable areas. GIS-based multi-criteria decision analysis combines geographical data and transforms many preferences to obtain significant information that aids decision-makers (Malczewski and Rinner, 2015). This technique has been successfully implemented in various studies from different parts of the world, ranging from flood hazard to coastal hazard management (e.g., Gigović et al., 2017; Rahmati et al., 2017; Ajjur and Mogheir, 2020; Mathew et al., 2020; Ariffin et al., 2023).

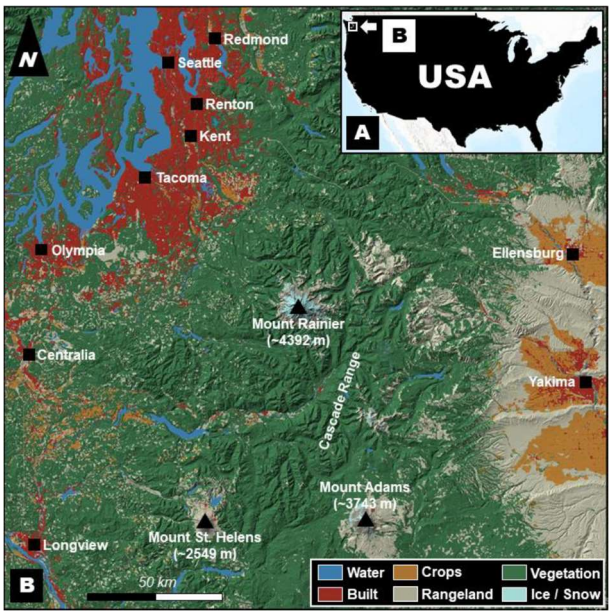

Figure 1. Location of Mount Rainier and Land Use Land Cover (LULC) characteristics of the stratovolcano and proximal (100 km radius) regions.

The approach adopted in this study to identify regions highly vulnerable to lahars involved determining and defining the aforementioned criteria. Following this, we transformed the values of each criterion to a common, relative, dimensionless scale (standardisation). We then weighted the significance of each criterion and, finally, combined and aggregated the criteria. In the occasion of an adverse lahar event, our results demonstrate that Seattle, Tacoma, Longview and surrounding areas are eminently at risk and require priority in terms of management strategies. Additionally, high-risk hotspots are identified around Olympia, Kent and Renton also due to their high population density. Areas of moderate risk within proximity to Mount Rainier emphasise the importance of protecting campgrounds and information centres within the National Park, due to their location along river valleys and near steep topography. We propose requisite and tailored mitigation strategies based on the characteristics of each location, vulnerability level and existing mitigation strategies. Examples of these include extending the early warning alert system beyond the Puyallup Valley to cover more urban areas and an enhanced education system for vulnerable groups. Within the National Park, recommendations included distributing leaflets to tourists on arrival and increased signage at campsites. Our work provides

valuable insights into lahar vulnerability and risk mapping, informing evidence-based mitigation strategies that can be utilised by policymakers and communities to safeguard against these geohazards in volcanic landscapes elsewhere.

References

Ajjur, S.B., Mogheir, Y.K., 2020. Flood hazard mapping using a multi-criteria decision analysis and GIS (case study Gaza Governorate, Palestine). Arabian Journal of Geosciences 13(2), 44.

Ariffin, E.H., Mathew, M.J., Roslee, A., Ismailluddin, A., Yun, L.S., Putra, A.B., Yusof, K.M.K.K., Menhat, M., Ismail, I., Shamsul, H.A., Menier, D., 2023. A multi-hazards coastal vulnerability index of the east coast of Peninsular Malaysia. International Journal of Disaster Risk Reduction 84, 103484.

Brown, S.K., Jenkins, S.F., Sparks, R.S.J., Odbert, H., Auker, M.R., 2017. Volcanic fatalities database: analysis of volcanic threat with distance and victim classification. Journal of Applied Volcanology 6 (15), 1–20.

Gigović, L., Pamučar, D., Bajić, Z., Drobnjak, S., 2017. Application of GIS-interval rough AHP methodology for flood hazard mapping in urban areas. Water 9(6), 360.

Malczewski, J., Rinner, C., 2015. Multicriteria decision analysis in geographic information science (Vol. 1, pp. 55-77). New York: Springer.

Mathew, M.J., Sautter, B., Ariffin, E.H., Menier, D., Ramkumar, M., Siddiqui, N.A., Delanoe, H., Del Estal, N., Traoré, K. and Gensac, E., 2020. Total vulnerability of the littoral zone to climate change-driven natural hazards in north Brittany, France. Science of the Total Environment 706, 135963.

Pierson, T.C., Wood, N.J., Driedger, C.L., 2014. Reducing risk from lahar hazards: concepts, case studies, and roles for scientists. Journal of Applied Volcanology 3, 1-25.

Rahmati, O., Zeinivand, H., Besharat, M., 2016. Flood hazard zoning in Yasooj region, Iran, using GIS and multi-criteria decision analysis. Geomatics, Natural Hazards and Risk 7(3), 1000-1017.

Thouret, J.C., Antoine, S., Magill, C., Ollier, C., 2020. Lahars and debris flows: Characteristics and impacts. Earth-Science Reviews 201, 103003.

Vinnell, L.J., Hudson-Doyle, E.E., Johnston, D.M., Becker, J.S., Kaiser, L., Lindell, M.K., Bostrom, A., Gregg, C., Dixon, M., Terbush, B., 2021. Community preparedness for volcanic hazards at Mount Rainier, USA. Journal of Applied Volcanology 10(1), 10.

Poster 15: Reconstructing paleosalinity in the Patuxent Estuary through diatom assemblages

Dylan Pilling[1*], Glenn Havelock[1]

[1]*Department of Geography, Geology and the Environment, Kingston University London, Kingston upon Thames KT1 2EE, United Kingdom*

*Corresponding author:
E-mail address: k2154442@kingston.ac.uk (Dylan Pilling)

Anthropogenic climate change is causing sea levels to rise worldwide, threatening coastal habitats such as tidal marsh with saltwater inundation. An understanding of environmental change in tidal marsh over recent history provides context for assessing current sea level rise dynamics. Here we analysed a 3-metre sediment core recovered from a tidal marsh on the Patuxent, a sub-estuary of Chesapeake Bay. We used diatom assemblages to reconstruct paleosalinity over the late Holocene. Diatoms were extracted by digesting samples with heated H_2O_2 and centrifuging. The samples were placed on microscope slides with Naphrax mountant, and diatoms were identified using a binocular microscope at 100x magnification with immersion oil. Loss on ignition tests for organic, moisture, and carbonate content and grain size data were also taken to reconstruct environmental change on the site. A second core went to James Madison University, where an age model was constructed to provide a geochronology. Our results indicate that from the base of the core, approximately 1k years ago, the site was a brackish tidal flat, with predominately silty sediment that supported a mixture of freshwater and marine diatom taxa. At 84 cm, approximately 1820, the site transitioned to an argillaceous depositional environment with an abundance of freshwater diatom taxa such as *Amphora Copulata*. However, from 54 cm, approximately 1970, this trend started to reverse, with an abundance of brackish-marine species being observed, particularly *Melosira Nummuloides,* and a higher proportion of sand. These results indicate that the site initially transitioned to a freshwater and argillaceous environment mainly as a result of slower relative sea level rise and higher levels of precipitation. Early industrial development

may have also played a role in increasing sediment input to the site. Marine intrusion from accelerating sea level rise is now inundating the marsh and driving it further inland, leading to coastal squeeze. This project could act as a pilot study for further research and would greatly benefit from higher-resolution sampling and a deeper core.

Poster 16: A multi-variable coastal vulnerability evaluation of the east Sussex coast, UK

Nataphon Reuangkhum[1], Manoj Mathew[1*], Ikhmal Siddiq[2], Effi Helmy Ariffin[2], David Menier[3], Benjamin Sautter[3], Mu Ramkumar[4], David Kidd[1]

[1]*Department of Geography, Geology and the Environment, Kingston University London, Kingston upon Thames KT1 2EE, United Kingdom*
[2]*Institute of Oceanography and Environment, Universiti Malaysia Terengganu, Kuala Nerus, Terengganu 21030, Malaysia*
[3]*Geo-Ocean, UMR CNRS 6538, Université Bretagne Sud, 56017, Vannes, France*
[4]*Department of Geology, Periyar University, Salem 636011, India*

*Corresponding author:
E-mail address: m.mathew@kingston.ac.uk (Manoj Mathew)

Global changes in atmospheric and oceanic mechanisms are projected to increase in frequency and magnitude due to anthropogenically increased uses of carbon-emitting fossil fuels, which will greatly induce several natural hazards, especially within coastal regions. This will profoundly impact the world's population, which is expected to grow to 9.1 billion by 2050, and even more significantly affect one-third of the population who live within 100 km proximity of the coast. The southern coast of England is experiencing climate-driven sea-level rise, natural hazards (e.g., landslides, floods, cliff retreat, mass movement, debris flow, rock fall, etc.) and increasing storm frequency and magnitude. Among the most affected coasts of the UK is East Sussex because of the geomorphology, geology and geographic context of the zone. This study aims to identify areas at risk, which are vulnerable to coastal hazards. To facilitate this research, we endeavoured to understand shoreline dynamics along the coast of east Sussex by quantifying cliff retreat rates in the study area, identifying zones undergoing intense coastal erosion and accretion, and calculating coastal vulnerability using a multi-variable approach organised within a GIS environment. In this study, a DEM of Difference using LiDAR digital terrain models of one-meter resolution was produced to analyse cliff retreat rates over 14 years between 2008 and 2022. The results produced using LiDAR data exhibit an average of 10 m cliff retreat over the past 14 years. Moreover, a multivariate statistical analysis using six variables (geology, superficial soils, population density, mean annual rainfall, land use cover, and slope) was quantified to infer nuanced interpretations of the most vulnerable wards to climate-induced natural hazards. The results show that the majority of the wards along the west coast of east Sussex that have moderate to high population densities (per 1 km²), such as Peacehaven East Ward, Newhaven South Ward, and Seaford West Ward, are at higher risk due to highly elevated cliffs and steep slopes along the beach line. When compared to the LiDAR results, areas along these wards show significant levels of cliff retreat averaging 10 meters. Additionally, an assessment of the shoreline dynamics was employed to investigate the rate of erosion and accretion in zonal areas along the east Sussex coast through the statistics of net shoreline change, linear regression rate, and weighted linear regression. The results produced from the analysis illustrate moderate to high rates of erosion throughout the entire study area. However, the Meads Ward, which encompasses the heavily urbanised and densely populated city of Eastbourne and the natural capital and

habitat-rich Seven Sisters Country Park, has the highest level of erosion. The ward also exhibits the highest level of cliff retreat due to its high steep sloped chalk cliffs and highest level of rainfall, compared with other wards. The following wards - Peacehaven East, Newhaven South, Seaford West, Seaford South, South Downs, and Meads - are highly vulnerable to climate change, sea-level rise, erosion, and coastal hazards. This vulnerability stems from the soft geology of the area, which includes chalk, mudstones, and clays. These geological formations are easily eroded due to moderate to high annual precipitation rates that the wards experience at an annual average of 799.189 – 961.695 mm (over 19 years). Furthermore, these wards feature low-angled gravel beaches that are bordered by high, steep cliffs ranging from 47.077 to 88.921 degrees. These cliffs are prone to failure, slumping, and sinkholes, heightening the vulnerability of these areas. If forward modelling climate analysis proves accurate, escalation of atmospheric and oceanic changes will increase coastal vulnerabilities of coastal communities and damage coastal habitats that provide humans with valuable natural capital assets and ecosystem services. This is a critical issue for the coastal region of East Sussex. Business infrastructure, residential homes, and marine and terrestrial habitats along the most vulnerable wards highlighted from the analysis will all be detrimentally affected if Representative Concentration Pathways (RCP) reach global temperatures of 4.3°C (RCP 8.5). These wards are anticipated to experience detrimental effects within the next 14 years if the average cliff retreat rate of 10 meters per year continues and may increase in severity if global warming rates reach RCP 8.5. To address these challenges, a comprehensive shoreline management plan is needed to mitigate the potential impacts of climate change.

Poster 17: Types, distribution and origins of micro-continents in the ocean

Wang Guangzeng[a,b*], Li Sanzhong[a,b*], Suo Yanhui[a,b], Wang Pengcheng[a,b], Zhu Mengjia[a], Song Taihai[a]

[a]*Frontiers Science Center for Deep Ocean Multispheres and Earth System, Key Lab of Submarine Geosciences and Prospecting Techniques, MOE and College of Marine Geosciences, Ocean University of China, Qingdao, 266100, China*
[b]*Laboratory for Marine Mineral Resources, Qingdao Marine Science and Technology Center, Qingdao, 266237, China*

*Corresponding authors:
E-mail address: Wangguangzeng@ouc.edu.cn (Wang Guangzeng); Sanzhong@ouc.edu.cn (Li Sanzhong)

The complexity of continental plate composition is undeniable, but oceanic plates are also not as simple as described in plate tectonics theory. Geological and geophysical surveys, as well as seabed drilling, have confirmed that the internal structure of ocean basins is equally complex. Within the major oceans on Earth, there are numerous small blocks embedded like patches, reflecting a variety of tectonic events that the oceanic plates have experienced during their formation and evolution, including their inception, growth, translocation, rotation, shifting, drifting, subduction, and collision. Along with these processes, not only the giant oceanic plates but also numerous microplates in them are formed, in which many submerged or isolated microcontinents are involved, such as Jan Mayen Ridge (Kandilarov et al., 2012), Seychelles Plateau (Ashwal, 2019) and Lord Howe Plateau (Schellart et al., 2006). Global magnetic and gravity anomaly maps show that these blocks are mainly located in the Atlantic, Indian, and Pacific Oceans, not far from continental margins. They are formed by tectonic processes possibly related to back-arc spreading, ridge jumping, extensional rifting, and transform faulting, which lead to the separation of micro-continents from continental margins. Therefore, based on their origins, microcontinental blocks in the oceans can be classified into detachment-derived (Péron-Pinvidic and Manatschal, 2010), ridge jumping-derived (Péron-Pinvidic et al., 2012; Misra et al., 2015), rifting-derived (van den Broek et al., 2020), transform-derived micro-continents (Bennett et al., 2013). The first two are mainly formed at passive continental margins, while the latter two develop at active continental margins. As oceanic plates subduct, different types of microcontinents in the oceans may

collide and accrete onto continents, forming accretion-related microcontinents like the Philippine Island arc. Thus, in geotectonic study, it is important not only to search for vanished oceans in ancient orogenic belts but also to look for submerged or isolated continents in modern oceans, in order to more accurately understand the oceanic-continental transformation and evolution and to reconstruct the true geological history of Earth's tectonics.

References:

Ashwal. L.D., 2019. Wandering continents of the Indian Ocean. South African Journal of Geology 122, 397–420 https://doi.org/10.25131/sajg.122.0040

Bennett, S. E. K., Oskin, M. E., Iriondo, A., 2013. Transtensional rifting in the proto–Gulf of California near Bahía Kino, Sonora, México. GSA Bulletin 125, 1752–1782.

Kandilarov, A., Mjelde, R., Pedersen, RB. Hallevang, B., Papenberg, C., Petersen, C.J., Planert, L., Flueh, E., 2012. The northern boundary of the Jan Mayen microcontinent, North Atlantic determined from ocean bottom seismic, multichannel seismic, and gravity data. Marine Geophysical Research 33, 55–76. https://doi.org/10.1007/s11001-012-9146-4

Péron-Pinvidic, G., Manatschal, G., 2010. From microcontinents to extensional allochthons: witnesses of how continents rift and break apart? Petroleum Geoscience 16, 189–197

Peron-Pinvidic, G., Gernigon, L., Gaina, C., Ball, P., 2012. Insights from the Jan Mayen system in the Norwegian–Greenland Sea—II. Architecture of a microcontinent. Geophysical Journal International 191, 413–435

Misra, A. A., Sinha, N., Mukherjee, S., 2015. Repeat ridge jumps and microcontinent separation: insights from NE Arabian Sea. Marine and Petroleum Geology 59, 406–428

Schellart, W.P. Lister, G.S., Toy. V.G.A., 2006.Late Cretaceous and Cenozoic reconstruction of the Southwest Pacific region: Tectonics controlled by subduction and slab rollback processes. Earth-Science Reviews 76, 191–233

van den Broek, J.M., Magni, V., Gaina, C., Buiter, S.J.H., 2020. Theformation of continental fragments in subduction settings: The importance of structural inheritance and subduction system dynamics. Journal of Geophysical Research: Solid Earth, 125,e2019JB018370. https://doi.org/10.1029/2019JB018370

Poster 18: Apatite geochemical perspectives on the maturation of continental arc crust via mush remobilization during magmatic flare-up

Long Chen[1,2,*], Peng Gao[3,4,*], Ian Somerville[5], San-Zhong Li[1,2], Jiang-Hong Deng[6], Dong-Yong Li[1,2], Sheng-Yao Yu[1,2], Xiao-Hui Li[1,2], Hua-Hua Cao[1,2], Zi-Fu Zhao[3,4], Zhi-Feng Yin[7,8]

[1]*Frontiers Science Center for Deep Ocean Multispheres and Earth System, Key Lab of Submarine Geosciences and Prospecting Techniques, MOE and College of Marine Geosciences, Ocean University of China, Qingdao 266100, China*
[2]*Laboratory for Marine Mineral Resources, Qingdao National Laboratory for Marine Science and Technology, Qingdao 266061, China*
[3]*CAS Key Laboratory of Crust-Mantle Materials and Environments, School of Earth and Space Science, University of Science and Technology of China, Hefei 230026, China*
[4]*Center of Excellence for Comparative Planetology, Chinese Academy of Sciences, Hefei 230026, China*
[5]*UCD School of Earth Sciences, University College Dublin, Belfield, Dublin 4, Ireland*
[6]*Center of Deep-Sea Research, Institute of Oceanology, Center for Ocean Mega–Science, Chinese Academy of Sciences, Qingdao 266071, China*
[7]*School of Materials Science and Engineering, Yancheng Institute of Technology, Yancheng, 224051, China*
[8]*Key Laboratory for Ecological-Environment Materials of Jiangsu Province, Yancheng Institute of Technology, Yancheng, 224051, China*

*Corresponding authors:
E-mail address: chenlong@ouc.edu.cn (L. Chen); gaopeng05@ustc.edu.cn (P. Gao)

In volcanic arcs, magma evolves from basaltic to intermediate and felsic compositions, known as volcanic arc maturation. The role of magma mushes during flare-ups is unclear. This study revealed a three-stage evolution of plutonic rocks from mafic (~94 Ma) to intermediate (~92–88 Ma) to felsic (~88 Ma) during a magmatic flare-up event in the Gangdese arc, Tibet, with increasing radiogenic Sr–Nd

isotope enrichment. Apatite in mafic and felsic rocks have $\varepsilon_{Nd}(t)$ values similar to their hosts, while intermediate rocks show higher values. The elemental composition of apatite in mafic and intermediate rocks is similar but differs from those in felsic rocks. Triangular and linear covariation relationships between apatite-compatible (e.g., La) and -incompatible (e.g., Rb) elements with SiO_2, respectively, for all three rock stages as a whole, confirm the incorporation of apatite-rich mushes into the mixing process. Textural and compositional features indicate varying degrees of influence of mafic rock compositions by accumulation. These findings suggest that mafic magma crystallized into apatite-rich mush, which was later remobilized and mixed with felsic magma to form intermediate magma. Felsic rocks represent end-member magmas resulting from crustal anatexis and/or mafic magma differentiation. Thus, the Gangdese arc's maturation during the magmatic flare-up progressed sequentially through mafic magma crystallization and mush formation, mush remobilization and mixing with felsic magma, and the eventual accumulation and segregation of felsic magma. This sequence of events during flare-ups illustrates a common crustal maturation process in volcanic arcs, as also seen in the Andean Cordillera.

Poster 19: Deformation and Mineralization at Paramanahalli Gold Deposit: Insights from Microstructures

Manju Sati[1*], Rajagopal Krishnamurthi[1], Sakthi Saravanan Chinnasamy[2]

[1]*Department of Earth Sciences, Indian Institute of Technology, Roorkee-247667, India*
[2]*Department of Earth Sciences, Indian Institute of Technology, Powai, Mumbai-400076, India*

*Corresponding author:
E-mail address: msati@es.iitr.ac.in (Manju Sati)

The Paramanahalli gold deposit, located approximately 7 km west of the Chitradurga Shear Zone (CSZ) within the Chitradurga Greenstone Belt (CGB) in Karnataka, exhibits significant shear zone-controlled gold mineralization. The CGB has experienced major three notable deformation phases (Roy et al., 2020) where the first phase (D1) is characterized by isoclinal folding and the development of foliations parallel to bedding planes within metasedimentary rocks. The second deformation phase (D2) led to the formation of the regional "Chitradurga Fold" and the development of the N-S trending CSZ (Kolb et al., 2004). During the third phase (D3), these D1 and D2 structures were refolded into E-W trending warps and kink folds (Mukhopadhyay et al., 1981; Roy et al., 2020). Gold mineralization is hosted within altered metabasalt and Banded Iron Formation (BIF) of the Hiriyur Formation, part of the Chitradurga Group, which has undergone ductile-brittle deformation. Microstructures observed in this study, comparable to those in many orogenic gold deposits, reveal significant ductile deformation features such as strain fringes made by quartz adjacent to pyrite (**Fig.1a**), rotation of foliation (**Fig.1b**), mica fish (**Fig.1d**), kink bands, micro folds (**Fig.1e**), quartz pods (**Fig. 1f**), and pinching and swelling of veinlets. Brittle deformation is evidenced by the brecciation of quartz (**Fig.1c**) and displacement of bands in BIF. This research analyzes these deformation phases and their impact on gold mineralization within the CGB. Gold mineralization is associated with the D2 deformation phase, where CSZ has played a crucial role as a conduit for ore-bearing hydrothermal fluids, forming auriferous quartz veins.

The quartz grains within veins show bulging recrystallization and deformation lamellae, pointing to low-temperature dynamic recrystallization at approximately 300-350˚C (Passchier and Trouw, 2005). Characterizing these microstructural features enhances our understanding towards gold metallogeny in CGB and provides valuable insights for future exploration and resource discovery.

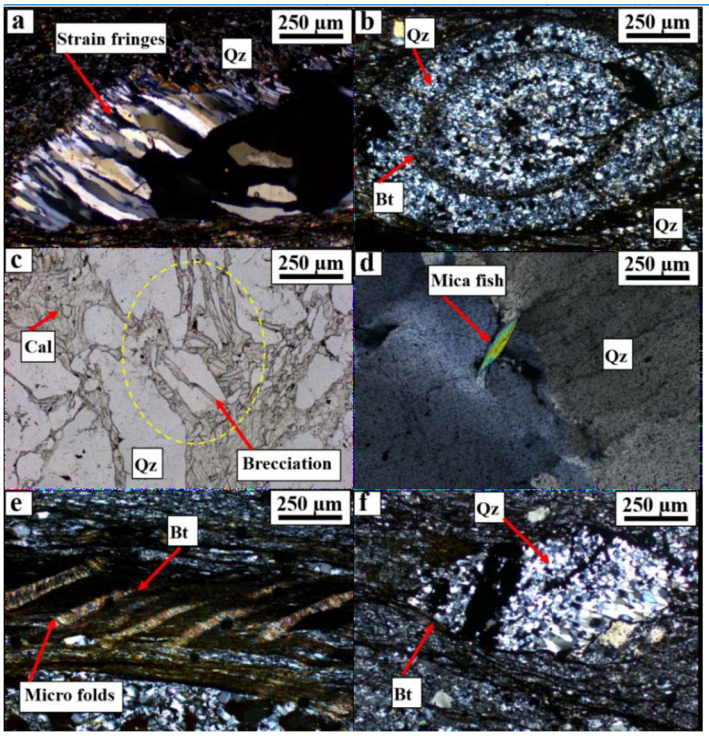

Figure 1. Photomicrographs: (a) Strain fringes consist of quartz in phyllite. (b) Circular foliation in metagraywacke. (c) Brecciation of quartz by later filled calcite. (d) Mica fish adjacent to quartz. (e) Micro folds consist of biotite within phyllite. (f) Quartz filling metagraywacke. Qz-quartz, Bt-biotite, Cal-calcite.

Keywords: Microstructures, Deformation, Orogenic gold, Paramanahalli, Gold metallogeny

References

Kolb, J., Hellmann, A., Rogers, A., Sindern, S., Vennemann, T., Böttcher, M. E., Meyer, F. M., 2004. The role of a transcrustal shear zone in orogenic gold mineralization at the Ajjanahalli Mine, Dharwar Craton, South India. Economic Geology 99(4), 743–759.

Mukhopadhyay, D., Baral, M. C., Ghosh, D., 1981. A tectonostratigraphic model of the Chitradurga schist belt, Karnataka, India. Journal of the Geological Society of India 22(1), 22–31.

Passchier, C. W., Trouw, R. A. J., 2005. Microtectonics. Springer Science & Business Media.

Roy, A., Ramachandra, H. M., Sengupta, S., 2020. Interpretation of stratigraphy and structure of the Neoarchaean Dharwar Supergroup of rocks in Chitradurga area, Dharwar Craton. Journal of Earth System Science 129(1), 1–21. https://doi.org/10.1007/s12040-020-1350-z.

Poster 20: Quantification of metasomatic alterations in Jahaz U-deposit, Khetri Belt, Aravalli Craton, India: Using Lithogeochemical approach

Priyanka Mishra[1*] and Rajagopal Krishnamurthi[1]

[1]*Department of Earth Sciences, Indian Institute of Technology Roorkee, Uttarakhand-247667, India*

*Corresponding author:
E-mail address: pmishra@es.iitr.ac.in (Priyanka Mishra)

Jahaz U-deposit, located along the *"albitite line"* of the North Delhi Fold Belt, India, and hosted within the Meso-Proterozoic metamorphic rocks of the Delhi Supergroup. U-mineralization is medium-tonnage (~8000 tU), low-grade (0.06% U_3O_8), metasomatic type, and shear-hosted. The major metamorphic rocks found in the Jahaz area are quartzite, quartz biotite schist, and amphibolite, which have undergone deformation and alteration. The altered rocks are classified into two types based on petrography: *(i)* least to moderately altered (LTMA) and *(ii)* intensely altered (albitized). Presently the samples are litho-geochemically assessed using PER (Pearce element ratio) and GER (General element ratio). This study aims to quantify the material transfer in altered rocks and delineate uranium-mineralized zones to explore the radioactive minerals using GER/PER analyses. The Zr, Hf, and Ta are found to be less mobile during fluid-rock interaction. The GER plot identifies alteration and accurate quantification of the extent of alteration. The (Na + K)/Al versus Na/Al, the data points fall along the

line joining the albite node to the muscovite node. It indicates the predominance of albite in the albitized rocks as compared to LTMA rocks (**Fig. 1a**). The (Na + K)/Al versus K/Al also confirms the clustering of samples around the albite node, and a few samples trend towards the chlorite node from albite, suggesting the presence of chlorite in albitized rocks (**Fig. 1b**). The (Na+K)/Al versus (Fe+Mg)/Al plot corroborates the trend of chloritization in the altered rocks (**Fig. 1c**). The albitized rocks exhibit higher molar (2Ca+Na+K)/Al and lower molar K/Al ratios than LTMA rocks, indicating the depletion of K and enrichment in Ca and Na in the albitized rocks (**Fig. 1d**). The positive correlation found between U and Na, whereas negative with K in the albitized rocks (**Fig. 1e**). The higher enrichment of Na, Ca, Mg, and depletion of K observed in the albitized rocks. The enrichment of K shows more formation of sericite and biotite formation in LTMA rocks. Hence, albitization, chloritization, calcitization, sericitization, and biotitization are common metasomatic alterations identified in the mineralized zones of the Jahaz U deposit.

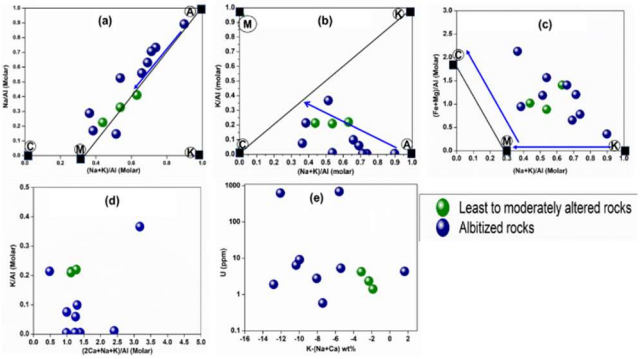

Fig. 1. (a–e) GER (molar ratio) scatter plots: **(a)** (Na+K)/Al vs. Na/Al indicate a predominance of albite as compared to chlorite, the blue arrow shows K enrichment; **(b)** (Na+K)/Al vs. K/Al shows the albitization followed by sericitization, the blue arrow shows K enrichment; **(c)** (Na+K)/Al vs. (Fe+Mg)/Al, showing the trend of chloritization; **(d)** (2Ca + Na + K)/Al vs. K/Al showing the presence of albite and calcite; **(e)** K-(Na+Ca) vs. U depicting positive correlation with U and Na, Ca. Nodes of albite (A), K-feldspar (K), chlorite (C), muscovite (M), and biotite (B) are shown.

Keywords: Metasomatism, U-mineralization, Pearce element ratio, General element ratio, North Delhi Fold Belt

Poster 21: Detrital zircon U–Pb geochronology revealing an early formation of proto-Japan: Reconstruction of Ordovician arc along the Terra Australis Orogen of northeastern Gondwana

Keisuke Suzuki[a,*], Toshiyuki Kurihara[b], Hidetoshi Hara[a], Kenichi Ishikawa[c], Takeru Otsuki[d], Hayato Ueda[b]

[a]*Geological Survey of Japan, AIST, 1–1–1 Higashi, Tsukuba, Ibaraki 305–8567, Japan*
[b]*Department of Geology, Faculty of Science, Niigata University, Niigata 950–2181, Japan*
[c]*Asahi Kohmatsu Co. Ltd, Ueno 110–0002, Japan*
[d]*East Japan Railway Company, 2–2–2 Yoyogi, Shibuya-ku, Tokyo, Japan*

*Corresponding author:
E-mail address: suzuki.k@aist.go.jp (Keisuke Suzuki)

Detrital zircon U–Pb geochronology has been widely applied to lower Paleozoic sedimentary rocks in the sutures and orogens of Asia, which have advanced our understanding of the complex orogenic histories between the Proto-Tethys and Paleo-Pacific oceans and northeast Gondwana, such as in India and Australia (Li et al., 2018). Recently, the author applied this approach to the Devonian–Permian strata of the Hida Gaien belt in southwest Japan, in terms of the content of Precambrian zircons and their sediment supply in each period, suggesting the involvement of the breakup of Gondwana in the paleogeographic transition of proto-Japan (Suzuki et al., 2023). However, it is still uncertain whether

the reconstructed position of proto-Japan in the early evolution of Gondwana is the Proto-Tethys or Paleo-Pacific oceans.

To further understand the paleogeographic relationship between proto-Japan and northeastern Gondwana in the early Paleozoic, we focused on the South Kitakami belt (SKB) in northeast Japan. In the western SKB, lower Paleozoic metamorphic rocks (the Motai and Matsugadaira metamorphic complexes) derived from accretionary complexes are unconformably overlain by Upper Devonian shallow-marine strata (the Tobigamori and Ainosawa formations). A plant fossil (*Leptophloeum*) in the Upper Devonian strata is a traditional indicator for the paleogeographic link between northeastern Gondwana regions, such as eastern and northwestern Australia, southern China, and Inner Mongolia (Saito and Hashimoto, 1982). Therefore, detrital zircons from these rocks can provide important data for understanding the formation of subduction zones and magmatic arcs in northeastern Gondwana.

Here, we report detrital zircons in Ordovician psammitic and siliceous schists of the western SKB. Their age peaks consist mainly of 480–470 Ma, 650–550 Ma, and 1300–900 Ma, which can be interpreted as a Pacific Gondwana signature (Purdy et al., 2016), indicating a tectonic association with the Terra Australis Orogen that developed along the northeastern Gondwanan margin and Paleo-Pacific Ocean, extending from eastern Australia (i.e., the Thomson, Lachlan, and Delamerian orogens) to Antarctica (i.e., the Ross Orogen). In northeast Asia, the Pacific Gondwana detrital zircons and 480–470 Ma zircons occur in the Bainaimiao arc belt along the northern margin of the North China Craton and in the Jiangyu continental arc in the Jilin area (Zhang et al., 2014). The magmatic arcs of proto-Japan and these regions were part of the Terra Australis Orogen during the Ordovician. Although previous studies have interpreted Proto-Japan as originating from the eastern margin of the South China Block (Isozaki, 2023), the U–Pb age spectra of the block have a pattern with affinity to the provenance on the Proto-Tethyan and northern Indian realms (Chen et al., 2021), which is distinctly different from our data.

References

Chen, Q., Zhao, G., Sun, M., 2021. Protracted northward drifting of South China during the assembly of Gondwana: Constraints from the spatial-temporal provenance comparison of Neoproterozoic–Cambrian strata. Geological Society of America Bulletin 133, 1947–1963. https://doi.org/10.1130/B35791.1

Isozaki, Y., 2023. Ordovician Japan: geotectonic setting and palaeogeography. Geological Society, London, Special Publications 533, 505–517. https://doi.org/10.1144/SP533-2022-8

Li, S., Zhao, S., Liu, X., Cao, H., Yu, S., Li, X., Somerville, I., Yu, S., Suo, Y., 2018. Closure of the Proto-Tethys Ocean and Early Paleozoic amalgamation of microcontinental blocks in East Asia. Earth-Science Reviews 186, 37–75. https://doi.org/10.1016/j.earscirev.2017.01.011

Purdy, D. J., Cross, A. J., Brown, D. D., Carr, P. A., Armstrong, R. A., 2016. New constraints on the origin and evolution of the Thomson Orogen and links with central Australia from isotopic studies of detrital zircons. Gondwana Research 39, 41–56. https://doi.org/10.1016/j.gr.2016.06.010

Suzuki, K., Kurihara, T., Sato, T., Ueda, H., Takahashi, T., Wilde, S. A., Satish-Kumar, M., 2023. Detrital zircon U–Pb ages and geochemistry of Devonian–Carboniferous sandstones and volcanic rocks of the Hida Gaien belt, Southwest Japan: Provenance reveals a Gondwanan lineage for the early Paleozoic tectonic evolution of proto-Japan. Gondwana Research 115, 224–255. https://doi.org/10.1016/j.gr.2022.12.005

Saito, Y., Hashimoto, M., 1982. South Kitakami region: an allochtohonous terrane in Japan. Journal of Geophysical Research: Solid Earth 87, 3691–3696. https://doi.org/10.1029/JB087iB05p03691

Zhang, S. H., Zhao, Y., Ye, H., Liu, J. M., Hu, Z. C., 2014. Origin and evolution of the Bainaimiao arc belt: Implications for crustal growth in the southern Central Asian Orogenic Belt. Geological Society of America Bulletin 126:1275–1300. https://doi.org/10.1130/B31042.1

Poster 22: Palaeogeomorphic reconstruction and influence of current in Taiwan orogenic belt and adjacent areas

Ze Liu[a,b,*], Sanzhong Li[a,b], Shaoqing Zhang[c,d],Pengcheng Shu[a,b], Jinping Liu[a,b], Ruixin Zhang[a,b], Pengcheng Wang[a,b], Yanyan Zhao[a,b], Jianping Zhou[a,b]

[a]*Frontiers Science Center for Deep Ocean Multispheres and Earth System, Key Lab of Submarine Geosciences and Prospecting Techniques, MOE, College of Marine Geosciences, Ocean University of China, Qingdao*

266100, China
[b]*Laboratory for Marine Mineral Resource, Qingdao Marine Science and Technology Center, Qingdao 266237, China*
[c]*Key Laboratory of Physical Oceanography, Ministry of Education/Institute for Advanced Ocean Study, Frontiers Science Center for Deep Ocean Multispheres and Earth System (DOMES), College of Oceanic and Atmospheric Sciences, Ocean University of China, Qingdao 260003, China*
[d]*Laoshan Laboratory, Qingdao 266201, China.*

*Corresponding author:
E-mail address: liuze@ouc.edu.cn (Ze Liu)

The Earth's surface response around Taiwan orogenic belt and adjacent areas commonly display complex 3D spatial and temporal evolution, which are still difficult to study the geological process. Coupled deep and surface process models based on Badlands software represent a powerful tool to investigate the structural development and the associated sedimentation. In order to study the palaeogeomorphic reconstruction, the paleo-bathymetry was restored using Badlands and data assimilation technique since Miocene to the recent based on the published geological data. We established forth representative end-member patterns associated with the different forcing. Our numerical simulation focuses on reconstructing the ancient paleogeomorphology and examining the impact of ocean currents in the Taiwan orogenic belt and its surrounding regions. According to simulation results, sedimentary areas influenced by ocean currents have gradually migrated eastward since the Miocene, which began approximately 15 Ma. We observed that the impact of the Taiwan Warm Current and the Kuroshio on sediment deposition was relatively limited between 15 Ma and 10 Ma. Furthermore, we found that the uplift of the Taiwan orogeny around 5 Ma intensified the sedimentary transport function of the Taiwan Warm Current, facilitating the sedimentation in the Taiwan Strait and the South China Sea continental shelf basin. Cenozoic paleogeomorphic reconstruction of the study area can not only help us understand the evolutionary process of the Taiwan orogenic belt, but also provide fundamental paleogeomorphic data for the other subjects.

Keywords: Palaeogeomorphic reconstruction; Coupled deep and surface process modeling; Deep dynamic process; Earth's surface system; Taiwan orogenic belt.

Poster 23: Reconstruction of provenances and magmatic protoliths of Ediacaran and Silurian clastic rocks of the Uzbek South Tien-Shan

Perfilova A.A.[1], Safonova I.Y.[2], Konopelko D.L.[3], Mirkamalov R.K.[4], Biske Y.S.[3]

[1]*Novosibirsk State University, Pirogova St. 1, Novosibirsk, 630090, Russia*
[2]*South-West Jiaotong University, Chengdu 610031, Sichuan, China*
[3]*Institute of Earth Sciences, St. Petersburg State University, St. Petersburg, 199034, Russia*
[4]*Institute of Mineral Resources, Tashkent, 100064, Uzbekistan*

*Corresponding author:
E-mail address: p.alina2808@mail.ru (Perfilova, A.A.)

The South Tien-Shan (STS) is located in the southwestern Central Asian Orogenic Belt (CAOB). STS formed by the closure of the Turkestan branch of the Paleo-Asian Ocean (PAO) and collision of the Paleo-Kazakhstan continental block in the north and the Karakum microcontinent and Tarim continent in the south in late Carboniferous time (Biske and Seltmann, 2010). The STS represents an accretion-

collisional belt consisting of oceanic plate stratigraphy (OPS) rocks: oceanic floor basalts, pelagic and hemipelagic sediments, turbidites, limestones and, to a lesser degree, supra-subduction ophiolites and metamorphic rocks.

We studied clastic rocks of Ediacaran and Silurian formations of the Kyzylkum and Nurata segments of the western STS cropped out in the Tamdytau and Bukantau ranges (Kyzylkum) and northern Nuratau Range. The Ediacaran formations (Besapan, Kaltadavan) consist of thick rhythmically bedded flyshoid-type sediments. The Silurian Baimen Fm. is dominated by turbidites occurring as tectonic sheets. The sandstones are spatially associated with OPS lithologies (oceanic pillow basalt, pelagic chert, hemipelagic siliceous mudstone, siltstone, shale) as well as with volcanic rocks of supra-subduction origin and limestones of various origins. The Ediacaran and Silurian ages of the sedimentary rocks were constrained by microfossils (conodonts, brachiopods, graptolites) (Akhmedov et al., 2001). However, the siliciclastic sedimentary rocks (sandstones) seldom contain well-preserved fossils and there remains a deficiency of up-to-date geochronological and geochemical data from such rocks that would allow reconstructing their geodynamic origins.

The U-Pb ages of detrital zircons show two Ediacaran major peaks at 624 and 608 Ma and a Silurian peak at 445 Ma (Konopelko et al., 2022). The Ediacaran samples yielded maximum depositional ages (MDA) of 580–540 Ma (Ediacaran-early Cambrian). The MDA of the Silurian samples is ca. 440 Ma (Llandovery). All samples display similar U-Pb detrital zircon age patterns with major peaks at 650–570, 870–730, 1050–900 and 2400 Ma and a smaller peak at ca. 1800 Ma all those indicating similar depositional environments and sources. The age patterns are similar to the summarized U-Pb age spectra of zircons from various igneous rocks of the basement of the Tarim Craton (Zhang et al., 2013).

Petrographically, the clastic rocks under study are fine-medium grained poorly- to medium sorted sandstones, which can be classified as litharenites, feldspathic litharenites, and lithic feldsarenites (Folk, 1980). According to the classification of Pettijohn (Pettijohn et al., 1972) they are litharenites and greywackes. The values of the index of chemical variability, ICV (Cox et al., 1995), span 0.9 - 2.6, indicating that the sandstones are immature and mature sedimentary rocks. The chemical indexes of alteration, CIA (Nesbitt and Young, 1982), are from 47 to 72 implying a provenance dominated by weak to strongly weathered rocks. The systematics of Dickinson (Dickinson et al., 1983) indicates that the sandstones were derived from a recycled orogen, which could be either a supra-subduction complex or a fold-and-thrust belt. The concentrations of major oxides are generally higher than those of PAAS (Taylor and McLennan, 1985). In the binary diagrams sandstones have clearly negative correlation between SiO_2 and TiO_2, Al_2O_3, Fe_2O_3, MgO. Their trace element compositions resemble those of arc-related igneous rocks. The La/Th – Hf (Floyd and Leveridge, 1987) and TiO_2 – Fe_2O_3+MgO (Bhatia, 1983) tectonic discrimination systematics indicate that the sandstones were derived by erosion of continental arc and/or active continental margin, respectively.

The Ediacaran sandstones are characterized by the negative values of εNd(t) ranging from –15 to –7 with crustal Nd model ages (T_{DM}) from 2.1 to 1.8 Ga. The values of εNd(t) for Silurian sandstones are also negative ranging from –16 to –9 with T_{DM} from 2.5 to 1.7 Ga suggesting the presence of recycled Precambrian continental crust in the provenance. The Ediacaran sandstones are characterized by a wide range of εHf(t) from −20 to +10 that suggests compositionally diverse provenances including both ancient continental crust and juvenile sources. The Silurian sandstones also yielded variable εHf(t) values ranging from −20 to +4.

As some of the 650–570 Ma detrital zircons from the Ediacaran sandstones possess juvenile Hf isotope characteristics, we suggest that they were derived from a mature intra-oceanic arc. On the contrary, the predominance of recycled 500–400 Ma detrital zircons in the Silurian samples indicates erosion of a continental arc or an active continental margin. Thus, the U-Pb zircon age data, the dominantly greywacke composition of the sandstones and the trace element data are all indicative of two periods of subduction-related orogeny: latest Neoproterozoic – earliest Cambrian and Silurian. The overall U-Pb ages of detrital zircons from the Kyzylkum and Nurata sandstones and adjacent regions show a middle-late Cambrian-Ordovician magmatic lull, that could be related to a shift of tectonic regime from the western Pacific-type (immature to mature intra-oceanic arcs) to the eastern Pacific-type (continental arc/active continental margin).

Acknowledgement: This work was founded by Russian Science Foundation (project № 21-77-20022), Fundamental Research Funds for the Central Universities of China (project № 2682023CX016).

References

Bhatia, M.R., 1983. Plate tectonics and geochemical composition of sandstone. The Journal of Geology 91, 611–627.
Biske, Yu.S., Seltmann, R., 2010. Paleozoic Tian-Shan as a transitional region between the Rheic and Urals–Turkestan oceans. Gondwana Research 17, 602–613.
Cox, R., Lowe, D.R., Cullers, R., 1995. The influence of sediment recycling and basement composition on evo- lution of mudrock chemistry in the southwestern United States. Geochimica et Cosmochimica Acta 59 (14), 2919–2940.
Dickinson, W.R., Berad, L.S., Brakenridge, G.R., Erjavec, J.L., Ferguson, R.C., Inman, K.F., Knepp, R.A., Lindberg, F.A., Ryberg, P.T., 1983. Provenance of North American Phanerozoic sandstones in relation-to-tectonic-setting. GSA Bulletin 94 (2), 222–235.
Floyd, P.A., Leveridge, B.E., 1987. Tectonic environment of the Devonian Gramscatho basin, south Cornwall: Framework mode and geochemical evidence from turbiditic sandstones. Journal of the Geological Society 144(4), 531–542.
Folk, R.L., 1980. Petrology of sedimentary rocks: Hemphill. Austin, Texas, 182 p.
Konopelko, D., Safonova, I., Perfilova, A., Biske, Y., Mirkamalov, R., Divaev, F., Kotler, P., Obut, O., Wang, B., Sun, M., Soloshenko, N., 2022. Detrital zircon U-Pb-Hf isotopes and whole-rock geochemistry of Ediacaran-Silurian clastic sediments of the Uzbek Tienshan: sources and tectonic implications. International Geology Review 64(21), 3005–3027.
Nesbitt, H.W., Young, G.M., 1982. Early Proterozoic climates and plate motions inferred from major element chemistry of lutites. Nature 299, 715–717.
Zhang, C.-L., Zou, H.-B., Li, K.-K., Wang, H.-Y., 2013. Tectonic framework and evolution of the Tarim Block in NW China. Gondwana Research 1306–1315.

Poster 24: Preliminary Study on Conversion of Bamboo Waste into Biochar via Pyrolysis Process

Yi Zheng Lim[1], Bridgid Lai Fui Chin[1,2*], Evelyn Chiong Tung[1], Angnes Ngieng Tze Tiong[1], Yie Hua Tan[3], Chai Yee Ho[4,5], Nor Adilla Rashidi[4,5]

[1]*Department of Chemical and Energy Engineering, Faculty of Engineering and Science, Curtin University Malaysia, CDT 250, 98009, Miri, Sarawak, Malaysia*
[2]*Centre of New and Sustainable Energy Research and Ventures (CoNSERV), Curtin University Malaysia, CDT 250, 98009, Miri, Sarawak, Malaysia*
[3]*Petroleum and Chemical Engineering, Faculty of Engineering, Universiti Teknologi Brunei, Gadong, BE1410, Brunei Darussalam*
[4]*Chemical Engineering Department, Universiti Teknologi PETRONAS, 32610, Seri Iskandar, Perak, Malaysia*
[5]*HICoE-Centre for Biofuel and Biochemical Research, Institute of Self-Sustainable Building, Universiti Teknologi PETRONAS, 32610, Seri Iskandar, Perak, Malaysia*

*Corresponding author:
E-mail address: bridgidchin@curtin.edu.my (Bridgid Chin L.F.)

Pyrolysis process of biomass is defined as the decomposition process whereby the biomass is decomposed by heat with limited amount of oxygen in producing products such as bio-oil, biochar, and syngas. Pyrolysis can be separated into slow and fast pyrolysis, whereby fast pyrolysis utilizes fast heating rate with bio-oil as the main product. Slow pyrolysis utilizes slow heating rate up to hours and days of residence time and produces biochar as the main product. Biochar has been widely studied as an adsorbent into ranges of containment including but not limited to microplastics and nano plastics, Hg (II) adsorption, Adsorption of chromium (VI), sulfamethoxazole and ethofumesate, phenol (Bhatia and Saroha, 2024; Ji et al., 2024; Li et al., 2024; Lopez-Cabeza et al., 2024; Masuku et al., 2024). Bamboo biochar has a high carbon to nitrogen value allows for a stronger biochar stability. Utilization of bamboo biochar in soil remediation is usually studied in reducing significant amount of specific heavy metal such as arsenic and cadmium above the safety level (Tang et al., 2024; Wei et al., 2024). Biochar has great potential but faces many issues in wide-scale implementation such as secondary pollution, limited equipment, limited research, long-term stability of biochar, and large initial start-up cost. While this study would be focus on the yield of the bamboo biochar and the yield of paddy in

paddy plant implementation. The research will focus on pyrolysis of bamboo biomass of three different sizes (0.05, 0.05-1.00, 1.00-2.00mm) and three different pyrolysis temperature of 300, 400, 500 °C using muffle furnace. The preliminary result has shown that biochar in 300, 400, and 500 °C has a yield range of 55.88 – 64.58, 36.13 – 41.62 and 26.67 – 33.50% respectively, which shows a generally higher yield compared to the yield of bamboo from a fixed bed reactor by Chen, D et al. (2016).

Acknowledgement: This work was supported by Curtin Malaysia Higher Degree Research (CMHDR) Grant and Sarawak Research and Development Council (RDCRG02/CAT/2023/110). In addition, the authors would like to thank Curtin University Malaysia for their technical assistant.

References:

Bhatia, D., Saroha, A. K. 2024. Biochar derived from pyrolysis of rice straw as an adsorbent for removal of phenol from water. Journal of Water Process Engineering 59, 105003. https://doi.org/10.1016/J.JWPE.2024.105003

Chen, D., Yu, X., Song, C., Pang, X., Huang, J., Li, Y., 2016. Effect of pyrolysis temperature on the chemical oxidation stability of bamboo biochar, Bioresource Technology 218, 1303-1306. https://doi.org/10.1016/j.biortech.2016.07.112.

Ji, G., Xing, Y., You, T. 2024. Biochar as adsorbents for environmental microplastics and nanoplastics removal. Journal of Environmental Chemical Engineering 12(5), 113377. https://doi.org/10.1016/J.JECE.2024.113377

Li, H., Zhen, F., Zhang, Q., Song, Y., Zhang, L., Qu, B., 2024. Preparation of porous lignocellulose biochar adsorbent by cold isostatic pressing pretreatment and study on Hg (II) adsorption properties of C and N dual activity sites. International Journal of Biological Macromolecules 274, 133479. https://doi.org/10.1016/J.IJBIOMAC.2024.133479

López-Cabeza, R., Cox, L., Gámiz, B., Galán-Pérez, J. A., Celis, R., 2024. Adsorption of sulfamethoxazole and ethofumesate in biochar- and organoclay-amended soil: Changes with adsorbent aging in the laboratory and in the field. Science of The Total Environment 939, 173501. https://doi.org/10.1016/J.SCITOTENV.2024.173501

Masuku, M., Nure, J. F., Atagana, H. I., Hlongwa, N., Nkambule, T. T. I., 2024. Pinecone biochar for the Adsorption of chromium (VI) from wastewater: Kinetics, thermodynamics, and adsorbent regeneration. Environmental Research 258, 119423. https://doi.org/10.1016/J.ENVRES.2024.119423

Tang, L., Xiong, L., Zhang, H., Joseph, A., Wang, Y., Li, J., Yuan, X., Rene, E. R., Zhu, N., 2024. Reduced arsenic availability in paddy soil through Fe-organic ligand complexation mediated by bamboo biochar. Chemosphere 349, 140790. https://doi.org/10.1016/J.CHEMOSPHERE.2023.140790

Wei, B., Zhang, D., Jeyakumar, P., Trakal, L., Wang, H., Sun, K., Wei, Y., Zhang, X., Ling, H., He, S., Wu, H., Huang, Z., Li, C., Wang, Z., 2024. Iron-modified biochar effectively mitigates arsenic-cadmium pollution in paddy fields: A meta-analysis. Journal of Hazardous Materials 469, 133866. https://doi.org/10.1016/J.JHAZMAT.2024.133866

Poster 25: Quantifying Fracture Clustering in Chiang Mai Granite: A Methodological Approach Using Normalized Correlation Count with Implications for Tectonic Evolution and CO_2 Sequestration

Natchanan Doungkaew[1*]

[1]*Department of Geological Sciences, Faculty of Science, Chiang Mai University, 239 Huay Kaew Road, Chiang Mai, 50200, Thailand*

*Corresponding author:
E-mail address: natchanan.d@cmu.ac.th (Natchanan Doungkaew)

Doi Suthep, a prominent geological feature in Chiang Mai, Thailand, is renowned for its cultural significance, touristic appeal, and rich tectonic history. This study introduces a novel approach to quantify fracture clustering in granite outcrops at Doi Suthep using the Normalized Correlation Count (NCC) method. The NCC method quantifies the spatial arrangement of fractures by comparing the observed fracture spacing distribution to that expected from a random arrangement, allowing for the detection of fracture clustering or regular spacing across multiple length scales. The objectives are: (1) to employ the NCC method, integrated within the CorrCount Program, to analyze the spatial distribution of fractures in granitic outcrops at Huay Kaew, Wang Bua Ban, and Pha Ngoep waterfalls; (2) to investigate the tectonic history of the area through the NCC results; and (3) to explore the applicability

of this method in evaluating the integrity of potential CO_2 sequestration sites in similarly fractured rock reservoirs.

Detailed mapping reveals distinct fracture patterns across the study sites. Wang Bua Ban and Pha Ngoep waterfalls exhibit a combination of random and regularly-spaced fracture clusters, while Huay Kaew waterfall displays predominantly regularly-spaced clusters. Fracture orientations are categorized into two main sets: a north-south set at Wang Bua Ban and Huay Kaew waterfalls, parallel to the slickenlines, and a NW-SE set at Pha Ngoep, perpendicular to the slickenlines. These variations are attributed to localized stress field rotation or reorientation associated with the uplift of the Doi Suthep metamorphic core complex. The observed fracture patterns may be linked to specific deformation events in the region's tectonic history, such as the Oligocene-Miocene extension associated with the development of the Chiang Mai Low-Angle Normal Fault (CMLANF) and older tectonic events like the Triassic collision of the Sibumasu Terrane with the Indochina Block or the Cretaceous-Tertiary metamorphism.

This study presents a methodological framework for quantifying fracture distributions using NCC, contributing to the understanding of the geology of Chiang Mai. The findings offer insights into the processes that formed the fracture network and have direct implications for assessing the CO_2 sequestration potential of fractured rock reservoirs. The results emphasize the importance of site-specific fracture distribution assessments, which consider the influence of different fracture network characteristics and spatial distribution on reservoir permeability and, thus, fluid or CO_2 flow in rocks.

Keywords: Normalized Correlation Count, NCC method, Doi Suthep, Chiang Mai granite, CO_2 sequestration, fracture clustering, geological methodology, slickenlines, Chiang Mai Low-Angle Normal Fault, CorrCount Program.

Poster 26: Neoproterozoic mafic to felsic magmatism of the Longmenshan Thrust Belt, western Yangtze Block: from supra-subduction to extensional settings

Li Yabo[1*], Inna Safonova[1], Alexandra Gurova[2], Gan Baoping[1]

[1]*South-West Jiaotong University, FGEE, Chengdu 610031, Sichuan, China*
[2]*Novosibirsk State University, Pirogova St. 1, Novosibirsk, 630090, Russia*

*Corresponding author:
E-mail address: liyabo@my.swjtu.edu.cn (Li Yabo)

The Longmenshan Thrust Belt (LTB) is located in the western margin of the Yangtze Block, at the junction zone between the Sichuan Basin and Songpan-Ganze terrane. The western Yangtze Block, a core of the South China Craton, consists of Proterozoic mafic-ultramafic plutons and granitoids intrusions, Paleozoic volcanogenic-sedimentary formations linked to the evolution of the Tethys Ocean, and Mesozoic continental sedimentary cover. The LTB is dominated by Neoproterozoic granitoids and mafic dikes and early-middle Paleozoic volcanogenic-sedimentary units. It has a complicated thrust-nappe structure that formed in Mesozoic to Cenozoic time during the early Mesozoic orogeny, late Mesozoic post orogenic extension and Cenozoic duplexing (Xue et al., 2022). The LTB is characterized by multiple NE trending faults zones and is a tectonically and seismically active area. Previous U-Pb geochronological data show that the Neoproterozoic magmatism of the western Yangtze Block during ca. 910-730 Ma (Xiong et al., 2023). We studied Neoproterozoic mafic to felsic plutonic intrusions and dikes exposed in the southern part of the LFB, near Ya'an City of the Tianquan County, Sichuan Province. The study area is located within the Xianshuihe fault zone and its stratigraphy also includes Ordovician carbonates, siliciclastic rocks (conglomerate, sandstone, siltstone and mudstone), chert, and

Silurian siliciclastic rocks (sandstone, siltstone, mudstone shale), and subordinate Mesozoic sedimentary strata. We sampled plutonic magmatic rocks, gabbroids and granitoids, exposed along the Da and Laba rivers. The gabbros typically occur as separate stocks and dikes cutting the granitoids. The sampled rocks were studied for U-Pb ages, major and trace element composition, Hf-in-zircon and whole-rock Nd isotopes.

According to the TAS classification, the samples are gabbro and monzogabbro, gabbrodiorite and monzodiorite, diorite and monzonite. The gabbroids are high-Ti and low-Ti. We separated zircons from high-Ti monzogabbro and monzodiorite and low-Ti gabbro, gabbrodiorite, diorite, and monzonite and performed their U-Pb dating. The low-Ti gabbro, gabbrodiorite, diorite and monzonite yielded mean U-Pb zircon ages of 816 ± 3Ma, 813 ± 3Ma, 809 ± 3Ma and 807 ± 3 Ma. The two high-Ti gabbroids yielded similar weighted mean ages of 787 ± 3Ma and 783 ± 3 Ma.

The groups of gabbroids (gabbro, gabbrodiorite, monzodiorite) and granitoids (diorite and monzonite) are characterized by variable compositions each. The low-Ti gabbroids show the lower concentrations of TiO_2 = 1.0-1.5 wt.% and FeO = 7.2-8.8 wt.% compared to the high-Ti gabbros (TiO_2 = 2.0-3.4, FeO = 11.5-11.9 wt.%). The granitoids can be divided into low-Si diorites (including monzodiorite) and "normal" diorites including monzonite. The low-silica diorites are characterized by higher concentrations of FeO (6.4-9.3 wt.%), MgO (2.7-5.7 wt.%) and CaO (5.2-6.9 wt.%) compared to the diorites (FeO = 5.2-7.3, MgO = 2.3-2.7, CaO = 2.7-4.5 wt.%). According to the alkalis-FeO-MgO classification, the sub-alkaline samples belong to the calc-alkaline series. In the low-Ti rocks, the concentrations of CaO and FeO decrease with increasing SiO_2 suggesting fractionation of olivine or orthopyroxene and clinopyroxenes. Such a correlation is not observed in the high-Ti gabbro indicating that the crystalline differentiation was not hardly responsible for the observed compositional variations.

The high-Ti gabbro are more enriched in the rare-earth elements (REE) compared to the low-Ti gabbro (ΣREE = 157 vs 88). They are typically enriched in light REE (LREE; La/Yb_N = 3.0-9.7), show a notable differentiation of heavy REE (HREE; Gd/Yb_N = 1.5-2.7) and have Zr/Nb ratios spanning 8.7-27.0. They are weakly depleted in Nb (Nb/Th_N = 0.3-1.0, Nb/La_N = 0.3-0.9). The low-Ti gabbroids are also enriched in LREE (La/Yb_N = 2.6-9.4), are characterized by moderately differentiated HREE (Gd/Yb_N = 1.3-2.2), but have higher Zr/Nb ratios (19-34). They are also depleted in Nb, but to a higher degree (Nb/Th_N = 0.2-0.3, Nb/La_N = 0.2-0.5) that is typical of supra-subduction igneous rocks (Pearce, 1982).

The low-silica diorites are also enriched in rare elements (La/Yb_N = 2.9-10.7) and have differentiated HREE (Gd/Yb_N = 1.0-2.5) and moderate Zr/Nb (18-33). The rocks are also depleted in Nb (Nb/Th_N = 0.2-0.6, Nb/La_N = 0.3-0.4). The diorites have similar features, but higher Zr/Nb (23-48) suggesting more evolved character. They are also enriched in LREE, moderately differentiated in HREE (La/Yb_N = 3.0-6.0, Gd/Yb_N = 1.6-1.8) and depleted in Nb (Nb/Th_N = 0.2-0.4, Nb/La_N = 0.3-0.4). All groups are characterized by positive εNd(t) values: 3.9-6.0 for the high-Ti gabbros, 3.1-4.3 for the low-Ti gabbroids, 4.3-4.4 for the low-silica diorites and 1.9 for diorite. The zircons from a low-Ti gabbro, low-silica diorite and diorite yielded positive εHf(t) values of 10.3, 11.2, and 11.1 respectively.

Thus, the Tianquan study area of the Longmenshan thrust belt obviously hosts at least two magmatic series of rocks: an older calc-alkaline series (816 to 807 Ma) represented by low-Ti gabbroids and diorites and a younger alkaline series (787-783 Ma) of high-Ti gabbro and monzodiorite. The calc-alkaline igneous series was evolving during almost 10 myr through crystalline differentiation from gabbro to diorite suggesting one or more intermediate chambers. The plutonic rocks of this series are characterized by typical features of supra-subduction igneous rocks: wide ranges of concentrations of most major oxides, medium to low concentrations of TiO_2, enrichment of LREE, depletion in Nb-Ta. The parental melts were derived from mantle wedge juvenile mantle sources (εNd(t) = +1.9-4.4; εHf(t) = +1.9-4.4), possibly, lherzolite or harzburgite (Gd/Yb_N = 1.3-2.2). They could be emplaced in a tectonic setting of a young active continental margin or evolved/mature island arc. The parental melts of the younger high-Ti gabbroids could be formed by mixing of enriched and depleted mantle sources (εNd(t) = +3.9-6.0) in an extensional tectonic setting. The extension was probably provided by active margin rifting or intra-arc rifting that has been fixed before in the western Yangtze for the 790-780 Ma time period (Wu et al., 2024).

Acknowledgement: This work was supported to the Russian Science Foundation (project № 21-77-20022), Fundamental Research Funds for the Central Universities of China (project № 2682023CX016) and Key R&D Program of Sichuan (Project #Q113523S01015).

References

Pearce, J.A., 1982. Trace element characteristics of lavas from destructive plate boundaries, In: Thorpe, R.S. (Ed.), Orogenic Andesites and Related Rocks. John Wiley and Sons, Chichester, England, pp. 528-548.

Wu L., Zhao G., Gao J., Dong X., Zhang A., Peng T., 2024. Intra-arc rifting induced the fragmentation of microplate from the continental margin. Geological Society of America Bulletin https://doi.org/10.1130/B37397.1

Xiong F, Zhong H, Huang H, Liu X., Hou M., 2023. Petrogenetic and tectonic implications of Neoproterozoic igneous rocks from the western Yangtze Block, South China. Precambrian Research 387, 106977.

Xue Zh., Lin W., Chu Y., Faure M., Chen Y., Ji W., Qiu H., 2021. An intracontinental orogen exhumed by basement-slice imbrication in the Longmenshan Thrust Belt of the Eastern Tibetan Plateau. Geological Society of America Bulletin 134 (1/2), 15-38.

Poster 27: Origin and geodynamic setting of Early Cretaceous bimodal volcanic rocks in the Karda area, South Tibet: Implications for the breakup of eastern Gondwana

Qiu-Ming Pei[a, *], Ying-Wei Yan[b], Li Zhang[a], Ding-Cheng Dai[a], Xiang Ren[a]

[a] *Faculty of Geosciences and Engineering, Southwest Jiaotong University, Sichuan, China*
[b] *Research Center of Applied Geology, China Geological Survey, Sichuan, China*

*Corresponding author:
E-mail address: pqm@swjtu.edu.cn (Q.-M. Pei)

The subduction of the Neo-Tethys Ocean and subsequent India-Asia collision formed the largest Himalaya-Tibetan Orogen on our planet. The voluminous igneous rocks generated within this notable orogen record a long-lived history of amalgamation process and have been used extensively to trace subduction–collision event. Early Cretaceous igneous rocks were reported to occur on a large scale in the Tethyan Himalaya. These voluminous magmatic rocks show genetic evidence of the Kerguelen mantle plume signatures, with ages ranging from ca. 141 to 117 Ma, and have been identified as the remnant Comei-Bunbury Large Igneous Province (LIP). However, the debate is still ongoing as to the origin of Early Cretaceous igneous rocks within the Tethyan Himalaya, for example, in contrast to the mantle plume model, some scholars argue that they were triggered by the rifting of the Australia–Antarctic Plate and Indian Plate.

In previous studies, extensive bimodal igneous rocks from the Late Jurassic to Early Cretaceous sedimentary-volcanic rocks in the study area have been reported, but they are mainly concentrated in the Sangxiu Formation (Fm), Lakang Fm, and Weimei Fm, and are mostly combinations of "gabbro + granite" or "basalt + dacite". However, little attention has been paid to the bimodal volcanic rocks in the Zhela Fm. On the other hand, there is also controversy over the formation age of the Zhela Fm. The 1:25,000 scale Longzi Country regional geological survey defined the age of the Zhela Fm as the Middle Jurassic. However, recent studies on the volcanic rocks of the Zhela Fm exposed in the Zhuode and Taga area of the Tethyan Himalaya have indicated that the Zhela Fm was deposited during the Late Jurassic-Early Cretaceous.

Based on the previous geological survey work, this study focuses on the newly discovered bimodal volcanic rocks in the Zhela Fm of the Karda area in southern Tibet. The basic end-member of the bimodal volcanic rocks of the Zhela Fm is basalt and the acid end-member is rhyolite. Zircon and monazite LA-ICP-MS U–Pb analyses obtained $^{206}Pb/^{238}U$ ages of 136.1−132.4 Ma for the sampled Zhela Fm bimodal volcanic rocks. Our new U–Pb ages, combined with the recent published chronological data, indicates that the Zhela Fm volcanic rocks erupted during the Late Jurassic–Early

Cretaceous, rather than the Middle Jurassic. Whole-rock geochemistry and Sr-Nd-Pb isotope analyses indicated that the basalt shows OIB-type geochemical features and suggests a mantle plume origin. The rhyolite samples might be the product of partial melting of the ancient crust influenced by the underplating of coeval mantle plume-derived magma. The bimodal volcanic rocks of the Zhela Fm were formed at the peak of the Early Cretaceous Tethyan Himalaya multistage magmatic activity, which records the important rift event of the Tethyan Himalaya. It was linked to the initial breakup of eastern Gondwana that start from nearly the earliest pulse (~141 Ma) of the Early Cretaceous magmatism in the Tethyan Himalaya.

Poster 28: Geochemical distribution of Heavy Metal in the Baram River MSCRNP- Corel reef section in the South China Sea, Borneo

Abdulmajid Muhammad Ali[a*], R. Nagarajan[a,b], Tewodros Rango Godebo[c], R.Sharveen[a], Jens Zinke[d], Nicola Browne[e], Jennifer McIlwain[f]

[a]*Department of Applied Sciences (Applied Geology), Curtin University, 98009 Miri, Sarawak, Malaysia*
[b]*Curtin Malaysia Research Institute, Curtin University, Malaysia*
[c]*Department of Environmental Health Sciences, School of Public Health and Tropical Medicine, Tulane University, New Orleans, LA 70112, USA*
[d]*School of Geography, Geology and Environment, Centre for Palaeobiology, University of Leicester, Leicester, UK*
[e]*School of the Environment, University of Queensland, Brisbane, QLD, 4067, Australia*
[f]*Molecular and Life Sciences, Curtin University, Bentley, WA 6102, Australia*

*Corresponding author:
E-mail address: a.ali@postgrad.curtin.edu.my (Abdulmajid Muhammad Ali)

Heavy metal pollution from urban rivers is a growing environmental concern, particularly in urban areas of developing countries, where industrial and agricultural activities contribute to elevated contaminant levels. The Miri Sibuti Coral Reef National Park (MSCRNP) is located adjacent to Miri City, with major rivers such as the Baram, Miri and Sibuti rivers draining into the South China Sea near the study area. This research project supports SDG 14 by targeting heavy metal pollution impacting coral reefs. Previous research in the region highlighted concerns regarding heavy metal contamination in rivers and coastal environments and its potential impacts on coral reefs (Prabakaran et al., 2019; Anandkumar et al., 2022; Nagarajan et al., 2023). Addressing these impacts is crucial for preserving coral reef ecosystems. Here, we try to understand the geochemical distribution of HM (heavy metals), which is expected to be supplied majorly from the Baram River and significant content is from the Miri and Sibuti Rivers to the MSCRNP. A spatial and temporal sampling of 18 both surface water and surface sediments (Fig.1A) was conducted and also the in situ physical parameters of the water samples (Temperature, dissolved oxygen, electric conductivity, salinity, turbidity and pH). The samples were analyzed using Inductively Coupled Plasma Mass Spectrometry (Agilent 7900 ICP-MS; Santa Clara, CA). With the results obtained, the heavy metal evaluation index (HEI), heavy metal pollution index (HPI), and degree of contamination (Cd) for the water samples were calculated to assess the pollution levels and understand the impacts of the HMs being supplied to the coral reefs. While for the sediments, the pollution load index (PLI), potential ecological risk index (RI), contamination factor (CF), enrichment Factor (EF) and geo-accumulation index (Igeo) were calculated collectively to provide a detailed picture of sediment contamination and will enable effective management, remediation, and conservation strategies to protect the MSCRNP. The HEI, HPI and Cd obtained from the water results shows that the pollution levels are higher during the wet season compared to the dry season. Based on

the geo-accumulation index (Igeo) values, the sediments show a high index (class 3) for As from both seasons. The contamination factor (CF) is low for all HMs except arsenic (As), which has a higher CF. Antimony (Sb) and tungsten (W) exhibit medium contamination factors. Enrichment factors (EF) show severe to extremely severe for As, Sb and W for but seasons and Minor to Moderately severe for other HMs. The potential ecological risk index (RI) is classified as low to medium across all samples. The pollution load index (PLI) is <1 for all samples, indicating low pollution levels overall. The source of the HMs and their geochemical mechanisms in the coastal regions (River vs estuary and sea) will be further studied and a way of mitigating the pollutants and impacts of these HMs on coral reefs.

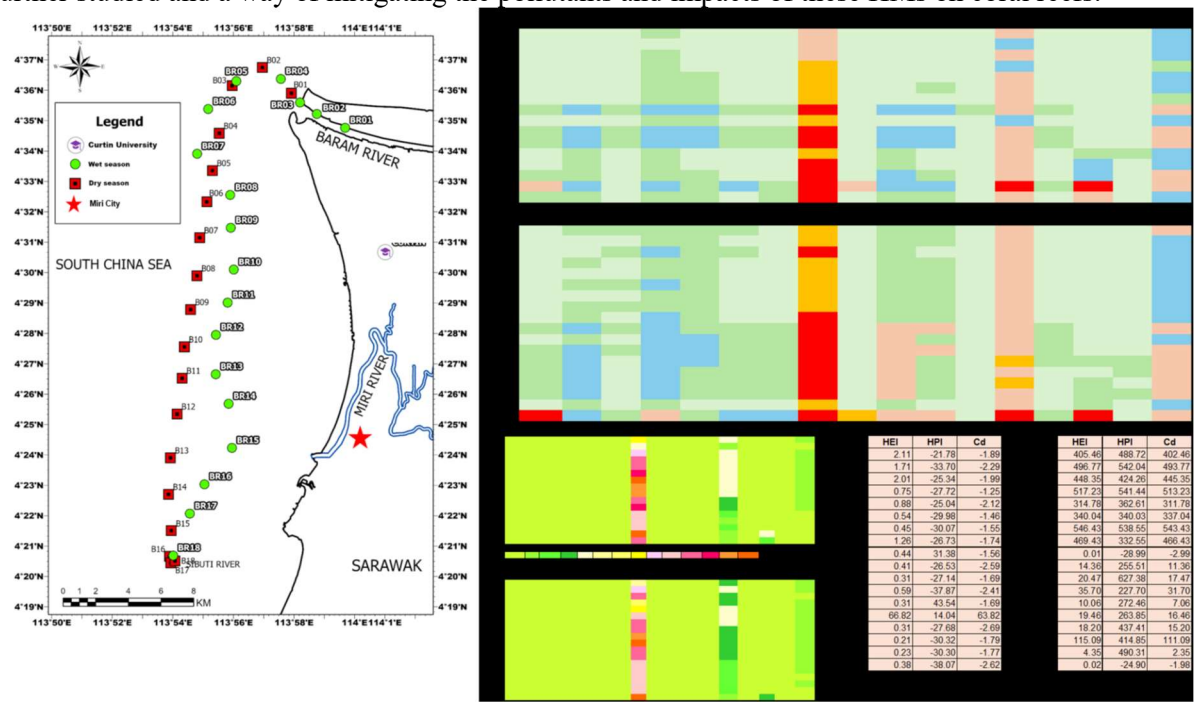

Poster 29: Distribution of Benthic Foraminifera in Reef Associated Kavaratti Island, Lakshadweep Archipelago, India

Euniksha Mohapatra[a], and Babu Nallusamy[a*]

[a]*Department of Geology, Central University of Karnataka, Kalaburagi, 585367, India*

*Corresponding author:
E-mail address: babun@cuk.ac.in (Babu Nallusamy)

Surface sediment samples across 9 locations of Kavaratti island of Lakshadweep archipelago, India were sampled to study the benthic foraminiferal assemblage. Kavaratti Island is a densely populated island in the Lakshadweep archipelago. In the current study, the distribution of benthic foraminifera and its ecosystem preference is reviewed. The benthic forams were handpicked under a stereozoom microscope after thorough processing. Amphisteginidae, and Calcarinidae were the dominant families of benthic forams identified from the region. *Amphistegina lessonii, Neorotalia calcar, Sorites orbiculus, Planorbulinella larvata, Cornuspira involvens,* and *Elphidium crispum* were the dominant species identified. *Amphistegina lessonii* dominated in numbers across all the sampling stations followed by *Neorotalia Calcar.* The genus *Amphistegina*, consisting of large symbiont-bearing foraminifera, is an excellent water quality indicator and hosts diatoms as symbionts. Higher numbers

of *Amphistegina lessonii* indicate the healthy nature of reefs at the time of sampling. *Neorotalia Calcar*, like other larger benthic foraminifera, prefers warm, shallow water associated with reefs and shelves. *Neorotalia Calcar* is also a large symbiont-bearing foraminifera and indicates healthy coral reefs. *Sorites orbiculus,* another symbiont-bearing functional group, hosts dinoflagellates as symbionts. A higher abundance of *Sorites orbiculus* suggests good fringing coral covers and abundant seagrass coverage. Genera *Quinqueloculina* is a small and heterotrophic foraminifera. They are basically stress resistant in nature and found scarcely in the sampling sites. *Genus Uvigerina and Cornuspira* also belong to small and heterotrophic functional groups of benthic foraminifera, which bear the ability to thrive in stressed atmospheres. They also found extremely less in numbers. The lower abundance of heterotrophic and opportunistic benthic foraminiferal functional groups indicates a very low supply of organic matter, low pollution, and higher oxygenated waters. The greater abundance of symbiont-bearing functional groups of benthic foraminifera indicates a healthy reef ecosystem in the Kavaratti islands at the time of sampling. Increased human interference has not yet affected this pristine coral reef environment. Continued monitoring and research are needed to preserve this ecosystem for future generations.

Keywords: Foraminifera, ecological status, environmental conditions, climate reconstruction and Kavaratti Island.

Poster 30: Sediment Quality Assessment and Estimation of Pollution Indices in the Mandapam Group of Islands, Gulf of Mannar Marine Biosphere Reserve, Southeastern India

Rakhil Dev[a*], Mohammed Noohu Nazeer[a], Babu Nallusamy[b*]

[a]*Department of Marine Geology and Geophysics, Cochin University of Science and Technology, Kochi, 682016, India*
[b]*Department of Geology, Central University of Karnataka, Kalaburagi, 585367, India*

*Corresponding authors:
E-mail address: rakhildev@cusat.ac.in (Rakhil Dev); babun@cuk.ac.in (Babu Nallusamy)

Sediment samples were collected during the NE monsoon from 20 locations around seven coral islands to decipher the ecological implications and to ascertain the pollution impacts in the Mandapam group of islands of the Gulf of Mannar Marine Biosphere Reserve (**Fig.1**). The proximity to the Rameswaram city on the Indian mainland, the higher load of household and municipal sewage, extra pollution from tourists and devotees, and monsoonal runoff and discharge can potentially affect the coral reefs and associated ecosystems. Pollution indices were plotted to understand the current status of the region's health. The quality of sediments from various environments of the Shingle, Krusadai, Poomarichan, Pullivasal, Manoli, Manoliputti, and Hare islands was studied. This study obtained trace metal concentrations from sediments and calculated pollution indices of sediments associated with coral reefs, seagrass, and mangroves. The decreasing order of heavy metal concentrations in the sediments is ranked as Fe> Mn> Cr> Nd> Ni> Zn> Rb> As> Th> Pb> Sm> Cu> Co> Cd> Ag. The Contamination factor (*CF*) shows values <1 in all stations except in KS-1, which is moderately contaminated with Cr. The degree of contamination (C_d) indicates that SH-1 has moderate contamination. In contrast, the modified degree of contamination (mC_d) indicates every station is falling under nil to a very low degree of contamination. The Pollution Load Index (PLI) also suggests that the area is under no pollution category (PLI<1). Similarly, the geoaccumulation index (I_{geo}) indicates that the whole area is unpolluted, i.e., Class 1=$I_{geo} \leq 0$. Sediment Pollution Index (SPI) suggests every every sample contains natural sediment (0<SPI<2). Similarly, the potential ecology risk coefficient (E^i_r) shows values <40, and the potential

ecological risk index (*PERI*) shows values <150 in all stations; both indicate the region is under low ecological risk (**Table 1**). Based on these indices, the overall contamination level of heavy metals from the Mandapam group of island sediments suggests that the area falls under the low-risk category and is highly conducive to coral reefs and associated ecosystems. The pressure of the urban population, tourism activities, and purported monsoonal runoff have not yet impacted the quality of sediments and reef health. The routine monitoring of the region is proposed to maintain the ecosystem's health.

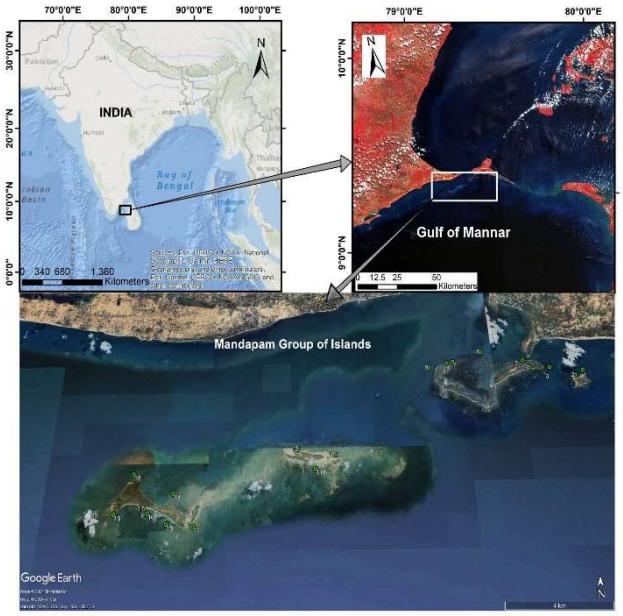

Fig.1. The map showing surface sampling locations around the Mandapam Group of Islands in the Gulf of Mannar Marine Biosphere Reserve, Southeastern India.

Table 1. The values of the Contamination factor (*CF*), Potential ecological risk coefficients (E^i_r), Sediment Pollution Index (*SPI*), Pollution Load Index (*PLI*), and Potential Ecological Risk Index (*PERI*) from the sediments of Mandapam group of islands, Gulf of Mannar.

Station number	Contamination factor (CF) and Potential ecological risk coefficients (E^i_r) of single heavy metal																		(SPI)	(PLI)	(PERI)
	Cr		Mn		Co		Ni		Cu		Zn		As		Cd		Pb				
	CF	E^i_r	*CF*	E^i_r	*CF*	E^i_r	*CF*	E^i_r	*CF*	E^i_r	*CF*	E^i_r	*CF*	E^i_r	*CF*	E^i_r	*CF*	E^i_r			
MP 4	0.26	0.05	0	0.04		0.07	0	0.08	0.12	0.05	0	0.06	0.04	2.94	0.09	10.23	0.01	3.46	0.27	0.07	16.99
PL 4	0.98	0.2	0	0.09	0	0.27	0	0.26	0.37	0.17	0	0.06	0.16	11.4	0.02	2.38	0.04	11.63	0.41	0.14	26.44
PM 1	0.37	0.07	0	0.08	0	0.08	0	0.09	0.12	0.06	0	0.02	0.06	4.05	0.02	2.78	0.02	4.46	0.18	0.06	11.69
KS 3	0.41	0.08	0	0.08	0	0.12	0	0.1	0.13	0.06	0	0.03	0.15	10.85	0.03	4.15	0.02	7.06	0.35	0.09	22.53
H 7	0.41	0.08	0	0.06	0	0.09	0	0.07	0.08	0.04	0	0.02	0.17	12.1	0.06	7.21	0.01	4.3	0.37	0.09	23.97
M 3	0.4	0.08	0	0.04	0	0.09	0	0.15	0.18	0.08	0	0.03	0.04	3.1	0.04	4.99	0.01	4.02	0.2	0.07	12.58
H 1	0.47	0.09	0	0.06	0	0.14	0	0.11	0.16	0.07	0	0.03	0.07	5.00	0.02	2.36	0.02	6.53	0.22	0.07	14.39
H 4	0.66	0.13	0	0.12	0	0.18	0	0.06	0.04	0.02	0	0.03	0.07	5.48	0.02	2.14	0.01	3.66	0.18	0.05	11.82
KS 1	0.24	0.05	0	0.06	0	0.06	0	0.05	0.05	0.02	0	0.01	0.12	9.13	0.04	5.24	0.02	4.448	0.3	0.06	19.08
PM 9	0.33	0.07	0	0.04	0	0.08	0	0.09	0.12	0.05	0	0.02	0.05	3.7	0.04	5.33	0.01	4.03	0.21	0.07	13.45
H 5	0.2	0.04	0	0.03	0	0.06	0	0.05	0.04	0.02	0	0.002	0.11	8.31	0.02	2.98	0.01	2.9	0.22	0.05	14.39
M 10	0.23	0.05	0	0.04	0	0.05	0	0.06	0.05	0.02	0	0.01	0.06	4.12	0.07	8.99	0.01	2.66	0.25	0.05	15.99
H 8	0.4	0.08	0	0.06	0	0.09	0	0.06	0.05	0.02	0	0.02	0.06	4.78	0.04	4.42	0.01	2.98	0.19	0.06	12.46
KS 6	1.08	0.22	0	0.04	0	0.04	0	0.26	0.09	0.04	0	0.02	0.03	2.41	0.04	5.36	0.01	2.94	0.18	0.07	11.33
SH 1	6.8	1.36	0	0.08	0	0.21	0	1.77	0.38	0.17	0	0.01	0.12	8.50	0.03	3.66	0.02	6.68	0.35	0.18	22.44
PL 10	0.19	0.04	0	0.05	0	0.05	0	0.04	0.07	0.03	0	0.01	0.04	3.11	0.02	2.1	0.01	3.42	0.14	0.04	8.85
SH 6	0.17	0.03	0	0.04	0	0.07	0	0.04	0.05	0.02	0	0.02	0.08	5.99	0.02	2.65	0.01	3.87	0.2	0.05	12.74
H 17	0.15	0.03	0	0.03	0	0.05	0	0.04	0.06	0.03	0	0.012	0.05	3.84	0.01	1.31	0.01	3.43	0.14	0.04	8.77
H 9	0.16	0.03	0	0.03	0	0.05	0	0.03	0.05	0.02	0	0.02	0.05	3.7	0.03	3.54	0.01	2.42	0.15	0.04	9.86
H 11	0.1	0.02	0	0.03	0	0.04	0	0.02	0.03	0.01	0	0.007	0.04	2.95	0.05	5.47	0.01	2.28	0.17	0.03	10.84

SPI=Sediment Pollution Index; PLI=Pollution Load Index; PERI= Potential ecological risk index

Keywords: Gulf of Mannar, Ecological Indices, Heavy Metal Contamination, Ecosystem Health, Monsoon

Poster 31: Experimental study of mobility of titanium and niobium during low-temperature hydrothermal transformation of pyrochlore, lueshite, and rutile in humid climate

D.A. Chebotarev[1*], B.Yu. Saryg-ool[1], E.N. Kozlov[2], E.N. Fomina[2], M.Yu. Sidorov[2]

[1] *Sobolev Institute of Geology and Mineralogy Siberian Branch Russian Academy of Sciences, Novosibirsk, Russia*
[2] *Geological Institute, Kola Science Center, Russian Academy of Sciences, Apatity, Russia*

*Corresponding authors:
E-mail address: chebotarev@igm.nsc.ru (D.A.Cheborarev)

Titanium and niobium are considered as low-mobility elements during low-temperature hydrothermal processes and weathering (Kurtz et al., 2000; Ewing et al., 2004). However, polymorphs of titanium oxides (Ti-oxides) are often found in high (400-300 °C), medium (300-150 °C) and low temperature (150-50 °C) hydrothermal veins, including associated with alkaline rocks (syenites and carbonatites) (Rabbia and Hernandez, 2012; Schirra and Laurent, 2021; Bollaert et al., 2023). Often these Ti-oxides exhibit oscillatory and sectorial zoning in Ti, Fe, Si, Nb and other elements., which also indicates their formation in an open system, and the Nb_2O_5 impurity content can reach tens of mass percent in the rims, providing industrial concentrations. As striking examples, we can name the following carbonatite complexes, containing industrial rare metal deposits: the Chuktukon massif of the Chadobetsky complex (Russia) (Chebotarev et al., 2017), the Vuoriyarvi massif in the Kola Alkaline Province (KAP) (Russia) (Fomina and Kozlov, 2022; Kozlov et al., 2018), Bear Lodge (USA) (Andersen et al., 2016), Morros dos Seis Lagos (Brazil) (Giovannini et al., 2017, 2020). In the weathering crust of the Morros dos Seis Lagos carbonatites, Ti-oxides formed both at the late low-temperature hydrothermal stage and weathering described (Giovannini et al., 2017, 2020) and a characteristic feature of most of these deposits is their formation in a humid (subtropical) climate.

At the moment, an experimental basis for studying the properties of titanium and niobium minerals in a wide range of temperatures and pressures at different geological settings was developed (for example, Shapovalov et al., 2019). However, there are no estimates of the mobility of titanium and niobium under conditions simulating low-temperature hydrothermal transformation of a mixture of titanium-niobium minerals in a humid climate. Therefore, we carried out a series of experiments at 50 and 200 °C on the effect of rutile, anatase, pyrochlore and luesite on a mixture of minerals with solutions of acids HF, HCl, and H_2SO_4.

For the experiments, 1.0 M solutions of mineral acids were prepared from extra pure concentrated HCl, HF and H_2SO_4 acids. Crystals of rutile (from the Kuura-Vara eclogites, Kola region, Russia), anatase (Dodo, Subpolar Ural mountains, Russia), pyrochlore (from the Seblyavr carbonatites, KAP, Russia) or lueshite (from the Sallanlatva carbonatites, KAP, Russia) weighing at least 10 mg of each variety were placed in autoclaves made of high-pressure polytetrafluoroethylene (PTFE) with a volume of 50 ml. The composition of minerals was analyzed by scanning electron microscopy (SEM) on a MIRA3 LMU scanning electron microscope (TESCAN, Czech Republic) with an INCA Energy 450+ microanalysis system based on an X-MAX 80 energy-dispersive spectrometer (Oxford Instruments NanoAnalysis, UK) before and after the experiments. 10 ml of solutions of acids were added to the mineral mixture (**Table 1**) and then the autoclaves were closed and placed in a HOT BOX 300 heating block (Siberian Analytical Systems, Russia). The experiments were carried out at 50°C and 200°C for 4 hours after establishing of temperature and then the autoclaves were cooled to room temperature. Element content in solutions of acids after the experiments were analyzed using inductively coupled plasma atomic emission spectrometry (ICP-AES) (iCAP Pro XP Duo, Thermo Scientific, USA). The mixtures of

minerals were washed twice with distilled water and dried at room temperature for re-examination using the specified scanning electron microscopy method. Analytical and mineralogical studies were carried out at the Analytical Center for multi-elemental and isotope research Siberian Branch Russian Academy of Science (Novosibirsk, Russia).

Table 1. Contents of titanium and niobium in the initial mixtures and in solutions after experiments.

		TiO_2 mg in mixture	**Nb_2O_5** mg in mixture	**TiO_2** mcg (in solution)	**Nb_2O_5** mcg (in solution)	**TiO_2** mg (in solution) / mg (in mixture) *100	**Nb_2O_5** mg (in solution) / mg (in mixture) *100
HCl,	Pcl+Ru+An	22.9	5.8	0.67	0.40	<0.10	<0.10
50 °C	Lue+Ru+An	21.0	9.6	0.59	0.20	<0.10	<0.10
HCl,	Pcl+Ru+An	22.7	5.6	5.5	4.8	<0.10	<0.10
200 °C	Lue+Ru+An	22.0	8.6	1.6	1.9	<0.10	<0.10
H_2SO_4,	Pcl+Ru+An	21.3	5.7	0.77	2.6	<0.10	<0.10
50 °C	Lue+Ru+An	21.3	8.6	0.52	0.84	<0.10	<0.10
H_2SO_4,	Pcl+Ru+An	25.7	6.9	32	250	0.12	3.6
200 °C	Lue+Ru+An	22.0	8.7	7.7	9.0	<0.10	0.10
HF,	Pcl+Ru+An	21.5	5.5	500	5000	2.3	91
50 °C	Lue+Ru+An	21.0	8.2	28	62	0.13	0.76
HF,	Pcl+Ru+An	22.4	5.5	730	4000	3.3	73
200 °C	Lue+Ru+An	23.9	8.2	380	780	1.6	9.5

The analytical results showed that chloride solutions were weakly saturated and transferred titanium and niobium, with the effect being slightly enhanced at elevated temperatures. Sulfate solutions are also practically not saturated with titanium and niobium at 50 °C, but at 200 °C they show a slightly higher saturation with titanium and significantly saturated with niobium - up to 3.7% of the initial content of Nb_2O_5 dissolved into solution in experiments with of pyrochlore. Fluoride solutions are most intensively saturated with titanium and niobium: in the case of pyrochlore, 2.3% of TiO_2 at 50 °C and about 3% of TiO_2 at 200 °C dissolved, while for Nb_2O_5 these values are about 91% and 74% respectively. For samples with lueshite, these values are less than 1% at 50 °C and 1.6% of TiO_2 and 9.5% of Nb_2O_5 at 200 °C. According to SEM analyses, it is also clear that lueshite was resistant to the effects of the used acid solutions, and rutile and anatase did not undergo dissolution, while pyrochlore was unstable upon contact with HF and was actively replaced by fluorite in all experiments. At the same time, no individual newly formed phases of niobium or titanium were detected.

The conducted studies show that titanium and niobium are indeed mobile in low-temperature hydrothermal solutions. Their mobility is controlled by the composition of fluids and temperature - the greatest effect is achieved in the presence of F-ions, and sulfate ions may also cause mass transfer of niobium and titanium during low-temperature hydrothermal processes.

Acknowledgement: The research was carried out with funds from the basic research project No. 22041400241-5 (consumables for experiments) and the Russian Science Foundation grant No. 23-77-01075 (starting substances, analytical work).

References

Andersen A.K., Clark J.G., Larson P.B., Neill O.K., 2016. Mineral chemistry and petrogenesis of a HFSE (+HREE) occurrence, peripheral to carbonatites of the Bear Lodge alkaline complex, Wyoming. American Mineralogist 101, 7, 1604-1623. https://doi.org/10.2138/am-2016-5532

Bollaert Q., Chassé M., Neto A.B., Baptiste B., Courtin A., Galoisy L., Mathon O., Quantin C., Vantelon D., Calas G., 2023. Mechanisms leading to exceptional niobium concentration during lateritic weathering: The key role of secondary oxides. Chemical Geology 121767. https://doi.org/10.1016/j.chemgeo.2023.121767

Chebotarev D.A., Doroshkevich A.G., Klemd R., Karmanov N.S., 2017. Evolution of Nb-mineralization in Chuktukon carbonatite massif, Chadobets upland (Krasnoyarsk territory, Russia). Periodico di Mineralogia 86, 99-118.

Fomina E.N., Kozlov E.N., 2022. A comprehensive study of rare earth carbonatites of the Vuorijärvi massif (Kola region) and a model of their formation. Bulletin of the Kola Scientific Center of the Russian Academy of Sciences 2. https://doi.org/10.37614/2307-5228.2022.14.2.002 (in Russian)

Giovannini A.L., Bastos Neto A.C., Porto C.G., Pereira V.P., Takehara L., Barbanson L., Bastos P.H.S., 2017. Mineralogy and geochemistry of laterites from the Morro dos Seis Lagos Nb (Ti, REE) deposit (Amazonas, Brazil). Ore Geology Reviews 88, 461-480.

https://doi.org/10.1016/j.oregeorev.2017.05.008.
Giovannini A.L., Mitchell R.H., Bastos Neto A.C., Moura C.A.V., Pereira V.P., Porto C.G., 2020. Mineralogy and geochemistry of the Morro dos Seis Lagos siderite carbonatite, Amazonas, Brazil. Lithos 360–361, 105433, https://doi.org/10.1016/j.lithos.2020.105433.
Ewing R.C., Weber W.J., Lian J., 2004. Nuclear waste disposal-pyrochlore ($A_2B_2O_7$): Nuclear waste form for the immobilization of plutonium and ''minor'' actinides. Journal of Applied Physics 95, 5949–5971.
Kozlov E., Fomina E., Sidorov M., Shilovskikh V., 2018. Ti-Nb Mineralization of Late Carbonatites and Role of Fluids in Its Formation: Petyayan-Vara Rare-Earth Carbonatites (Vuoriyarvi Massif, Russia). Geosciences 8, 8, 281. https://doi.org/10.3390/geosciences8080281
Kurtz A.C., Derry L.A., Chadwick O.A., Alfano, M.J., 2000. Refractory element mobility in volcanic soils. Geology 28, 683–686
Rabbia O.M., Hernandez L.B., 2012. Mineral chemistry and potential applications of natural-multi-doped hydrothermal rutile from porphyry copper deposits. Rutile: Properties, Synthesis and Applications, ISBN 978-1-61942-233-9, Editor: It-Meng (Jim) Low, 209-228
Schirra M., Laurent O., 2021. Petrochronology of hydrothermal rutile in mineralized porphyry Cu systems. Chemical Geology 581, 120407. https://doi.org/10.1016/j.chemgeo.2021.120407.
Shapovalov Y.B., Chevychelov V.Y., Korzhinskaya V.S., Kotova N.P., Redkin A.F., Konyshev A.A., 2019. Physical and chemical parameters of processes producing rare-metal deposits in granitoid systems with fluorine: experimental data. Petrology 2019, 27, 567–584. https://doi.org/10.1134/S0869591119060067

Poster 32: The pockmarks and associated fluid migration in the Baiyun canyon-channel system in the South China Sea

Junjiang Zhu[a, b*], Sanzhong Li[a, b], Yonggang Jia[c], Xingquan Chen[a, b], Qinglong Zhu[a, b], Xiaoxiao Ding[a, b], Zhengyuan Liu[a, b], Yuhan Jiao[a, b], Yongjiang Liu[a, b]

[a]*Frontiers Science Center for Deep Ocean Multispheres and Earth System, Key Lab of Submarine Geosciences and Prospecting Techniques, MOE and College of Marine Geosciences, Ocean University of China, Qingdao 266100, China*
[b]*Laboratory for Marine Mineral Resources, Qingdao Marine Science and Technology Center, Qingdao 266237, China*
[c]*Shandong Provincial Key Laboratory of Marine Environment and Geological Engineering, Ocean University o f China, Qingdao 266100, China*

*Corresponding authors:
E-mail address: zhujunjiang@ouc.edu.cn (Junjiang Zhu)

The hydrothermal vents and pockmarks are two remarkable features in the global ocean and indicate direct evidence for the extensive seabed fluid emission and fluid seepage process. The pockmarks are one of the typical types of seafloor crater-like depressions associated with fluid escape from the seabed and are considered to contribute to the transfer of methane into the ocean and ultimately into the atmosphere. Based on the newly acquisitioned multibeam bathymetry and sub-bottom profile data in the Baiyun channel system in the Pear River Mouth Basin, twelve large pockmarks are recognized and these isolated pockmarks are found to situate on the inter-channel ridges (ICRs). The shapes of pockmarks identified by the bathymetric data and geophysical data in the sedimentary basins in the South China Sea are mainly circular, elliptical, crescent-shaped, comet-shape, elongated, irregular and horseshoe shapes from the plan view. We propose that three types of pockmarks in the South China Sea may explain the formation of different pockmarks in the sedimentary basins. Type-1 pockmarks are related to the gas chimney structure and it is used to interpret the formation of the unit-pockmarks in the shallow water area. The Type-2 pockmarks commonly explain the normal and large pockmarks in the sedimentary basins and the Type-3 pockmarks termed as channel-related pockmarks are mainly located on the ICRs in the submarine channel system and the formation of the isolated large pockmarks is associated with the dissociation of gas hydrates in the deep. All types of pockmarks were produced by the vertical migration of fluid and free gas along the faults and sources of fluid and gas are from the deep to the shallow reservoirs.

Poster 33: *Parvancorina* : The anchor-shaped Ediacaran organism from Sonia Sandstone Formation of Marwar Supergroup, India

Hukma Ram[a*], Anshul Harsh[a], Pawan Kumar[a], V. S. Parihar[a]

[a]*Jai Narain Vyas University, Jodhpur, Rajasthan, India, 342005*

*Corresponding author:
E-mail address: hukmaramchouhan@gmail.com (Hukma Ram)

The current study records and characterizes the anchor-shaped Ediacaran organisms on the sandstone bedding plane of the Sonia Formation in the Marwar Supergroup of India that are attributed to the genus *Parvancorina*. This is the first report of *parvancorina* from the Indian sub-continent. The specimens are preserved as small, posterior shield-shaped, rounded to ovate imprints with a posterior anchor-shaped structure and an anterior-lateral expanded part. The Ediacaran period remains a captivating chapter in Earth's history and within its fossil record lies the mysterious entity, *Parvancorina*. This abstract ventures into the depths of ancient oceans to illuminate the story of *Parvancorina*. This discovery adds a novel dimension to the understanding of *Parvancorina's* paleobiology and distribution, providing a crucial link to the broader Ediacaran biota in India and contributing valuable insights into the ecological dynamics of this enigmatic period in Earth's history. Methodology includes the Field work and data collection this includes noting the geological context (stratigraphy, lithology) of the site where the fossil was found, as well as recording measurements, dimensions, and morphological features of the Parvancorina structures. Studied more than 30 specimens and their slab in the Sonia sandstone Formation, the recovered (two) *P. minchami* specimens have been found in size ranges of 1.2 × 1.5 to 4.0 × 4.2 cm^2 (length × width), suggesting preservation of adult and larger forms. The allure of *Parvancorina* lies not only in its peculiar morphology but also in the questions it raises about the evolutionary experimentation preceding the Cambrian explosion. The aim of the study is to find out the linkage between the *Parvancorina* and the Trilobites with the help of morphological feathers of the animals. Based on the *Parvancorina* and associated Ediacaran fossils assemblages, this study suggests terrestrial to marginal marine habitats with moderate hydrodynamic forces. The preservation of the *parvancorina* in the orientation also shows the important direction of the paleo-environment.

Keywords: *Parvancorina*, Ediacaran Biota, Marwar Super Group, Rajasthan, India

Poster 34: Geochemistry of Eocene – Oligocene Carbonates of Northern Sarawak, Borneo

C.Ranjen[a*], R.Nagarajan[a,b], M.Ramkumar[c], S. Vijay Anand[a]

[a] *Department of Applied Sciences (Applied Geology), Curtin University, 98009 Miri, Sarawak, Malaysia*
[b] *Curtin Malaysia Research Institute, Curtin University, Malaysia*
[c] *Department of Geology, Periyar University, Salem, India*

*Corresponding Author
E-mail address: ranjen95@gmail.com (C.Ranjen)

The geochemistry and petrography of carbonates are indispensable and potent tools for understanding depositional environments (Mehrabi and Tavakoli, 2024) and diagenetic transformations (Wei and Zhang, 2024). Traditionally, geologists have routinely employed these techniques. Recently, with the

rising interest in the exploration of rare earth elements (REE) in sedimentary deposits, such studies have gained renewed vigor (Balaram, 2023). This paper documents the geochemical and petrographic data of the Eocene–Oligocene carbonates in the Batu Gading area of Northern Sarawak to unravel the depositional environment and potential sources of REEs.

The Batu Gading Limestone (**Fig. 1**) refers to a group of carbonate rocks located about 80 kilometers southeast of Miri, Sarawak (Wannier, 2009; Wilson et al., 2013; Madden et al., 2017), along the Baram River. It is part of the Melinau Limestone Formation, which trends NE-SW in Sarawak. This formation is known for its variable thickness and lateral extension, as well as its diverse depositional environmental settings (Ali, 2013).

Sample collection was carried out horizontally along the carbonate sequence at 1-meter intervals. Two thin sections (parallel and perpendicular to the bed) were prepared for each interval of the carbonate sequence. The concentrations of major and trace elements were analyzed using Inductively Coupled Plasma-Atomic Emission Spectrometry (ICP-AES) and Inductively Coupled Plasma Mass Spectrometry (ICP-MS) for REE content. Petrographic analysis of these deposits revealed that foraminifera grainstone (**Figs. 2a and b**) is the most common facies type. Previous studies have identified four different depositional textural types—mudstone, wackestone, packstone, and grainstone—indicating variations in the depositional environment (Hutchison, 2005; Ali, 2013; Madden et al., 2017; Kessler & Jong, 2017) and the impact of post-depositional processes such as micritization, compaction, cementation, and recrystallization.

Among the major oxides, CaO was found to be dominant, followed by SiO_2, while Sr was the dominant trace element. Negative cerium anomalies (Ce/Ce*) (average 0.849 ppm) and positive europium anomalies (Eu/Eu*) (average 1.117 ppm) were recorded in the current study. The high abundance of CaO suggests calcite dominance in the carbonate phase, with minimal dolomitization. The average Sr concentration was 401.9 ppm, while the second most abundant trace element, vanadium, averaged 38.8 ppm. Several factors, such as Sr incorporation in diagenetic carbonates due to the weathering of detrital input, may explain the dominance of Sr concentration (Salih et al., 2021).

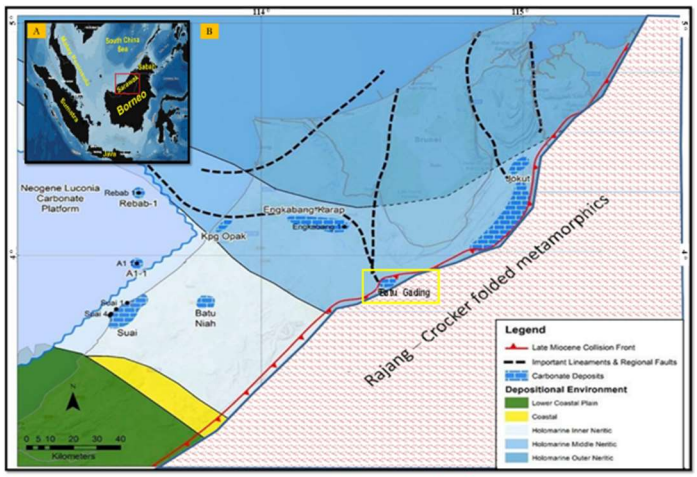

Figure 1. Location Map of the study area (modified from Kessler and Jong, 2017)

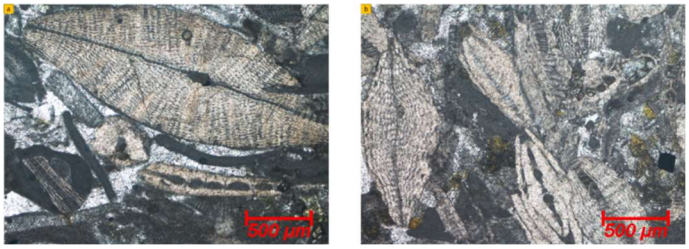

Figure 2a. Close-up view of the foraminifera with recrystallised calcite cement. The presence of pyrite, the absence of micrite, and the different types of foraminifera can be seen in b.

Negative Ce anomalies in carbonate sediments and rocks strongly indicate precipitation in an oxic environment, which is common in most modern oxygenated waters (Adelabu et al., 2021). PAAS-normalized positive Eu anomalies could be the result of intense diagenetic processes or the weathering

of detrital input (Salih et al., 2021; Singh et al., 2023). The positive Eu anomaly suggests that certain siliclastic sediments were incorporated into the limestone. The CaO content results from chemical and biological processes, while the negative Ce anomaly indicates that the REEs were supplied directly from seawater under oxic conditions.

This study highlights additional factors that influenced the deposition of the limestone and the potential source of REEs under oxic conditions. It enhances our understanding of the Batu Gading limestone by elucidating depositional environmental conditions and the possible inclusion of REEs into the limestone, which provides insights into tectonic activity, climatic changes, and resource potential.

Keywords: rare earth elements, geochemistry, Eocene - Oligocene limestone, Batu Gading, Sarawak

References

Adelabu, I., Opeloye, S., Oluwajana, O., 2021. Petrography and geochemistry of Paleocene-Eocene (Ewekoro) limestone, eastern Benin basin, Nigeria: implications on depositional environment and post-depositional overprint. Heliyon, 7(12).

Ali, M.Y., 2013. An Integrated Analysis of the Depositional Control, Sedimentology and Diagenesis of Cenozoic Carbonates from the Sarawak Basin, East Malaysia. Dissertation, Imperial College London

Balaram, V., 2023. Potential future alternative resources for rare earth elements: Opportunities and challenges. Minerals, 13(3), 425

Hutchison, C. S., 2005. Geology of North-West Borneo: Sarawak, Brunei and Sabah. Elsevier Science, Amsterdam. 421 p.

Kessler, F. L., Jong, J. 2017. Carbonate banks and ramps on the northern shore of Palaeogene and Early Neogene Borneo: Observations and implications on stratigraphy and tectonic evolution. Bulletin of the Geological Society of Malaysia 63, 1–26.

Madden, R. H., Wilson, M. E., Mihaljević, M., Pandolfi, J. M., Welsh, K., 2017. Unravelling the depositional origins and diagenetic alteration of carbonate breccias. Sedimentary Geology 357, 33-52.

Mehrabi, H., Tavakoli, V., 2024. Editorial for the special issue: Deposition, Diagenesis, and Geochemistry of Carbonate Sequences. Minerals 14(3), 269.

Salih, N., Préat, A., Gerdes, A., Konhauser, K., Proust, J., 2021. Tracking the origin and evolution of diagenetic fluids of upper Jurassic carbonate rocks in the Zagros Thrust Fold Belt, NE-Iraq: water 13(22), 3284.

Singh, A., Singh, B. P., Kanhaiya, S., Qasim, M. A., Patra, A., Singh, S., 2023. Geochemistry of Palaeo-Proterozoic Kajrahat Limestone, Vindhyan Supergroup, Central India: Insights into Depositional Conditions and Sources of Rare Earth Elements. Research Square.

Taylor, S.R., McLennan, S.M., 198.5 The Continental Crust: Its Composition and Evolution: An Examination of the Geochemical Record Preserved in Sedimentary Rocks. Blackwell Science, Oxford, 312.

Wannier, M., 2009. Carbonate platforms in wedge-top basins: An example from the Gunung Mulu National Park, Northern Sarawak (Malaysia). Marine and Petroleum Geology 26(2), 177–207.

Wei, G., Zhang, F., 2024. Pristine or altered, what can early diagenesis tell us in shallow-water carbonates? Earth and Planetary Science Letters 641, 118806.

Wilson, M. E., Wah, E. C. E., Dorobek, S., Lunt, P., 2013. Onshore to offshore trends in carbonate sequence development, diagenesis and reservoir quality across a land-attached shelf in SE Asia. Marine and Petroleum Geology 45, 349–376.

Poster 35: Heavy Metal Distribution and Environmental Significance in Miri and Sibuti Rivers And MSCRNP, South China Sea, Borneo

R. Sharveen[1*], R. Nagarajan[1,2], Jens Zinke[3], Tewodros Rango Godebo[4], Nicola Browne[5], Jennifer McIlwain[6], Abdulmajid Muhammad Ali[1]

[1]*Department of Applied Sciences (Applied Geology), Faculty of Engineering and Science, Curtin University, Malaysia*
[2]*Curtin Malaysia Research Institute, Curtin University, Miri, Sarawak, Malaysia*
[3]*School of Geography, Geology and Environment, Centre for Palaeobiology, University of Leicester, Leicester, UK*
[4]*Department of Environmental Health Sciences, School of Public Health and Tropical Medicine, Tulane University, New Orleans, LA 70112, USA*
[5]*School of the Environment, University of Queensland, Brisbane, QLD, 4067, Australia*
[6]*Molecular and Life Sciences, Curtin University, Bentley, WA 6102, Australia*

[*] Corresponding author:
E-mail address: Sharveengeo@gmail.com (R.Sharveen)

Miri Sibuti Coral Reef National Park (MSCRNP) in Northern Borneo holds an important ecosystem for marine animals due to its special biodiversity of turbid reefs. MSCRNP is crucial to the Sarawak state's tourism sector. The aquatic system faces pressing problems due to sediment load, quality, and heavy metal influx from the rivers. In this study, we are comparing the sediment quality from the Miri and Sibuti rivers (downstream to the coral reef area) from 10 years ago to the present. In the present study, a total of 26 samples were collected from Miri and Sibuti Rivers towards MSCRNP in 2023, shown in **Figure 1**. Trace metal concentration was obtained using ICP-MS. The heavy metal and major elements were used to assess the contamination levels of the samples based on the geoaccumulation index (Igeo), Contamination index (CF), and Enrichment factor (EF). According to Nagarajan et al. (2023), the upstream of Miri River was moderate to considerably contaminated by Sb, As and Cu in 2014. It is also stated that CF in downstream of the Miri River is higher, for example, As and Sb represent very high contamination. The average Igeo value in the river was in an increasing trend (Mn < Ba< Sn < Ni < Pb < V < Cr < U < Zn < Mo < Cu < Sb < As) and As was severely polluted. William et al. (2024) reported that the heavy metal evaluation index (HEI) values in water significantly increased during the dry season compared to the wet season in 2021 and 2022. Similarly, Maharjan et al. (2021) reported that the heavy metals (in the water body) in the Miri River are high and not safe for domestic and recreational purposes such as fishing and water usage. Saifullah et al. (2014) reported that the estuary of the Sibuti River is experiencing low anthropogenic activity. In our study, the concentration of heavy metals is quite similar to the study conducted by Nagarajan et al. (2023) in the Miri River system. Igeo concentration in Miri River shows a similar pattern of increasing trend (Ba>Cu>Ni>Co>Mn>Mo>V>Zn>Pb=U>Cr>Sb>As), and As is severely polluted as well. Similarly, the CF values are similar to the previous study with As and Sb representing high contamination. While the Sibuti River also has a similar contamination pattern to the Miri River. CF values show high contamination of As and Sb in the river and Igeo values in increasing order (Ba>Cu>Ni>Co>Mo>V>Mn>Zn>Pb=U>Cr>Sb>As) showing severe pollution by As. This concludes that Arsenic contamination since 2014, reported by Nagarajan et al. (2023), has continued to present in the Miri River. Arsenic contamination could be associated with pesticides, agriculture fertilizers, sewage discharge and natural occurring (leaching from weathered rock or soil). While Sibuti River has changed from slightly polluted to moderately polluted since 2013 (Saifullah et al. 2014). This study will further explore geochemical mechanisms and the source of HM in Miri's coastal ecosystem. Thus, the impact on MSCRNP can be minimized, contributing to sustainable ecotourism and reducing the bioaccumulation of HM in aquatic organisms.

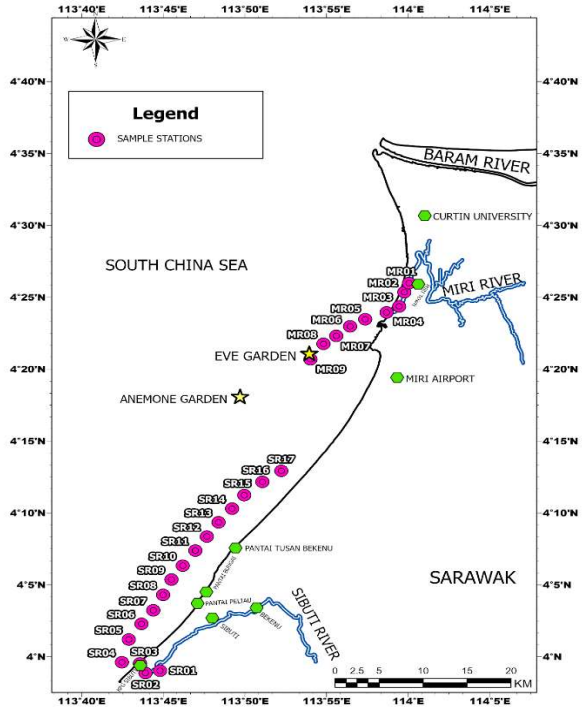

Figure 1. Location map of the study area

References:

Saifullah A. S. M., Abu Hena M. K., Idris M. H., Rajaee A.H., Johan I. 2014. Seasonal variation of water characteristics in Kuala Sibuti River estuary in Miri, Sarawak, Malaysia. Malaysian Journal of Science 33(1), 9–22. https://doi.org/10.22452/mjs.vol33no1.3

Maharjan, A. K., Wong, D. R., Rubiyatno, R. 2021. Level and distribution of heavy metals in Miri River, Malaysia. Tropical Aquatic and Soil Pollution, 1(2), 74–86. https://doi.org/10.53623/tasp.v1i2.20

Nagarajan, R., Eswaramoorthi, S. G., Anandkumar, A., Ramkumar, M. (2023). Geochemical fractionation, mobility of elements and environmental significance of surface sediments in a tropical river, Borneo. Marine Pollution Bulletin 192, 115090. https://doi.org/10.1016/j.marpolbul.2023.115090

William, F. B., Mohan Viswanathan, P., Ramasamy, N. 2024. Spatial and temporal distribution of geochemical elements and their processes in different size fractions–Miri river (NW Borneo). Kuwait Journal of Science 51(1), 100136. https://doi.org/10.1016/j.kjs.2023.10.004

Poster 36: Mesoarchean emergence of continents: Evidence from the Coorg Block, southern India

Cheng-Xue Yang[1*], M. Santosh[1,2]

[1]*Institute of Earth Science, China University of Geosciences Beijing, Beijing 100083, China*
[2]*Department of Earth Science, University of Adelaide, Adelaide, Australia*

[*] Corresponding author:
E-mail address: chengxue.yang@qq.com (Chengxue Yang)

The Coorg Block in southern India represents one of the oldest crustal blocks, and the felsic and mafic rock suites here provide important clues to the formation and growth of continental crust in the Early Earth. Charnockites and associated rock suites are the dominant lithology in this block and petrological and geochemical studies were carried out in order to elucidate the formation growth of the continental crust. The results indicate that they were derived possibly through fractionation of a reduced primary magma in a Mesoarchean subduction-related setting. Zircon U-Pb geochronology shows peak magmatism and crust building at ca. 3.15 Ga. This was immediately followed by high to ultrahigh-

temperature metamorphism at 3.0 Ga under a P-T range of 8–11 kbar at 950-1000 °C. Zircon Lu-Hf analyses suggest that the magma sources involved both juvenile and reworked Paleoarchean components. The mafic and ultramafic rock suites in this block represent the roots of an island arc built through slab dehydration and mantle wedge melting with geochemical features attesting to magma derivation from a refractory mantle source followed by the metasomatic enrichment of lithospheric mantle wedge through the influx of subduction-derived fluids/melts. The building of the Coorg block coincided with the formation of Earth's oldest supercontinent 'Ur' and also marks the emergence of early continents on the globe.

Poster 37: Petrography and Geochemistry of the Au-Polymetallic Deposit in Tawau, Sabah, Malaysia

R. Natasha Cindy[1*], S. Vijay Anand[1,*], R. Nagarajan[1,2], M. Santosh[3,4]

[1]*Department of Applied Sciences (Applied Geology), Curtin University, 98009, Miri, Sarawak, Malaysia.*
[2]*Curtin Malaysia Research Institute, Curtin University Malaysia, 98009, Miri, Sarawak, Malaysia.*
[3]*School of Earth Sciences and Resources, China University of Geosciences Beijing, 29 Xueyuan Road, Beijing, 100083, China.*
[4]*Department of Earth Science, University of Adelaide, Adelaide, SA, 5005, Australia.*

[*]Corresponding authors:
E-mail address: cindyrpie@postgrad.curtin.edu.my (Natasha Cindy); vijay.anand@curtin.edu.my (Vijay Anand)

The Bukit Mantri Au-polymetallic ore field is located within the Tawau, Sabah, Malaysia. The orebodies are hosted in altered andesite volcanic rocks with an intruded quartz vein dated Middle to Late Miocene, which overlay on the Kalumpang Formation. The study of this research includes field, petrography and whole-rock geochemistry. The field excursions were conducted around the Tawau, Sabah area, including Bukit Mantri goldmine, and the rock samples were collected based on their lithological variation and characteristics. The mineralogical studies were conducted using the thin, polished section under an optical microscope. In contrast, the concentration of major elements and trace elements was determined by using X-ray Fluorescence (XRF) analysis. This study reveals the petrographic data of the Bukit Mantri goldmine's host and mineralized rock to determine the mineral assemblages, textural features and alteration of the gold deposit and find the relationship of the ore mineralization in the study area along with the volcanic rock samples collected surround the Tawau area. The Au (gold) deposit is hosted by quartz gauge and associated with poly-metallic sulphides such as pyrite, chalcopyrite, galena, and sphalerite, and formed in different alterations like argillic, silicification along with sericitization. The most dominant sulphide mineral in the mineralized rock is fine to medium-grained pyrite, which occurs as a single or aggregated grains with the shape of cubic and octahedral within the quartz minerals. Furthermore, the content of Au in the study area with ore texture is confirmed to be high due to the presence of colloform, crustiform, cockade, comb and zonal texture in the minerals. The fluid inclusion petrography shows that the mineralized veins consist of liquid-rich and vapour-rich carbonic inclusion, which mostly displayed Type 3 (monophase) inclusion. As for the volcanic rock samples, the petrography result shows that the volcanic rocks are mostly display orthophyric and sieve texture and composed mainly of normal and continuously zoned twinning of plagioclase feldspar. The other minerals, such as biotite, pyroxene (orthopyroxene and clinopyroxene) and quartz, occur as secondary minerals with a percentage less than 20%. Additionally, the geochemical data of the volcanic rocks collected surrounding Tawau, Sabah that consist of the volcanic bomb, matrix of the volcanic bomb and andesite show insight into the composition and geochemical pattern of the volcanic rocks to elucidate the area's type, characteristics and tectonic setting relationships. Based on

the geochemical data, the volcanic rocks range in composition from basaltic andesite to andesite with calc-alkaline magmatic signature. The major oxide of all the volcanic rock samples shows high concentration, particularly on SiO_2 and Al_2O_3, with an overall average of 58.6 wt.% and 17.0 wt.%. Meanwhile, the MgO, MgO, Na_2O, and K_2O content exhibit low concentration for all samples with a range of 1 wt.% to 4 wt.% where the other major oxide such as TiO_2, MnO and P_2O_5 appear to be lower abundances in all samples with values of <1 wt.%. As for the rare earth elements (REEs), the volcanic bomb recorded a higher content of both light rare earth elements (LREEs) and high field strength elements (HFSEs) compared to the matrix of volcanic bombs and andesite. The ΣREE concentration is recorded high in volcanic bombs (avg. 72.88), followed by andesite (avg. 70.50) and matrix of volcanic bombs (avg. 68.49). Other than that, the pattern of chondrite normalized REEs shows enrichment in LREE with negative Eu anomaly, which confirms the fractionation of plagioclase feldspar that is rich in Ca in the rocks and undergoes magmatic differentiation. The negative Nb, Ta, and Ti anomalies in the primitive mantle elucidate the calc-alkaline subduction-related setting. In addition, the tectonic setting of the volcanic rocks shows that the mantle-derived basaltic magma formed the volcanic rocks from the subduction zone in the oceanic crust with the involvement of the arc materials caused by volcanic activity. This condition suggests that both the volcanic and mineralized rock can contribute to the economy of the state of Sabah, which can be considered a commercial venture. Other than that, this study is executed to provide reliable data and information to the exploration sector. Therefore, it is possible to explore the potential possibility of the Au-polymetallic deposit in the area for a better understanding by using a new constraint method regarding geodynamic processes, which can be used to develop the exploitation of the deposit to maximum profit.

Keywords: Tawau, Au-Polymetallic deposit, volcanic rocks, petrography, fluid inclusion, geochemistry

Poster 38: The unveiling of episodic volcanism at the onset of Celebes Sea subduction: Evidence from the Semporna volcanic complex

A. Manobalaji[a*], S. Vijayanand[a], R. Nagarajan[a,b], M. Ramkumar[c]

[a]*Department of Applied Science (Applied Geology), Curtin University Malaysia, Miri, Sarawak, Malaysia.*
[b]*Curtin Malaysia Research Institute, Curtin University Malaysia, Miri, Sarawak, Malaysia.*
[c]*Department of Geology, Periyar University, Salem, India.*

[*] Corresponding author:
E-mail address: manobalaji@postgrad.curtin.edu.my (Manobalaji, A)

The Semporna Volcano-Sedimentary Complex (SVSC) is a Miocene volcanic sequence associated with the Volcanogenic Massive Sulphide (VMS) deposits (**Fig 1a**). Previous studies have been done regarding the Plio-Pleistocene magmatism in Tawau and Kunak areas (Macpherson et al., 2010), the formation of geode (James et al., 2020), and K-Ar dates for volcanic rock in the Semporna peninsula (Bergman et al., 2000). Most research has been conducted in the entire Semporna Peninsula to understand the tectonic evolution of northern Sabah with an additional subsidiary focus on the Semporna region (Macpherson et al., 2010; Bergman et al., 2000; Burton-Johnson et al., 2020). Previous studies overlooked prevalent magmatism, particularly in Semporna. This disregard is of considerable significance, as magmatism is essential for tectonic evolution and the formation of mineral deposits. This study uses petrography studies via thin sections to discuss the spatial and textural variation of volcanic rock with multiple tectono-magmatic events/volcanic events. Preparing a petrography thin section requires cutting, grinding, and polishing a rock sample to a thickness of about 0.03mm for microscopic analysis. Six volcanic units associated with hydrothermal veins have been distinguished based on petrographic features and field investigation: The volcanic unit 1 is classified as

Andesite with limestone. It may be auto breccia or quench fragmentation because of fractured coherent lava. The selected region is composed of loose, blocky, irregular clast (**Fig 1b**), which is mainly composed of plagioclase and quartz as phenocrysts. The groundmass is lath feldspar with clinopyroxene, K-feldspar, and bioclasts such as bivalve, foraminifera, gastropods, coral and rostrum microstructure on cephalopods (**Fig 2a**). Andesite has a seriate texture (**Fig 2b**) with normal zoning of plagioclase. The volcanic unit 2 is classified as rhyolite, consisting of sanidine, plagioclase, and biotite as phenocrysts, and the groundmass is fine quartz (**Fig 2d**). It has a porphyritic texture with oscillatory zoning (**Fig 2c**). The volcanic unit 3 (maybe latite or leucocratic andesite) is mainly plagioclase as phenocrysts with felty feldspar (**Fig 2e**) that is strongly aligned. At Semporna quarry, the occurrence of volcanic units 4, 5 and 6 in the stratigraphic column (in the order of rhyo-trachyte, dacite, and trachyte from the top). The volcanic unit 4 is classified as rhyo-trachyte which has a columnar joint structure (**Fig 1e**). The upper colonnade is composed of plagioclase, sanidine, and less content of quartz with lath alkaline feldspar, and amphibole (**Fig. 2f, g, h**), which has a pilotaxitic texture. Dacite (Volcanic unit-5) (**Fig. 2g**) exhibits a glomeroporphyritic texture (**Fig. 2i & j**), which is characterised by clusters of mafic minerals, plagioclase and feldspar microlites. The volcanic unit 6 (trachyte) is mainly composed of K- feldspar as phenocrysts. The groundmass is lath feldspar with amphibole. Andesite is formed by polybaric crystallisation during magma ascent/gradual decrease of temperature during the crystallization (Adam and MacKenzie, 1998). It could have caused the tectonic stress on the Miocene limestone (MacKenzie et al., 1998). Rhyolite is formed by a process of a combination of slow cooling at depth (forming the phenocrysts), followed by poikilitic quartz nucleated at a depth of 5 to 10 km (Blundy and Cashman, 2001; Gill and Fitton, 2022) (forming the fine-grained quartz groundmass), and fluctuating conditions in the magma chamber (Winter, 2014). Flow direction near the surface is confirmed by vesicular, and the size of plagioclase decreases to the south direction, which is observed from megascopic and texture observation in Volcanic Unit 3 (Gill and Fitton, 2022).

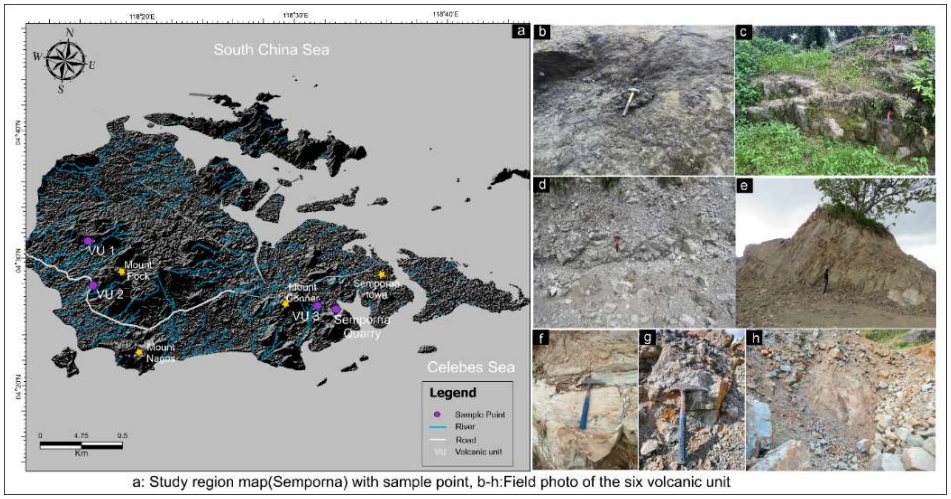

a: Study region map(Semporna) with sample point, b-h:Field photo of the six volcanic unit

Figure 1: Location map showing study area various lithology

The texture of the rhyo-trachyte is indicative of both flow-induced alignment and later-stage cooling-induced contraction (Winter, 2014), resulting in a striking appearance where fine crystal alignment is preserved within geometrically regular columns. Feldspar microlites of dacite indicate it formed as magma ascended from 4 km to 1 km (Gill and Fitton, 2022). Each volcanic unit showed variation in crystallisation, and it has been concluded that episodic volcanism (multiple volcanic intrusions/ extrusion) occurred in the Semporna region. The absence of olivine and the presence of feldspar is evidence of silica-saturated rock (Best, 2013). Carbonate veins have intruded into volcanic and sedimentary (pyroclastic rock). The presence of hydrous minerals (biotite and amphibole) in the rhyo-trachyte, dacite and rhyolite indicates that they crystallized under hydrous magmatic conditions (Best, 2013). These rocks were formed in the intra-oceanic island arcs and active continental margins above subduction zones (Gill and Fitton, 2022). The subduction that occurred in the Celebes Sea might have

caused the eruptions/intrusion of volcanic rock into overlying volcanic products, such as tuff, with geothermal fluid movement across the rocks (James et al., 2021).

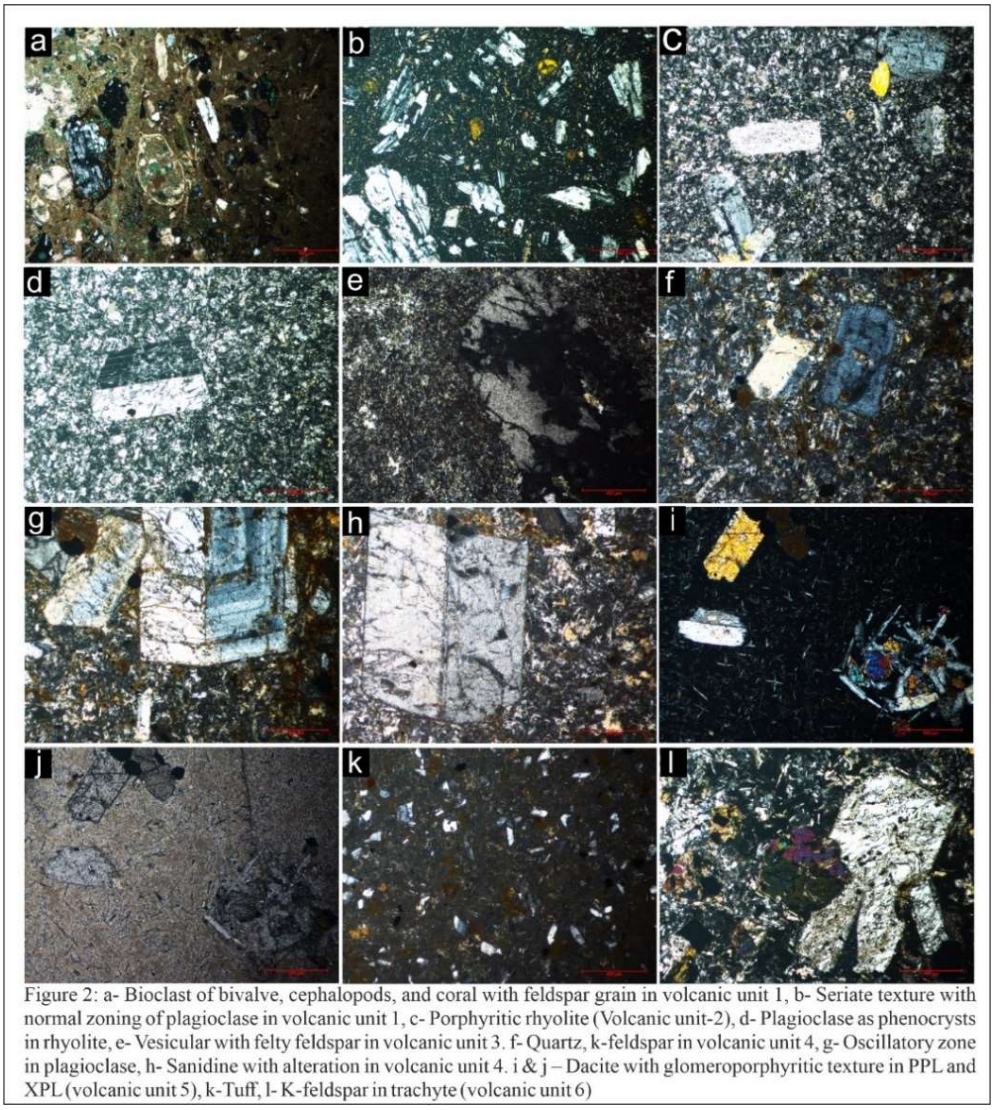

Figure 2: a- Bioclast of bivalve, cephalopods, and coral with feldspar grain in volcanic unit 1, b- Seriate texture with normal zoning of plagioclase in volcanic unit 1, c- Porphyritic rhyolite (Volcanic unit-2), d- Plagioclase as phenocrysts in rhyolite, e- Vesicular with felty feldspar in volcanic unit 3. f- Quartz, k-feldspar in volcanic unit 4, g- Oscillatory zone in plagioclase, h- Sanidine with alteration in volcanic unit 4. i & j – Dacite with glomeroporphyritic texture in PPL and XPL (volcanic unit 5), k-Tuff, l- K-feldspar in trachyte (volcanic unit 6)

References:

Adams, A., MacKenzie, W. S., 1998. Carbonate sediments and rocks under the microscope: a colour atlas. CRC Press.

Bergman, S.C., Hutchison, C.S., Swauger, D.A., Graves, J.E. 2000. K:Ar ages and geochemistry of the Sabah Cenozoic volcanic rocks. Geological Survey of Malaysia, Borneo Region, Bulletin, 44, 165-171.

Best, M. G. 2013. Igneous and metamorphic petrology. John Wiley & Sons. PP 33

Burton-Johnson, A., Macpherson, C.G., Millar, I.L., Whitehouse, M.J., Ottley, C.J., Nowell, G.M., 2020. A Triassic to Jurassic arc in north Borneo: Geochronology, geochemistry, and genesis of the Segama Valley Felsic Intrusions and the Sabah ophiolite. Gondwana Research, 84, 229-244.

Blundy, J., Cashman, K., 2001. Ascent-driven crystallisation of dacite magmas at Mount St Helens, 1980–1986. Contributions to Mineralogy and Petrology, 140, 631–650.

Gill, R., Fitton, G., 2022. Igneous rocks and processes: a practical guide. John Wiley & Sons.

James, E., Ghani, A.A., Akinola, O.O., Asis, J.B., 2021. Petrology and Geochemical Features of Semporna Volcanic Rocks, South-east Sabah, Malaysia. *Sains Malaysiana, 50*, 9-21.

MacKenzie, W.S., Donaldson, C.H., Guilford, C. 1982. Atlas of igneous rocks and their textures (Vol. 148). Harlow: Longman.

Macpherson, C.G., Chiang, K.K., Hall, R., Nowell, G.M., Castillo, P.R., Thirlwall, M.F., 2010. Plio-Pleistocene intra-plate magmatism from the southern Sulu Arc, Semporna peninsula, Sabah, Borneo: Implications for high-Nb basalt in subduction zones. Journal of Volcanology and Geothermal Research 190(1-2), 25-38.

Winter, J.D., 2014. Principles of igneous and metamorphic petrology (Vol. 2). Harlow, UK: Pearson education.

Poster 39: Tectonic Evolution of the Okcheon Fold-Thrust Belt: Insights into Paleozoic Tectonics and Orogenic Processes along the East Asian Continental Margin

Changyeob Kim[1,*], Jungrae Noh[1], Dawon Kim[1], Sanghoon Kwon[1*], Yirang Jang[2]

[1]*Department of Earth System Sciences, Yonsei University, Seoul 03722, Republic of Korea*
[2]*Department of Geological and Environmental Sciences, Chonnam National University, Gwangju 61186, Republic of Korea*

[*] Corresponding author:
E-mail address: kcy0202@yonsei.ac.kr (Changyeob Kim); skwon@yonsei.ac.kr (Sanghoon Kwon)

The Okcheon fold-thrust belt, located in the southern Korean Peninsula, serves as a crucial example for understanding the formation and evolution of the orogenic belts along the East Asian continental margin during the Paleozoic era. The belt preserves a variety of sedimentary basins developed at different geological times and tectonic settings, which have experienced various orogenic events forming an area of significant scientific debate, which characterize the complex Paleozoic tectonics of East Asia. This study integrates biomarker analysis, and U-Pb detrital and igneous zircon geochronology to redefine the stratigraphy of the Okcheon belt. Using the redefined stratigraphy, structural interpretations based on detailed field survey and down-plunge projections were conducted to figure out major structures and will provide new insights into the structural evolution of the belt. Together with all the information from this study and the previously reported publications, the spatiotemporal scenarios for the evolution of the Okcheon fold-thrust belt are as follows. (1) The Okcheon Belt was formed during the Neoproterozoic intracontinental rifting, which resulted in the creation of a rift basin in the Taebaeksan Zone. This resulted in the subsequent deposition of miogeoclinal sediments, known as the Joseon Supergroup. Throughout this time, the Okcheon Zone remained a basement high without sedimentation. (2) During the Devonian, sporadic magmatic events and contractional deformation in the Gyeonggi Massif supported the higher structural relief of the Gyeonggi Massif than the Okcheon Belt. In addition, the Taebaeksan Zone was higher relative to the Okcheon Zone in the Okcheon Belt. The differences in basement geometry before the deposition of the Carboniferous clastic wedge resulting in differences in depositional environments and lithologic variations in the Okcheon and Pyeongan Supergroups, and are supported by the previously reported Devonian detrital zircon U-Pb age dates from the meta-sedimentary rocks in the Okcheon Belt, the existence of angular unconformity between the Joseon Supergroup and the subsequent sequences, and the distinct lithologic differences between the lower parts of two Supergroups etc. (3) Finally, in the Late Permian to Early Triassic period, southeast-vergent thrust faulting affected the Paleozoic sequence in the study area.

By integrating these findings with previously reported data, this study provides a comprehensive model of the tectonic evolution of the Okcheon fold-thrust belt, offering significant insights into the tectonic processes along the East Asian continental margin during the Paleozoic era.

Poster 40: Multistage submarine landslides and their effects on widespread seeps, shallow gas and gas hydrate occurrences

Xiujuan Wang[1,2*], Jilin Zhou[2], Sanzhong Li[1,2], Jiapeng Jin[2]

[1]*Frontiers Science Center for Deep Ocean Multispheres and Earth System, Key Lab of Submarine Geosciences and Prospecting Techniques, MOE and College of Marine Geosciences, Ocean University of China, Qingdao 266100, China*
[2]*Laboratory for Marine Science and Technology (Qingdao) Qingdao 266237, China*
Center for Ocean Mega-Science &Key Laboratory of Marine Geology and Environment, Institute of Oceanology, Chinese Academy of Sciences, Qingdao 266071, China

[*] Corresponding author:
E-mail address: wangxiujuan@ouc.edu.cn (Xiujuan Wang)

Multistage mass transport deposits (MTDs) or submarine landslides have been delineated using three-dimensional (3D) seismic data in the sedimentary basins of the world oceans, especially in the deep-water basins. In the northern slope of the South China Sea, gas hydrate, shallow gas and numerous paleo-seeps or active seeps have been widely distributed, which are identified from 3D seismic data, drilling, in situ detection and multibeam data. Gas hydrates are confirmed from the logging-while-drilling and coring, which show the different morphologies and even coexistence with free gas in some areas. Gas hydrates are found below or within MTDs above the base of the gas hydrate stability zone (BGHSZ) showing layered or mounded-like structures which is controlled by the internal structure of MTD and the fluid flow.

Multi-attributes, such as RMS, coherence, dip and others are extracted from 3D seismic data along different horizons to show the reservoir changes, faults, and fractures. Most of the seeps and the highly concentrated gas hydrate are found in the sand-rich reservoir above the shallow gas-trapped zones, where the faults and gas chimney zones root from basement uplift. More than 200 chimney- and mounded-like structures are identified above MTD near the BGHSZ from 3D seismic data in the Qiongdongnan basins, South China Sea. The thrust faults and fractures are found within the MTD using coherence and RMS attributes, which can provide pathways for fluid flow migrations from deeper sediments to shallower sediments.

The thermogenic gas of the deep oil and gas reservoir migrates to the upward sediments along the structural faults, the side wall of central canyons and the tensile faults directly, which are just located above the basement uplift. They contribute to the accumulation of shallow gas, seeps and gas hydrate in the submarine fan and channel-levee system below MTD. Moreover, we found that the shallow gas trapped in the sand-rich reservoir below MTD shows the change from west to east. In the west zone, the gas resource shows biogenic gas, while the gas source shows thermogenic in the east part due to long-distance migration along the side wall of canyons. By modeling, we quantitatively reveal that a similar vertical distribution of gas hydrate saturation can be formed around the open faults above the base of the hydrate stability zone and the thermogenic gas migration along faults contributes to the enrichment of gas hydrate. The integrated studies provide a better understanding of how the fluids can pass through the MTD and form seeps, shallow gas and concentrated gas hydrate.

Keywords: Mass transport deposits, Paleo- and active seeps; gas hydrate; mounded-like; fluid flow.

Poster 41: Dynamic properties of black shale slip zone under acidic corrosion

Xin Liao[1*], Maoji Fan[1], Mingyao Zhong[1]

[1] *Faculty of Geoscience and Engineering, Southwest Jiaotong University, Chengdu, China*

[*] Corresponding author:
E-mail address: xinliao@swjtu.edu.cn (Xin Liao)

The black shale is prone to evolve to the slip zone as it exists in the bedding slope through the water-rock interactions. The study investigates how acidic conditions impact the dynamic mechanical properties of black shale slip zones. It shows that acid erosion significantly degrades these properties, with reductions in dynamic shear modulus and damping ratio, and an increase in permanent dynamic deformation. Microscopic examination indicates that acidic corrosion leads to the dissolution of carbonates, a rise in gypsum content, changes in clay particle shape, transitions in particle contact patterns and the expansion of fissures. These microstructural alterations diminish the stability and strength of the soil within the slip zone, thereby increasing the susceptibility to deformation and rupture under dynamic loading. They also highlight that acid erosion significantly degrades the mechanical properties of black shale. This paper utilizes the Duncan-Zhang and hyperbolic models to forecast the dynamic mechanical properties of slide zone soils subjected to acid erosion. It develops predictive models for permanent deformation under such conditions. The models' accuracy is confirmed through a comparison of calculated and measured values. The results are expected to provide further understanding of the mechanism of black shale degradation and bedding slope instability under seismic action.

Poster 42: Investigating the Mechanical Effects of Plant Roots on Slope Stability Using Global Root Strength Data

ADHJ. Perera[1,2*], Taro Uchida[2]

[1] *National Building Research Organization, Sri Lanka*
[2] *The Graduate School of Life and Environmental Sciences, University of Tsukuba, Japan,*

[*] Corresponding author:
E-mail address: harshisl@yahoo.com (Adhj. Perera)

Among all the natural disasters in the world, sediment disasters become one of the most destructive phenomena resulting in uncountable losses to the environment in recent history. Soil erosion and sediment disasters like slope failures, landslides, debris flows, river closure, volcanic disasters and avalanche disasters are becoming more serious problems in recent history causing numerous economic and human losses each year. The influence of climatic changes also promotes extreme weather conditions and it results in more sediment disasters throughout the world. In the last 100 years, global precipitation has increased from 1% and by 2100, the global rainfall is predicted to be increased by 16%-24%. Thus, we can expect more rainfall-related disasters and the world should be prepared to reduce the risk to both environment and human lives due to such natural disasters.

In terms of landslide disaster management, slope protection and stabilization methods can be efficiently used to minimize the effect of sediment disasters and simply these methods are two types, structural and non- structural or non-living and living. The structural measures are constructing rigid structures while non-structural measures include vegetation improvement, land use development, awareness and so on. As a non-living/ non-structural method, soil bioengineering methods, which use plants and their traits for slope stabilization is becoming a good practice all over the world. It is also applicable to control natural hazards, restore or reintroduce plant and animal species onto degraded lands and distributed environments and increase soil, air and water quality resulting in a sustainable society.

Apart from its major functions like photosynthesis, biodiversity enhancement and soil-water balancing, plants have hydrological and mechanical functions, which help to reduce soil erosion and enhance slope stability. The mechanical effects like catching, armouring, supporting, reinforcing and anchoring influence the mechanical strengthening of soil. The roots play a major role in slope stability and its characteristics influence the magnitude of the reinforcement provided. The presence of roots in soil produces a reinforced matrix in which stress is transferred to the roots during the loading of the soil. The magnitude of this reinforcement depends on the development of the root system as a function of plant properties and environmental conditions.

Different numerical models and experimental methods are introduced to quantify the effect of plants on slope stability and widely used models are Wu-Waldron model (Waldron, 1975; Wu et al., 1979), Fibre Bundle model (Pollen and Simon, 2005) and Root Bundle model (Schwarz et al. 2010). One of the key parameters in these models is root tensile strength. The tensile strength has been evaluated for various vegetation through laboratory experiments and in situ tests. There are commonly inverse relationships between root diameter and root tensile strength and the relationship between tensile strength (Ts) and root diameter(d) has been often expressed using the following power relationship.

$\mathbf{Ts = \alpha\, d^{\beta}}$ (The coefficients α and β are the regression parameters significant for species).

Since testing plant roots to quantify the effects is time and cost-consuming, it would be important to have a compiled database for root tensile strength data. Furthermore, if we can clarify controlling factors of root tensile strength and develop a predicting method of root tensile strength will be important for further effective use of bioengineering methods to mitigate sediment disasters. To overcome this, the data of regression parameters of the power relationship between root diameter and root strength were collected from previously published papers in scientific journals from 1979 to 2021. 178 dataset in terms of three different vegetation types as trees, shrubs and herbs from various continents like North America, Europe, Asia and Australia were used for the analysis.

During, the correlation of α and β, variations of those parameters with vegetation types and also with different diameters and the calculated tensile strength with respect to root diameter, leaf and root type and root system depth were analysed.

According to the results obtained, there is no significant correlation between the two experimental parameters, and they got higher values in tree species while lower values in herb species. Among the two parameters, β is more significant and the numerical contribution of diameter to the root strength depends on β. When β is zero, the strength is equal to α and the strength value decreases than α when β gets more negative values.

According to the diameter analysis, coarser roots of trees and finer roots of herb have relatively higher strength values. Most of the herbaceous species have simple and fine root systems and according to their strength values, they are more suitable to use as erosion control measure and stable topsoil layers. On the other hand, most tree species have deeply penetrating complex root systems and they can anchor the loos soil layers to the hard layers and it is believed that plant species with both fine and coarse root systems are most suitable for slope stabilization and a more number of fine roots are believed to contribute more on slope stabilization than a lesser number of coarse roots. The deep rooted and shallow rooted species show no difference, and the rooting depth is highly affected by the soil conditions and nutrient availability.

According to **Figure 1**, fine roots, herb and grass species show higher strengths while coarse roots and tree species show higher strengths. According to the schematic diagram, the root strength of herb and grass species shows a higher variation than that of tree species. Also, grass and herb have the highest

range of regression parameter β of all according to this study and β is the diameter-dependent variable when calculating root strength using the power law equation. The wide range of β in herbs and grasses also influences the higher range of strength values shown in the schematic diagram. So, it is clear that even within the same vegetation type, the strength properties of roots vary depending on the species and the local growth conditions.

Compared to tree species, herb and grass species show higher diameter dependency on root strength. That means the variation of root strength is high with changing the diameter. In tree species, the dependence of diameter is low so, the variation of root strength is low. This is influenced by the higher negative values of β of herb & grass species than trees.

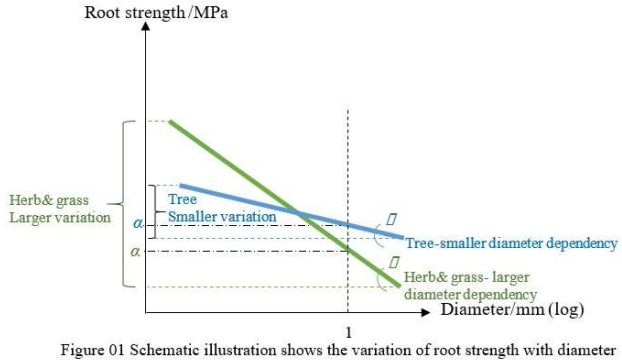

Figure 01 Schematic illustration shows the variation of root strength with diameter

Table 1. Mean Tensile strength-Mpa

Vegetation type	Mean α	Mean β	D=0.1mm	D=1mm	D=10mm
Tree	42.44±28.65	(-0.58)±0.25	210.74±269.87	42.44 ±28.65	12.39 ±12.61
Shrub	29.71 ±19.16	(-0.72)±0.26	165.93 ±137.85	29.71 ±19.16	6.84 ±6.34
Herb	24.16±16.99	(-1.01) ±0.43	283.44 ±422.66	24.16 ±16.99	4.87 ±6.76

Keywords: Natural Disasters, Climatic Changes, Disaster Management, Plants, Slope Stability, Tensile Strength, Root Diameter

References:

Pollen, N., Simon, A., 2005. Estimating the mechanical effects of riparian vegetation on stream bank stability using a fiber bundle model. Water Resources Research 41 http://dx.doi.org/10.1029/2004WR003801 W07025.

Schwarz, M., Cohen, D., Or, D., 2010. Root–soil mechanical interactions during pullout and failure of root bundles. Journal of Geophysical Research 115. http://dx.doi.org/10.1029/2009JF001603F04035.

Waldron, L., 1977. The shear resistance of root-permeated homogeneous and stratified soil. Soil Science Society of America Journal 41(5), 843-849

Wu, T.H., McKinnell III., W.P., Swanston, D.N., 1979. Strength of tree roots and landslides on Prince of Wales Island, Alaska. Canadian Geotechnical Journal 16(1), 19-33.

Poster 44: Mineralization Potential of the Ngoc Tu Granitoid Block in Kontum

Nguyen Duc Do[1,*], Niem Van Nguyen[1], Tien Cong Dinh[1],

[1]*Vietnam Institute of Sciences and Mineral Resources, Vietnam*

[*] Corresponding author:
E-mail address: nguyen180@gmail.com (Nguyen Duc Do)

The object of study is the mineralization potential of Ngoc Tu granitoids, located in the Po Co structural zone in the Kon Tum massif, Kon Tum province, Vietnam. The Ngoc Tu area includes the Triassic (T_2)-aged Ba Na complex granitoids and the Proterozoic (PR_{1-2})-aged plagioclase and biotite gneiss of the Tac Po Formation, where there is weak albitization and greisenization at their contact margins. Granitoid khối Ngọc Tu gồm các dạng granite porphyr và granite hạt trung This research mineralization potential integrated the field data, petrography and geochemistry. The K/Rb ratios of granitoids range from 88.19 to 135.25, indicating extreme evolution and deep differentiation. At the same time, the Sm/Eu (2.7-14.1), Zr/Hf (11.8-42.6) and K/Rb ratios; while the Rb/Sr (4.1-14.0) and Ce/Y (2.7-14.2) ratios indicate the potential molybdenum (Mo) and wolfram (W) mineralization. Determining the oxidation-reduction environment of magma by the content of (CO_2, H_2O) of quartz inclusions in magma on RAMAN equipment to know the potential of the granite mass. On that basis, it was determined that the Ngoc Tu granitoid mass is in a moderate to strong oxidation environment, indicated by the increase in the content of the main CO_2-rich impurities from porphyritic granite to medium-grained granite, showing the mineralization potential of molybdenum (Mo) and wolfram (W) of the Ngoc Tu granitoid.

Keywords: granitoid, mineralization potential, Ngoc Tu.

Author Index